Antti Ahola

STRESS COMPONENTS AND LOCAL EFFECTS IN THE FATIGUE STRENGTH ASSESSMENT OF FILLET WELD JOINTS MADE OF ULTRA-HIGH-STRENGTH STEELS

ACTA UNIVERSITATIS LAPPEENRANTAENSIS 937

Antti Ahola

STRESS COMPONENTS AND LOCAL EFFECTS IN THE FATIGUE STRENGTH ASSESSMENT OF FILLET WELD JOINTS MADE OF ULTRA-HIGH-STRENGTH STEELS

Dissertation for the degree of Doctor of Science (Technology) to be presented with due permission for public examination and criticism in the Auditorium 1316 at Lappeenranta-Lahti University of Technology LUT, Lappeenranta, Finland on the 4th of December, 2020, at noon.

Acta Universitatis
Lappeenrantaensis 937

Supervisor Professor Timo Björk
LUT School of Energy Systems
Lappeenranta-Lahti University of Technology LUT
Finland

Reviewers PhD Henri-Paul Lieurade
Technical Centre for Mechanical Industry (CETIM)
France

PhD Majid Farajian
GSI – Gesellschaft für Schweißtechnik International mbH
Germany

Opponents Professor Thomas Ummenhofer
Steel and Lightweight Structures
Karlsruhe Institute of Technology
Germany

PhD Majid Farajian
GSI – Gesellschaft für Schweißtechnik International mbH
Germany

ISBN 978-952-335-594-1
ISBN 978-952-335-595-8 (PDF)
ISSN-L 1456-4491
ISSN 1456-4491

Lappeenranta-Lahti University of Technology LUT
LUT University Press 2020

Abstract

Antti Ahola
Stress components and local effects in the fatigue strength assessment of fillet weld joints made of ultra-high-strength steels
Lappeenranta 2020
88 pages
Acta Universitatis Lappeenrantaensis 937
Diss. Lappeenranta-Lahti University of Technology LUT
ISBN 978-952-335-594-1, ISBN 978-952-335-595-8 (PDF), ISSN-L 1456-4491, ISSN 1456-4491

Ultra-high-strength steels (UHSSs) enable a significant reduction in material usage compared to mild steels and, thus, provide energy-efficient solutions for structural applications. In welded steel components, an increase in material strength does not necessarily result in enhanced fatigue strength, unless post-weld treatments (PWTs) are introduced. Consequently, the fatigue strength of welded UHSS components is amongst the most important design criteria, and fatigue assessments should be conducted using appropriate and accurate approaches.

This dissertation's objective is to evaluate the effect of stress components and local behavior on the fatigue strength assessments of fillet-welded UHSS joints. In this thesis, the effects of the cyclic membrane and bending loads on the fatigue strength of load-carrying (LC) and non-load carrying (NLC) fillet weld joints are investigated considering both weld root and weld toe failures. Furthermore, the local effects on the fatigue performance are addressed. The local effects are evaluated at a structural level, i.e. the effect of geometrical symmetry and asymmetry on the fatigue performance of fillet weld joints. In addition, the effect of stress components on notch stress is evaluated. Notch stress analysis applies a generic fatigue strength assessment model – namely the 4R method – to evaluate the combined effects of notch stress, residual stress, material strength and applied stress ratio on the fatigue strength of welded UHSS components. The thesis applies both experimental and numerical methods to examine the fatigue performance of fillet-welded LC and NLC joints. Experiments are conducted for joints made of S960MC and S1100QL UHSS grades, and numerical studies carried out for investigating structural stresses, notch stresses, and crack propagation of these joints.

The results demonstrate the importance of stress components and structural symmetry when assessing the fatigue strength of fillet-welded UHSS joints. Furthermore, PWT and its effect on the fatigue strength of UHSS components requires particular attention to notch geometry in association with the residual stresses and applied stress ratio in the fatigue strength assessments – for which the 4R method provides an efficient means of assessing the influencing factors.

Keywords: fatigue, welded joints, ultra-high-strength steel, stress component, local effect, fillet weld

Acknowledgments

Intensive work for the last few years has now come to an end – a doctoral thesis. The work was carried out in the Laboratory of Steel Structures at LUT University. Although my doctoral studies officially started in April 2017, one could say that the inspiration for research work initiated already in May 2013 when I set foot in the Laboratory of Steel Structures as a research assistant for the first time.

I would like to express my greatest gratitude to my supervisor, Professor Timo Björk, for providing the opportunity to work in the research group of Steel Structures, together with all support and trust that I have received in the past years. His supportive, unique, and highly qualified guidance has successfully guided me through research problems, simultaneously leaving room for finding my own path and approach.

I would like to gratefully acknowledge PhD Henri-Paul Lieurade and PhD Majid Farajian for their contribution to review, pre-examine and comment this thesis, and Professor Thomas Ummenhofer and PhD Majid Farajian for agreeing to act as opponents in the defense. I also want to thank my co-authors, PhD Timo Nykänen, Professor Zuheir Barsoum, PhD Tuomas Skriko, Moritz Braun, and Arttu Muikku for their valuable comments and contribution which played a significant role to enhance the content and quality of the articles included in this thesis.

A great appreciation is expressed to all research colleagues and friends in the Laboratory of Steel Structures. Versatile and valuable discussions and conversations, on and off the topic, have widened my thinking and knowledge. In addition, experimental testing is an essential step to verify applied concepts, theories and ideas. In the context of this thesis, any of the applied experimental research methods would not have been realized without the help of the skillful and cooperative personnel in the Laboratory of Steel Structures and other laboratories in the field of Mechanical Engineering – thank you all. For the last few months, Jenny and Antti Wihuri Foundation has helped me to finalize this thesis and will provide a support to continue the research work of this thesis. Their grant has been and will be received with a great respect.

To have an equilibrium in life, family and friends are needed to act as a counterbalance. I would like to thank my parents, Tiina and Kare, for providing a supportive and encouraging home to live and grow. Finally, thank you Miia, for acting as a great source of inspiration to finalize this thesis, and for being alongside with me for all these years.

Antti Ahola
November 2020
Lappeenranta, Finland

Contents

List of publications

This dissertation contains material from the following papers. The rights have been granted by publishers to include the material. Hereafter, the publications are referred to in the text as P-I–P-V.

I. Ahola, A., Nykänen, T., and Björk, T. (2017). Effect of loading type on the fatigue strength of asymmetric and symmetric transverse non-load carrying attachments. *Fatigue and Fracture of Engineering Materials and Structures*, 40 (5), pp. 670–682

II. Ahola, A., and Björk, T. (2020). Fatigue strength of misaligned non-load-carrying cruciform joints made of ultra-high-strength steel. *Journal of Constructional Steel Research*, 175, 106334

III. Ahola, A. Björk, T., and Barsoum, Z. (2019) Fatigue strength capacity of load-carrying fillet welds on ultra-high-strength steel plates subjected to out-of-plane bending. *Engineering Structures*, 196, 109282

IV. Ahola, A., Skriko, T., and Björk, T. (2020). Fatigue strength assessment of ultra-high-strength steel fillet weld joints using 4R method. *Journal of Constructional Steel Research*, 167, 105861

V. Ahola, A., Muikku, A., Braun, M., and Björk, T. (2021) Fatigue strength assessment of ground fillet-welded joints using 4R method. *International Journal of Fatigue*, 142, 105916

Author's contribution

The author was the principal investigator and corresponding author of all the above-listed publications. The author was responsible for the designing and managing of experiments, conducting finite element analyses, and preparing manuscripts for the articles. In P-V, A. Muikku assisted in the determination of literature data points and carried out the finite element analyses under the author's supervision.

Supporting studies

Björk, T., Ahola, A., and Tuominen, N. (2018) On the design of fillet welds made of ultra-high-strength steel. *Welding in the World*, 62, pp. 985–995

Ahola, A., Skriko, T., and Björk, T. (2018) Fatigue performance of GMA-brazed non-load carrying joints made of ultra-high-strength steel. In: K. Jármai and B. Bolló (Eds.): *Vehicle and Automotive Engineering 2*, pp. 157–169

Björk, T., Mettänen, H., Ahola, A., Lindgren, M., and Terva, J. (2018) Fatigue strength assessment of duplex and super-duplex stainless steels by 4R method. *Welding in the World*, 62, pp. 1285–1300

Nomenclature

Latin alphabet

A	elongation	%
a	crack depth	mm
a_f	final crack depth	mm
a_i	initial crack depth	mm
a_{tcd}	critical distance	mm
a_w	weld throat thickness	mm
$a_{w,eff}$	effective weld throat thickness	mm
b	base plate width	mm
C	crack propagation coefficient	da/dN in mm/cycles, K in N·mm$^{-3/2}$
C_f	Fatigue capacity	MPa^m
c	crack width	mm
E	Young's modulus	GPa
e	plate misalignment	mm
F	axial force	N
f	enhancement factor	–
f_y	yield strength	MPa
H	strength coefficient	MPa
I	second moment of area	mm^4
K	stress intensity factor	N·mm$^{-3/2}$
K_s	structural stress concentration factor	–
$K_{s,b,b}$	structural bending stress concentration factor under bending loading	–
$K_{s,b,m}$	structural bending stress concentration factor under membrane loading	–
$K_{s,m,b}$	structural membrane stress concentration factor under bending loading	–
$K_{s,m,m}$	structural membrane stress concentration factor under membrane loading	–
$K_{t,m}$	notch stress concentration factor under membrane stress	–
$K_{t,b}$	notch stress concentration factor under bending stress	–
K_{tot}	total stress concentration factor	–
k_b	bending bonus factor	–
k_m	stress magnification factor	–
k_s	thickness correction factor	–
L	gusset length	mm
L_j	joint width	mm
M	bending moment	Nmm
m	slope parameter of S-N curve or Paris' law	–
N	fatigue life	cycles
N_f	fatigue life	cycles
n	strain hardening exponent	–
n_{ts}	number of specimens	–
P_s	survival probability	%
p	weld penetration depth	mm

R	applied stress ratio	–
R_{eff}	effective applied stress ratio	–
R_m	ultimate tensile strength	MPa
$R_{p0.2}$	proof strength, 0.2% plastic strain	MPa
r	weld toe radius	mm
r_{ref}	reference radius, see also ENS	mm
r_{true}	actual weld toe radius	mm
S	stress	MPa
s	stress multiaxiality factor	–
T_σ	scatter range	–
t	plate thickness	mm
w	infusible weld root length	mm
x	x-coordinate (through thickness direction)	mm
x_g	stress gradient exponent	–
y	y-coordinate (plate width direction)	mm
z	z-coordinate (longitudinal direction)	mm

Greek alphabet

γ_f	partial safety factor for fatigue	–
Δ	range	–
ε	strain	–
ε_e	elastic strain	–
ε_p	plastic strain	–
θ	weld flank angle	°
ν	Poisson’s ratio	–
ρ	actual notch radius	mm
ρ^*	micro-support length	mm
ρ_f	fictitious radius	mm
σ	stress	MPa
σ_b	bending stress	MPa
σ_{ens}	effective notch stress	MPa
σ_{eff}	effective stress	MPa
$\sigma_{hs,eff}$	effective hot-spot stress	MPa
σ_{hs}	hot-spot stress	MPa
σ_m	membrane stress	MPa
σ_{nom}	nominal stress	MPa
σ_k	notch stress	MPa
$\sigma_{k,ref}$	reference notch stress, see 4R	MPa
σ_{res}	residual stress	MPa
σ_w	weld stress	MPa

Subscripts

avg	average

char	characteristic
max	maximum
min	minimum

Abbreviations

2D	two-dimensional
3D	three-dimensional
4R	notch stress-based fatigue strength assessment method
AW	as-welded
DNV-GL	Det Norske Veritas-Germanischer Lloyd
DOB	degree of bending, bending stress divided by total stress
DQ	direct-quenching
EC3	Eurocode 3
FAT	fatigue class
FEA	finite element analysis
G&P	ground and peened
GMAW	gas metal arc welding
HAZ	heat-affected zone
HFMI	high frequency mechanical impact
HS	hot-spot
HSS	high-strength steel
IIW	International Institute of Welding
LG	longitudinal gusset
LC	load-carrying
LCX	load-carrying cruciform
LSE	linear surface extrapolation
MSSPD	minimization of sum of squared perpendicular distances
NLC	non-load-carrying
NLCT	non-load-carrying transverse (single-sided transverse attachment)
NLCX	non-load-carrying cruciform (double-sided transverse attachments)
NWS	nominal weld stress
PWT	post-weld treatment
QC	quenched and cold-formable
QL	quenched and tempered
R-O	Ramberg-Osgood
SCF	stress concentration factor
SIF	stress intensity factor
STDV	standard deviation
SWT	Smith-Watson-Topper
UHSS	ultra-high-strength steel
TCD	theory of critical distance
TG	toe ground
TIG	tungsten inert gas
TTWT	through thickness at weld toe

WP	weld profiled
XRD	X-ray diffraction

1 Introduction

1.1 Background and motivation

Steels are used as structural materials in engineering applications due to their high structural performance and economical profitability. Steel materials include a wide range of applications, e.g. in civil engineering, working machines, cranes, transportation equipment, and marine and offshore structures. To assemble components and products, sheet metals typically incorporate welding as a joining method. Welding-related thermal cycles with unequal heating and cooling rates cause welding residual stresses and deformations. Tensile residual stresses cause an increase in the mean stress level of cyclic stress and, consequently, fatigue crack initiation and propagation can also occur under compressive cyclic loads. Welding deformations may introduce geometrical imperfections, such as axial misalignments and angular distortions in plate components, which act as stress raisers with respect to externally applied loads. In addition, a severe transition from the base material to weld metal, together with potential initial flaws, causes weld toes to be susceptible to fatigue crack initiation and propagation. In the case of fillet welds with a lack of full penetration, infusible weld root can act as an initial crack for crack propagation, and a fatigue crack can propagate through the weld or base metal under propitious cyclic load conditions. Due to these circumstances, fatigue strength capacity is amongst the most important design criteria in welded joints and components subjected to cyclic or fluctuating load conditions.

On the other hand, increasing demand for reducing CO_2 emissions has led to a pressing need for structural optimization and lightweight design in various applications. To conform to these requirements, redundant material usage and over-dimensioning should be avoided. In structures subjected to cyclic loads, fatigue strength assessments should aim for finite rather than infinite fatigue life of structural components in service but without forgetting structural integrity. In weight-critical steel structures, an attractive way to increase structural performance-to-weight ratio is to introduce the usage of high-strength and ultra-high-strength steel (HSS/UHSS) materials, which due to high static strength enable high load-bearing capacity. In welded components, the design and fabrication of UHSS constructions may initiate new design issues in comparison to components made of mild steels, such as local reduction and increase of material strength at heat-affected zones (HAZ) and fusion lines (Amraei et al., 2016, 2019; Björk et al., 2018) and metallurgical mismatch effects (Neuvonen et al., 2020; Ran et al., 2019). Such phenomena require detailed scrutiny from both design and fabrication perspectives.

The use of UHSS materials is favored to achieve an increase in stress levels, both static and cyclic, so that the material can be utilized to its full capacity. Nevertheless, prior investigations have unambiguously recognized that, with the welded steel joints, an increase in material strength does not necessarily improve the fatigue performance of welded components, as exemplified in Figure 1.1. This factor highlights the need for understanding the fatigue behavior of welded UHSS materials so that HSS and UHSS

materials can become as feasible options for structural applications (Skoglund et al., 2020). Potential requirements for high fatigue strength can be overcome by the implementation of post-weld treatments (PWTs), e.g. high-frequency mechanical impact (HFMI) treatment, weld profiling, weld toe grinding, or tungsten inert gas (TIG) dressing. These methods can significantly enhance the fatigue strength of welded joints compared to their untreated counterparts in the as-welded (AW) condition. In general, PWT methods can be divided into two categories; methods providing geometrical improvement at the weld toes, and methods modifying the residual stress state at weld toe, or both (Haagensen, 2011). Furthermore, a higher fatigue strength improvement level can typically be claimed for joints made of higher material strength. In residual stress-related methods, however, a consideration of external load conditions is required because the beneficial effects obtained by PWT might be severely diminished in the case of the high mean stress level of cyclic loading, and during overload peaks in external loading (Haagensen & Maddox, 2013).

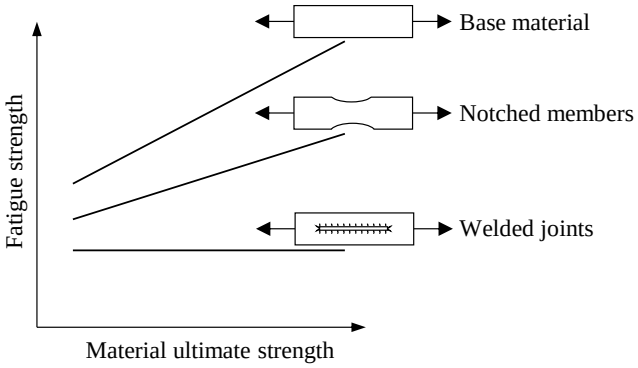

Figure 1.1: Correlation between material strength and fatigue strength in the base material, notched members and welded joints in the AW condition, after Maddox (1991).

As the use of UHSS material targets a reduction of material usage and plate thicknesses, the role of bending loads becomes pronounced. A reduction of plate thickness increases the share of bending stress in total stress, as the section modulus is proportional to the quadrature of plate thickness and the axial membrane stress is directly proportional to plate thickness. In addition, the role of imperfections is pronounced in thin-walled UHSS structures since the magnitude of structural stress concentrations increases when plate thickness is reduced. Therefore, further understanding of the effect that bending stresses have on the fatigue strength of welded components is required. In addition, the fatigue strength improvement gained by PWTs requires accurate approaches to avoid conservative and unconservative fatigue strength assessments.

This thesis investigates the role of stress components in the fatigue analysis of fillet-welded UHSS joints. In addition, the local effects at a structural level, i.e. whether weld reinforcement and welded detail are single-sided or double-sided, are addressed. The misalignment effects in the double-sided details are also covered in this context. To

account for the local effects at the notch level – i.e. weld toe radius and residual stress, in the fatigue strength assessments – this thesis also presents and further verifies the notch stress-based approach, namely the 4R method, for assessing the fatigue strength of UHSS fillet weld joints. The consideration of stress components and notch effects are studied experimentally, conducting geometry and residual stress measurements and fatigue tests on welded joints and, numerically, performing finite element analyses (FEAs) to investigate the stress concentrations and crack propagation properties of fillet-welded joints. The study addresses the importance of considering stress components in the fatigue analysis of welded joints and shows an efficient method for assessing the fatigue strength of UHSS joints using notch stress-based analysis in respect of the joint and external load conditions.

1.2 Objectives of the study

Together with the estimation of acting service loads, one of the main concerns in fatigue design is stress analyses and the achieving of efficient methods for assessing the fatigue strength properties of welded joints and components (Haglund et al., 2019). From an engineering viewpoint, a common practice has been to select a most conservative approach to obtaining safe-side predictions but an increasing need for optimizing structures necessitates a more comprehensive understanding of the fatigue behavior of welded components. This issue also incorporates consideration for stress components and local effects in fatigue design. Some of the design codes and standards include consideration of stress components in the fatigue analysis of welded joints. However, the most common practice is to obtain the maximum nominal or structural hot-spot (HS) stress regardless of the degree of bending (DOB) – i.e. bending stress divided by the total stress – and also to use a similar fatigue class (FAT) for both axial and bending loads.

The incoherence and lack of information present in current fatigue design standards and guidelines regarding the role of stress components, together with the importance of fatigue strength assessments in welded UHSS joints, combine to pose the research questions and main objectives of this study. This thesis aims to analyze the effects of the membrane and bending stress components, as well as the local effects on the fatigue strength of welded UHSS joints in fillet weld joint configurations, in respect of both non-load-carrying (NLC) and load-carrying (LC) joint types. Factors influencing fatigue strength at structural and notch levels in fillet weld UHSS joints are examined. In addition, this thesis examines efficient methods for taking stress components and local effects into account to further the scope of fatigue strength assessments. Figure 1.2 summarizes the study's objectives and research questions in conjunction with the publications included.

Objective

To determine the effect of stress components, and local structural and notch geometry on the fatigue strength of fillet-welded UHSS joints and to obtain efficient methods for fatigue strength assessments.

Research questions	Publications
Q1. What is the effect of stress components on the notch stresses and fatigue behavior of fillet-welded UHSS joints?	P-I, P-II, P-III
Q2. How do the joint symmetry and misalignments affect the notch stress concentrations, and what is the role of stress components?	P-I, P-II
Q3. How should the bending stresses be considered in the fatigue analysis of load-carrying fillet welds in the case of weld root fatigue failure?	P-III
Q4. What factors influence fatigue strength of UHSS joints and how they can be considered in the fatigue strength assessments?	P-IV, P-V

Figure 1.2: Research objectives and questions in association with publications included in this thesis.

1.3 Scope and limitations

Experiments within this study are conducted for fillet-welded UHSS joints to reflect the main focus of this thesis. Consequently, the experimental findings obtained in this study are principally applicable for joints made of UHSS grades. Nevertheless, literature reviews on experimental fatigue test data also includes results from joints made of mild and high-strength steels. Therefore, the presented theoretical concepts are extended to cover various steel grades.

When considering the applications of thin-walled UHSS components, gas metal arc welding (GMAW) is a widely used process applied to produce fillet welds and, thus, is the only welding process applied in the study's experiments. However, similar fillet welds (weld size and heat input) can be also produced with other methods of shielded metal arc welding or hybrid laser and arc welding techniques, meaning that the results are not only limited to GMAW processes. In addition, the thesis investigates fillet weld joints in both the AW and post-weld-treated conditions, including the HFMI treatment, TIG dressing, grinding methods (burr grinding and weld profiling), and a combined method in which grinding is followed by peening treatments. Other PWT methods are not addressed in this thesis.

Fillet welds are usually used to adjoin transverse or longitudinal plate components to a base plate; namely transverse attachment and longitudinal gussets. Depending on the load configuration, transversely fillet-welded joints can either be LC or NLC, or both. In this thesis, the fatigue behaviors of both LC and NLC joint types are addressed but, for simplicity, they are investigated individually, i.e. it is assumed that the ends of the fillet-welded adjoined plate components can deform freely under loading at the base plate.

Furthermore, all joint experiments are conducted in an atmosphere at room temperature using load-controlled uniaxial constant amplitude loading.

Due to the limited number of test specimens in each study, the thesis does not majorly address the statistical aspects usually present in fatigue tests conducted for various weld qualities. The fillet welds are prepared using robotic welding to produce uniform geometrical and metallurgical quality throughout the fatigue test specimens, and reduce thus the scatter of fatigue test results within the test series. Although a welding robot is employed in the preparation of the specimens, the specimens in the AW condition are aimed to represent fillet weld joints without initial flaws in normal workshop quality, resulting in a rather sharp transition from the base metal to the weld reinforcement.

1.4 Scientific contribution

This thesis investigates the fatigue behavior of fillet-welded UHSS joints, focusing on the role of stress components and local effects in fatigue strength assessments using numerical, experimental and analytical methods. Results are provided on the effect of axial and bending loads on the fatigue behavior of fillet-welded NLC and LC joints. In this context, UHSS components have not been widely studied in prior research and, consequently, the role of joint symmetry and misalignments has not been comprehensively recognized. Consequently, the thesis provides a novel insight into this topic. These viewpoints are principally focused in P-I and P-II.

The thesis also investigates the fatigue behavior of LC joints prepared with double-sided fillet welds and subjected to bending loads. Prior investigations and current fatigue design guidelines mainly address the fatigue analysis of such joints subjected to cyclic axial loads. Through the numerical and experimental findings, an analytical approach for assessing weld stress under bending loading for fatigue strength assessments is proposed. P-III covers this topic.

The fatigue strength of welded steel components failing at the weld toes, particularly in the case of UHSSs, can be significantly improved with PWT methods. The use of conventional approaches, complete with improved fatigue class and enhancement factors, hinders the methodological understanding of the fatigue performance of welded joints as such approaches are generally applicable for certain experimentally verified conditions. This thesis furthers work related to the novel notch stress-based model – namely the 4R method – by applying it for fillet weld UHSS joints in the AW and post-weld-treated condition. Also, applying literature data, the 4R method is implemented for joints made of various steel grades (from mild steels to UHSSs) post-weld-treated with grinding, and also combined grinding and peening, through which both geometrical and residual stress improvement is introduced. The thesis demonstrates that the 4R method enables accurate fatigue strength assessments for joints in the AW and post-weld-treated conditions, as well as supporting its utlization as a generic model for predicting the fatigue strength of welded joints. P-IV and P-V concentrate on the 4R method applications.

1.5 Structure of the thesis

The thesis comprises six chapters. Chapter 1 outlines the topics of the thesis, introduces background and motivation, and defines study's scope and limitations. Chapter 2 presents the theoretical foundation and current craft associated with the topics the thesis covers, i.e. the consideration of stress components and local effects in the fatigue assessments of welded joints. In addition, Chapter 2 describes the current design guidelines for a fatigue strength assessment of welded joints, including an introduction for considering the influencing factors in assessments. Plus, Chapter 2 also theorizes the principles of the multi-parametric fatigue strength assessment approach – the 4R method – that is later applied for the fatigue strength assessments in Chapter 4.4. In Chapter 3, the basic principles of the applied experimental and numerical research methods, together the literature review conducted for collecting fatigue test data are introduced. The experimental results, numerical analyses, and fatigue analyses are presented in Chapter 4. Chapter 5 reflects the study results with respect to the objectives and research questions of the thesis, as well as discussing the significance of the research findings in comparison with previous approaches. Chapter 6 summarizes the thesis and draws the main conclusions.

2 Theoretical foundation

This chapter presents the theoretical foundation applied in this thesis. Chapter 2.1 gives the background of classical stress analysis and insights on the role of primary stress components in the secondary and tertiary levels of stresses. Chapter 2.2 presents the theoretical concepts related to factors influencing the fatigue strength of welded joints. Chapter 2.3 introduces the basic principles of current fatigue design codes and guidelines, and, last, Chapter 2.4 presents the 4R method concept.

2.1 Categorization of stress components

By nature, stress at a welded joint can be divided into primary, secondary and tertiary level stresses (Radaj et al., 2006):

- Primary-level stresses can be regarded as stresses induced directly by external load components. In the context of this thesis, primary stresses are either membrane or bending stresses, or else a combination of both. They can be derived analytically by means of axial normal force and cross-sectional area, as well as bending moment and section modulus. From the fatigue design viewpoint, the primary stresses are usually regarded as nominal stresses, and are applied in the fatigue analysis as global approaches. Macro-geometric stresses induced by angular distortion, for example, can be also regarded as primary-level stresses.
- Secondary-level stresses are caused by structural discontinuities. In welded details, together with primary-level stresses, they are usually regarded as structural in nature. In an individual cross-section, e.g. in the front of a longitudinally welded detail, the secondary stresses are positive but they are self-balanced in the whole cross-sectional area and, consequently, alongside the welded structural detail, secondary stresses can be negative. Secondary stresses are comprised of the membrane and bending stress components. Structural stresses can be evaluated obtained numerically with FEA by deriving the stress distribution in the through-thickness direction and linearizing the stress distribution, or using the analytical formulation of structural stress concentration factors (SCFs), K_s, if available. In the fatigue analysis, structural stresses are applied using the structural hot-spot (HS) stress methods.
- Tertiary-level stresses are caused by notched details, due to the cross-sectional change, while in the welded details, they are caused by a (severe) transition from the base metal to weld metal. Tertiary-level stresses are invariably self-balanced in each longitudinal cross-section, i.e. the integration of a notch stress distribution in the through-thickness direction gives zero membrane and bending stress.

Tertiary level stresses are incorporated by the fatigue analyses when employing notch stress-based approaches.

The main focus of this thesis is on transversely welded joints, i.e. transverse NLC and LC fillet weld joints in which primary stresses are superposed with angular distortion-induced macro geometric bending stresses only. However, to exemplify the nature of primary-, secondary- and tertiary-level stress components in welded joints, a fillet-welded single-sided longitudinal gusset (LG) joint is analyzed with FEA using a three-dimensional (3D) solid element model. Figure 2.1 presents a quarter symmetry model of the studied geometry. The LG joint is analyzed using both axial membrane stress (DOB = 0), and pure bending loading (DOB = 1) at the loaded surface. In the analysis, the magnitude of the nominal membrane and bending stresses are $\sigma_{nom,m}$ = 1 MPa and $\sigma_{nom,b}$ = 1 MPa.

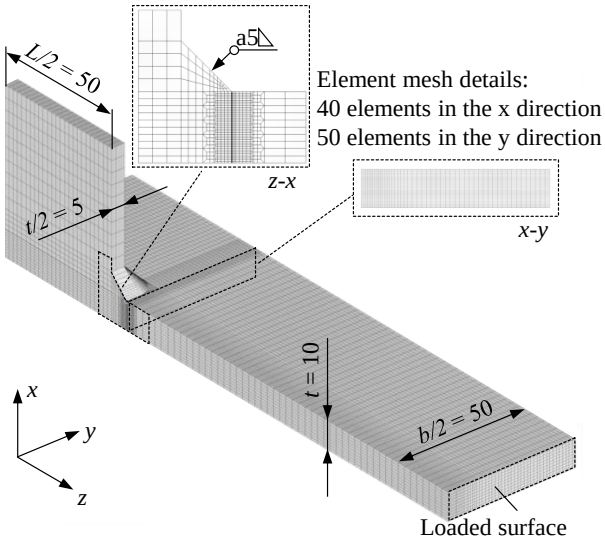

Figure 2.1: Element mesh model and geometry used for analyzing the stress components. *L* is the gusset length, *t* is the plate thickness, and *b* is the base plate width.

The primary and secondary membrane and bending stress components, and the tertiary-level non-linear stress component can be determined using the following formulae (modified from Hobbacher, 2016):

$$\sigma_m(y) = \frac{1}{t}\int_0^t \sigma(x,y)dx\,, \tag{2.1}$$

$$\sigma_b(y) = \frac{6}{t^2}\int_0^t \left(\sigma(x,y) - \sigma_m\right)\left(\frac{t}{2} - x\right)dx\,, \tag{2.2}$$

$$\sigma_{nl}(x,y) = \sigma(x,y) - \sigma_m(y) - \sigma_b(y)\left(1 - \frac{2x}{t}\right), \tag{2.3}$$

where $\sigma_m(y)$ is the membrane stress at the y location, $\sigma(x,y)$ is the normal stress distribution in the through-thickness direction ($x = 0$ at the plate surface, and $x = t$ at the bottom of the plate) at the y location, $\sigma_b(y)$ is the bending stress at the y location, and $\sigma_{nl}(x,y)$ is the non-linear tertiary stress at an arbitrary location of the x-y plane (see Figure 2.1). Using Equations (2.1–2.3), 3D stress distribution plots are obtained for all stress components. Figure 2.2 presents the stress distributions for the joint subjected external membrane stress.

Under axial loading, both secondary membrane and bending stresses (see Figure 2.2c–d) occur, caused by a one-sided structural stiffener. In the case of a double-sided stiffener, bending stresses do not occur due to the symmetry of the joint, and secondary stress is only increased by a membrane stress concentration in the front of the gusset. It is also noticeable that the counter-reaction forces and moments, are present next to the gusset ($y \approx 10$–50 mm), i.e. secondary-level stresses are negative and, thus, balancing the structural stresses at the front of the gusset. Naturally, the notch stress is only present at the front of the gusset (Figure 2.2e), and fades out and diminishes to zero next to the gusset. To conform to the force and moment equilibrium, the primary nominal stresses must meet the following formulae:

$$\sigma_{nom,m} = \frac{1}{b}\int_0^b \sigma_m(y)\mathrm{d}y, \tag{2.4}$$

$$\sigma_{nom,b} = \frac{1}{b}\int_0^b \sigma_b(y)\mathrm{d}y, \tag{2.5}$$

where $\sigma_{nom,m}$ and $\sigma_{nom,b}$ are the nominal (external) membrane and bending stress, respectively. For the LG joint subjected to external bending stress (see Figure 2.3) similar structural stress components to the membrane stress loaded LG joint can be found. However, in this case, the most interesting finding is that membrane stress is unequal to zero, i.e. the external bending stress also causes redistribution of membrane stresses (see Figure 2.3d). In addition, the magnitude of secondary-level membrane stress is even higher in the case of external bending stress than external membrane stress loading.

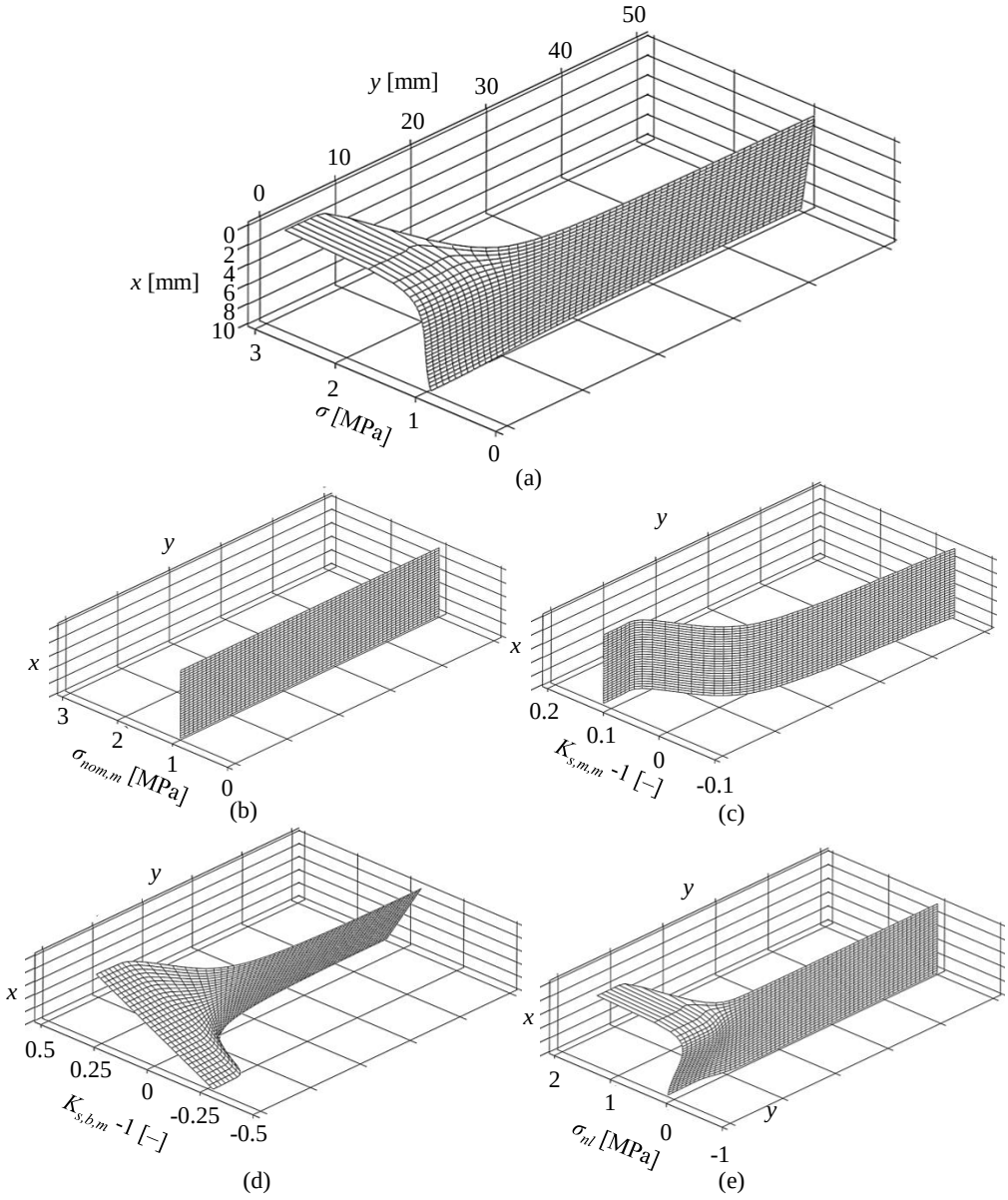

Figure 2.2: The stress plots of welded longitudinal gusset under axial membrane stress: (a) total stress distribution including all stress components, (b) nominal (primary) membrane stress, (c) secondary membrane stress, and (d) secondary bending stress distributions, and (e) the non-linear distribution of tertiary-level stresses. $K_{s,m,m}$ and $K_{s,b,m}$ are the structural membrane and bending SCFs under the membrane loading, respectively.

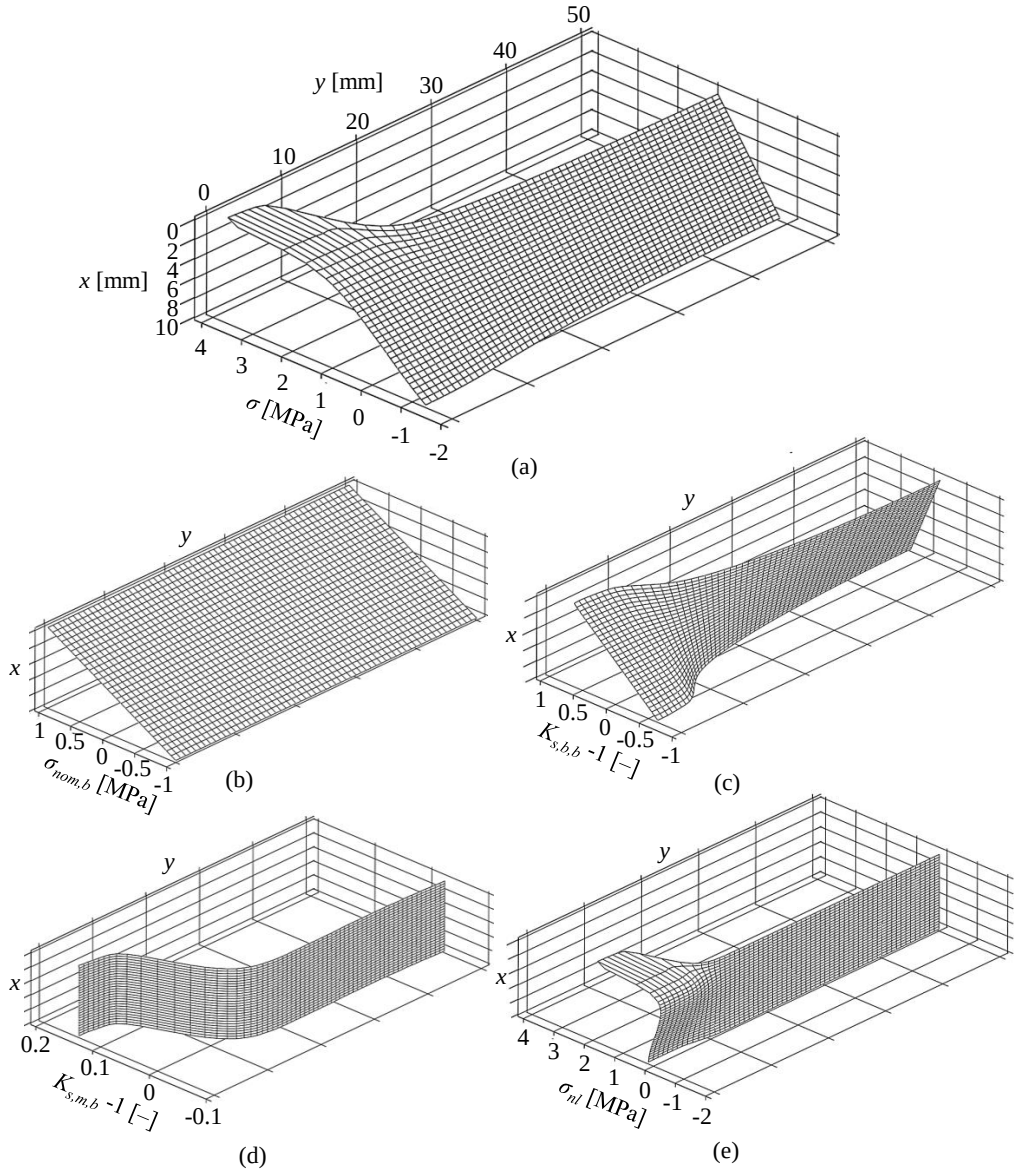

Figure 2.3: The stress plots of welded longitudinal gusset under bending stress: (a) total stress distribution, including all stress components, (b) nominal (primary) bending stress and (c) secondary bending stress, and (d) secondary membrane stress distributions, and (e) the non-linear component of tertiary-level stresses. $K_{s,m,b}$ and $K_{s,b,b}$ are the structural membrane and bending SCFs under the bending loading, respectively.

To explain the stress analysis in accordance with the stress components, the notch stress at the weld toe can be formulated as follows (for simplicity σ_m and σ_b now represents the stress values at the weld toe position $y = 0$):

$$\sigma_m = \sigma_{nom,m} + (K_{s,m,m} - 1)\sigma_{nom,m} + (K_{s,m,b} - 1)\sigma_{nom,b}\,, \tag{2.6}$$

$$\sigma_b = \sigma_{nom,b} + (K_{s,b,m} - 1)\sigma_{nom,m} + (K_{s,b,b} - 1)\sigma_{nom,b}\,. \tag{2.7}$$

Using the membrane and bending stresses, the superposed notch stress σ_k can be calculated accordingly for a finite notch radius r:

$$\sigma_k(r) = K_{t,m}(r)\sigma_m + K_{t,b}(r)\sigma_b\,, \tag{2.8}$$

where $K_{t,m}$ and $K_{t,b}$ are the notch SCFs under the membrane and bending stress, respectively. In Figure 2.2 and Figure 2.3, the stress distributions were exemplified for a single geometry configuration. To evaluate the effect of geometrical parameters on the magnitude of stress concentrations, the geometry of the LG joint was altered. In this observation, of base plate width and gusset length (see Figure 2.1) were varied to study their effect on the stress concentrations. These parameters were regarded as the main influencing factors for the stress concentrations. In addition, in this analysis, a symmetric double-sided gusset was analyzed. Figure 2.4 presents the stress components and Figure 2.5 presents the notch stress concentrations at the weld toe of LG for the single-sided and double-sided LG joints subjected to the external membrane and bending stresses.

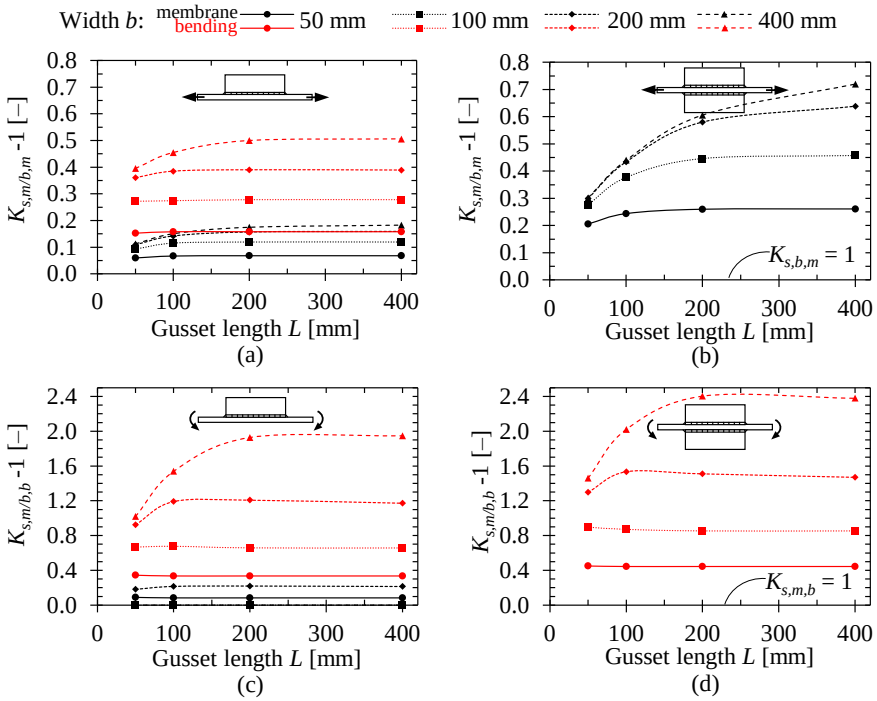

Figure 2.4: The effect of base plate width and gusset length on the secondary membrane and bending stresses: (a) single-sided and (b) double-sided LG joint under axial membrane stress, and (c) single-sided and (d) double-sided LG joint under bending stress.

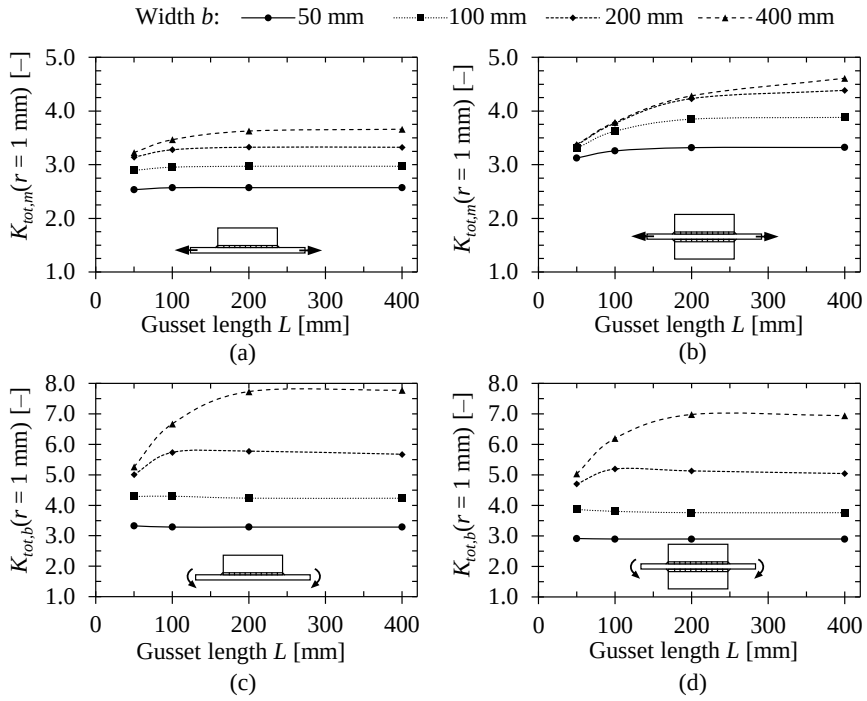

Figure 2.5: The effect of base plate width and gusset length on the total notch stress using a reference radius of r_{ref} = 1.0 mm at the weld toe and maximum principal stress criterion: (a) single-sided and (b) double-sided LG joint under axial membrane stress, and (c) single-sided and (d) double-sided LG joint under bending stress. K_{tot} is the total SCF (comprising both structural and notch stress concentrations).

2.2 Fatigue strength of welded joints – Influencing factors

The following subchapters introduce influencing factors that have been recognized to affect the fatigue behavior of welded joints. Following the scope and limitations of the study given in Chapter 1.3, some aspects are excluded, such as thickness effects, low-cycle fatigue characteristics, and environmental effects. Each subchapter focuses on its own topic but as the factors and their effects are closely related to each other, their combined effects are also discussed.

2.2.1 Residual stresses

Welding incorporates local thermal cycles at the joint areas, an unevenly distributed temperature field at the adjoined plate components, and the expansion and subsequent contraction of filler material during the thermal cycle. In association with the structural stiffness of adjoined components, which may cause high tensile residual stresses. By their nature, the residual stresses can be global, i.e. occurring at the whole structural component corresponding to the external loading, or local residual stresses (Hensel et al., 2018;

Schroepfer et al., 2019). The local stresses occur at the structural details (secondary level) or at the notched members, such as weld toes (tertiary level). Local residual stresses are characterized by the fact that they reach self-equilibrium. Furthermore, it is noticeable that the global residual stresses, similar to external load components, are superposed at the local level. Due to these circumstances, high tensile residual stresses, equal to up to the yield strength of material, are typically assumed to occur at the weld toes in the AW condition. This is a valid assumption, particularly regarding large-scale welded components. In the small-scale test specimens usually applied in the fatigue testing, the magnitude of residual stresses can be significantly lower, or even compressive, depending on the joint configuration and applied base and filler materials (Farajian, 2013; Gkatzogiannis et al., 2017).

High tensile residual stresses combined with the external cyclic loading normally cause a high mean stress level of cyclic behavior. This high mean stress level is recognized to substantially decrease the fatigue strength of metallic materials. In welded components, the high mean stress – in association with the local stress raisers at the weld toes such as notches or crack-like defects – significantly lowers the fatigue performance with respect to the unwelded counterparts, making welded components susceptible to fatigue failures. The presence of high tensile residual stresses diminishes the effect of stress ratio on the fatigue behavior in welded joints, as the cyclic loading causes local plasticity – and the local cyclic behavior is identical whether the cyclic loading is pulsating tension ($R \geq 0$) or fully reversed ($R = -1$). To improve the fatigue performance of welded components, the tensile residual stresses can be decreased using various techniques, such as using low transformation temperature (LTT) filler materials in GMAW (Bhatti et al., 2013) or introducing alternatively gas metal arc brazing in joining (Ahola et al., 2018).

Another means for modifying and reducing local or global residual stresses is to apply PWTs. Various PWT methods can be applied either to modify the residual stresses thermally, e.g. by stress relieving or spot heating, or mechanically introducing peening techniques or overloads (Haagensen, 2011). Thermal methods cause redistributions of residual stresses, and are mainly used to change the secondary level of residual stresses, while mechanical methods primarily affect residual stresses at the local notches. The reduction of tensile residual stresses, particularly with PWT methods that induce compressive residual stresses in welded joints, can significantly improve fatigue capacity.

2.2.2 **Material strength**

In steel components with blunt notches and negligible low stress residual stresses, increase in the material ultimate tensile strength typically provides higher fatigue performance. Nevertheless, as demonstrated in Chapter 1.1, an increase in the material strength does not contribute to achieving high fatigue strength in the welded joints in the AW condition. This observation has been widely supported by the experimental findings, e.g. see the works undertaken by Lieurade et al. (2008) and Sonsino (2009). In plain specimens and unnotched members, e.g. for cut and machined edges with high surface quality, higher fatigue strength can be claimed for HSS and UHSSs (Sperle, 2008). In

welded components, multiple factors affect the fatigue strength, and the use of HSS and UHSS grades does not necessarily provide any fatigue strength improvement. Such fatigue behavior found with UHSS grades is affected by multiple factors:

- A higher material strength of metallic materials decreases the micro-support length (see Chapter 2.2.4) and, thus, increases the fatigue notch sensitivity (Stephens et al., 2000);
- The magnitude of welding residual stresses typically increase along with the increase in material strength (Farajian, 2013), and tensile residual stresses equal up to the yield strength of the material can be assumed (Hobbacher, 2016);
- UHSS materials may experience severe changes in local microstructure due to the welding, as well as a reduction of material strength at the fatigue-critical fusion lines and HAZ (Lieurade et al., 2008; Skriko & Björk, 2015).

In spite of these concerns, welded HSS and UHSS grades may achieve significantly higher fatigue strength than mild steels. Again, the introduction of PWTs is essential for materials with higher strength. Particularly, peening methods can lead to high fatigue strength in HSS and UHSS grades (Marquis & Barsoum, 2016). Nykänen and Björk (2016) examined the effect of material strength on the compressive residual stresses in the joints post-weld-treated with peening methods. Based on the literature data, they found a conservative correlation between the material ultimate tensile strength and residual stress, equal to the residual stress of $\sigma_{res} = -0.255R_m$, which indicate achievement of high fatigue strength in the peened joints made of HSS and UHSS grades. Furthermore, recent experimental studies on the fatigue performance of HFMI-treated joints have shown that significantly higher fatigue strength improvement can be claimed for joints with higher steel grade (Yıldırım, 2017). For other PWT methods, unambiguous conclusions cannot be drawn although the design recommendations do allow a higher fatigue class for the steels with yield strength of more than 355 MPa. Maddox (2011) showed a slight increase in burr ground and TIG-dressed joints along with the increasing material strength while a recent study undertaken by Baumgartner et al. (2019) found a slight decrease in the fatigue strength of TIG-dressed joints when using local approaches.

2.2.3 **Applied stress ratio**

Due to a premise of high tensile residual stresses in joints in the AW condition, the applied stress ratio of external loading does not have a major influence on the fatigue strength capacity of welded joints (Sonsino, 2009). Regardless of the magnitude of maximum loading, the presence of high tensile residual stresses causes the plastic deformation of material at the notch root (as illustrated in Figure 2.6b). Consequently, the local cyclic behavior is quite similar for fully reversed ($R = -1$) and pulsating cyclic load conditions ($R \geq 0$), with a similar fatigue performance.

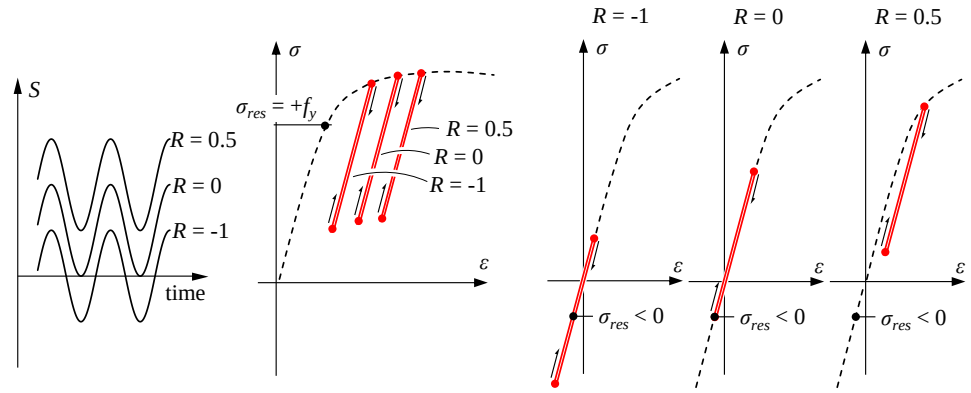

Figure 2.6: Cyclic behavior at different applied stress ratios: (a) constant amplitude loading, and cyclic behavior under (b) high ($\sigma_{res} = +f_y$) and (c) compressive residual stresses.

The negligibly small effect of applied stress ratio on the fatigue strength of welded joints is, however, valid for joints with high tensile residual stresses. In the case of low or compressive residual stresses, the applied stress ratio plays an important role because the local stress ratio is affected by the external loading (see Figure 2.6c). This has been clearly demonstrated by Baumgartner and Bruder (2013b) for S460 LG joints with high tensile residual stresses in the AW condition and, subsequently, stress-relieved with thermal methods: for joints in the AW condition, an almost identical fatigue strength was obtained under pulsating (R = 0) and fully reversed (R = -1) load conditions. In contrast, for the stress-relieved joints, a distinctly higher fatigue strength was experimentally obtained for joints tested under fully reversed conditions. Similarly, for joints with compressive residual stresses, the stress ratio effects are significant. For instance, a significant reduction of fatigue strength improvement has been demonstrated for the HFMI-treated joints with an increasing mean stress level (Mori et al., 2012; Wang et al., 2009; Yonezawa et al., 2019).

2.2.4 Notch effects

Welding without any PWT methods generally produces a severe transition from the base material to the filler material. The AW condition typically provides rather small radius, and a actual weld toe radius of r_{true} = 0 is assumable based on the worst-case condition. The sharp transition causes a notch stress, unevenly distributed stress distribution over the plate thickness and local increase in stress at the fatigue critical notch, see Chapter 2.1 for exemplifying illustrations. The infinite small radius at the weld toe basically causes an infinitely high stress peak which, however, tends to be neglected in fatigue assessments when applying notch stress methods. Instead, fatigue phenomenon occurs at a certain volume underneath the notch root and, as a result, fatigue assessments accounts for the notch stresses by applying fatigue-effective notch stress. Consequently, the term ‘notch effect’ rather refers to the fatigue behavior affected by the notch than the

geometrical notch and its notch stress, which can be infinite, at sharp transitions. Few methods for describing the fatigue-effective stress gradient underneath the notch have been developed, of which two have been most widely applied for the fatigue analysis of welded joints (Radaj et al., 2006):

- Stress averaging concept following Neuber's (1968) work
- Critical distance approach originally proposed by the early work of Peterson (1959), followed by later works in a larger scope by Taylor (2007)

The basic notion of Neuber's notch effect concept is to derive the fatigue-effective averaged notch stress in the vicinity of the notch root, as follows (see Figure 2.7a):

$$\sigma_{eff} = \frac{1}{\rho^*}\int_0^{\rho^*} \sigma(x)\mathrm{d}x\,, \tag{2.9}$$

where σ_{eff} is the effective stress, ρ^* is the micro-support length, and $\sigma(x)$ is the notch stress distribution. Due to the lack of computational resources at the time when the approach was developed, alternative methods were suggested. Consequently, Neuber's notch theory is more widely known by its applications for substituting the actual notch radius with a fictitious radius ρ_f to account for the fatigue-effective notch stress. Using the fictitious notch radius, the effective stress can be determined at the notch root ($x = 0$), and the fictitious notch radius can be determined as follows (see Figure 2.7b):

$$\rho_f = \rho + s\rho^*, \tag{2.10}$$

where ρ is the actual notch radius, and s is the stress multiaxiality factor. Although the fictitious radius concept was based on the low notch opening angle, it has been extended for seam-welded joints. Radaj (1990) suggested the use of a stress multiaxiality factor of $s = 2.5$ and micro-support length of $\rho^* = 0.4$ mm for welded steels joints made of mild steel, resulting in fictitious radius of $\rho_f = 1.0$ mm. Hereafter, in the fatigue strength assessments of welded joints, this approach has been referred to as the effective notch stress (ENS) concept, and a reference radius of $r_{ref} = 1.0$ mm with the fatigue class of FAT225 has been suggested for welded joints with the plate thicknesses $t \geq 5$ mm.

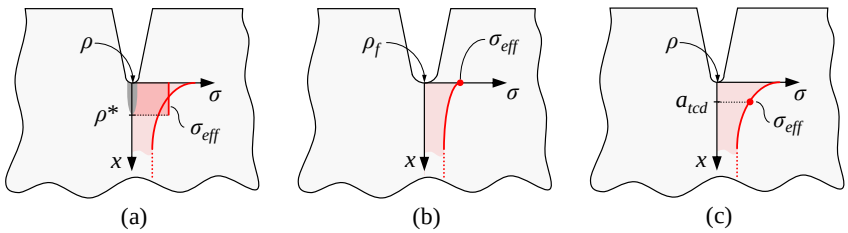

(a) (b) (c)

Figure 2.7: Effective stress concepts: (a) stress averaging over the micro-support length and (b) substituted fictitious notch radius, and (c) concept of critical distance.

Another means of considering notch effects is to apply critical distance approaches. In principle, there are two alternative theory of critical distances (TCD) methods, entitled line and point methods. Characteristically, the line method corresponds with Neuber's stress averaging concept (Figure 2.7a), but in the point method, the fatigue effective notch stress is derived at a certain distance from the notch, i.e. at a critical distance a_{tcd} (as shown Figure 2.7c). The effective stress can be formulated as follows:

$$\sigma_{eff} = \sigma(a_{tcd}) \tag{2.11}$$

Compared to the ENS concept, standardized concepts for the theory of critical distances (TCD) have not been established for the fatigue strength assessment of welded joints. Despite this, in recent years, the TCD has been increasingly applied to evaluate the fatigue strength of welded components. The main concern is related to the characterization of the value of critical distance. A statistical evaluation of critical distances – i.e. minimization of the scatter in fatigue test data – has served as one approach to evaluating an appropriate critical distance for fatigue analysis purposes. Baumgartner et al. (2015, 2019) evaluated the critical distances of a_{tcd} = 0.14 mm (thin- and thick-walled specimens) and a_{tcd} = 0.6 mm for welded steel joints in the AW and TIG-dressed conditions. The use of stress averaging and critical distance concepts have been justified by their capabilities for considering the stress gradients more comprehensively than fictitious radius concepts. To some extent, this is supported by the experimental findings, for instance, Karakaş et al. (2018) found a statistically lower scatter for the fatigue test data using stress averaging and critical distances concept compared to the fixed reference radii of r_{ref} = 1.0 mm and r_{ref} = 0.05 mm. In contrast to these findings, Möller et al. (2017) exemplified higher accuracy with the fictitious radius concept than with stress averaging concepts in butt welds. In addition, structural stress, determined at the 1 mm depth below a notch (Xiao & Yamada, 2004), can be regarded as a structural stress-level description of the TCD. Due to the lack of theoretical consistency, together with the volatile results regarding the scatter of test data, extensive and standardized applications of stress averaging and critical distances approaches have not been established, meaning that the ENS concept based on the fictitious radius has firmly become a standardized notch stress method. Although the notch effects are considered in the fatigue analysis covering notch geometry and, in some extent, the material behavior through the fatigue effective volume, they fall short of addressing the effect of residual stresses and applied stress ratio. Chapter 2.4 presents the concept of the 4R method, which is based on the ENS concept but also covers the mean stress correction affected by the residual stresses and applied stress ratio.

2.2.5 **Loading type**

Conventionally, cyclic bending loads are assumed to lead to a higher fatigue strength than axial loads, and the implementation of bending fatigue tests is more difficult than axial tests (Kang et al., 2002). Consequently, the stress-fatigue life (*S*-*N*) curves of design codes and guidelines are principally derived from the experimental fatigue data tested under axial load conditions (Maddox, 2015). The higher fatigue strength of joints subjected to

cyclic bending loads is supported by crack propagation-based predictions; bending load produces lower stress intensity factors (SIFs) and, thus, lower crack propagation rate than axial load (Bowness & Lee, 1996). If initial cracks and flaws are present, fatigue life is predominantly comprised of crack propagation (CP) period, which makes fracture mechanics-based predictions justifiable. However, in weldments with moderate or even high welding quality, it is not valid to assume the presence of initial flaws, and total fatigue life is comprised of both crack initiation (CI) and CP periods. In such an example, notch stresses might have a significant influence on fatigue strength. Many researchers have also recognized the discrepancies between notch SCFs under axial and bending loading in fillet weld joint configurations (Anthes et al., 1993; Brennan et al., 2000; Dabiri et al., 2017; Oswald et al., 2019).

Experimental bending effect studies have principally focused on crack propagation analyses and comparisons with design curves. Baik et al. (2009, 2011) found that bending fatigue tests complied with the design curves, and developed equations for SIFs in semi-elliptical cracks under bending loading. Xiao et al. (2012) concluded that lower bounds can be extracted using a linear elastic fracture mechanics (LEFM) approach. One-class higher fatigue strength was also suggested for bending-loaded joints when applying stress at the 1 mm depth below weld toe. Ottersböck et al. (2015) performed axial and bending fatigue tests on thin-walled (t = 5 mm) fillet-welded non-load-carrying T (NLCT) joints. Contrary to prior implications, they found lower fatigue strength for bending-loaded joints than axially-loaded.

Previous studies have not been comprehensively addressed the following aspects:

- Comparisons between the fatigue strengths of axially- and bending-loaded joints are conducted using nominally applied loads. Due to the thermal cycles of welding, angular distortions are generally present. In the case of axial loads, the angular distortion induces macro-geometric bending stresses while in the case of bending loads, the angular distortion does not superpose any additional stresses. Consequently, by neglecting the bending stresses in axially loaded joints, severe misinterpretation about the higher fatigue strength of bending loaded joints can be conducted. In addition, *S-N* curves for the nominal stress approach include a certain degree of angular distortion and, thus, should be conservative for joints tested under bending loading.
- Comparisons do not address the joint type. As described in Chapter 2.1, axial loading leads to a higher notch stress concentration than bending loading in symmetric structures (double-sided welded details), while bending loading produces a higher notch stress concentration than axial loading in asymmetric structures (single-sided welded details). Consequently, dissimilar results for bending effects can be derived for single- and double-sided welded details.

2.3 Design codes and guidelines for fatigue strength assessments

Starting from the latter half of the 20th century, great efforts have been made to investigate the fatigue behavior of welded joints. To guide engineering practice, research work has resulted in many fatigue design codes and guidelines. The generic design codes and guidelines in a pan-European context can be listed as:

- Eurocode 3 (EC3): Design of steel structure – Part 1-9: Fatigue (EN 1993-1-9, 2005);
- Guide to fatigue design and assessment of steel products (BS7608:2014 +A1:2015, 2015);
- Recommendations for Fatigue Design of Welded Joint and Components by International Institute of Welding (IIW) (Hobbacher, 2016);

followed by many steel application-specific standards and guidelines, such as:

- Recommended practice for offshore structures by Det Norske Veritas-Germanischer Lloyd (DNV-GL) (DNVGL-RP-C203, 2016);
- European standard for fatigue design of cranes (EN 13001-3-1, 2018);
- European standard for fatigue design of unfired pressure vessels (EN 13445-3, 2018).

Currently, the EC3 with its extension standard (EN 1993-1-12, 2007) and BS7608 cover HSS grades, with a yield strength of up to f_y = 700 MPa. DNV-GL (2016) and the IIW Recommendations (Hobbacher, 2016) enable the use of UHSS grades, with a yield strength of less than 960 MPa.

2.3.1 Basic principles and existing methods

The standards and guidelines listed above have some special features, e.g. regarding the survival probabilities and covered fatigue strength assessment approaches, although the basic principles are relatively similar. Most of them cover fatigue design using the stress- and fracture mechanics-based fatigue strength assessments based on characteristic (char) design parameters representative for a survival probability of P_s = 97.7%, i.e. mean minus two standard deviations (STDVs) (Radaj et al., 2006). The stress-based approaches comprise the nominal stress method as a global approach, the structural HS method, and the ENS concept with the reference radius of r_{ref} = 1.0 mm as local approaches. The basic equation of the stress-based approaches is:

$$\Delta\sigma_i^{\,m} N_f = \left(\frac{k_s \mathrm{FAT}_i}{\gamma_f} \right)^m 2 \cdot 10^6 = C_f \,, \tag{2.12}$$

where $\Delta\sigma_i$ is the stress range corresponding to the applied method (i = *nom*, *hs*, *ens*), N_f is the fatigue life, k_s is the thickness correction factor, γ_f is the partial safety factor for fatigue, FAT_i is the fatigue class corresponding to the fatigue strength at two million cycles – again referring to the applied method – and C_f is the fatigue capacity. Furthermore, the fatigue class can address other correction or improvement factors, e.g. due to the applied PWTs (see Chapter 2.3.3). Another, widely accepted method for assessing fatigue crack growth in welded joints is to apply linear elastic fracture mechanics (LEFM). SIF can be determined using analytical equations, weight functions or numerically with crack growth analyses. Crack propagation rate can be determined with, for example, a simple Paris' equation:

$$\frac{\mathrm{d}a}{\mathrm{d}N} = C\left(\Delta K\left(a\right)\right)^m, \tag{2.13}$$

of which the fatigue life can be derived as follows:

$$N_f = \int_{a_i}^{a_f} \frac{\mathrm{d}a}{C\Delta K(a)^m}, \tag{2.14}$$

where a is the crack depth, a_i is the initial crack depth, a_f is the final crack depth, C is the crack propagation coefficient, $\Delta K(a)$ is the stress intensity factor range as a function of the crack depth, and m is the slope parameter of Paris' law. One critical step in the LEFM analyses is the determination of the initial crack size (Hobbacher, 2011). In the case of a fatigue crack propagating from the weld root, the infusible weld root acts as an initial crack, and the crack propagation analysis can be carried out accordingly. Respectively, when assessing the crack propagation starting from the weld toe, the size of the potential initial crack must be critically evaluated. An initial crack depth of a_i = 0.15 mm can be assumed if no further information is available.

2.3.2 Weld root fatigue strength assessment

This content of this chapter differs from previously described topics, as the previous chapters mainly focus on the fatigue failures starting from weld toes. Depending on the load and joint configuration, weld root can be a fatigue-critical location of the joint. Typically, this refers to the joints prepared with fillet welds and lack of full penetration, and subjected to cyclic loads at the adjoined plate component, i.e. load-carrying (LC) fillet weld joints. Weld root fatigue strength capacity cannot be improved with PWTs and, consequently, usually limits the fatigue performance of fillet weld joints. Again, welded UHSS grades do not provide any benefit for weld root fatigue capacity compared to mild steels and, consequently, should also be considered as an important design criterion in the case of fillet-welded UHSS joints.

Fatigue cracks can propagate insidiously from the weld root and cannot usually be monitored until the fatigue crack has propagated through the weld reinforcement or plate

components. The fatigue design against weld root failures in fillet-welded joints is mainly based on the weld sizing and/or proper groove preparation to decrease the infusible weld root acting as an initial crack. The existing stress-based concepts for the fatigue strength assessment of weld root failures are covered by the nominal stress and ENS concepts. Two alternative design proposals for assessing weld root fatigue strength using a structural HS approach have also been given by Fricke et al. (2006) for the weld leg section and Sørensen et al. (2006) for the weld throat section, but the proposed approaches have yet become official guidelines.

The nominal stress approach is the most elementary method for assessing the weld root fatigue strength; nominal weld stress (NWS) range is calculated based on the weld throat thickness a_w, or effective weld throat thickness $a_{w,eff}$ considering the weld penetration if it can be verified. In the case of axial membrane stress, the weld stress range $\Delta\sigma_{w,m}$ can be formulated simply:

$$\Delta\sigma_{w,m} = \frac{t}{2a_{w,eff}}\Delta\sigma_{nom,m} \tag{2.15}$$

In this case, a characteristic design curve of FAT36 is suggested by the design codes. Under bending loads, similar concepts for assessing weld root fatigue strength in double-sided fillet weld joints using the nominal stress approach have not been addressed in either the design codes and guidelines, or in prior investigations. Upon the date of this thesis being published (November 2020), the fatigue strength assessment procedure for bending-loaded double-sided fillet welds using the nominal stress approach is under discussion and development in the working group of the European Committee for Standardization, and the design guidelines are supposedly available in an upcoming version of the EN 1993-1-9 standard. It is noticeable that an increase in DOB predisposes the LC joints to weld toe failures (Jakubczak & Glinka, 1986) but understanding weld root fatigue behavior and analysis concepts under bending loads is still important. For partially and fully penetrated single-sided T joints subjected to bending loading, Sundermeyer et al. (2015) suggest that the linear elastic bending stress at the weld is derived at the throat section, with the results showing accordance with the FAT36 design curve. Using a similar concept, the NWS range under bending loading can be formulated, while the following NWS range is suggested for the fatigue analysis (P-III):

$$\Delta\sigma_{w,b} = \frac{\Delta M\,\frac{w}{2}}{I} = \frac{\Delta\sigma_{nom,b}\,\frac{t^2}{6}\,\frac{w}{2}}{\frac{\left(w+2a_{w,eff}\right)^3 - w^3}{12}} = \frac{\Delta\sigma_{nom,b}t^2 w}{6a_{w,eff}w^2 + 12wa_{w,eff}{}^2 + 8a_{w,eff}{}^3} \tag{2.16}$$

where ΔM is the bending moment range, I is the second moment of area, and w is the infusible weld root length. Figure 2.8 shows the NWSs for axial loading and the proposed model for bending loading.

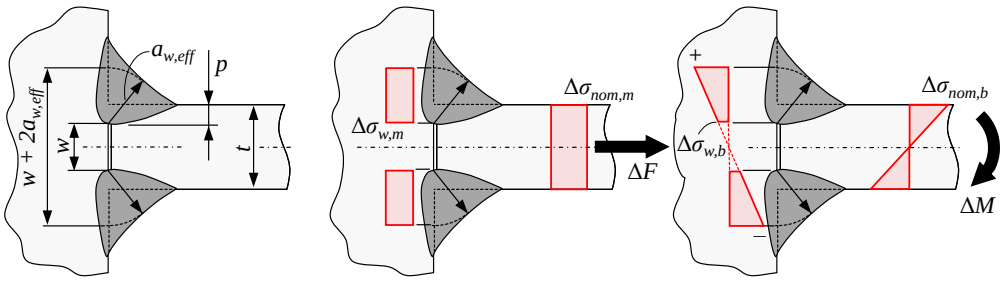

(a) (b) (c)

Figure 2.8: (a) dimensions of a double-sided fillet-welded LC-joint, and NWSs in the case of (b) axial and (c) bending loading. p is the weld penetration depth and ΔF is the axial force range.

2.3.3 Consideration of influencing factors

Chapter 2.2 addressed factors influencing the fatigue strength of welded joints. This chapter briefly describes the existing guidelines for addressing these effects in fatigue strength assessments. Principally, the presented concepts follow the recommendations provided by IIW, because these offer the latest and most novel methods for considering the influencing factors, and can be regarded as state of the art in the field. As described in Chapter 2.2, many of the influencing factors have a combined effect and, thus, one factor is considered in conjunction with another.

Residual stresses, material strength and applied stress ratio

According to the IIW Recommendations (Hobbacher, 2016), for moderate and low residual stresses, the applied stress ratio can be taken into account with the enhancement factor f to account for improved fatigue strength. In general, high tensile residual stresses are assumed as resulting in f = 1 (no enhancement). However, for stress-relieved weldments with low residual stresses, for enhancement factors of up to f = 1.6, and for thin-walled structural elements with short welds and moderate residual stresses, as key examples, a factor of f = 1.3 can be derived for fully reversed load conditions (as shown in Figure 2.9a).

The fatigue strength improvements gained by the PWT methods are also addressed with the design guidelines (Haagensen & Maddox, 2013). When improving the weld toe geometry using grinding techniques or TIG dressing, fatigue class can be increased with a factor of 1.3, resulting in a two-fatigue class improvement. For the peening methods, an improvement factor of up to 1.5 is allowable, corresponding to a three-fatigue class improvement, depending on material strength and applied stress ratio. These improvement factors are usually applicable when applying the nominal and structural HS stress approaches in the fatigue strength assessments. Geometrical improvement in terms of a higher weld toe radius cannot be considered in fatigue assessments. A later guideline for the HFMI treatment by IIW (Marquis & Barsoum, 2016), extends the use of the ENS concept with r_{ref} = 1.0 mm for the HFMI-treated welded joints. In addition, the material

strength is addressed by providing higher fatigue class for steels with higher yield strength. Figure 2.9b describes the step-model for the HFMI-treated joints as a function of material strength for low stress ratios. For higher stress ratios, the improvement level diminishes.

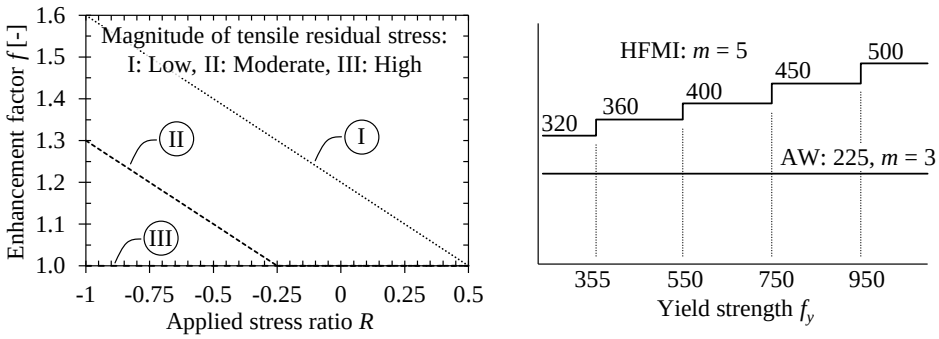

(a) (b)

Figure 2.9: (a) Fatigue enhancement factor for joints with low, moderate, and high residual stress as a function of applied stress ratio (Hobbacher, 2016) and (b) fatigue class of HFMI-treated joints according to the ENS concept at low stress ratios (Marquis & Barsoum, 2016).

Bending effects

Conventionally, the basis of the nominal and structural HS stress approaches has been to neglect the stress gradient effects of primary (nominal) and secondary (structural) stresses in the fatigue strength assessment. In other words, the fatigue strength assessment is carried out using the maximum nominal or structural stress acting at the plate surface or edge. This observation covers the EC3 standard (EN 1993-1-9, 2005) and IIW Recommendations (Hobbacher, 2016), although diverging expressions have also been given. For the structural stress approach, DNV-GL provides an effective HS stress range $\Delta\sigma_{hs,eff}$ in which a 40% reduction for bending stress has been allowed:

$$\Delta\sigma_{hs,eff} = \Delta\sigma_m + 0.6\Delta\sigma_b \tag{2.17}$$

Originally, the reduction is based on the findings of Kang et al. (2002). As guided by DNV-GL, the reduction is limited for special structural details and is not applicable to a general stress design. The reduction can be justified if a re-distribution of loads occurs together with a decrease in crack propagation rate, as the crack propagates at highly-stressed areas under displacement-controlled behavior, exemplified with a hopper corner joint of beams (Lotsberg & Sigurdsson, 2006). Consequently, the assumption is made on the major role of crack propagation time in total fatigue life and fatigue design *S-N* curve. Another bending bonus factor included in the design standards is provided in the revision of the BS7608 (2015) standard, which is based on the research work undertaken by

Maddox (2015). Based on the experimental findings, and supported by the crack propagation analyses, the following empirical equation has been formulated:

$$k_b = \left[1 + \left(\frac{0.7}{t^{0.2}} + 0.5 \log \frac{L_j}{t}\right) \mathrm{DOB}^{1.4}\right]^{x_g}, \tag{2.18}$$

where k_b is the bending bonus factor, L_j is the joint width, and x_g is the stress gradient exponent (x_g = 1 for decreasing, and x_g = -1 for increasing stress gradients). Assuming joint width to plate thickness ratio of L_j/t = 2, a bonus factor of up to k_b = 1.65 can be derived for thin-walled joints, as illustrated in Figure 2.10.

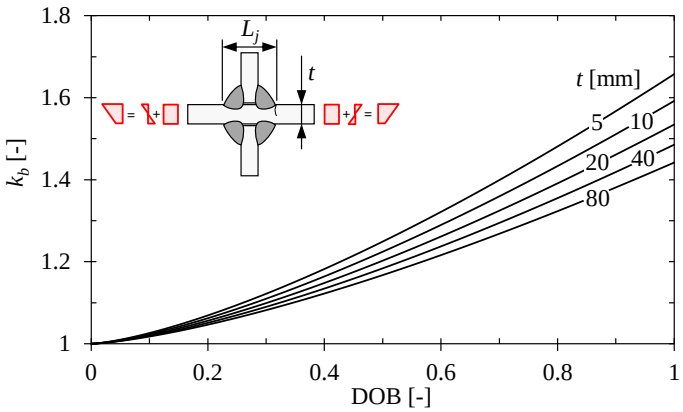

Figure 2.10: Bending bonus factor for decreasing stress gradients (x_g = 1) for a joint with various plate thicknesses (L_j/t = 2.0).

2.4 4R method

Chapter 2.2 presented the main factors that decisively influence the fatigue behavior of metallic materials, specifically focusing on welded joints. As discussed, many of the influencing factors are related to other factors, and it cannot be stated unambiguously how an individual parameter affects the fatigue strength without other parameters being known. Chapter 2.3.3 briefly addressed the state-of-art methods for considering these factors in the fatigue strength assessments according to design guidelines. Conventionally, different influencing factors are considered individually or in association with a second factor, such as the fatigue strength improvement gained by the HFMI treatment as a function of applied stress ratio or material strength or enhancement factor for low stress ratios under low or moderate residual stresses. Although such approaches may result in reasonable accuracy in fatigue strength predictions, they hinder a comprehensive understanding of the fatigue behavior of welded components and, for instance, show ambiguity when evaluating ‘moderate’ and ‘low’ residual stresses.

Nykänen and Björk (2015) extracted the fatigue test data of butt-welded details and evaluated the mean stress effect introduced by applied stress ratio and post-weld treatment. Subsequently, Nykänen and Björk (2016) conceptualized the applied method by implementing the Smith-Watson-Topper (SWT) mean stress correction (Smith et al., 1970) in a novel way: the SWT correction is conducted for the applied stress ratio considering the local stress ratio R_{local} as acting at the notch root. The notch stress approach was initially entitled as the '3R method' after the '*R*' parameters considered in the analysis, i.e. applied stress ratio *R*, residual stress σ_{res}, and material ultimate tensile strength R_m. At that time, the reference radius of r_{ref} = 1.0 mm was used for both joints in the AW and HFMI-treated conditions following the existing design guidelines for the ENS concept. Within this thesis, and in related research works, it has been noticed that a single reference radius does not characterize the improved weld toe transition. This means that the TIG-dressing and grinding PWT methods, as key examples, necessitate methodology modifications. Consequently, the approach was further developed to consider the actual weld toe radius r_{true}, so the method was renamed as the 4R method according to additional 'r_{true}' parameter included in the model. This chapter presents the concept of the 4R method.

The basis of the 4R method is to utilize the notch stress range $\Delta\sigma_k$ using a radius of $r = r_{true}$ + 1 mm, according to Neuber's fictitious notch radius concept. The actual weld toe radius can be chosen based on the geometry measurements, or, if the geometry measurements are not conducted or available, it can be characterized based on conservative assumptions, e.g. r_{true} = 0 for joints in the AW condition. In the notch stress analysis, it is essential to consider the joint symmetry and load components following the concepts presented in Chapter 2.1. The linear elastic ENS range is converted to cyclic elastic-plastic behavior at the notch root. Amongst various material models, the Ramberg–Osgood (R-O) true stress-true strain material model is well-known and widely applied for metallic materials (Dowling, 2006):

$$\varepsilon = \varepsilon_e + \varepsilon_p = \frac{\sigma}{E} + \left(\frac{\sigma}{H}\right)^{\frac{1}{n}} \tag{2.19}$$

In Equation (2.19), ε, ε_e and ε_p are the true, the elastic and plastic strain, respectively, σ is the true stress, *E* is Young's modulus, and *H* is the strength coefficient and *n* is the strain hardening exponent, respectively. When the kinematic hardening rule is assumed, the cyclic material behavior can be described using the cyclic R-O equation, as follows:

$$\Delta\varepsilon = \Delta\varepsilon_e + \Delta\varepsilon_p = \frac{\Delta\sigma}{E} + 2\left(\frac{\Delta\sigma}{2H'}\right)^{\frac{1}{n'}} \tag{2.20}$$

In Equation (2.20), the symbols are similar to those presented in Equation (2.19) but Δ describes corresponding range values, and H' and n' represent the cyclic strength coefficient and strain hardening exponent, respectively. If the cyclic parameters are not

known exactly, $H' = H$ and $n' = n$ can be assumed. Moreover, at the intermediate life, i.e. fatigue life of more than 50 000 cycles and particularly with UHSS grades, reversed plasticity does not occur. Consequently, cyclic behavior can solely be described with the elastic range and the cyclic plastic strain coefficients do not play a major role. The cyclic behavior for different residual stress states, as well as external stress amplitudes and mean stresses can be simulated with the welding simulation followed by the mechanical analysis using a materially non-linear analysis, but usually requires a high amount of computational efforts due to element mesh requirements for notch stresses, particularly in the case of large components. A simplified method for converting from the linear stress range to elastic-plastic behavior is to employ Neuber's notch theory, in association with the local residual stress $\sigma_{k,res}$ occurring at the weld. The rule can be formulated for monotonic and cyclic loads as follows:

$$\varepsilon = \frac{\left(\sigma_k + \sigma_{k,res}\right)^2}{\sigma E} \tag{2.21}$$

$$\Delta\varepsilon = \frac{\Delta\sigma_k^{\,2}}{\Delta\sigma E} \tag{2.22}$$

Local residual stresses can either be in compression or in tension depending on the location of the welded joint in the applications and potentially conducted PWTs. Furthermore, single tension or compression overloads might also significantly change the magnitude of compressive residual stresses (Leitner et al., 2017; Schubnell et al., 2020), while they can also be taken into account as modifying the residual stress in Equation (2.21). By setting equal Equations (2.19) and (2.21), and Equations (2.20) and (2.22), the maximum stress $\sigma_{\max}$, stress range $\Delta\sigma$ and, subsequently, the minimum stress $\sigma_{\min}$ can be determined based on the ENS range and applied stress ratio:

$$\frac{\sigma_{\max}}{E} + \left(\frac{\sigma_{\max}}{H}\right)^{\frac{1}{n}} - \frac{\left(\frac{\Delta\sigma_k}{1-R} + \sigma_{k,res}\right)^2}{\sigma_{\max} E} = 0 \tag{2.23}$$

$$\frac{\Delta\sigma}{E} + 2\left(\frac{\Delta\sigma}{2H'}\right)^{\frac{1}{n'}} - \frac{\Delta\sigma_k^{\,2}}{\Delta\sigma E} = 0 \tag{2.24}$$

$$\sigma_{\min} = \sigma_{\max} - \Delta\sigma \tag{2.25}$$

To take into account pre-stresses and self-weights, the applied stress ratio R can be replaced with an effective applied stress ratio R_{eff} in Equation (2.23). For instance, in the fatigue testing of small-scale specimens, the effect of clamping-induced stresses and geometrical non-linearities can be considered. Equations (2.23) and (2.24) do not have closed-form but do have single-valued solutions, and the maximum stress and stress range

can be determined with numerical approximations, e.g. using the Newton–Raphson method or commercial numerical solvers with various approaches. From the local cyclic behavior, the local stress ratio R_{local} is determined based on the maximum and minimum stresses as follows:

$$R_{local} = \frac{\sigma_{\min}}{\sigma_{\max}} \tag{2.26}$$

Subsequently, the local stress ratio is implemented in the SWT correction, conventionally presented in the form $\sigma_{\max}\varepsilon_a$ = constant, where ε_a is the local strain amplitude. By reformulating the SWT equation, a mean stress-corrected reference notch stress range $\Delta\sigma_{k,ref}$ is formulated as follows:

$$\Delta\sigma_{k,ref} = \frac{\Delta\sigma_k}{\sqrt{1-R_{local}}} \tag{2.27}$$

Figure 2.11 exemplifies the above-described concepts, and graphically presents the equations needed for analyzing the local stress ratio. The fatigue analysis can be summarized with the following steps (see sub-Figures 2.11a–d for a comparison):

a) Joint conditions (AW or post-weld-treated) characterize the weld toe radius and residual stress state. The fatigue-effective notch SCFs are obtained using fictitious radius of $r = r_{true}$ + 1 mm, i.e. $K_t(r_{true}$ + 1 mm), though separately for membrane and bending stress components.
b) Linear elastic notch stress history (σ_k) and corresponding notch stress range ($\Delta\sigma_k$) acting at the notch root are obtained using the externally applied nominal stresses ($\sigma_{nom,m}$ and $\sigma_{nom,b}$) and notch SCFs. For simplicity, the membrane and bending stress are presented to act proportionally but they can also be nonproportional. If structural SCFs are present in the joint, i.e. $\sigma_m \neq \sigma_{nom,m}$ and $\sigma_b \neq \sigma_{b,nom}$, the stress components should be calculated using Equations (2.6) and (2.7). The notch SCFs are determined considering r_{true} in accordance with the applied PWT method.
c) After welding, the magnitude of tensile residual stresses depends on the boundary conditions of plate components during the welding, together with welding sequence. High tensile residual stresses of up to $\sigma_{res} = +f_y$ can be assumed if the welding deformations and weld contractions are prevented. In the case of high tensile residual stresses, grinding or TIG dressing may decrease the magnitude of tensile residual stresses. Compressive residual stresses can be induced with HFMI treatment. During the cyclic loading, over- or underloads may change both tensile and compressive residual stresses. The residual stress value is moved to stress-strain curve (Figure 2.11d) as a starting point of cyclic behavior, see also Equation (2.23).

d) The cyclic behavior is approximated via an analytical approach using the applied notch stress history and residual stresses. As a result, the local maximum and minimum of cyclic stress at the notch root is received, and, based on those values, the local stress ratio of R_{local} is determined.

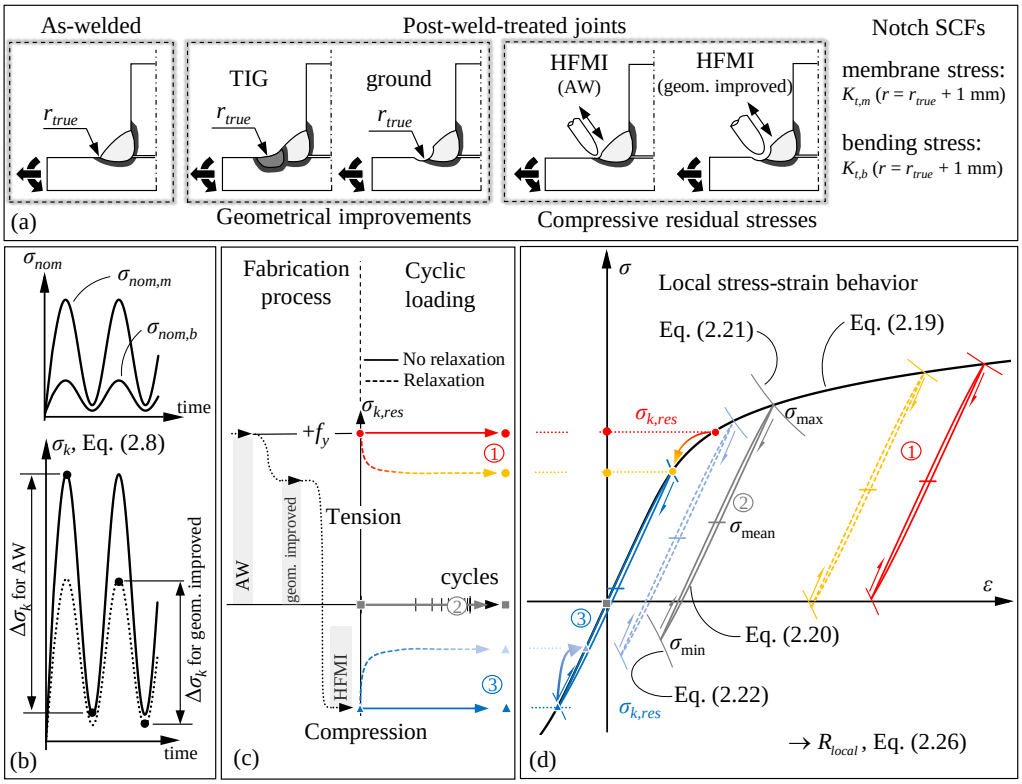

Figure 2.11: Schematic description of the determination of local stress ratio: (a) joint characteristics, (b) cyclic ENS, (c) residual stresses after fabrication processes and cyclic loading, (d) material behavior at the notch root.

3 Materials and Methods

Experimental studies, numerical analyses and literature studies are applied as research methods to investigate the topics covered in this thesis. Chapter 3.1 describes the experimental framework, i.e. fatigue tests and relevant measurements, conducted for UHSS weldments, and Chapter 3.2 presents the numerical FE models, principally applied for determining SCFs and SIFs for the notch stress and crack propagation analyses, respectively. Chapter 3.3 briefly describes the literature review on the existing fatigue test data, applied for supplementing the experimental work of this study. This chapter aims to present an overview of research methods, while more detailed descriptions of the materials and methods, specific to a certain topic covered by this thesis, can be found in the included publications.

3.1 Experiments

3.1.1 Materials

S960MC and S1100QL structural UHSS grades were applied in this study as base materials. Both grades are manufactured using controlled direct-quenching (DQ) after thermomechanical rolling although the S960MC grade applied in this study does not undergo any tempering phase and can be regarded as a QC-type (quenched and cold-formable) of UHSS grade, meeting the criteria of the EN 10149-2 (2013) standard. In the studied S1100QL UHSS grade, DQ is followed by a tempering phase, that is a QL-type (quenched and tempered) of UHSS grade (Kömi et al., 2016). S1100QL does not currently have an official European standard definition.

In both base materials, Böhler Union X96 (G 89 5 M21 Mn4Ni2,5CrMo) solid wire with a diameter of 1 mm was used as filler material. X96 is nominally strength-undermatching filler material but prior studies have shown that it has higher ultimate tensile strength than the studied base materials in both butt joint and fillet-welded joint configurations (Amraei et al., 2019; Björk et al., 2018). Table 3.1 and Table 3.2 present the mechanical properties and chemical compositions of the studied base and filler materials, respectively. For the test specimens, the sheet metals were taken from multiple batches, and the 'typical' values presented in Table 3.1 represent average (avg) values calculated based on the material certificates supplied by the manufacturer.

Table 3.1: Mechanical properties of the studied materials.

ID	type	Proof strength $R_{p0.2}$ [MPa]	Ultimate tensile strength R_m[MPa]	Elongation A [%]	Impact strength KV [J] (temp.)
S960MC	nominal	960	980-1250	7	27 (-40 °C)
	typical	1040	1160	11	65 (-40 °C)
S1100QL	nominal	1100	1130-1350	10	27 (-40 °C)
	typical	1150	1190	14	n/a
X96	nominal	930	980	14	47 (-50 °C)

Table 3.2: Chemical compositions ([wt-%], maximum values) of the studied materials, showing the most important alloying components.

ID	type	C	Si	Mn	P	S	Al[a]
S960MC	nominal	0.12	0.25	1.30	0.020	0.010	0.015
S1100QL	nominal	0.20	0.50	1.80	0.020	0.005	0.015
		C	Si	Mn	Cr	Ni	Mo
X96[b]	nominal	0.12	0.8	1.9	0.45	2.35	0.55

[a]minimum value
[b]undiluted filler material

3.1.2 **Test specimens**

Small-scale laboratory test specimens were manufactured to experimentally obtain the fatigue strength of welded joints made of UHSS grades. Two types of fillet-welded transverse NLC attachment joints were manufactured: single-sided non-load-carrying transverse (NLCT) joints and double-sided transverse attachments joints, i.e. non-load-carrying cruciform (NLCX) joints (as shown in Figure 3.1 and Figure 3.4). In addition, the effect of plate misalignment on the fatigue strength of NLCX joints was examined, introducing a different degree of plate misalignment e in NLCX joints (see Figure 3.4d). The weld root fatigue strength of double-sided fillet welds was examined using the load-carrying cruciform (LCX) joints presented in Figure 3.2. Table 3.3 summarizes the details of fatigue test specimens and the related publications examined in this thesis.

Table 3.3: Summary of fatigue test specimens. n_{ts} is the number of specimens.

Base material	Joint type	Figure	Load type[a]	n_{ts} [-]	Joint condition	t [mm]	R [-]	Publication
S960MC	NLCT	3.1a	A	2	AW	8	0.1	P-I
		3.1a	4B	4	AW	8	0.1	
	NLCX	3.1b	A	2	AW	8	0.1	
		3.1b	4B	4	AW	8	0.1	
	LCX	3.2a	A	4	AW, HFMI	9	0.1	P-III
		3.2b	4B	16	AW, HFMI	9	0.1	
S1100QL	NLCT	3.4a	A	14	AW, TIG, HFMI	8	0.1, 0.5	P-IV
		3.4b	4B	10	AW	8	0.1, 0.5	n/a[b]
	NLCX	3.4c	A	12	AW, HFMI	8	0.1, 0.5	P-II, P-IV
	NLCX[c]	3.4d	A	8	AW	8	0.1	P-II

[a]A = axial loading, 4B = four-point bending loading
[b]New, unpublished test results
[c]Joints with a plate misalignment e (see Figure 3.3 and Figure 3.4d), e = 6 mm, e = 9 mm and e = 16 mm

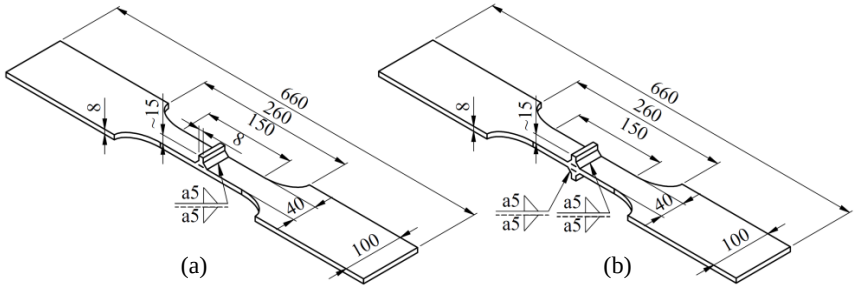

Figure 3.1: Shape and dimensions (in mm) of S960 NLC transverse attachment specimens tested under axial and bending loads: (a) NLCT joints and (b) NLCX joints.

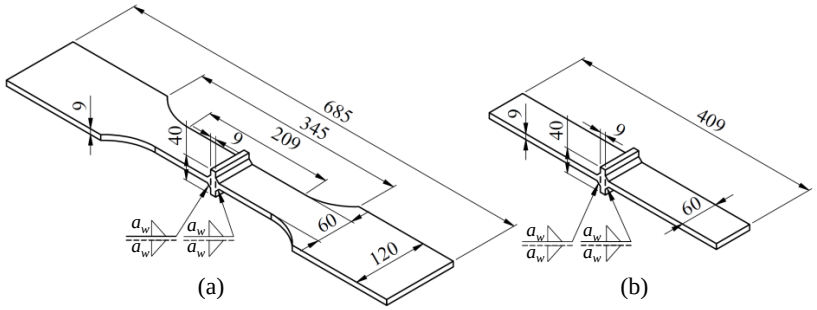

Figure 3.2: Shape and dimensions (in mm) of S960 LCX specimens with double-sided fillet welds. Joints subjected to (a) axial loads and (b) bending loads. Weld throat thickness was varied between a_w = 3–5 mm.

Distinguishing fatigue strength was found for the NLCT and NLCX joints under axial loading (see Chapter 4.2) and, consequently, a set of NLCX specimens were manufactured, in which the transverse attachments are not aligned. The effect of plate misalignment e on the fatigue strength was experimentally observed. Three different degrees of misalignment were chosen for the study, based on a preliminary FE study on SCFs in a misaligned NLCX joint (t = 8 mm, a_w =5 mm) in terms of structural and effective notch stresses – as presented in Figure 3.3.

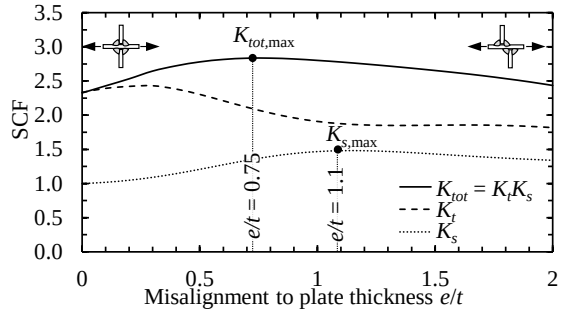

Figure 3.3: Results of a preliminary FE study conducted on the effect of plate misalignment, see also Figure 3.4d.

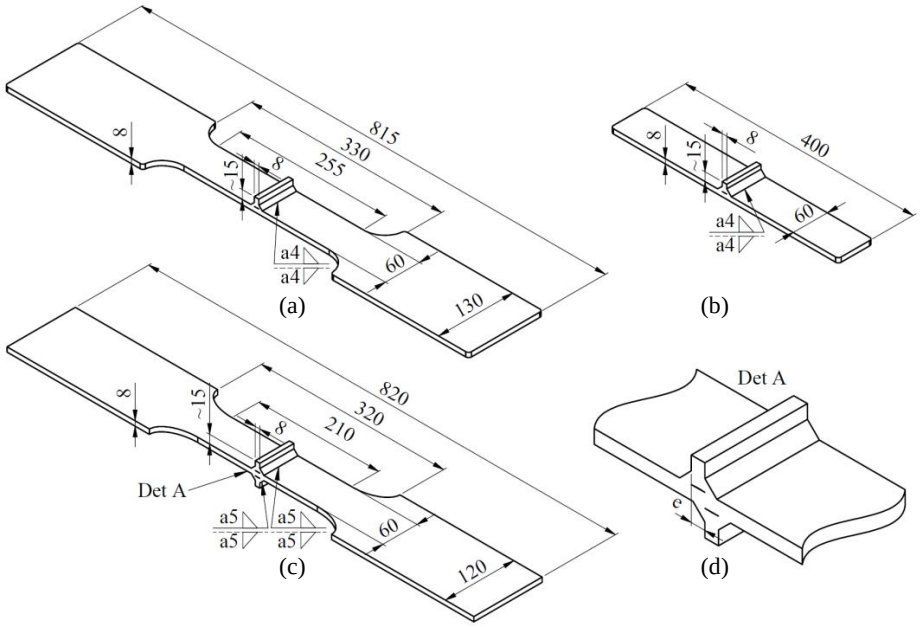

Figure 3.4: Shape and dimensions (in mm) of S1100QL specimens. NLCT joints subjected to (a) axial loads and (b) bending loads, (c) NLCX joints and (d) a detailed view of NLCX joints with plate misalignment.

The plate components were laser cut from larger sheet metals and, subsequently, cleaned with 5–10% citric acid to remove any impurities from the plate surfaces (mill scales, rust, and grease). The weldments were prepared using a single-pass robotic GMAW and the shielding gas was an argon-carbon dioxide (Ar-CO_2) mixed gas, i.e. Ar+8%CO_2 or Ar+10%CO_2. In all specimens, the welding position was horizontal-vertical (PB, the loaded plate orientated horizontally) producing rather sharp transition from the loaded base plate to the weld reinforcement. The welding sequence is presented in Figure 3.5 and the weld run-on and run-off widenings were machined and ground to flush before fatigue testing. No welding deformations were prevented during welding.

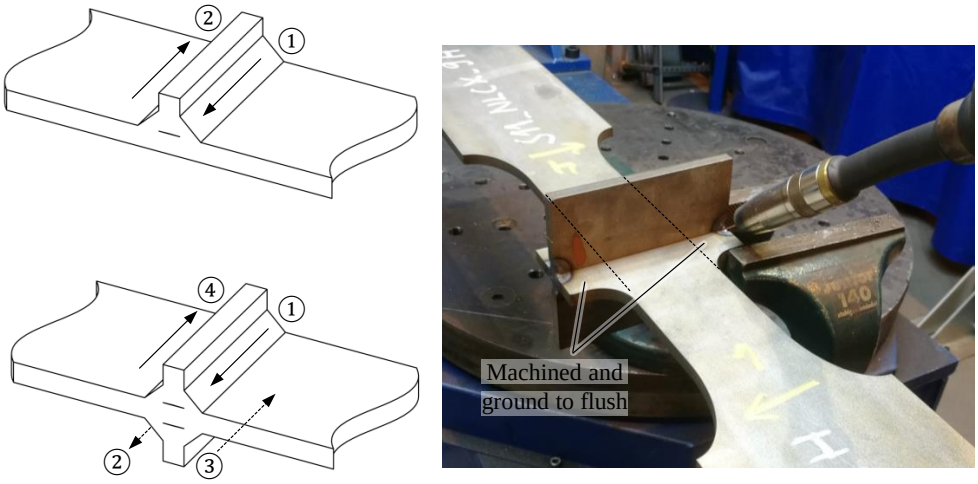

(a) (b)

Figure 3.5: (a) Welding sequence and directions of T and cruciform joints, and (b) welding preparation of test specimens.

3.1.3 Geometry and residual stress measurements

Before fatigue testing, geometry measurements were carried out to obtain the angular distortions, weld profiles, flank angles, and weld toe radii in the test specimens. The geometry measurements were principally carried out using a two-dimensional (2D) coordinate measuring device with an inductive displacement transducer and a laser transducer to measure the longitudinal coordinates and specimen shape, respectively (see Figure 3.6a). These measurements were conducted at the centerline of the specimens in the longitudinal (loading) direction of the test specimens. In chronologically later studies, 3D laser scanners were used for determining weld geometries: Hexagon Romer Absolute Arm for measuring *x*-*y*-*z* point clouds.

In the selected specimens, the transverse welding residual stresses, parallel to the loading direction, were measured with the X-Ray diffraction (XRD) technique using the Stresstech X3000 G3 device with the 1 mm spot size of the collimator (see Figure 3.6b). A common approach within the test series was to measure the longitudinal residual stress distribution with a 1–2 mm step size in one specimen representative for a test series (joint type and condition), while, in the other test series specimens, residual stresses were measured at the weld toes.

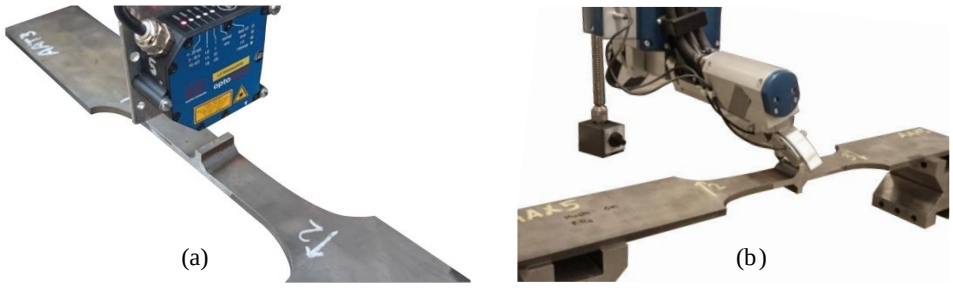

(a) (b)

Figure 3.6: (a) geometry measurement using a 2D coordinate measuring device, and (b) XRD residual stress measurement device.

3.1.4 Instrumentation and fatigue test setup

The studied joints types were transversely welded LCX, NLCT, and NLCX joints. Consequently, the structural stresses are equal to nominally applied stresses, and potentially superposed with macro geometric bending stresses, resulting from the angular distortion and axial loading. Each specimen was instrumented with, at least, one strain gage at the distance of 0.4*t* from the weld toe to measure the strain variation during the cyclic loading. The grid sizes of the applied strain gages were 0.6 mm and 1.5 mm, in accordance with the IIW Recommendations (Hobbacher, 2016) – i.e. less than 0.2*t*. Furthermore, the strain gages also were utilized to account for the magnitude of clamping stresses, i.e. the strain gages were engaged before attaching specimens to the fatigue test rigs, and the clamping-induced strains were recorded.

Carried out using servo-hydraulic fatigue testing machines with a constant amplitude loading, the fatigue tests were performed using load-controlled cyclic loading, with the total rupture of the specimens taken as the failure criterion of the test specimens. In the axial tests, fatigue test machines with maximum axial force capacities of 400 kN, 750 kN, and 1200 kN were applied. In the bending tests, load rigs with a lower force capacity, i.e. maximum force capacities of 100 kN and 150 kN, were used. The fatigue tests were also carried out with a four point-bending test setup, producing a constant moment and zero shear stress area between the inner press rolls. Figure 3.7 exemplifies the fatigue test setups for the axial and bending tests.

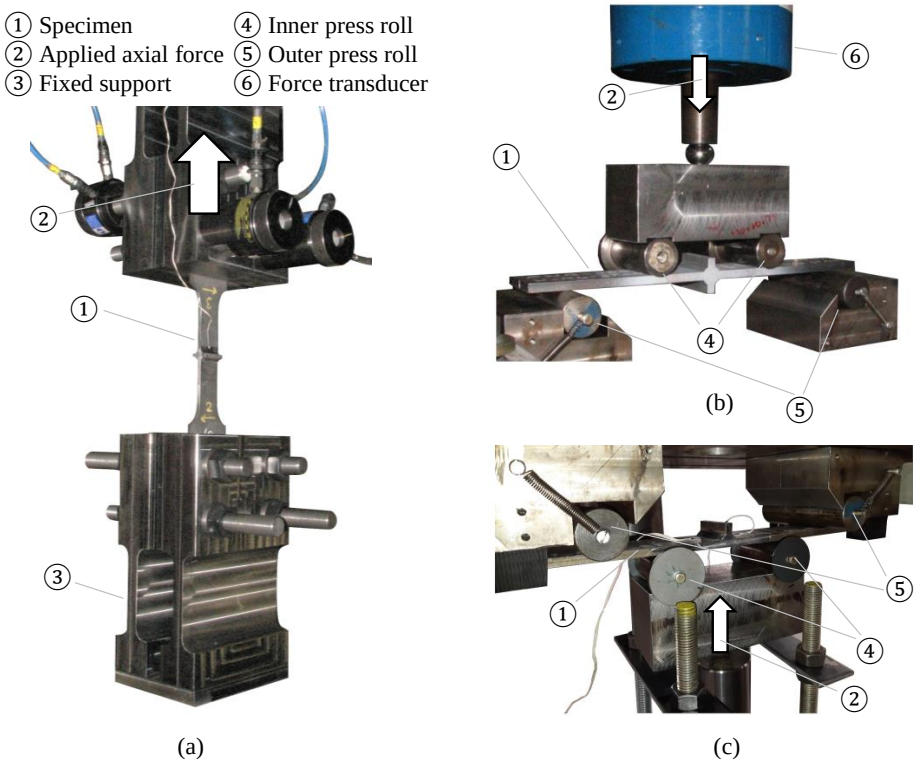

Figure 3.7: Fatigue test setups used in the (a) axial tests, and bending tests of (b) LCX joints and (c) NLCT joints.

3.2 Numerical finite element analyses

The FE analyses had two principal objectives. Firstly, structural and notch SCFs applied for analyzing the experimental fatigue test results in terms of structural HS stress, and notch stress-based approaches, such as the ENS concept and 4R method. Secondly, the FE models were employed to compare the computational fatigue strength with experimental results. Computational fatigue lives were also obtained using LEFM, and crack growth models were employed in these analyses to obtain SIFs.

The FE analyses were also utilized to evaluate the effect of geometrical parameters on the SCFs and SIFs and, subsequently, on the fatigue strength of welded joints. Such parametric FE studies were carried out to obtain the effect of misalignment degree on the SCFs of NLCX joints (see Figure 3.3 and Figure 3.4d), and to obtain the effect of weld penetration on the weld root fatigue strength of LC joints (see P-III).

3.2.1 Structural and notch stress analysis

The FE models were prepared according to the joint type. In the case of transverse weldments, continuous uniform stress along the weld can be assumed when cyclic loading is perpendicular to the weld and weld shape and dimensions do not vary along the weld. Therefore, 2D plane strain element models were employed in these cases. In P-V, ground fillet welds with various joint types (NLCT, NLCX, LCX and LG joints) were examined, with the weld toe radii equal up to 10 mm being found, which hinders the plane strain condition at the weld toe due to the low stress concentration. In the study of ground joints, 3D hexahedral element models were applied. In addition, 3D element models were used when investigating the stress components in the LG joints (see Figure 2.1. in Chapter 2.1). Symmetry constraints were applied where applicable, and linear material model, with E = 210 GPa and Poisson's ratio of ν = 0.3, was used.

The geometries of the FE models were prepared according to the measured geometries and polished sections, from which the weld penetration was obtained. However, the angular distortions were not modeled. Instead, the FE models were analyzed using 1 MPa membrane and bending stress seed loads, with the resulting stress values, therefore, corresponding directly to SCFs. Notch stresses superposed from the membrane and bending stresses were calculated on the basis of notch SCFs in accordance with Equations (2.6)–(2.8).

Three different evaluation methods were used for determining the structural HS stresses, and the FE models were prepared in accordance with the applied method (Niemi et al., 2018):

- Linear surface extrapolation (LSE)
- Through thickness at the weld toe (TTWT) method
- Structural stress at the 1 mm depth

The notch stress analyses were carried out using the fictitious radius at the weld toe after the ENS concept with r_{ref} = 1.0 mm, and the 4R method with $r = r_{true} + 1$ mm. To accurately determine the notch stresses, the element side length of $r/20$ was used as a basis of the mesh size, corresponding to 125 elements over a 360° arc, as per the mesh convergence study for notch stresses by Baumgartner and Bruder (2013a). The notch stresses were determined at the notch root using maximum principal stress criterion. Figure 3.8 presents the typical meshes applied in the FE analyses.

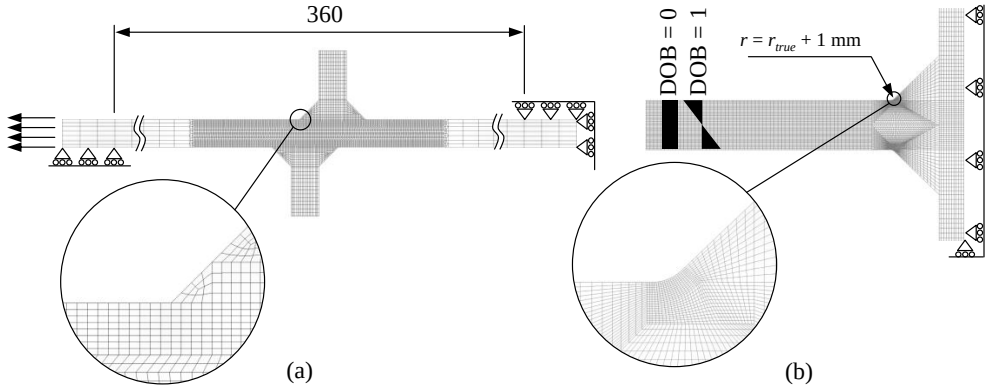

Figure 3.8: 2D FE models used to obtain (a) structural SCFs and (b) notch SCFs.

3.2.2 Crack growth analyses

Crack growth simulations were carried out to obtain SIFs for predicting fatigue strength using LEFM. The main interest of LEFM analyses was to assess the fatigue strength of LC joints because the infusible weld root acts as an initial crack. Comparisons with LEFM and stress-based analyses, however, were conducted for fatigue failures starting from weld toe, i.e. in the case of NLC joints. As transverse continuous weldments were studied, 2D plane strain models were employed in the analyses once again. This assumption regards planar cracks as having a crack depth to crack width ratio of $a/c \approx 0$.

Crack growth simulations were carried out using Franc2D software distributed by Cornell University (Cornell Fracture Group, 2020). Crack growth paths were computed using maximum tangential stress criterion, and SIFs (modes I and II) were obtained using the J-integral approach embedded in the Franc2D software. In the case of crack growth starting from the weld root, the weld penetration was taken into account in the geometry of FE models (as demonstrated in Figure 3.9). In the case of weld toe failures, a crack depth of $a = 0.025$ mm was inserted radially to the model at the maximum stress location, which was propagated to $a_i = 0.15$ mm as applied in the LEFM analyses (as shown in Figure 3.10).

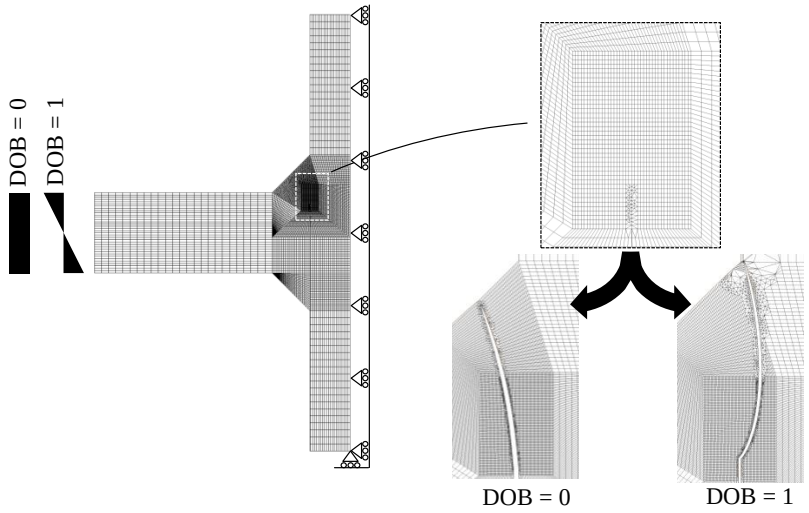

Figure 3.9. The Franc2D crack growth model of an LC joint: (a) load and boundary conditions, and (b) crack paths under axial and bending loads.

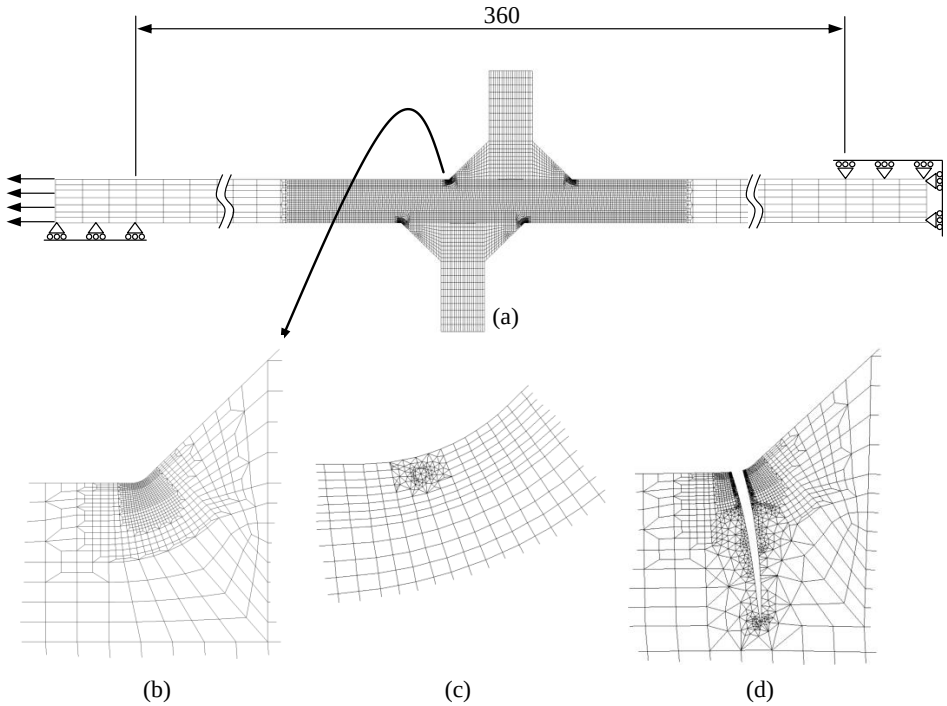

Figure 3.10. The Franc2D crack growth model of a misaligned NLCX joint: (a) load and boundary conditions (b) weld toe FE mesh, (c) inserted crack depth of a = 0.025 mm and (d) propagated crack at the crack depth of a = 1.5 mm.

3.3 Literature review on fatigue test data

The third research method, closely related to the experimental methods, was to conduct literature reviews on the fatigue test data of existing studies to supplement the fatigue test data-sets and to experimentally further-verify the proposed concepts for the fatigue strength assessments. In this thesis, literature reviews were carried out on experimental studies concerning fatigue strength of fillet-welded LC joints under bending loads and fatigue strength of ground fillet weld joints. The fatigue test data of fillet-welded LC joints under bending loading was used to experimentally verify the proposed analytical model for assessing the weld root fatigue strength, together with the experiments on UHSS grade conducted within this thesis. In both studies, the scope was extended to cover mild steels and HSSs, as opposed to UHSS grades only due to the lack of fatigue test data on welded UHSS grades.

Literature reviews and extracted data sets were limited to those studies in which the geometry details of specimens were comprehensively described. In the case of LC joints, the degree of weld penetration and weld throat thickness should have been available to compute NWS and ENS for geometry. In the ground joints, attention was paid to the reported weld toe radii as they were used as a basis for the FE models.

4 Results

4.1 Measurements

4.1.1 Residual stresses

Typical residual stress distributions for an S960MC LC joint in the AW and HFMI-treated conditions are demonstrated in Figure 4.1. Figure 4.2 summarizes the results of residual stress measurements at the weld toes, conducted for S960MC and S1100QL NLCT and NLCX specimens in the AW and post-weld-treated conditions. It should be noted that all experiments were conducted for small-scale specimens and negligible low tensile, while even compressive residual stresses were measured at the weld toes for joints in the AW condition. The compressive residual stresses at the plate components (far away from the weld toe) is a result from the manufacturing process of these UHSS grades.

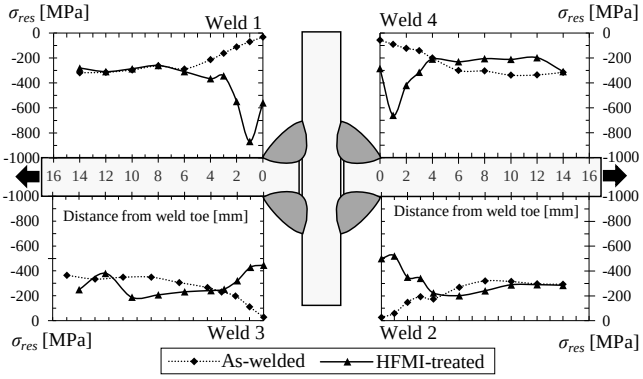

Figure 4.1: Transverse residual stress distributions (parallel to the loading direction) in the S960MC LC joints in the AW and HFMI-treated condition.

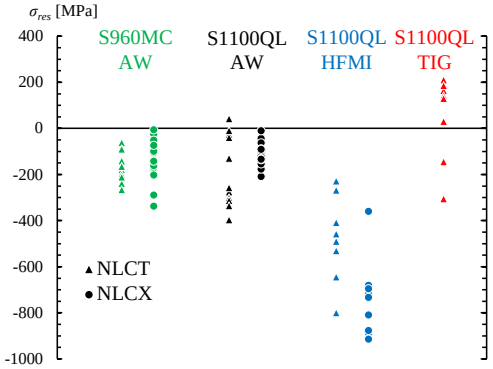

Material	Joint type	Joint cond.	$\sigma_{res,max}$ [MPa]	$\sigma_{res,avg}$ [MPa]
S960MC	NLCT	AW	-62	-156
S960MC	NLCX	AW	-6	-121
S1100QL	NLCT	AW	42	-171
S1100QL	NLCX	AW	-10	-110
S1100QL	NLCT	HFMI	-228	-450
S1100QL	NLCX	HFMI	-360	-745
S1100QL	NLCT	TIG	211	52

Figure 4.2: Summary of residual stress measurements at the weld toe positions in NLCT and NLCX joints in the AW, HFMI-treated and TIG-dressed conditions.

4.1.2 Specimen and weld geometries

From the geometry measurements, the actual weld toe radius, weld flank angle θ, and weld throat thickness were determined. Strain gage measurements were utilized in the determination of bending stresses induced by the angular distortions, that particularly occur in the single-sided NLCT joints due to their asymmetric heat input. The magnitude of bending stresses is denoted with the stress magnification factor $k_m = (\sigma_m + \sigma_b)/\sigma_m$. Table 4.1 presents a summary of the geometry measurements (average and STDV) together with stress magnification factor ranges. Figure 4.3 presents macro graphs of the S1100QL NLCT joints in the AW, HFMI-treated, and TIG-dressed condition, from which the weld penetration and effective throat thickness were obtained.

Table 4.1. Results of geometry and strain gage measurements.

Material	Joint type	Joint condition	Average r_{true} [mm]	Average θ [°]	Average a_w [mm]	STDV r_{true} [mm]	STDV θ [°]	STDV a_w [mm]	k_m [-]
S960MC	NLCT	AW	0.30	43	5.1	0.07	1.1	0.12	1.26–1.35
	NLCX	AW	0.29	43	5.2	0.07	1.5	0.17	1.00–1.01
S1100QL	NLCT	AW	0.35	36	4.5	0.22	1.2	0.16	1.14–1.19
	NLCT	HFMI	2.3	37	4.5	0.49	1.7	0.09	1.07–1.12
	NLCT	TIG	6.4	37	4.5	1.8	1.5	0.11	1.17–1.41
	NLCX	AW	0.30	44	5.2	0.11	1.9	0.18	1.00–1.06
	NLCX	HFMI	2.3	43	5.2	0.21	2.3	0.23	1.01–1.09

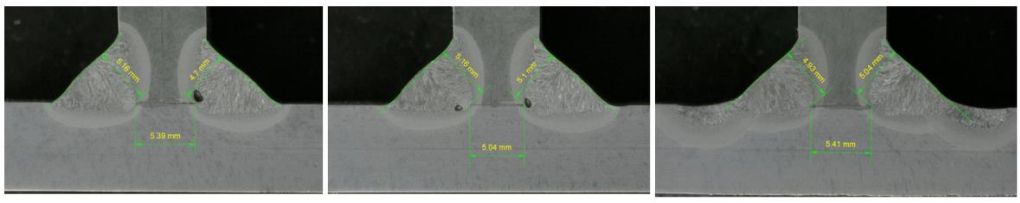

Figure 4.3: Macro graphs of NLCT joints in the (a) AW, (b) HFMI-treated, and (c) TIG-dressed conditions.

4.2 Fatigue strength of non-load-carrying joints

4.2.1 Notch stress concentration factors

Notch stress concentrations were determined for NLCT and NLCX joints using FEA. A fictitious radius concept was applied using the reference radius of r_{ref} = 1.0 mm, as per the ENS concept and considering actual weld toe radius, i.e. $r = r_{rtue}$ + 1 mm. Figure 4.4 presents the results of notch stress analyses in accordance with the geometrical details presented in Table 4.1.

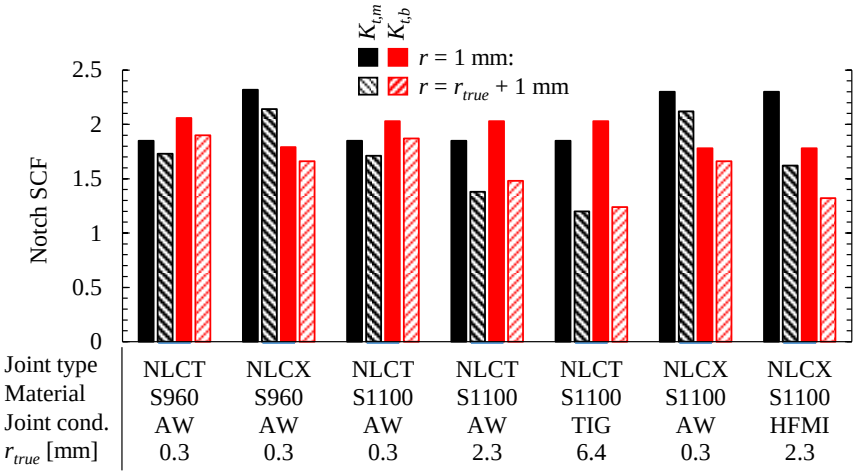

Figure 4.4: Notch SCFs for NLCT and NLCX joints under axial and bending loading.

4.2.2 Axial and bending fatigue behavior

Figure 4.5 and Figure 4.6 present the fatigue test results of S960 NLCT and NLCX joints subjected to axial and bending loading, respectively. Table 4.2 presents the mean fatigue strengths and slope parameters of the *S-N* curves. The results are plotted in terms of nominal stresses, structural HS stresses (considering the macro-geometric bending stresses), and ENSs. It is noticeable that, in the case of bending loading, nominal bending stress is equal to HS stress because angular distortion does not cause any additional stress at the joints.

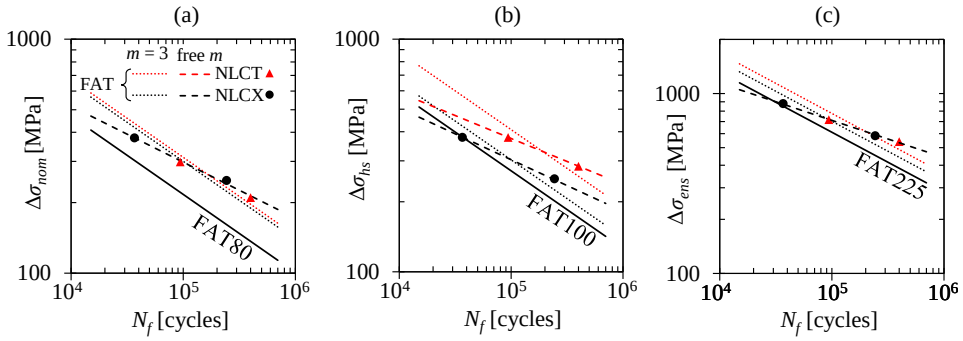

Figure 4.5: The fatigue test results of NLCT and NLCX S960MC specimens in the AW condition under axial loading: (a) nominal stress, (b) HS stress and (c) ENS. See Table 4.2 for further details regarding the *S-N* curves.

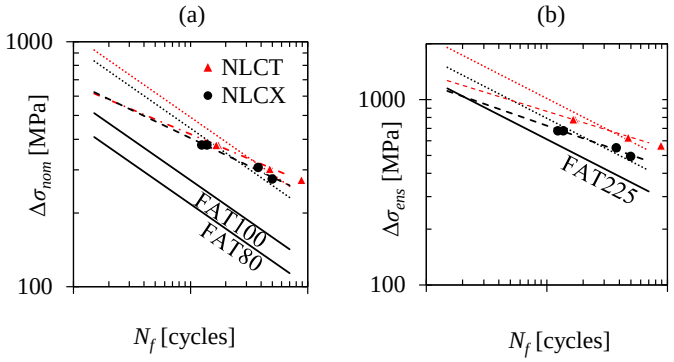

Figure 4.6: The fatigue test results of NLCT and NLCX S960MC specimens in the AW condition under bending loading: (a) nominal stress, and (b) ENS. See Table 4.2 for further details regarding the *S-N* curves.

Table 4.2: Mean (P_s = 50%) fatigue strengths [MPa] of S960MC specimens in the AW condition and tested under R = 0.1 using different stress criteria.

Approach		Nominal stress			HS stress			ENS		
Joint type	Load type	FAT (m = 3)	FAT	m	FAT (m = 3)	FAT	m	FAT (m = 3)	FAT	m
NLCT	Axial	115	147	4.18	150	207	5.07	286	383	4.83
NLCX	Axial	111			111	156	4.51	259		
NLCT	Bending	–	–	–	183	230	4.98	373	474	4.98
NLCX	Bending	–	–	–	163	204	4.40	292	366	4.40

In the second set of fatigue tests, NLCT joints made of S1100QL grade were tested under axial and bending loads. Figure 4.7 presents the results of these tests. The experimental program also concerned NLC joints post-weld-treated with HFMI treatment and TIG dressing. Figure 4.8 summarizes the fatigue test results of these experiments.

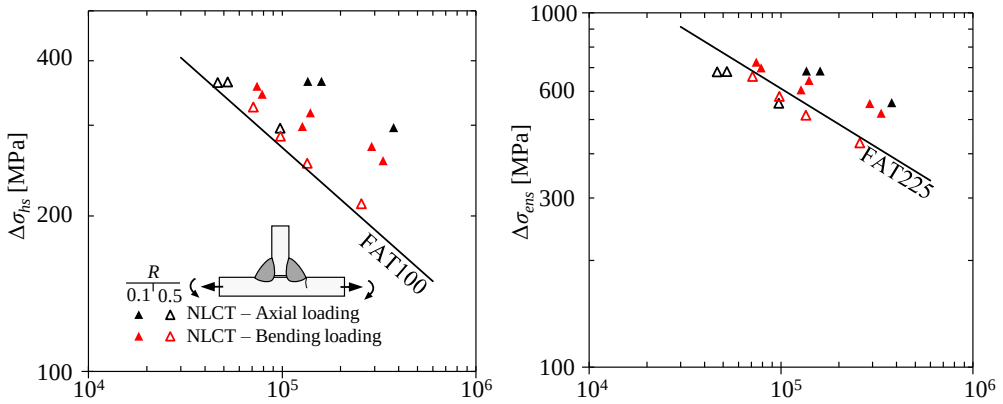

Figure 4.7: Fatigue test results of NLCT S1100QL specimens in the AW condition under axial and bending loading.

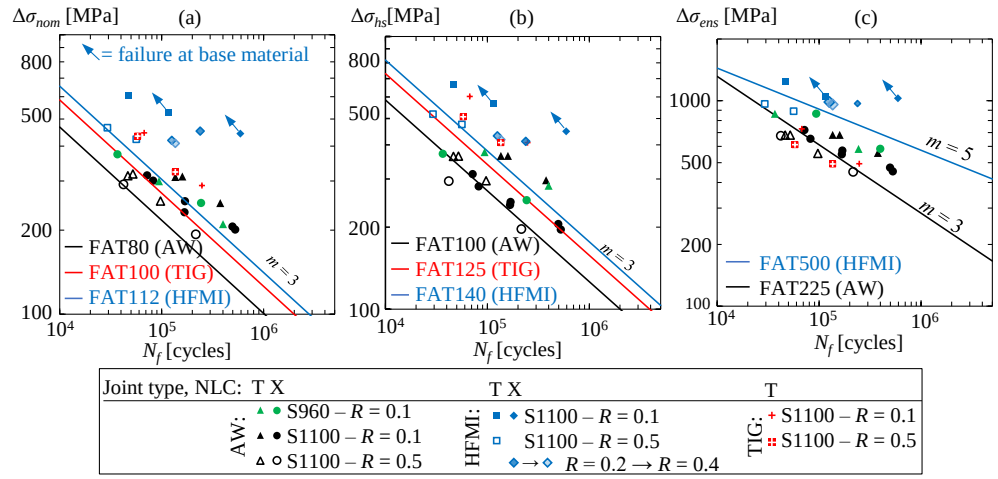

Figure 4.8: Summary of fatigue test results of axially tested NLCT and NLCX specimens in the AW and post-weld-treated conditions: (a) nominal stress, (b) structural HS stress, (c) ENS.

4.2.3 Misaligned transverse non-load-carrying attachments

A discrepancy was found in the fatigue strength of fillet-welded NLCT and NLCX joints, which raises a question about the fatigue behavior of misaligned NLCX joints, i.e. NLCX joints in which transverse attachments are not perfectly aligned. Consequently, a set of test specimens were prepared to investigate the effect of plate misalignment on the fatigue strength of NLCX joints. This study was limited to observe axially loaded misaligned NLCX joints with symmetrical fillet welds. Three different degrees of plate misalignment were chosen for fatigue testing, based on the numerical FE study on the effect of plate misalignment. Figure 4.9 demonstrates the applied misalignments and corresponding fatigue failures in NLCX joints.

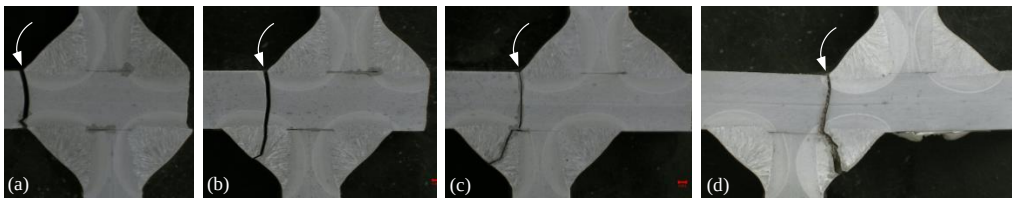

Figure 4.9: NLCX joints with different degrees of misalignments and fatigue failures: (a) e = 0, (b) e = 6 mm, (c) e = 9 mm and (d) e = 16 mm. The white arrows show locations of fatigue crack initiation.

FE analyses were employed to obtain structural and notch SCF, essential for determining fatigue strength using different approaches. Structural HS stresses were determined using the LSE method and stress at 1 mm depth. The TTWT method, for determining structural

stress, was not employed as it is not applicable in the case of a misaligned NLCX joint. Notch SCFs were determined in accordance with the ENS concept using r_{ref} = 1.0 mm at the weld toe. Figure 4.10 presents *S-N* data plots in comparison with design curves using different stress criteria, and Table 4.3 presents the fatigue strengths obtained for the different specimen configurations.

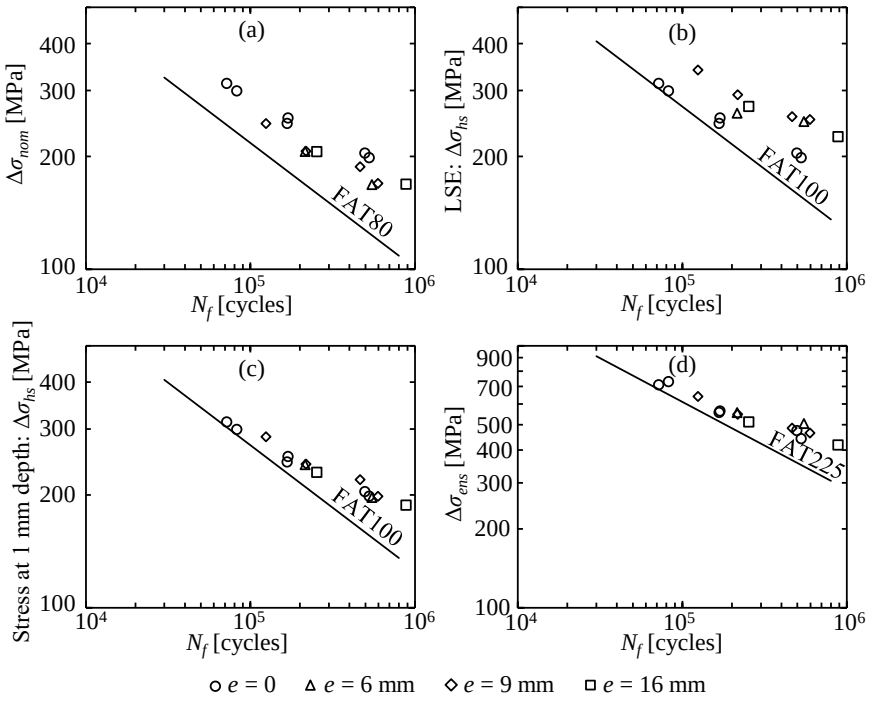

Figure 4.10: Fatigue test results of the misaligned NLCX joints.

Table 4.3: Mean fatigue strength for different misalignments and stress criteria. The slope parameters of *S-N* curves (*m*) were determined for all joints and fatigue strengths for the different degrees of misalignment using the obtained slope parameter.

			FAT_{mean} [MPa]			
Approach	*m*	e [mm]	0	6	9	16
Nominal	3.57		128	113	117	124
HS (LSE)	3.75		132	158	169	169
HS (1 mm)	4.47		147	147	152	150
ENS	4.53		337	359	346	336

4.3 Weld root fatigue strength of load-carrying fillet weld joints

4.3.1 Experimental results

The main focus of this thesis, as far as the fillet-welded LC joints made of UHSS are concerned, was to investigate fatigue behavior under out-of-plane bending and so establish an analytical approach to calculating NWSs for fatigue strength assessments. Consequently, the bending tests were in the main focus of the experiments, but axial tests were performed for comparison. In each specimen failing from the weld root, macrographs were taken from the failed specimens to obtain the throat thicknesses (nominal and effective) and infusible weld root length for stress analysis. Figure 4.12 demonstrates weld root crack paths in the axially and bending-loaded LC joints. NWSs were calculated in accordance with Chapter 2.3.2 using effective throat thickness. Furthermore, ENSs were obtained using r_{ref} = 1.0 mm by means of FE analysis. Figure 4.11 presents the fatigue test results in *S-N* plots using NWSs and ENSs for both axial and bending tests.

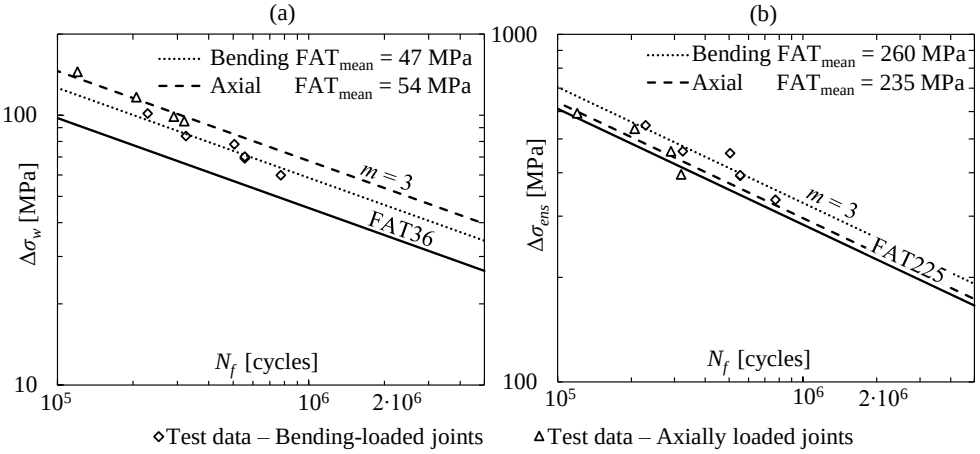

Figure 4.11: Fatigue test results and S-N curves of S960 LCX joints for (a) the nominal stress (NWS) approach and (b) the ENS concept.

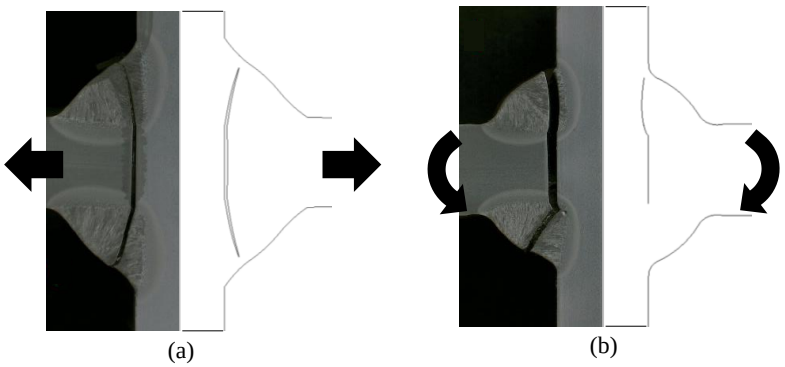

Figure 4.12: Experimentally (left) and numerically (right) obtained fatigue crack paths under (a) axial and (b) bending loading.

To further-verify the applicability of the proposed procedure for calculating NWSs in the bending-loaded LC joints with fillet welds, fatigue test results were extracted from the existing experimental studies. Bending fatigue tests have not been widely applied for investigating the fatigue behavior of fillet-welded LC joints but a few test series were found. Mori et al. (2009; 2010) studied the fatigue strength of GMA-welded LC fillet weld joints made of mild low-carbon structural steel (KA32, f_y = 362 MPa) under four-point bending and axial loading, and Ghafoori-Ahangar and Verreman (2019) studied two multi-pass TIG-welded stainless steel grades (AISI 415, $R_{p0.2}$ = 754 MPa; E316L, $R_{p0.2}$ = 395 MPa) under three-point bending. In these studies, the focus was on experimental work and fracture mechanics-based assessments, with analytical approaches not being proposed. Figure 4.13 presents the findings of a re-analysis conducted for these results.

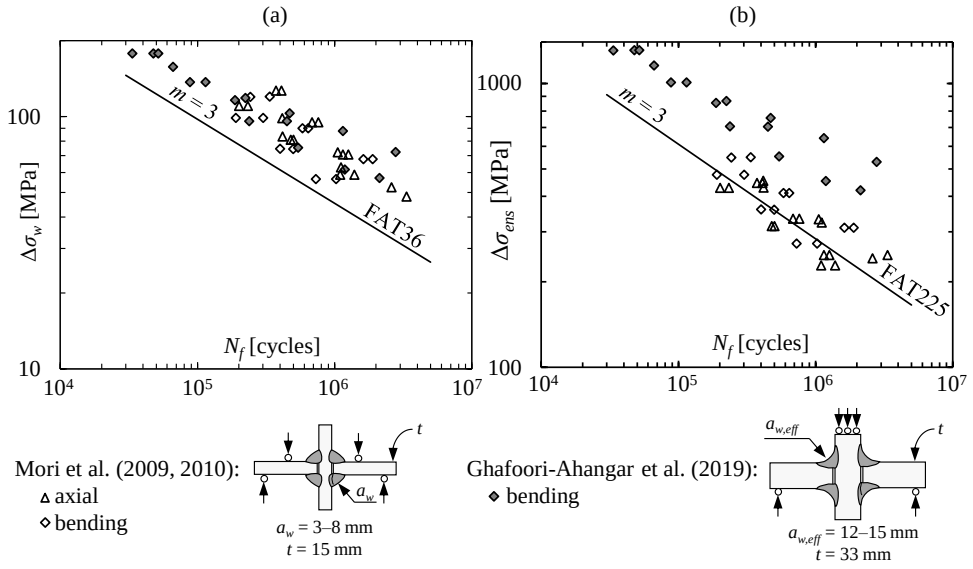

Figure 4.13: The findings of the re-analysis of fatigue test results with (a) the nominal stress (NWS) approach and (b) the ENS concept in comparison with the design curves.

4.3.2 Weld penetration effects on fatigue performance

Chapter 4.3.1 presented the fatigue test results by applying NWSs in association with the nominal stress approach. For the axially-loaded joints, NWSs were determined based on the acting force and cross-sectional area while, for bending loaded joints, linear stress distribution over the LC weld section was assumed. In both load cases, the effective weld throat thickness considering weld penetration was used as a basis for computing NWSs – see also Figure 2.8, together with Equations (2.15) and (2.16) in Chapter 2.3.2. The results showed good correspondence between joints fatigue-tested under axial and bending loads, as well as complying with the FAT36 design curve for NWSs. Nevertheless, to address the effects of weld penetration and chosen ligament size on the weld root fatigue strength capacity, crack growth simulations and LEFM analyses were carried using varying degrees of penetration.

A symmetric LC joint with double-sided 45-degree (isosceles) fillet welds without weld penetration was chosen as a basis for the observation. Weld throat thickness to plate thickness ratios (a_w/t) of 0.33, 0.50, and 0.66 were analyzed. The weld penetration p was increased from $p/t = 0$ (no penetration) to $p/t = 0.2$, then its beneficial effect on the fatigue strength was evaluated. In this context, NWSs were analyzed using ligament sizes of effective throat thickness ($a_{w,eff}$) and external throat thickness summed with weld penetration ($a + p$). The improvement gained by penetration was evaluated by a relative improvement compared to an LC joint without penetration ($k = \mathrm{FAT}_{\mathrm{penetrated}}/\mathrm{FAT}_{\mathrm{fillet\ weld}}$). Similarly, the improvement is estimated based on the increase of ligament sizes ($a_{w,eff}$ and $a_w + p$). Figure 4.14 and Figure 4.15 present the results of the analyses for LC joints subjected to axial and bending loads, respectively. In axially-loaded LC joints, the weld penetration enhancing the fatigue strength seemingly correlates with the NWS calculated based on the ligament size of $a_w + p$, whereas the ligament size of $a_{w,eff}$ follows the results obtained by LEFM analyses in bending-loaded joints.

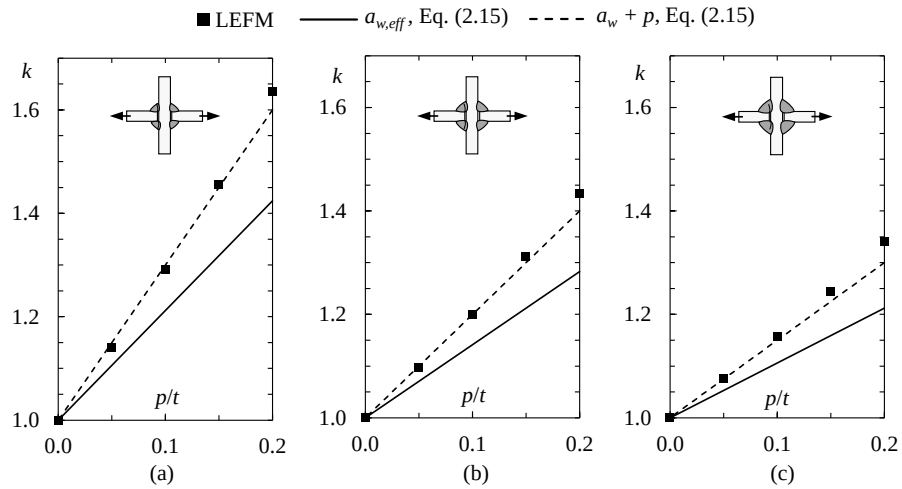

Figure 4.14: Fatigue strength improvement gained by weld penetration in axially loaded LC joints: (a) $a_w/t = 0.33$, (b) $a_w/t = 0.50$, and (c) $a_w/t = 0.66$.

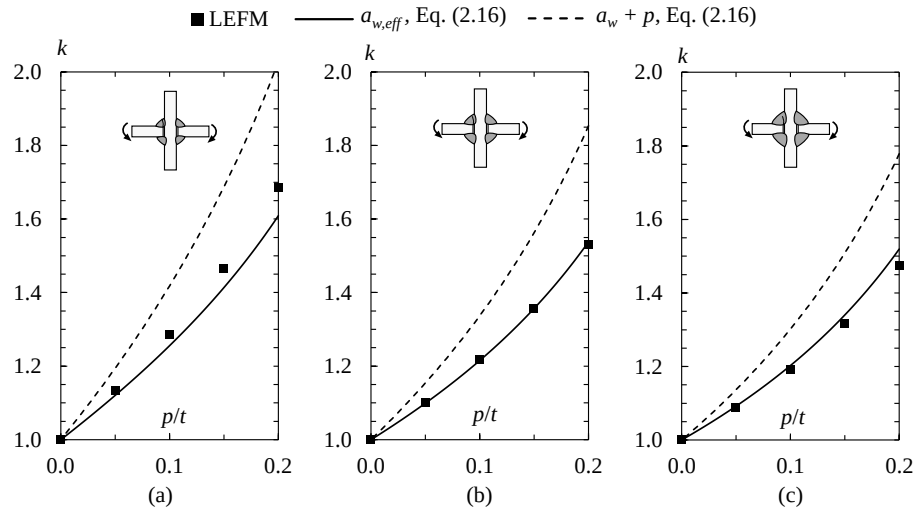

Figure 4.15: Fatigue strength improvement gained by weld penetration in bending loaded LC joints: (a) a_w/t = 0.33, (b) a_w/t = 0.50, and (c) a_w/t = 0.66.

4.4 Fatigue strength assessments using 4R method

4.4.1 Welded ultra-high-strength steel joints

This chapter presents the results of the 4R analysis conducted for fillet-welded UHSS joints tested in the AW, HFMI-treated and TIG-dressed conditions. In these assessments, the residual stress, geometry, and strain gage measurements were of paramount importance, accounting for the local stress ratio in association with the effective notch stresses. Residual stresses were chosen according to conservative assumptions, i.e. a maximum value in the test series (joint type and condition), as well as the average weld toe radii were chosen for the analysis, see Figure 4.1 and Table 4.1. Figure 4.16 presents the results of 4R fatigue strength assessments for fillet-welded UHSS joints.

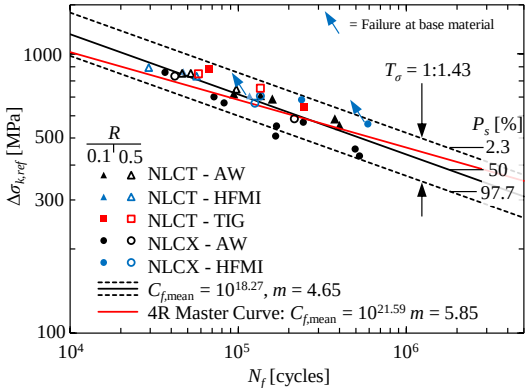

Figure 4.16: Fatigue test results of UHSS fillet weld joints.

Figure 4.17 presents a comparison between the design curves of the ENS concept and the 4R method for the fatigue strength assessment of welded joints in the AW and HFMI-treated condition as a function of material yield/proof strength. The 4R method provides an *S-N* curve in terms of the reference notch stress range (N_f, $\Delta\sigma_{k,ref}$), which does not have a direct correspondence with the conventional ENS curves because the reference ENS represents fictional mean stress-corrected stress. Nevertheless, a continuous *S-N* curve of the 4R method (N_f, $\Delta\sigma_k$), can be formulated using the following equation:

$$N_f = \frac{C_f}{\Delta\sigma_{k,ref}{}^m} = C_f \left(\frac{\sqrt{1 - R_{local}\{\Delta\sigma_k, R, \sigma_{res}, R_m\}}}{\Delta\sigma_k} \right)^m \tag{5.1}$$

By setting $N_f = 2 \cdot 10^6$ in Equation (5.1), $\Delta\sigma_k$ can be determined numerically and compared with the design curves for a given condition (R, σ_{res}, R_m). For the comparisons, the material yield strength to ultimate tensile strength ratios were estimated following the upper bound of the structural integrity assessment procedure by Webster and Bannister (2000), and residual stresses for the HFMI treatments were approximated using two values; σ_{res} = -0.255R_m (Nykänen & Björk, 2016) and higher compressive residual stresses, i.e. σ_{res} = -0.5R_m to visualize the residual stress effects on fatigue strength estimation after the 4R method.

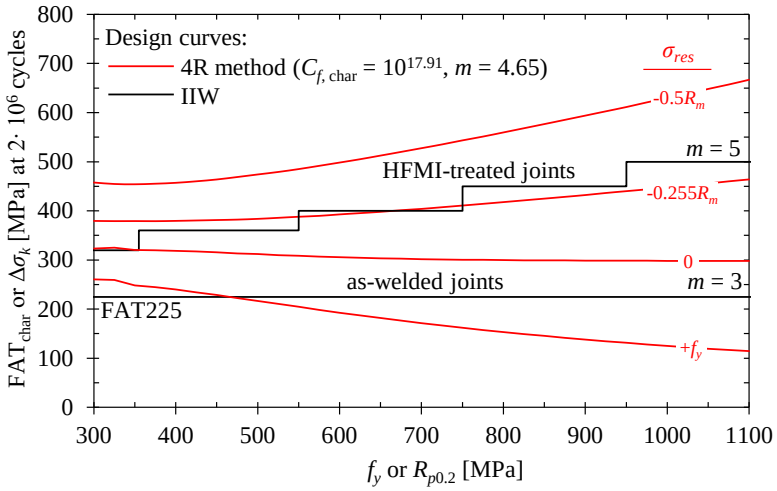

Figure 4.17: Comparison between the 4R method and the design curves of the ENS concept (r_{ref} = 1.0 mm) by the IIW Recommendations (Marquis & Barsoum, 2016) at R = 0.1.

4.4.2 Ground fillet weld joints

Prior studies of the 4R method, together with the results presented in Chapter 4.4.1, focused on the joints in the AW and post-weld-treated conditions, including HFMI treatment and TIG dressing. This chapter presents the results of fatigue strength

assessments conducted for fillet-welded joints post-weld-treated with grinding using the 4R method. In addition, the study considers joints in which the grinding treatment was followed by peening to induce compressive residual stresses at the notch root.

For this analysis, fatigue test data was extracted from existing studies. The extracted data consisted of fillet-welded NLC, LC and LG joints, post-weld treated with weld toe grinding, weld profiling (entire weld reinforcement profiled with grinding), and combined grinding and peening. Joints in the AW condition were also included in the 4R analysis to compare the assessment accuracy. In total, 607 data points were extracted. From these studies, *S-N* data points together with the geometrical details, including joint geometry, weld size and profile, and weld toe radius were determined. FE analyses were carried out to obtain notch SCFs to convert the nominal stresses to the fatigue-effective notch stress system, considering the radius of ground weld toe ($r = r_{true} + 1$ mm). For joints in the AW condition, $r_{true} = 0$ was conservatively assumed if no further information was provided. The angular distortions and/or stress magnification factors were not reported in all studies, and a stress magnification factor of $k_m = 1.25$ was assumed in those joints to account for the macro geometric bending stresses, as per the IIW Recommendations (Hobbacher, 2016).

Some of the extracted studies covered experimental work on residual stresses before and after the grinding treatment. In transversely welded joints, it was found that welding residual stresses, transverse to weld and parallel to the loading direction, were negligible small (near zero) in both AW and ground condition (Baptista et al., 2008; Braun, Hensel, et al., 2020; Gao et al., 2015), similar to the results found in this study for NLCT, NLCX and LCX joints in the AW condition and made of UHSS grades. Such results are fundamentally related to the characteristics of small-scale specimens.

In small-scale specimens of LG joints, the longitudinal weld cannot contract freely at the cooling phase due to the stiffness of plate components, while significantly higher residual stresses can be present. The experiments have demonstrated tensile residual stresses nearly equal to the yield strength of the material, and weld toe grinding in LG joints causes residual stress reduction (Huther et al., 2006; Miki & Tai, 2013). Based on these findings, conservative assumptions of residual stresses were made, as presented in Table 4.4.

Table 4.4: Residual stress approximations on fillet welded joints in the AW, ground and ground and peened condition.

Joint type	Joint condition	σ_{res}
Joints with transverse welds	AW	0
	Ground	0
	Ground and peened	$-0.5R_m$
LG joints	AW	$+f_y$
	Ground	$+0.5f_y$
	Ground and peened	$-0.5R_m$

Figure 4.18 presents the fatigue strength assessment results obtained using the 4R method in terms of data plots and statistically determined *S-N* curves. In the statistical analyses, both the minimization of the sum of squared perpendicular distances (MSSPD) approach and standard method ($\Delta\sigma$ is a known variable and N_f is an unknown variable) were used to obtain *S-N* curves. Furthermore, to enable a comparison between the fatigue strength assessments of joints in the AW, toe ground (TG), weld profiled (WP) and ground and peened (G&P) condition, the mean fatigue strengths were obtained for each joint condition category. Table 4.5 presents the results of statistical analyses.

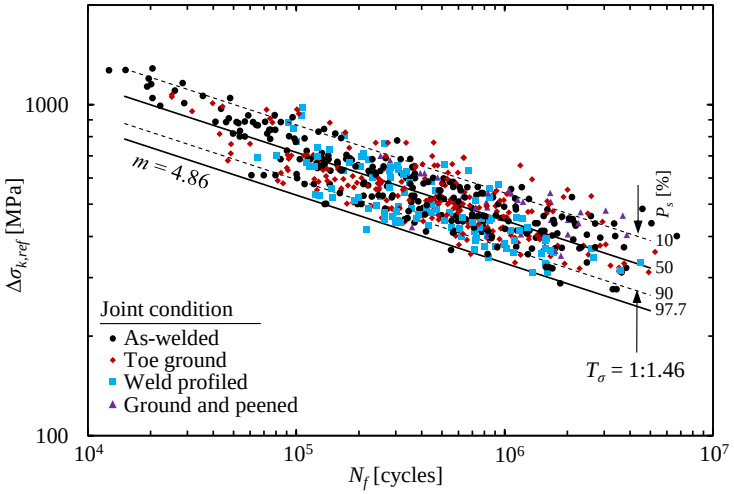

Figure 4.18: The fatigue test data and S-N curves of fillet weld joints in the AW, TG, WP, and G&P conditions using the 4R method. T_σ is the scatter range (corresponding to P_s = 90% and 10%).

Table 4.5: Results of statistical analyses.

Statistical approach	All specimens m [-]	All specimens FAT_{mean} [MPa]	All specimens FAT_{char} [MPa]	All specimens T_σ [-]	$FAT_{mean,i}$ [MPa] (ratio $FAT_{mean,i}/FAT_{mean}$) AW	TG	WP	G&P
Standard	3.55	345	243	1:1.57	345 (1.00)	344 (1.00)	325 (0.94)	395 (1.15)
MSSPD	4.86	388	288	1:1.46	393 (1.01)	387 (1.00)	366 (0.94)	418 (1.08)

The results indicate that the 4R method accounts for the fatigue strength improvement gained by geometrical and residual stress improvement, and approximately similar fatigue strength was found for all categories. Figure 4.19 provides a closer insight on the 4R results in respect of the data series in which joints in the AW, TG and/or WP, and G&P conditions were fatigue-tested.

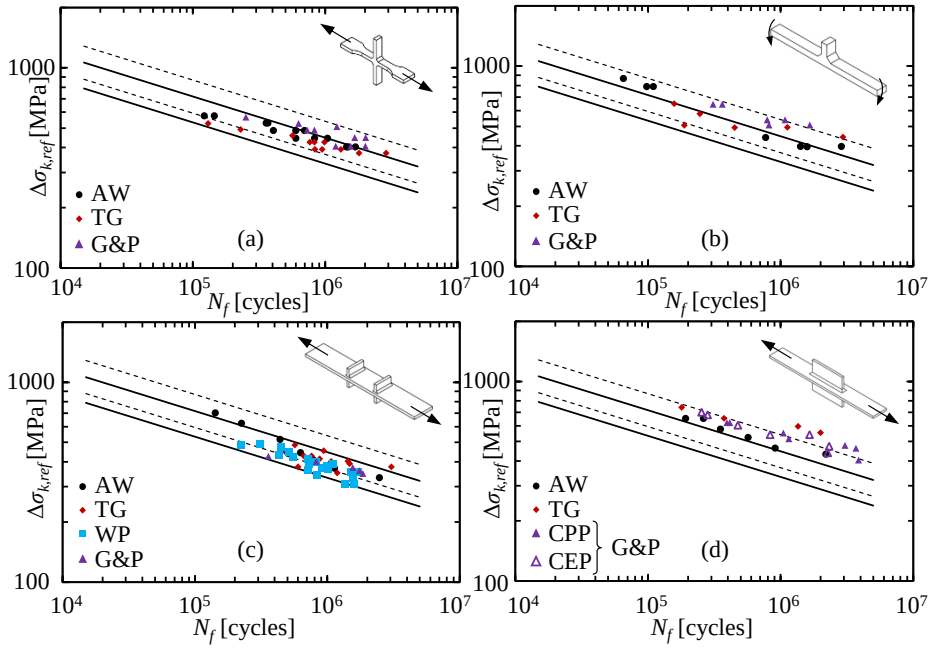

Figure 4.19: A comparison of 4R fatigue strength assessments in joints in the AW, ground, and ground and peened conditions: Data points of (a) Gao et al. (2015), (b) Haagensen (1993), (c) Gurney (1968), and (d) Miki and Tai (2013). The *S-N* curves correspond to the ones presented in Figure 4.18 and Table 4.5.

4.4.3 **Sensitivity analysis**

The 4R method considers the weld toe radius, residual stress, applied stress ratio and material strength in fatigue strength assessments. An increase in the number of parameters included in the analyses expectedly increase the accuracy of prediction. However, uncertainties related to the determination of the parameters can affect the accuracy of the fatigue strength assessments conducted using the 4R method. Figure 4.17 exemplified material strength effects using different residual stress assumptions. To comprehensively address the effect of a change in the 4R parameters on the reference ENS in a UHSS fillet weld joint, a sensitivity analysis was conducted. Furthermore, this analysis enables a consideration of the importance of an individual parameter in fatigue strength assessments at different joint and load conditions.

In the sensitivity analysis, a simple ‘one variable at a time’ approach was employed, and each parameter was varied with respect to the values of baseline scenarios. The effect of parameter change on the reference ENS was obtained, which was then compared to the corresponding value in a baseline scenario. To obtain the sensitivity of the parameters in different joint conditions, various cases were chosen for observation. Residual stress and applied stress ratio were altered in the baseline scenarios, resulting in nine different combinations. Table 4.6 presents the baseline scenarios and chosen ranges of variation in

each parameter. For simplicity, material strength was chosen to be a UHSS grade with $R_{p0.2}$ = 1100 MPa and A = 10%, while ultimate tensile strength was estimated based on the yield strength to ultimate tensile strength ratio, as per Webster and Bannister (2000). The chosen joint type was NLCT and the notch SCF for membrane loading was estimated following the analytical equation formulated by Ushikorawa (Iida & Uemura, 1996). The results of the sensitivity analyses are shown in Figure 4.20.

Table 4.6: Parameters in baseline scenarios and variation ranges in 4R parameters.

4R parameter	r_{true} [mm]	$R_{p0.2}$ [MPa]	σ_{res} [MPa]	R [-]
Baseline scenarios	0.5	1100	800; 0; -300	0.5; 0; -1
Variation ranges	±0.5	±100	±100	±0.2

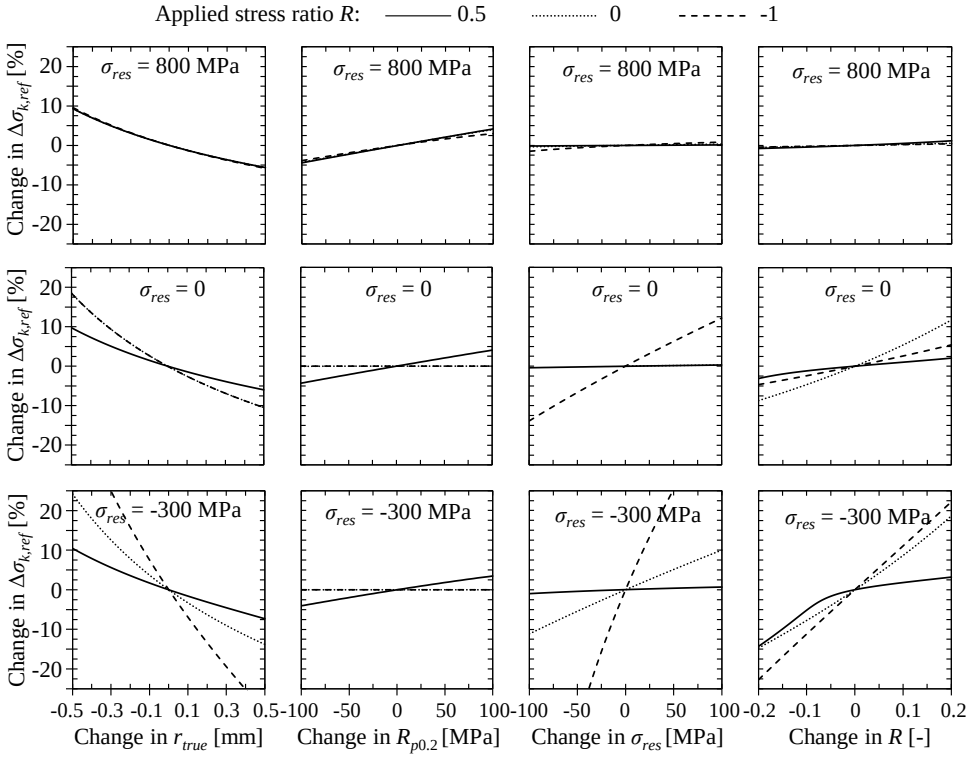

Figure 4.20: Results of the sensitivity analyses.

5 Discussion

This chapter analyzes the results and discusses about the implications and significance of the findings. Chapters 5.1–5.3 focuses specifically on certain topics of the thesis answering the research questions of the study, and Chapter 5.4 summarizes the topics of the thesis by compiling the findings.

5.1 Non-load-carrying joints under axial and bending loading

To summarize the numerical studies on SCFs, it is definite that axial loading and membrane stress induces higher notch SCF in symmetric joints – in double-sided details, than in asymmetric joints – in single-sided details. In contrast, bending stress cause higher notch factors in asymmetric joints than in symmetric joints, as demonstrated in Figure 4.4. When observing different joint types, notch SCFs are higher for bending stresses in asymmetric joints, whereas notch SCFs are higher for axial stresses in symmetric structures. It is of great importance, therefore, to consider the joint and load type when evaluating notch stress for a fatigue analysis. This applies to stress analyses, for example, in which a cross-sectional (plane strain) model is applied for computing notch stress based on the structural stresses determined from a global model. Stress components in joints should be distinguished and applied as load conditions in the cross-sectional model.

The fatigue test results also indicate that, under axial loading, higher fatigue strength can be claimed for NLCT joints than NLCX joints. It is noticeable that angular distortions should be considered in this observation – see Figure 4.5. For NLCX joints, negligibly small stress magnification factors of k_m = 1.0–1.06 were determined (Table 4.1), while for NLCT joints in the AW condition k_m = 1.14–1.35 were obtained. In the ENS criterion, the data points lie in a single *S-N* curve.

Some inconsistencies were found in the bending fatigue tests. In NLCX joints, expectedly higher fatigue strength was found under bending loading. In NLCT joints, due to the higher notch SCFs, a lower fatigue strength could be expected. Nonetheless, a higher fatigue strength was found in S960 NLCT specimens. Crack propagation periods were significantly higher than numerically obtained periods in those joints, and, possibly for that reason, higher fatigue strength was obtained – see Figure 4.6. However, it is worth mentioning that the number of test specimens in these series was low, and further tests should be carried out to verify these findings. In the second set of specimens, S1100QL specimens were fatigue tested under bending loading with applied stress ratios of R = 0.1 and R = 0.5. When taking angular distortions into account in axially-loaded specimens, lower fatigue strength was obtained for bending-loaded joints than for axially-loaded joints at both stress ratios – see Figure 4.7.

An increase in applied stress ratio decreased the fatigue strength of NLC joints and also in the joints in the AW condition. Negligibly small residual stresses were measured in the tested small-scale specimens and consequently, the fatigue strength was affected by the applied stress ratio. It is also worth noting that the R = 0.5 results did not exceed the

design curves indicating that they might lead to unconservative assessments in UHSS joints. The $R = 0.1$ results complied with the design curves, although it should be noted the design curves are determined for the applied stress ratio of $R = 0.5$

This study also addressed the PWT methods – namely HFMI treatment and TIG dressing – to enhance the fatigue strength of fillet-welded UHSS joints. Distinct improvements in fatigue strengths were found – see Figure 4.8. The present findings agree with current design recommendations for PWTs, although the use of the nominal and structural HS stress approaches might lead to conservative fatigue assessments. In contrast, this study was unable to demonstrate that no improvement is gained by the HFMI treatment at high stress ratios, as guidelines have recommended (Marquis & Barsoum, 2016). Expectedly, this can be reasoned by the geometrical improvement resulting from HFMI treatment, but might show material-dependency and would need further verification.

A discrepancy was found between the fatigue strength of NLCT and NLCX joints, i.e. higher fatigue strength was obtained for the NLCT joints than NLCX joints when using the nominal or structural HS stress approaches, which was due to the higher notch SCF in NLCX joints. Therefore, a series of misaligned NLCX specimens were manufactured and fatigue-tested. The fatigue strength was evaluated using nominal stresses, while structural stresses determined using the LSE method and structural stress at the 1 mm below depth. In addition, the ENS concept was employed. The results indicated that the misalignment decreases the fatigue strength of these joints by up to 12% compared to joints without misalignment, depending on the degree of misalignment – see nominal fatigue strengths in Figure 4.10a and Table 4.3. On the other hand, when the misalignment is large enough, the joint acts as an NLCT joint, and fatigue strength increases.

Earlier studies have tended to focus on the effects of plate misalignment on the fatigue strength of LCX joints, rather than NLCX joints. Recent studies undertaken by Zong et al. (2017) and Su et al. (2020) examined the plate misalignment effects in NLCX joints, finding a few percent decrease in fatigue strength. However, their studies were limited to the low degree of misalignments ($e/t < 0.25$) and numerical crack propagation simulations, excluding the effect of crack initiation period on fatigue strength. In this study, it was found that the notch stress and structural stress (at the 1 mm depth) accurately estimated the effect of misalignment on fatigue strength, while the LSE method was unable to predict the effect of the plate misalignment on fatigue strength.

5.2 Weld root fatigue strength of load-carrying joints

Experimental and numerical studies were carried out to investigate the fatigue behavior of LC joints with double-sided fillet welds under bending loading. Fatigue tests were carried out for LC joints made of an S960MC UHSS grade, tested under bending and axial loading with the applied stress ratio of $R = 0.1$. An analytical approach was proposed for calculating NWS under bending loading for fatigue assessments in accordance with the nominal stress method.

Through experimental verification, it was suggested that NWSs can be calculated using linear elastic stress distributions over the joint section defined by effective throat thickness – see Figure 2.8. Using the proposed method, a similar weld root fatigue strength was found for axially and bending-loaded LC joints, with the results in line with the FAT36 design curve – see Figure 4.11. The proposed method was also applied for data sets of existing experimental studies on LC joints made of mild structural steel and two stainless steels grades, showing similar results with the experiments of this study. Therefore, the proposed method can be suggested for assessing the fatigue strength of fillet-welded joints under bending loading.

An effective throat thickness was applied in the analysis of NWSs, while LEFM analyses were carried out to examine the effect of weld penetration on the fatigue strength capacity. The results indicated that in axially loaded joints, the improvement correlated with the NWS, computed based on the external throat thickness summed with weld penetration ($a_w + p$). Under bending loading, a correlation was found with NWS and fatigue strength improvement when using effective throat thickness ($a_{w,eff}$). With a small degree of penetration, the difference in NWS resulting from different ligament sizes is rather low but as penetration depth is higher, the effective throat thickness gives a distinctly lower NWS value. However, these findings are limited to fillet welds with flank angles of θ = 45° and the fatigue capacities should be analyzed using fillet welds with unequal leg lengths.

Fatigue crack paths from weld root were different for axially- and bending-loaded joints, as clearly demonstrated by both the numerical and experimental results shown in Figure 4.12. Within this study, fillet-welded LC joints were studied with either pure axial or bending loading, and the combined effect of axial and bending loads were not addressed. Due to the different failure paths under axial and bending loading, a superposition principle is expected to lead to safe side fatigue assessments. Such fatigue performance was also found by Anami et al. (2008) for fillet-welded LC joints subjected to a DOB = 0.2 loading. They also applied linear elastic stress distribution over a joint section to compute ENSs at the weld root under combined axial and bending loading.

Based on the experimental findings, the ENS method might give unconservative fatigue strength predictions with the FAT225 design curve. The mean fatigue strengths barely exceeded the design curve, which raises a question as to whether the UHSS materials have lower fatigue strength against weld root failures or whether the FAT225 design curve is unconservative for weld root failures. However, recent experimental studies on LC joints made of mild steel and failing from weld root have indicated that the FAT225 does not necessarily provide safe-side predictions (Braun, Milaković, et al., 2020; Sundermeyer et al., 2015). In addition, a recent review on the fatigue test data of LC joints with double-sided fillet welds has also expressed that one fatigue class lower, i.e. FAT200, is justifiable for assessing weld root fatigue strength (Rohani Raftar et al., 2020).

5.3 Applications of the 4R method for fatigue strength assessments

The results of the fatigue tests – see Figure 4.8 – demonstrated that the fatigue strength of fillet-welded UHSS joints can be significantly enhanced by introducing PWTs. Weld toe radius and notch effect, residual stress, applied stress ratio, and material strength are decisive factors influencing the fatigue performance of welded UHSS components. Conventionally, the fatigue strength improvements obtained by PWTs are considered in fatigue assessments by adopting a higher fatigue class or enhancement factors, influenced by material strength and applied stress ratio (Haagensen & Maddox, 2013).

In this thesis, the 4R method was applied for the fatigue assessments of fillet-welded UHSS joints in the AW, HFMI-treated and TIG-dressed conditions, and for fillet weld joints geometrically improved with grinding methods and made of various steel grades. In both studies, the *S-N* curves were determined for experimental data, and good correspondence was found between the data sets. The 4R method, via ENS with an SWT-correction using local stress ratio, commeasured data points into single *S-N* curves – see Figure 4.16 and Figure 4.18.

The current design codes and guidelines for the fatigue assessments of post-weld-treated joints are limited to individually conducted PWTs. For instance, prior studies have demonstrated that higher fatigue strength can be claimed for joints improved with grinding followed by peening treatment at the ground surface, when compared to joints improved solely with grinding or peening (Gao et al., 2015; Gurney, 1968; Haagensen, 1993; Miki & Tai, 2013). Logically, this is a result of both geometrical and residual stress improvement. The 4R method was able to accurately assess the fatigue strength of those joints, as demonstrated in Figure 4.18. In comparison with conventional local approaches, the 4R method enables a methodological and numerical consideration of material strength, applied stress ratio, residual stress and ENS, and can thus be regarded as a generic model for fatigue assessments. It can, therefore, be assumed that the 4R method can predict the fatigue strength welded joints treated with various combined PWTs, such geometrical improvements (grinding or TIG dressing) followed by residual stress modification method (shot peening, overloads or HFMI treatment).

The sensitivity analysis – see Chapter 4.4.3 – was carried out to examine the effect of the 4R parameters and their error or uncertainty on fatigue strength assessments. It clearly indicated that, under high tensile residual stress (an assumed condition for a UHSS joint was σ_{res} = 800 MPa in tension), fatigue strength is insensitive to changes in applied stress ratio and residual stresses. This result is in line with the current knowledge on stress ratio effects on the fatigue strength of welded joints in the AW condition, as exemplified in Figure 2.6. At low or compressive residual stress fields and low stress ratios, fatigue strength is severely affected by changes in the applied stress ratio and residual stresses. Material strength does not have a major effect on the fatigue strength in these cases when cyclic behavior occurs at the elastic regime and, consequently, affects the assessments of joints at high residual stress fields and loaded at high stress ratios. Of the 4R parameters,

the weld toe radius is the most insensible for changes in load and residual stress conditions.

The obtained slope parameters for *S-N* curves were slightly lower than found in the prior study (Nykänen & Björk, 2016), in which the 4R method (or the 3R method at that time) was established for butt welds in the AW condition. Such a difference is expected to be a result of different residual stress approximations. In this study, negligibly small tensile residual stresses ($\sigma_{res} \approx 0$) were assumed for transversely welded small-scale specimens based on experimental findings. This assumption particularly affects fatigue assessments at low ENS ranges and high strength materials by lowering the local stress ratio and, thus, giving a lower reference ENS range. The R_{local} effects on the reference ENS can be found in Equation (2.27) in Chapter 2.4. In addition, higher material strength in steels results in higher yield strength to ultimate tensile strength ratio (close to $f_y/R_m \approx 1$), which should be considered when determining material stress-strain curve for the 4R analysis. The results of quasi-static tests, together with material yield strength, ultimate tensile strength, and elongation were used for estimating the R-O curve parameters of UHSS grades and ground specimens made of various steel grades. Nevertheless, the data points of this study complied with the *S-N* curves of the prior study, as shown in Figure 4.16. By reflecting the results of this study for a larger scope with engineering applications, a slope parameter of $m = 5$ could be approximated for fatigue design purposes, similarly to that recommended for the HFMI-treated joints (Marquis & Barsoum, 2016). This proposal, however, would need a statistical re-analysis and verification with a high number of data points.

5.4 Summarizing remarks

The aim of this study was to investigate the fatigue behavior of fillet-welded NLC and LC UHSS joints under axial and bending loading considering local effects at the structural and notch levels. The findings of this study underline the need for consideration of these aspects in order to realize accurate fatigue assessments of welded UHSS components.

The results of this study imply that the local effects at a structural level, i.e. joint symmetry and misalignments, should be taken into account when computing notch stress analyses for fatigue assessments. In addition, a consideration of stress components is of paramount importance in these analyses. The parametric studies on LG joints – see Figure 2.4 and Figure 2.5 – exemplified that structural and notch stresses can be significantly higher for bending-loaded joints. Furthermore, these results indicated that structural stresses are significantly affected by the base plate width, not only the gusset length, as typically regarded in the fatigue classes of design guidelines for the nominal stress approach (Hobbacher, 2016). This aspect has also been found and addressed in a recent study of geometrical effects in longitudinal gussets (Ono et al., 2020).

Although the fatigue-effective notch stresses are computed precisely, such local approaches do not necessarily result in accurate fatigue strength assessments. The fatigue strength of fillet-welded UHSS joints is characterized by local effects at the notch level,

not only by notch stresses. To enable accurate fatigue strength assessments of weld toe failures, a consideration of weld residual stress and material strength, together with applied stress ratio and fatigue-effective notch stress is required. These factors are of paramount importance in the case of weld toe failures. Although PWTs are usually applied locally to enhance fatigue strength, it was also found that the PWTs conducted locally at weld toes affects angular distortions in specimens. HFMI treatment decreased, and TIG dressing increased angular distortions when compared to the AW specimens in the NLCT joints – see reported values in Table 4.1. Consequently, the local treatments might have an influence on the structural-level phenomena, and should be addressed if fatigue strengths are compared using the nominal stress approach.

The weld root fatigue strength of fillet-welded LC joints is characterized by an infinite sharp notch at the weld root acting as an initial crack for propagation. Fatigue performance is influenced by weld throat thickness and penetration, while applied stress ratio, for instance, does not have a major effect on the fatigue strength capacity (Ahola et al., 2019). Due to these conditions, the weld root fatigue strength cannot necessarily be described with a similar *S-N* curve to weld toe failures when applying local approaches. The use of NWSs in fatigue assessments resulted in good accuracy in both axially- and bending-loaded LC joints so can be recommended for fatigue assessments. Figure 5.1 summarizes the topics covered in this thesis and illustrates the fatigue assessment procedure considering the stress components and local effects in the fatigue assessments of fillet-welded UHSS joints.

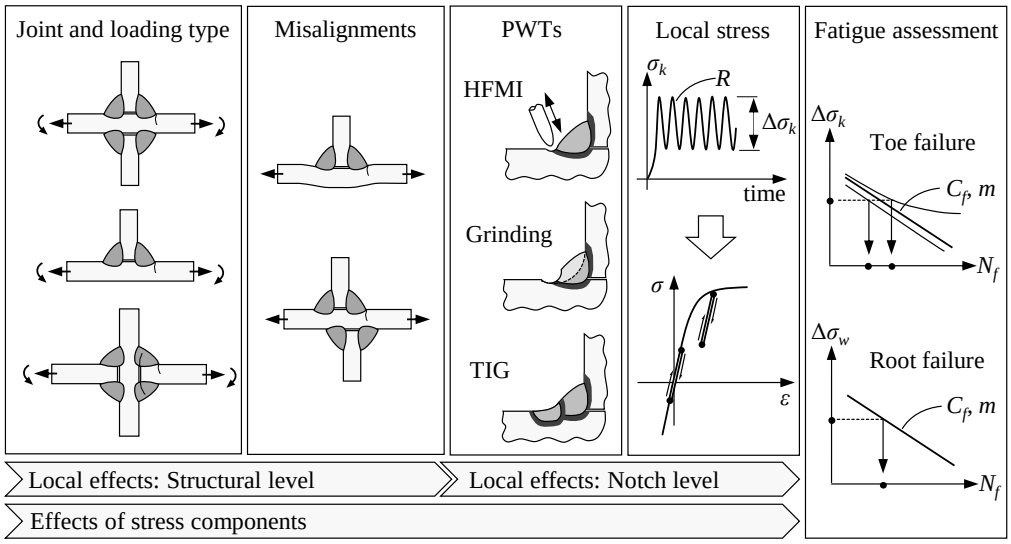

Figure 5.1: Consideration of stress components and local effects in the fatigue strength assessments of fillet-welded UHSS joints.

6 Conclusions

UHSSs enable a significant weight-reduction and high load-bearing capacity in structural applications with respect to conventional steels. However, higher material strength does not necessarily correlate with higher fatigue strength in welded steel components, however, meaning that welded UHSS joints and components are prone to fatigue failures. To make UHSSs a viable option for welded structural components, a comprehensive understanding of fatigue behavior is demanded.

Firstly, the thesis investigated the stress component and local effects on the fatigue strength of fillet-welded UHSS joints. Bending effects on the fatigue strength of fillet-welded UHSS joints are closely related to joint symmetry. In symmetric joint configurations, bending stress induce lower notch SCF than membrane stress, and a higher fatigue strength was experimentally found for bending loading. In asymmetric joints, higher SCF was found for bending loads. Experimental results showed some inconsistencies on the fatigue strength of asymmetric joints, and both lower and higher fatigue strength was found for bending loading when compared to axial loading. Concluding remarks cannot thus be drawn. In axially-loaded NLCX joints with plate misalignment, notch stress-based methods were able to predict the effects of misalignment on the fatigue performance.

Secondly, this thesis aimed to identify the fatigue strength capacity of fillet-welded LC UHSS joints subjected to bending and to examine efficient methods for fatigue strength assessments. An analytical method for computing NWSs under bending loads was proposed. Through experimental verifications, an elastic stress distribution, determined on the basis of effective throat thickness and infusible weld root length, over joint section can be applied together with the FAT36 design curve.

On the basis of the experiments conducted within this thesis, and relying on findings in prior studies, the fatigue strengths of UHSS components are decisively affected by residual stresses, notch effects, applied stress ratio. Thirdly, in this thesis, the 4R method was applied to consider these parameters in fatigue strength assessment. Good accuracy was found in the assessments for various joint and load conditions, meaning that the 4R method provides a methodological approach for taking these parameters into account in fatigue strength assessments.

These findings enhance our understanding of the importance of the consideration of stress components and local effects in the fatigue assessments of fillet-welded joints made of UHSS, considering both weld toe and weld root fatigue failures. The effect of local geometrical symmetry and stress components should be taken into account in fatigue assessments and in general, notch stress-based evaluation can fundamentally define the fatigue performance of joints. However, fatigue strength is also essentially characterized by local effects at the notch level. A consideration of residual stress, weld toe radius, applied stress ratio, and material strength provides higher accuracy in the fatigue strength assessments of welded joints made of UHSSs. For the fatigue strength assessment of weld

root failures in double-sided fillet weld LC joints under bending loading, this thesis proposed an analytical approach for computing NWSs that has not been univocally presented in design guidelines.

The experiments and subsequent analysis of the study were limited to small-scale specimens made of S960MC and S1100QL UHSS grades and manufactured in laboratory conditions. Significantly higher tensile residual stresses may occur in large-scale components, while engineering applications typically incorporate various weld qualities, and potentially defected weldments. Such welded UHSS components might show different fatigue performance, so careful consideration of these aspects is needed. The 4R method is founded on the flawless weldments and fatigue failures starting from weld toes, including at least some share of crack initiation period in total fatigue life. The present study also determines the weld root fatigue strength of LC joints under bending loading, and an analytical procedure for evaluating the weld stresses, complying with the FAT36 design curve, was proposed. The combined effects of axial and bending loads on the weld stresses were not observed, and further studies, taking the interaction of axial and bending loads through numerical and experimental observations into account will need to be undertaken.

The discrepancy between the fatigue strengths of S960MC and S1100QL NLCT joints bending loads still implies the need for careful consideration of crack initiation and propagation periods, which should be paid attention to in further investigations. This thesis accounts for the notch effects in fatigue assessments via the ENS concept using the fictitious notch stress concept, i.e. $r = r_{true} + 1$ mm, regardless of material strength, weld toe radius and notch opening angle. Successful results were acquired using this approach but further studies should carefully address the fatigue-effective notch effects for welded details. In the field of welded UHSS joints, the applicability of the 4R method for assessing the fatigue strength of joints in a high tensile residual field should be explored.

References

Ahola, A., Skriko, T., & Björk, T. (2019). Experimental investigation on the fatigue strength assessment of welded joints made of S1100 ultra-high-strength steel in as-welded and post-weld treated condition. In A. Zingoni (Ed.), *Proceedings of the 7th International Conference on Structural Engineering, Mechanics and Computation (SEMC 2019). Cape Town, South Africa, 2-4 September 2019* (pp. 1254–1259). https://doi.org/10.1201/9780429426506

Ahola, A., Skriko, T., & Björk, T. (2018). Fatigue performance of GMA-brazed non-load carrying joints made of ultra-high-strength steel. In K. Jármai & B. Bolló (Eds.), *Vehicle and Automotive Engineering 2 - Proceedings of the 2nd VAE2018* (pp. 157–169). https://doi.org/10.1007/978-3-319-75677-6_13

Amraei, M., Ahola, A., Afkhami, S., Heidarpour, A., Björk, T., & Zhao, X.-L. (2019). Effects of heat input on the mechanical properties of butt-welded high and ultra-high strength steels. *Engineering Structures*, *198*, 109460. https://doi.org/j.engstruct.2019.109460

Amraei, M., Dabiri, M., Björk, T., & Skriko, T. (2016). Effects of workshop fabrication processes on the deformation capacity of S960 ultra-high strength steel. *Journal of Manufacturing Science and Engineering*, *138*(12), 121007. https://doi.org/10.1115/1.4033930

Anami, K., Yokota, H., & Takao, R. (2008). Evaluation of Fatigue Strength of Load-Carrying Cruciform Welded Joint under Combination of Axial Loading and Out-of-Plane Bending. *International Journal of Steel Structures*, *8*(3), 183–188.

Anthes, R. J., Köttgen, V. B., & Seeger, T. (1993). Stress concentration factors for butt joints and double T-joints (in German). *Schweißen Und Scheiden*, *45*(12), 685–688.

Baik, B., Yamada, K., & Ishikawa, T. (2009). Fatigue strength of fillet welded joint subjected to plate bending. *International Journal of Steel Structures*, *8*, 163–169.

Baik, B., Yamada, K., & Ishikawa, T. (2011). Fatigue crack propagation analysis for welded joint subjected to bending. *International Journal of Fatigue*, *33*, 746–758. https://doi.org/10.1016/j.ijfatigue.2010.12.002

Baptista, R., Infante, V., & Branco, C. M. (2008). Study of the fatigue behavior in welded joints of stainless steels treated by weld toe grinding and subjected to salt water corrosion. *International Journal of Fatigue*, *30*, 453–462. https://doi.org/10.1016/j.ijfatigue.2007.04.011

Baumgartner, J., & Bruder, T. (2013a). An efficient meshing approach for the calculation of notch stresses. *Welding in the World*, *57*(1), 137–145. https://doi.org/10.1007/s40194-012-0005-3

Baumgartner, J., & Bruder, T. (2013b). Influence of weld geometry and residual stresses on the fatigue strength of longitudinal stiffeners. *Welding in the World*, *57*(6), 841–855. https://doi.org/10.1007/s40194-013-0078-7

Baumgartner, J., Schmidt, H., Ince, E., Melz, T., & Dilger, K. (2015). Fatigue assessment of welded joints using stress averaging and critical distance approaches. *Welding in the World*, *59*, 731–742. https://doi.org/10.1007/s40194-015-0248-x

Baumgartner, J., Yıldırım, H. C., & Barsoum, Z. (2019). Fatigue strength assessment of TIG-dressed welded steel joints by local approaches. *International Journal of Fatigue*, *126*, 72–78. https://doi.org/10.1016/j.ijfatigue.2019.04.038

Bhatti, A. A., Barsoum, Z., Mee, V. Van Der, Kromm, A., & Kannengiesser, T. (2013). Fatigue strength improvement of welded structures using new low transformation temperature filler materials. *Procedia Engineering*, *66*, 192–201. https://doi.org/10.1016/j.proeng.2013.12.074

Björk, T., Ahola, A., & Tuominen, N. (2018). On the design of fillet welds made of ultra-high strength steel. *Welding in the World*, *62*(5), 985–995. https://doi.org/10.1007/s40194-018-0624-4

Bowness, D., & Lee, M. M. K. (1996). Stress intensity factor solutions for semi-elliptical weld-tie cracks in T-butt geometries. *Fatigue & Fracture of Engineering Materials & Structures*, *19*(6), 787–797. https://doi.org/10.1111/j.1460-2695.1996.tb01323.x

Braun, M., Hensel, J., Song, S., & Ehlers, S. (2020). *Fatigue strength of normal and high strength steels joints improved by weld profiling (under preparation)*.

Braun, M., Milaković, A. S., Renken, F., Fricke, W., & Ehlers, S. (2020). Application of local approaches to the assessment of fatigue test results obtained for welded joints at sub-zero temperatures. *International Journal of Fatigue*, *138*, 105672. https://doi.org/10.1016/j.ijfatigue.2020.105672

Brennan, F. P., Peleties, P., & Hellier, A. K. (2000). Predicting weld toe stress concentration factors for T and skewed T-joint plate connections. *International Journal of Fatigue*, *22*(7), 573–584. https://doi.org/10.1016/S0142-1123(00)00031-1

BS7608:2014 +A1:2015. (2015). *Guide to Fatigue Design and Assessment of Steel Products*.

Cornell Fracture Group. (2020). *Software*. http://cfg.cornell.edu/software/

Dabiri, M., Ghafouri, M., Rohani Raftar, H., & Björk, T. (2017). Neural network-based assessment of the stress concentration factor in a T-welded joint. *Journal of Constructional Steel Research*, *128*, 567–578.

https://doi.org/10.1016/j.jcsr.2016.09.024

DNVGL-RP-C203. (2016). *Fatigue Design of Offshore Steel Structures*.

Dowling, N. E. (2006). *Mechanical Behavior of Materials. Engineering Methods for Deformation, Fracture, and Fatigue*. Prentice Hall.

EN 10149-2. (2013). *Hot rolled flat products made of high yield strength steels for cold forming – Part 2: Technical delivery conditions for thermomechanically rolled steels*.

EN 13001-3-1. (2018). *Cranes. General Design. Part 3-1: Limit States and proof competence of steel structure*.

EN 13445-3. (2018). *Unfired pressure vessels - Part 3: Design*.

EN 1993-1-12. (2007). *Eurocode 3: Design of steel structures - Part 1-12: Additional rules for the extension of EN 1993 up to steel grades S700*.

EN 1993-1-9. (2005). *Eurocode 3: Design of steel structures - Part 1-9: Fatigue*.

Farajian, M. (2013). Welding residual stress behavior under mechanical loading. *Welding in the World*, *57*(2), 157–169. https://doi.org/10.1007/s40194-013-0024-8

Fricke, W., Kahl, A., & Paetzold, H. (2006). Fatigue Assessment of Root Cracking of Fillet Welds Subject To Throat Bending Using the Structural Stress Approach Fatigue Assessment of Root Cracking of Fillet Welds Subject To Throat Bending Using the Structural Stress Approach for Structural Stress. *Welding in the World*, *50*, 64–74. https://doi.org/10.1007/BF03266538

Gao, W., Wang, D., Cheng, F., Deng, C., Liu, Y., & Xu, W. (2015). Enhancement of the fatigue strength of underwater wet welds by grinding and ultrasonic impact treatment. *Journal of Materials Processing Technology*, *223*, 305–312. https://doi.org/10.1016/j.jmatprotec.2015.04.013

Ghafoori-Ahangar, R., & Verreman, Y. (2019). Fatigue behavior of load-carrying cruciform joints with partial penetration fillet welds under three-point bending. *Engineering Fracture Mechanics*, *215*, 211–223. https://doi.org/10.1016/j.engfracmech.2019.05.015

Gkatzogiannis, S., Knoedel, P., & Ummenhofer, T. (2017). FE welding residual stress simulation: Influence of boundary conditions and material models. In J. Jönsson (Ed.), *Proceedings of Eurosteel 2017* (Vol. 1, Issues 2–3, pp. 443–452). Wiley. https://doi.org/10.1002/cepa.80

Gurney, T. R. (1968). Effect of peening and grinding on the fatigue strength of fillet

welded joints. *British Welding Journal*, *15*(12), 601–609.

Haagensen, P. J. (1993). The effect of grinding and peening on the fatigue strength of welded T-joints. *Transactions on Engineering Sciences*, *2*.

Haagensen, P. J. (2011). Fatigue strength improvement methods. In K. A. MacDonald (Ed.), *Fracture and Fatigue of Welded Joints and Structures* (pp. 297–329). Woodhead Publishing. https://doi.org/10.1533/9780857092502.2.297

Haagensen, P. J., & Maddox, S. J. (2013). *IIW Recommendations on Methods for Improving the Fatigue Strength of Welded Joints*. Woodhead Publishing.

Haglund, P., Khurshid, M., & Barsoum, Z. (2019). *Mapping of scatter in fatigue life assessment of welded structures - A Round Robin Study. IIW-document XIII-2827-19*.

Hensel, J., Nitschke-Pagel, T., Tchoffo Ngoula, D., Beier, H., Tchuindjang, D., & Zerbst, U. (2018). Welding residual stresses as needed for the prediction of fatigue crack propagation and fatigue strength. *Engineering Fracture Mechanics*, *198*, 123–141. https://doi.org/10.1016/j.engfracmech.2017.10.024

Hobbacher, A. (2011). The use of fracture mechanics in the fatigue analysis of welded joints. In *Fracture and Fatigue of Welded Joints and Structures* (pp. 91–112). https://doi.org/10.1533/9780857092502.1.91

Hobbacher, A. (2016). *Recommendations for Fatigue Design of Welded Joints and Components* (2nd ed.). Springer International Publishing.

Huther, I., Suchier, Y., & Lieurade, H. P. (2006). *Fatigue behaviour of longitudinal non-load-carrying joints improved by burr gringing, TIG dressing. IIW-document XIII-2108-06*.

Iida, K., & Uemura, T. (1996). Stress concentration factor formulae widely used in Japan. *Fatigue and Fracture of Engineering Materials and Structures*, *19*(6), 779–786. https://doi.org/10.1111/j.1460-2695.1996.tb01322.x

Jakubczak, H., & Glinka, G. (1986). Fatigue analysis of manufacturing defects in weldments. *International Journal of Fatigue*, *8*(2), 51–57. https://doi.org/10.1016/0142-1123(86)90053-8

Kang, W., Kim, W. S., & Paik, Y. M. (2002). Fatigue strength of fillet welded steel structure under out-of-plane bending. *International Journal of Korean Welding Society*, *2*(1), 33–39.

Karakaş, Ö., Zhang, G., & Sonsino, C. M. (2018). Critical distance approach for the fatigue strength assessment of magnesium welded joints in contrast to Neuber’s

effective stress method. *International Journal of Fatigue*, *112*, 21–35. https://doi.org/10.1016/j.ijfatigue.2018.03.004

Kömi, J., Karjalainen, P., & Porter, D. (2016). Direct-Quenched Structural Steels. In R. Colás & G. E. Totten (Eds.), *Encyclopedia of Iron, Steel and Their Alloys: Vol. I* (pp. 1109–1125). CRC Press.

Leitner, M., Khurshid, M., & Barsoum, Z. (2017). Stability of high frequency mechanical impact (HFMI) post-treatment induced residual stress states under cyclic loading of welded steel joints. *Engineering Structures*, *143*, 589–602. https://doi.org/10.1016/j.engstruct.2017.04.046

Lieurade, H. P., Huther, I., & Lefebvre, F. (2008). Effect of weld quality and postweld improvement techniques on the fatigue resistance of extra high strength steels. *Welding in the World*, *52*(7–8), 106–115. https://doi.org/10.1007/BF03266658

Lotsberg, I., & Sigurdsson, G. (2006). Hot Spot Stress S-N Curve for Fatigue Analysis of Plated Structures. *Journal of Offshore Mechanics and Arctic Engineering*, *128*(4), 330–336. https://doi.org/10.1115/1.2355512

Maddox, S. J. (1991). *Fatigue Strength of Welded Structures*. Woodhead Publishing.

Maddox, S. J. (2011). Fatigue design rules for welded structures. In K. A. MacDonald (Ed.), *Fracture and Fatigue of Welded Joints and Structures* (pp. 168–207). Woodhead Publishing. https://doi.org/10.1533/9780857092502.2.168

Maddox, S. J. (2015). Allowance for bending in fatigue design rules for welded joints. In *IIW-document XIII 2580-15*.

Marquis, G. B., & Barsoum, Z. (2016). *IIW Recommendations for the HFMI Treatment - For Improving the Fatigue Strength of Welded Joints*. Springer Singapore. https://doi.org/10.1007/978-981-10-2504-4

Miki, C., & Tai, M. (2013). Fatigue strength improvement of out-of-plane welded joints of steel girder under variable amplitude loading. *Welding in the World*, *57*(6), 823–840. https://doi.org/10.1007/s40194-013-0076-9

Möller, B., Baumgartner, J., Wagener, R., Kaufmann, H., & Melz, T. (2017). Low cycle fatigue life assessment of welded high-strength structural steels based on nominal and local design concepts. *International Journal of Fatigue*. https://doi.org/10.1016/j.ijfatigue.2017.02.014

Mori, T. (2009). *Assessment of fatigue strength of cruciform welded joints failing from weld roots under out-of-plane bending. IIW-document XIII-2287-09*.

Mori, T., Shimanuki, H., & Tanaka, M. (2012). Effect of UIT on fatigue strength of web-

gusset welded joints considering service condition of steel structures. *Welding in the World*, *56*(9–10). https://doi.org/10.1007/BF03321388

Mori, T., Uchida, D., Fukuoka, T., & Myoken, M. (2010). Assessment of fatigue strength of cruciform welded joints failing from weld roots under out-of-plane bending (in Japanese). *Japanese Society of Steel Construction*, *66*(3), 568–575. https://doi.org/10.2208/jsceja.66.568

Neuber, H. (1968). Über die Berücksichtigung der Spannungskonzentration bei Festigkeitsberechnungen. *Konstruktion*, *20*, 245–251.

Neuvonen, R., Skriko, T., & Björk, T. (2020). Use of quasi-static Johnson-Cook model in the failure assessment of tensile specimens with metallurgical constraints. *European Journal of Mechanics A/Solids*, *82*, 104011. https://doi.org/10.1016/j.euromechsol.2020.104011

Niemi, E., Fricke, W., & Maddox, S. J. (2018). Fatigue Analysis of Welded Components: Designer's Guide to the Structural Hot-Spot Stress Approach. In *Fatigue Analysis of Welded Components: Designer's Guide to the Structural Hot-Spot Stress Approach* (2nd editio). Springer Nature. https://doi.org/10.1533/9781845696665

Nykänen, T., & Björk, T. (2015). Assessment of fatigue strength of steel butt-welded joints in as-welded condition - Alternative approaches for curve fitting and mean stress effect analysis. *Marine Structures*, *44*, 288–310. https://doi.org/10.1016/j.marstruc.2015.09.005

Nykänen, T., & Björk, T. (2016). A new proposal for assessment of the fatigue strength of steel butt-welded joints improved by peening (HFMI) under constant amplitude tensile loading. *Fatigue and Fracture of Engineering Materials and Structures*, *39*(5), 566–582. https://doi.org/10.1111/ffe.12377

Ono, Y., Baptista, C., Kinoshita, K., Yıldırım, H. C., & Nussbaumer, A. (2020). *Influence of geometric size effect on fatigue strength of longitudinal welded gusset joints in as-welded and HFMI-treated state. IIW-document XIII-2854-2020*.

Oswald, M., Mayr, C., & Rother, K. (2019). Determination of notch factors for welded cruciform joints based on numerical analysis and metamodeling. *Welding in the World*, *63*(5), 1339–1354. https://doi.org/10.1007/s40194-019-00751-y

Ottersböck, M., Leitner, M., & Stoschka, M. (2015). *Effect of loading type on welded and HFMI-treated T-joints. IIW-document XIII-2584-15*.

Peterson, R. E. (1959). Notch sensitivity. In G. Sines & J. L. Waisman (Eds.), *Metal Fatigue* (pp. 293–306). McGraw-Hill Inc.

Radaj, D. (1990). *Design and Analysis of Fatigue Resistant Welded Structures*.

Woodhead Publishing.

Radaj, D., Sonsino, C. M., & Fricke, W. (2006). *Fatigue Assessment of Welded Joints by Local Approaches* (2nd editio). Woodhead Publishing.

Ran, M. M., Sun, F. F., Li, G. Q., Kanvinde, A., Wang, Y. B., & Xiao, R. Y. (2019). Experimental study on the behavior of mismatched butt welded joints of high strength steel. *Journal of Constructional Steel Research*, *153*, 196–208. https://doi.org/10.1016/j.jcsr.2018.10.003

Rohani Raftar, H., Dabiri, M., Ahola, A., & Björk, T. (2020). *Re-evaluation of weld root fatigue strength for load-carrying fillet welded joints using the notch stress concept (under work)*.

Schroepfer, D., Kromm, A., & Kannengiesser, T. (2019). Formation of multi-axial welding stresses due to material behaviour during fabrication of high-strength steel components. *Welding in the World*, *63*, 43–51. https://doi.org/10.1007/s40194-018-0650-2

Schubnell, J., Carl, E., Farajian, M., Gkatzogiannis, S., Knödel, P., Ummenhofer, T., Wimpory, R., & Eslami, H. (2020). Residual stress relaxation in HFMI-treated fillet welds after single overload peaks. *Welding in the World*. https://doi.org/10.1007/s40194-020-00902-6

Skoglund, O., Leander, J., & Karoumi, R. (2020). Overview of Steel Bridges Containing High Strength Steel. *International Journal of Steel Structures*. https://doi.org/10.1007/s13296-020-00360-2

Skriko, T., & Björk, T. (2015). Welding metallurgy and fusion line softening of direct quenched ultra-high-strength steel. *68th IIW Annual Assembly and International Conference: High Strength Materials - Challenges and Applications*.

Smith, K. N., Watson, P., & Topper, T. H. (1970). A stress–strain function for the fatigue of metals. *J Materials*, *5*(4), 767–778.

Sonsino, C. M. (2009). Effect of residual stresses on the fatigue behaviour of welded joints depending on loading conditions and weld geometry. *International Journal of Fatigue*, *31*(1), 88–101. https://doi.org/10.1016/j.ijfatigue.2008.02.015

Sørensen, J. D., Tychsen, J., Andersen, J. U., & Brandstrup, R. D. (2006). Fatigue Analysis of Load-Carrying Fillet Welds. *Journal of Offshore Mechanics and Arctic Engineering*, *128*(1), 65. https://doi.org/10.1115/1.2163876

Sperle, J. O. (2008). Influence of parent metal strength on the fatigue strength of parent material with machined and thermally cut edges. *Welding in the World*, *52*(7–8), 79–92. https://doi.org/10.1007/BF03266656

Stephens, R. I., Fatemi, A., Stephens, R. R., & Fuchs, H. O. (2000). *Metal Fatigue in Engineering* (2nd editio). Wiley.

Su, H., Wang, J., & Du, J. (2020). Fatigue behavior of uncorroded non-load-carrying bridge weathering steel Q345qDNH fi llet welded joints. *Journal of Constructional Steel Research*, *164*, 105789. https://doi.org/10.1016/j.jcsr.2019.105789

Sundermeyer, W., Fricke, W., & Paetzold, H. (2015). Investigation of weld root fatigue of single-sided welded T-joints. In C. Soares Guedes & R. A. Shenoi (Eds.), *Analysis and Design of Marine Structures V* (pp. 309–315). Taylor & Francis Group.

Taylor, D. (2007). *The Theory of Critical Distances: A New Perspective in Fracture Mechanics*. Elsevier Ltd. https://doi.org/10.1016/B978-0-08-044478-9.X5000-5

Wang, T., Wang, D., Huo, L., & Zhang, Y. (2009). Discussion on fatigue design of welded joints enhanced by ultrasonic peening treatment (UPT). *International Journal of Fatigue*, *31*, 644–650. https://doi.org/10.1016/j.ijfatigue.2008.03.030

Webster, S., & Bannister, A. (2000). Structural integrity assessment procedure for Europe - of the SINTAP programme overview. *Engineering Fracture Mechanics*, *67*(6), 481–514. https://doi.org/10.1016/S0013-7944(00)00070-9

Xiao, Z. G., Chen, T., & Zhao, X. L. (2012). Fatigue strength evaluation of transverse fillet welded joints subjected to bending loads. *International Journal of Fatigue*, *38*, 57–64. https://doi.org/10.1016/j.ijfatigue.2011.11.013

Xiao, Z. G., & Yamada, K. (2004). A method of determining geometric stress for fatigue strength evaluation of steel welded joints. *International Journal of Fatigue*, *26*(12), 1277–1293. https://doi.org/10.1016/j.ijfatigue.2004.05.001

Yıldırım, H. C. (2017). Recent results on fatigue strength improvement of high-strength steel welded joints. *International Journal of Fatigue*, *101*, 408–420. https://doi.org/10.1016/j.ijfatigue.2016.10.026

Yonezawa, T., Shimanuki, H., & Mori, T. (2019). Influence of cyclic loading on the relaxation behavior of compressive residual stress induced by UIT. *Welding in the World*, *64*, 171–178. https://doi.org/10.1007/s40194-019-00821-1

Zong, L., Shi, G., Wang, Y. Q., Li, Z. X., & Ding, Y. (2017). Experimental and numerical investigation on fatigue performance of non-load-carrying fillet welded joints. *Journal of Constructional Steel Research*, *130*, 193–201. https://doi.org/10.1016/j.jcsr.2016.12.010

Publication I

Ahola, A., Nykänen, T., and Björk, T.
Effect of loading type on the fatigue strength of asymmetric and symmetric transverse non-load carrying attachments

Reprinted with permission from
Fatigue & Fracture of Engineering Materials & Structures
Vol. 40, pp. 670-682, 2017

Publication II

Ahola, A., and Björk, T.
Fatigue strength of misaligned non-load-carrying cruciform joints made of ultra-high-strength steel

Reprinted with permission from
Journal of Constructional Steel Research
Vol. 175, 106334, 2020

Journal of Constructional Steel Research 175 (2020) 106334

Contents lists available at ScienceDirect

Journal of Constructional Steel Research

Fatigue strength of misaligned non-load-carrying cruciform joints made of ultra-high-strength steel

A. Ahola *, T. Björk

Laboratory of Steel Structures, School of Energy Systems, Lappeenranta-Lahti University of Technology LUT, P.O. Box 20, FI-53851 Lappeenranta, Finland

ARTICLE INFO

Article history:
Received 27 March 2020
Received in revised form 28 August 2020
Accepted 3 September 2020
Available online 13 September 2020

Keywords:
Fatigue
Welded joint
Misalignment
Fillet weld
Ultra-high-strength steel
4R method

ABSTRACT

Misalignments and distortions in welded plate components act as stress raisers and can significantly decrease the fatigue strength of welded connections. This paper investigates the effect of the plate misalignment of transverse attachments on the fatigue behavior of axially-loaded non-load-carrying cruciform (NLCX) joints. Experimental fatigue tests with and without the plate misalignment are carried out for fillet-welded NLCX joints. The test specimens were fabricated of S1100 ultra-high-strength steel grade, and the fatigue tests were conducted using an applied stress ratio of $R = 0.1$. Numerical finite element analyses were conducted to obtain the stress concentrations induced by the misalignment. In addition, varied geometry parameters were applied to investigate their effect on the magnitude of stress concentrations. Stress concentrations were obtained using the structural hot spot stress method applying linear surface extrapolation and 1 mm below depth methods, and the effective notch stress concept with the reference radius of 1 mm. Experimental fatigue tests showed a decrease of up to 12% in fatigue strength depending on the degree of misalignment. The highest stress concentration was induced when the misalignment to the joint width ratio was $e/L = 0.2$–0.4. Structural stresses cannot be estimated using the linear surface extrapolation. Instead, structural stress at the 1 mm depth and effective notch stress concept accurately evaluated the misalignment effect on the fatigue performance of NLCX joints, and provided a good correspondence between the theoretical and experimental fatigue strength estimations.

1. Introduction

Use of high- and ultra-high-strength steels (HSS/UHSS) in welded steel constructions enables weight reduction with similar static strength capacity, unlike their counterparts manufactured from mild steel. Consequently, HSS and UHSS materials prove profitable particularly in weight-critical structures and devices to increase payloads, e.g. in the fields of civil engineering, transportation, lifting and the automotive industry [1]. Such structures are typically subjected to fluctuating or cyclic load conditions, making them susceptible to fatigue failures. Whereas it is well-known in the prior art that increasing the static strength capacity of steel material does not contribute to high fatigue strength in welded components [2–4] unless specific post-weld treatments, see e.g. [5,6], are employed to improve the fatigue strength. On the other hand, a decrease in plate thickness predisposes UHSS components for different manufacturing imperfections, particularly those associated with welded details, i.e. welding deformations and the assembly accuracy of plate components. Structural misalignments and macrogeometric imperfections act as stress raisers, which may drastically decrease the fatigue strength capacity of welded joints and, thus, necessitate the consideration of fatigue performance in welded UHSS components.

The consideration of different misalignments and imperfections has been addressed in design codes and guidelines [7–9] providing parametric equations to analyze structural stress concentrations, typically denoted with k_m or k_s factors. In recent studies, significant interest has been placed on butt-welded details. Indeed, several studies have been conducted to consider misalignments in the structural HS system [10–12] but SCFs based on notch stress concepts have also been under investigation [13–15]. In cruciform joints with double-sided fillet welds and subjected to axial loading in the adjoined plate components – see Fig. 1a, i.e. in the case of load-carrying X-joints (LCX) – the effect plate and angular misalignments on fatigue performance and failure location have been well recognized in prior investigations [16–20]. Together with these plate misalignments, the fatigue behavior of the LCX joints is influenced by the size of weld throat thickness, the depth of weld penetration, potentially conducted post-weld treatments at the weld toes [21], residual stress state [22], and loading type [23,24].

Although extensive research has been carried out on the misalignment of LCX joints, far too little attention has been paid to the effect of the plate misalignment of transverse attachments in similar cruciform joints but subjected to axial loading at the base plate, i.e. non-load-carrying cruciform (NLCX) joints, see Fig. 1b. Henceforth in this paper,

* Corresponding author.
E-mail address: antti.ahola@lut.fi (A. Ahola).

https://doi.org/10.1016/j.jcsr.2020.106334
0143-974X/

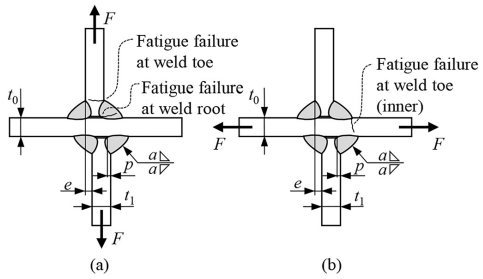

Fig. 1. Potential fatigue failure paths in axially loaded (a) LCX joint with plate misalignment and (b) NLCX joint with plate misalignment.

the term 'plate misalignment' signifies the misalignment of transverse attachments of NLCX joints. In such components, the misalignment can be introduced as a result of manufacturing inaccuracy, or design and functional purposes. The fatigue failure in a misaligned NLCX joint typically occurs, as also demonstrated in this study, at the inner weld toe. In recent studies, Zong et al. [25] and Su et al. [26] conducted numerical analyses based on linear elastic fracture mechanics (LEFM) to explore the effect of NLCX joint plate misalignment on fatigue strength capacity. In both studies [25,26], a relatively small degree of the misalignment was investigated, i.e. maximum of $e = 3$ mm for plate thicknesses of 8 mm and 12 mm, respectively, and a fatigue-life decrease of approximately 10% was found due to such misalignment. Some insights on the topic can also be found in [27]. In thin-walled UHSS components, relatively higher misalignments can potentially occur. Moreover, in UHSS weldments in the as-welded condition, the crack initiation time might become predominant in terms of total fatigue life [28,29] and, in such cases, fatigue strength assessment using LEFM might significantly underestimate the capacities. Furthermore, the lack of experimental data on the fatigue strength of misaligned NLCX joints restricts further conclusions being made on the issue.

This study aims to experimentally and numerically investigate how plate misalignment affects stress concentrations using different fatigue design criteria, i.e. structural HS stress and ENS concepts, together with what the efficient methods are for assessing the fatigue strength of a UHSS NLCX joint with plate misalignment. Finite element (FE) analyses are carried out to numerically investigate the structural and notch

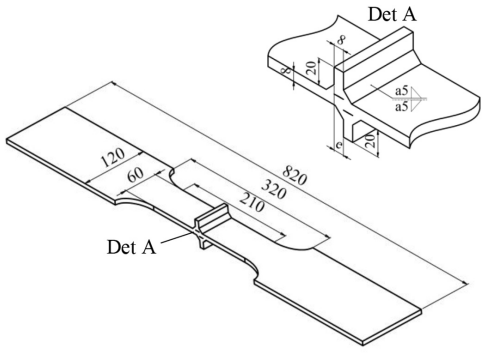

Fig. 2. Shape and dimensions of the test specimens (all dimensions in mm).

Table 1
Mechanical properties of the studied materials (nominal values).

Material	Proof strength	Ultimate strength	Elongation	Impact energy
	$R_{p0.2,min}$ [MPa]	R_m [MPa]	$A_{5,min}$ [%]	KV [J] (at temp.)
S1100	1100	1130–1350	10	27 (−40 °C)
Union X96[a]	930	≥980	14	47 (−50 °C)

[a] Mechanical properties of undiluted weld metal.

SCFs introduced by the plate misalignment in fillet-welded NLCX joints. Stress distributions along the base plate from the weld toe are obtained, and the structural stresses are obtained using linear surface extrapolation (LSE) method [30], and 1 mm below the surface approach, most commonly recognized as the Xiao–Yamada method [31]. For comparison, the effective notch stress (ENS) concept with a reference radius of $r_{ref} = 1.0$ mm [32] is employed to evaluate the fatigue effective notch stress. Subsequently, the numerically obtained findings on the effects of the plate misalignment are verified by conducting experimental fatigue tests on fillet-welded NLCX joints made of $t = 8$ mm S1100 UHSS steel plates prepared with and without plate misalignment. The S–N curves for joints with a different degree of plate misalignment are evaluated using different stress criteria, i.e. the nominal stress, structural HS stress and ENS concepts, and efficient methods for evaluating the effect of plate misalignment are addressed. This study is limited to NLCX joints for which the transverse attachments are unconstrained and so will not carry any axial forces or suffer bending moments.

2. Materials and methods

2.1. Experimental fatigue tests

2.1.1. Specimen design and preparation

Experimental fatigue tests were carried out for NLCX joints made of S1100 UHSS plates with the base and adjoined plate thicknesses of $t_0 = t_1 = 8$ mm, respectively. Union X96 (Ø1.0 mm) solid wire was used in the gas metal arc welding (GMAW) of the test specimens. Fig. 2 shows the shape and dimensions of the test specimens, and Table 1 and Table 2 present the mechanical properties and chemical compositions of the studied materials, respectively.

As the aim of this study is to investigate the effect of plate misalignment on the fatigue strength of NLCX joints made of UHSS, the misalignments in the test specimens were intentionally produced. A preliminary numerical FE analysis study on the stress concentrations induced by the plate misalignment, observed at the structural stress (LSE method) and notch stress (ENS method, $r_{ref} = 1.0$ mm) level, was carried out to choose misalignment levels. The model details regarding the FE analysis correspond to the specifications given in Section 2.2.1, and the analyses were carried out for $t_0 = t_1 = 8$ mm with four symmetric welds with a throat thickness of $a = 5$ mm, and no weld penetration was assumed. Fig. 3 shows the SCFs in terms of structural HS stress (K_s) and ENS (K_{tot}) as a function of plate misalignment. Fig. 3 reveals that the maximum structural SCF ($K_{s,max}$) and notch SCF ($K_{tot,max}$, including both structural and notch stress) occur at the different degree of misalignment. The notch SCF accounts for the geometrical symmetry at the joint section, while structural SCF depends on the position of neutral

Table 2
Chemical compositions of the studied materials (nominal values).

Material	C_{max}	Si_{max}	Mn_{max}	P_{max}	S_{max}	Al_{min}
S1100	0.20	0.50	1.80	0.02	0.005	0.015
	C_{max}	Si_{max}	Mn_{max}	Cr_{max}	Ni_{max}	Mo_{max}
Union X96[a]	0.12	0.8	1.9	0.45	2.35	0.55

[a] Chemical composition of undiluted weld metal.

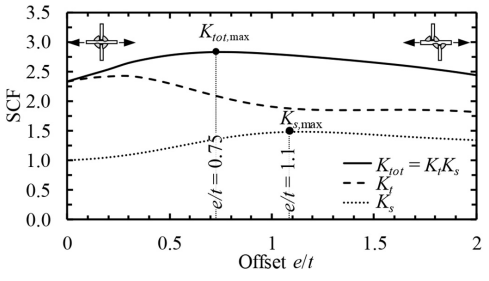

Fig. 3. SCFs for NLCX joint with $t_0 = t_1 = 8$ mm and $a = 5$ mm. K_t represents pure notch SCF, i.e. the total stress divided by the structural stress.

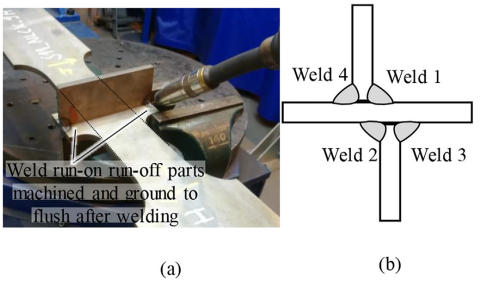

Fig. 4. (a) Welding preparation of the test specimen with a robotic GMAW and (b) sequence of welds in the misaligned specimens.

axis and stress flow over the attachments. It is also worth mentioning that the structural SCFs were determined using the LSE method resulting in different structural SCFs in comparison with the Xiao-Yamada method (see Section 3.2).

Three different degrees of misalignment were chosen according to the FEA study, i.e. $e/t = 0.75$, $e/t = 1.1$, and $e/t = 2.0$ corresponding to misalignments of $e = 6$ mm, 9 mm and 16 mm, based on the maximum values of SCFs, see Fig. 3. In addition, the reference specimens without plate misalignment were also manufactured, with the test results were initially reported in a previous study [33]. A total number of 14 specimens were fabricated and tested, with Table 3 showing the geometry and load configuration for each. To diminish the effect of metallurgical and geometrical scatter within the test specimen, the NLCX joints were prepared using a robotic GMAW process, and the target throat thickness of $a = 5$ mm was applied, according to the conducted preliminary FEA study. Fig. 4 shows the GMAW preparation of test specimens and a welded specimen, with Table 4 presenting the key values of the welding specification procedure (WPS).

2.1.2. Geometry and residual stress measurements

To evaluate the plate misalignment effect on the residual stresses, and to consider the welding quality in the joint fatigue strength assessment, residual stresses and weld geometries were determined before conducting the fatigue tests. Residual stresses were measured using an X-ray diffractometer (XRD, Stresstech X3000 G3 device) parallel to the loading direction. The collimator's spot size was 1 mm and the exposure time was 40 s. The average scatter of the residual stress measurements (including all points) was ±20 MPa. Residual stress distributions along the specimens' longitudinal direction were obtained in one reference specimen and one misaligned specimen. In the rest of the specimens, only the residual stresses at weld toes were measured (see Table 5). In the misaligned specimens, it was assumed that the fatigue critical weld toes are weld IDs 1 and 2, see Fig. 4 welding sequence, and the residual stress measurements were only carried out at these welds. Fig. 5 shows the residual stress distributions in the longitudinal direction of a reference specimen (ID S11_NLCX_1, $e = 0$) and a misaligned specimen (ID S11_NLCX_15, $e = 9$ mm). As demonstrated in Fig. 4, no welding deformations were prevented in the test specimens and, thus, low and even compressive residual stresses were measured at the weld toes despite the specimens being in the as-welded condition, similarly to reported in Refs. [33, 34].

The weld geometries were measured using a 2D coordinate measuring device and the weld profile determined with a laser displacement sensor and inductive displacement transducer. From these measurements, the average weld toe radius of $r_{true,avg} = 0.3$ mm, flank angle of $\theta_{avg} = 44°$, and external throat thickness of $a_{avg} = 5.1$ mm were evaluated.

2.1.3. Fatigue test set-up

Fatigue tests were carried out using a servo-hydraulic fatigue testing machine with the test frequency of $f = 1$–3 Hz, using a constant amplitude uniaxial loading with an applied stress ratio of $R = 0.1$. Fig. 6 shows the specimen attached to the test rig. The failure criterion for the fatigue tests was the total rupture of the specimen.

2.2. Numerical analyses

2.2.1. Model configuration and validation

The principal aim of the numerical analyses is to obtain the stress concentration factors induced by NLCX joint plate misalignment. Following the separation of stress components into three categories, i.e. nominal stress, structural HS stress, and notch stress, the numerical analyses are carried out to obtain both structural and notch stresses. In a previous investigation [28], it was well recognized that the transverse attachment (NLCT) joint has significantly lower stress concentration than the NLCX joint. Consequently, notch and joint detail must be taken into account in the notch stress analysis, instead of only determining the structural stresses. Three different approaches are employed in the numerical study:

- Structural stress approach using the LSE method [35]
- Structural stress approach using the Xiao–Yamada method [31]
- Notch stress approach using the ENS concept ($r_{ref} = 1.0$ mm) [32]

Table 3
Test matrix.

Misalignment e [mm]	No. of specimens	Specimen ID
0	6	S11_NLCX_1–6
6	2	S11_NLCX_13–14
9	4	S11_NLCX_15–18
16	2	S11_NLCX_19–20

Table 4
GMAW parameters applied in the test specimen preparation. Shielding gas was Ar + 8% CO_2, and travel angle and working angle were 18° (pushing) and 45°, respectively.

Voltage U [V]	Current I [A]	Travel speed v_{travel} [cm/min]	Wire feed rate v_{wire} [m/min]
28.0–28.4	235–240	35.4	13.2

Table 5
Summary of residual stress measurements. n/a signifies not analyzed (welds 3 and 4 were not fatigue critical).

Offset	Residual stress σ_{res} [MPa]				Measured specimens
	Weld 1	Weld 2	Weld 3	Weld 4	
$e = 0$	−101	−117	−129	−93	S11_NLCX_1 – S11_NLCX_4
$e = 6$ mm	12	−22	n/a	n/a	S11_NLCX_13 – S11_NLCX_14
$e = 9$ mm	4	−8	n/a	n/a	S11_NLCX_15 – S11_NLCX_18
$e = 16$ mm	−44	36	n/a	n/a	S11_NLCX_19 – S11_NLCX_20

As the studied joint is assumed to represent a continuous transverse joint, a two-dimensional (2D) plane strain FE model is used in the analysis to obtain the stress concentrations. The geometries of the models were obtained from the fatigue tested specimens; base and attached plate thickness of $t_0 = t_1 = 8$ mm, and welded with the throat thickness of $a = 5.1$ mm and the flank angle of $\theta = 44°$ corresponding to the measured geometries described in Section 2.1.2.

In the LSE method, two different types of hot spot stresses are presented, i.e. type 'a' and type 'b', depending on whether there is a distinct through-thickness stress distribution or not. In the misaligned NLCX joint, the division into two types is indeterminable since the increase in misalignment changes the joint type from type 'a' to type 'b'. Thus, both methods are applied in the present study. A fine mesh is applied in accordance with the guided mesh sizes [35], see FE mesh details shown in Fig. 7, and the stresses are extrapolated from the proposed distances, as follows:

$$\sigma_{hs} = 1.67\sigma_{0.4t} - 0.67\sigma_{1.0t} \quad (1)$$

$$\sigma_{hs} = 1.5\sigma_{4\text{ mm}} - 1.5\sigma_{8\text{ mm}} + \sigma_{12\text{ mm}} \quad (2)$$

For the ENS method, the reference radius of $r_{ref} = 1.0$ mm was applied to assume the worst-case scenario for the transition from the base material to the weld ($r_{true} = 0$). For the fatigue life predictions using the 4R method [33], the radius of $r = r_{true} + 1$ mm $= 0.3$ mm $+ 1$ mm $= 1.3$ mm, was also applied. Otherwise, the models of the 4R method correspond to those of the ENS concept. As the notch stresses have been obtained from these models, a high mesh density and quadrilateral shape of elements are required for the convergence. The FE mesh size of r/20 was applied according to the study by Baumgartner and Bruder [36].

2.2.2. Parametric study on the effects of geometry parameters

In Section 2.2.1, the FE model geometry was specified according to the fatigue tested geometries. From these FEAs, the stress concentrations (HS and ENS methods) for the determination of *S–N* curves can be obtained. Nevertheless, it is worth noting that the magnitude of plate misalignment effect on the stress concentrations and, subsequently, on the fatigue strength of fillet-welded NLCX joints might vary based on the geometry configuration of the NLCX joint. Consequently, a parametric analysis of the effect of change in the geometry parameters on the magnitude of stress concentrations is investigated by conducting FEA.

The base plate thickness $t_0 = 8$ mm is held as a reference value, with the attached plate thickness and throat thickness varied. In considering a real joint configuration, the parametric study concerns are limited to only single-pass GMAW, for which a throat thickness of $a = 3.0$–6.0 mm can easily be reached with single-pass welding and, consequently a/t_0 ratios of 0.33, 0.50 and 0.66 were chosen for the analyses. In addition, three different plate thicknesses were tested: similar plate, and thinner and thicker plate thickness, see Fig. 8. Also, the infusible weld root width w was altered. In all cases, the fillet welds are modeled with a 45° flank angle. As a result, 27 geometry combinations are achieved, and when the plate misalignment was modeled using a 0.8 mm step size with a total number of 35 increments for each geometry combination (constant step size was used to simplify the element mesh modeling) from the ratios of $e/L = 0$ to $e/L = 1$. A total number of 1890 element models and analysis results are obtained.

2.2.3. Linear elastic fracture mechanics

2D LEFM analyses were carried out to evaluate the effect of misalignment on the fatigue strength prediction using a crack propagation-based analysis. In the conducted experiments, no initial defects or flaws, such as cold laps or sharp undercuts, were present, but LEFM analysis provides an insight into the results for NLCX joints with initial flaws. In addition, when considering the crack propagation of the studied joint types, it is noticeable that the early crack propagation is influenced by the presence of a notch induced by the weld toe. Whereas

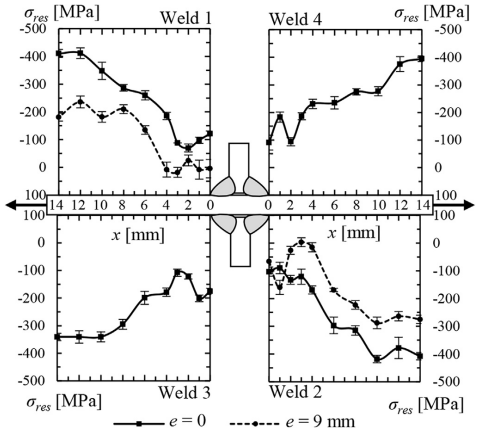

Fig. 5. Residual stress distribution and scatter values in a reference (ID S11_NLCX_1, $e = 0$) and a misaligned specimen (ID S11_NLCX_15, $e = 9$ mm).

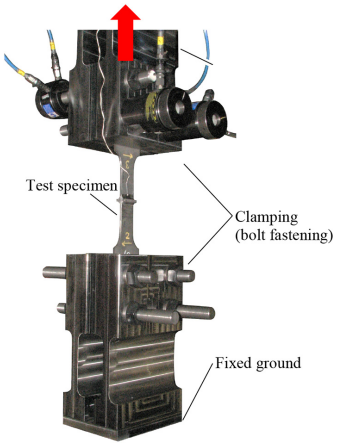

Fig. 6. Fatigue test set-up.

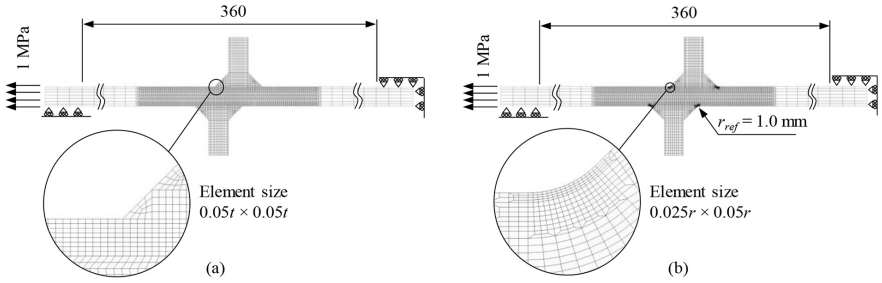

Fig. 7. FE model configurations: (a) HS models, and (b) ENS model.

for large fatigue cracks, general stress state and crack shape dominates the crack propagation.

Numerical analyses were carried out using the Franc2D software provided by Cornell University [37]. 2D element meshes of the studied NLCX joints were modeled, corresponding to the geometry presented in Section 2.2.1, see Fig. 9a. However, for the sake of similarity with the fatigue tested joints, a weld toe radius was modeled according to the measured average weld toe radius, $r_{true,avg} = 0.3$ mm. For the design purposes, IIW recommends an initial crack depth of $a_i = 0.1$ mm for sharp notches. In the FE modeling, crack of 0.025 mm was applied to the model, see Fig. 9b, which was subsequently propagated to achieve an initial crack depth of 0.1 mm. From a fatigue life viewpoint, the final crack depth does not have a major effect on the results. In this case, the final crack depth was $a_f = 7$ mm, i.e. $a_f/t = 0.875$, to confirm the stability of FE re-meshing when reaching the plate surface. The crack path was obtained using the maximum tangential stress criterion. A seed load of 1 MPa was used in the model, and afterwards multiplied with the stress range corresponding to the test load, see Table 6 in Section 3.1.

From the LEFM models, the SIF values (K_I and K_{II}) were obtained using a J-integral approach embedded in the software. The magnitude of K_{II} values is negligibly low in this case with respect to K_I values, so it can be ignored when assessing fatigue life. The crack propagation fatigue life can be obtained using Paris' law:

$$\frac{da}{dN} = C(\Delta K(a))^m \tag{3}$$

where a is crack depth, N is the number of cycles, C is the crack propagation coefficient, $\Delta K(a)$ is the SIF as a function of crack depth, and m is the slope of Paris' law.

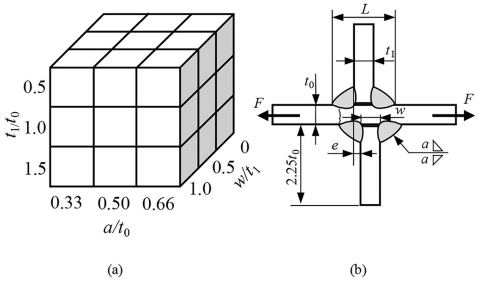

Fig. 8. (a) Analyzed geometry combinations, and (b) dimensions of the joint.

3. Results

3.1. Fatigue test results

A total number of 14 NLCX specimens, including six reference specimens without plate misalignment, and eight specimens with misalignment, were fatigue tested using uniaxial loading with an applied stress ratio of $R = 0.1$. All specimens failed at the weld toe, and, in the case of misaligned NLCX, the specimens failed at the inner weld toe, as shown in Fig. 10, due to the stress concentration induced by the plate misalignment. Numerical analyses were conducted, see Section 2.2, to obtain SCF for different stress criteria, i.e. structural HS stress using the LSE and Xiao–Yamada methods, together with the ENS approach with the reference radius of $r_{ref} = 1.0$ mm.

Table 6 summarizes the fatigue testing details, and Fig. 11 shows the fatigue data plots and obtained mean fatigue strength and scatter ranges values in a log-log coordinate system in comparison with the standard curves using different stress criteria, i.e. the nominal stress, structural HS stress (LSE and 1 mm depth methods), and ENS approaches. In the nominal stresses, the macrogeometric stresses induced by the angular distortions were also considered.

Using a free slope parameter and standard statistical evaluation of S–N curves, the mean fatigue strength can be evaluated for each series (misalignments of $e = 0$, 6, 9 and 16 mm). First, the slope parameters of S–N curves are evaluated for all data points, subsequently, the mean fatigue strength at two million cycles with a survival probability of $P_s = 50\%$ is obtained for each series, see Fig. 12. The characteristic design curves ($P_s = 97.7\%$) were not obtained within this study due to the low number of test specimens in the experimental program.

The angular distortions due to the welding were negligibly low and, consequently, no bending stress was present in the fatigue tests, and strain gages were not always positioned in the vicinity of failing weld toe. However, Fig. 13 exemplifies the strain gage measurements in the fatigue tests where strain gage was next to the failing weld toe. Based on the changes in the strain range $\Delta\varepsilon$, the crack initiation (CI) and crack propagation (CP) periods can be estimated.

3.2. Stress distributions and stress concentration factors

Numerical analyses were conducted to evaluate the stress concentration factors induced by the plate misalignment. Fig. 14 exemplifies the normal stress distributions at plate surfaces in the NLCX joint with equal plate thicknesses ($t_1 = t_0 = 8$ mm), and with a throat thickness of $a = 4$ mm. The structural stresses, obtained using the LSE method (type 'a'), are extrapolated at the given points. Fig. 14c shows that the inner and outer weld toe have identical notch stress but, due to the stress distribution at joint area, the LSE method estimates a structural SCF of less than 1.

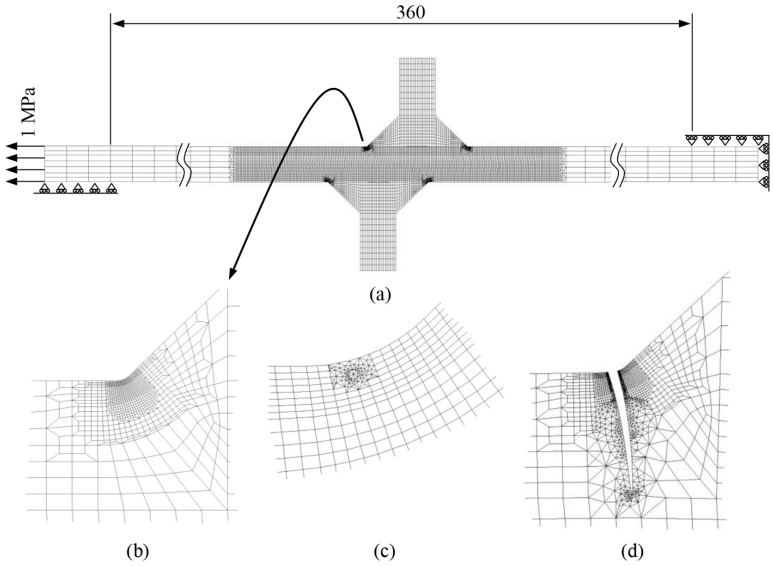

Fig. 9. 2D LEFM models: (a) full model with boundary conditions, (b) detailed view of the weld toe mesh, (c) initial crack of $a_i = 0.025$ mm, and (d) a propagated crack with the depth of $a = 1.5$ mm.

Table 6
Results of fatigue testing.

ID	e [mm]	$\Delta\sigma_{nom}$ [MPa]	$K_{s,m,\mathrm{LSE}}$ [−]	$K_{s,m,1\mathrm{mm}}$ [−]	$K_{tot,m}$ [−]	$N_{f,exp}$ [cycles]
S11_NLCX_1	0	312	1.0	1.0	2.30	72,872
S11_NLCX_2	0	317	1.0	1.0	2.30	82,578
S11_NLCX_3	0	247	1.0	1.0	2.30	169,415
S11_NLCX_4	0	241	1.0	1.0	2.30	169,322
S11_NLCX_5	0	205	1.0	1.0	2.30	496,828
S11_NLCX_6	0	196	1.0	1.0	2.30	528,328
S11_NLCX_13	6	206	1.37	1.17	2.85	214,769
S11_NLCX_14	6	168	1.37	1.17	2.85	547,795
S11_NLCX_15	9	206	1.48	1.17	2.74	217,244
S11_NLCX_16	9	244	1.48	1.17	2.74	124,297
S11_NLCX_17	9	169	1.48	1.17	2.74	596,207
S11_NLCX_18	9	188	1.48	1.17	2.74	463,560
S11_NLCX_19	16	206	1.34	1.12	2.48	253,715
S11_NLCX_20	16	168	1.34	1.12	2.48	883,148

To determine the effect of geometrical parameters, i.e. plate thickness (t_1/t_0), throat thickness (a/t_0), and degree of weld penetration (w/t_1) on the magnitude of SCF, parametric analyses were carried out. Fig. 15 summarizes the results of structural SCFs determined using the applied structural stress methods, and Fig. 16 presents the results of SCFs obtained using $r_{ref} = 1.0$ mm, i.e. the ENS method denoted with K_{tot}, including both the structural stress and notch effect.

3.3. Fatigue strength predictions

This section summarizes the numerical results obtained to evaluate the structural behavior of misaligned NLCX joints, as well as to predict the fatigue strength of such joints using different fatigue strength assessment approaches in comparison with the experimental fatigue test results. Table 7 presents the reference S–N curves of each stress-based fatigue strength assessment method and the crack propagation coefficients for LEFM. In both cases, the values are representative of characteristic values with the survival probability of $P_s = 97.7\%$.

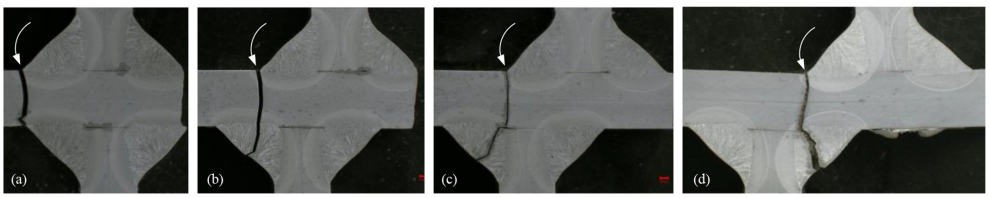

Fig. 10. Fatigue failures of the test specimens: (a) a reference specimen (S11_NLCX_1), (b) $e = 6$ mm, (c) $e = 9$ mm, and (d) $e = 16$ mm. White arrows show the weld toe location of an initiated fatigue crack.

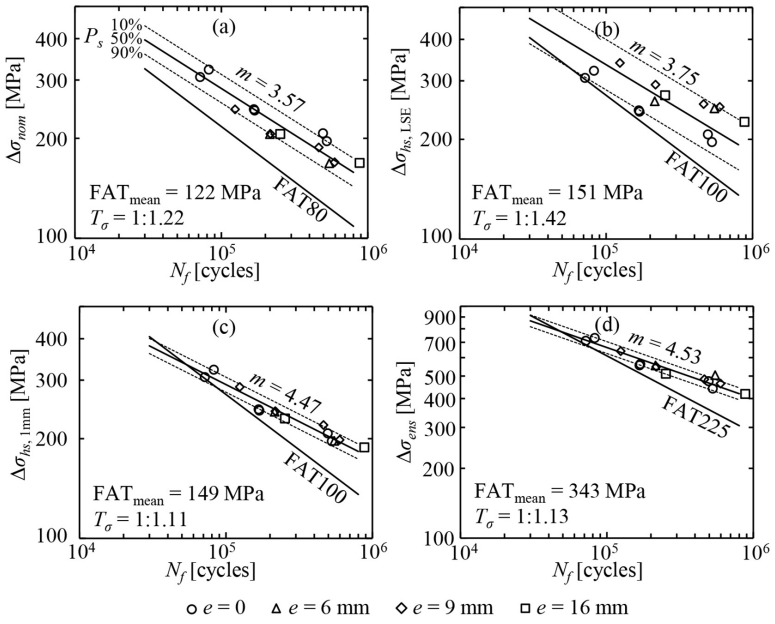

Fig. 11. *S–N* data plots using different stress criterion: (a) nominal stress, (b) structural HS stress using the LSE method, (c) structural HS stress using the Xiao-Yamada 1 mm depth stress, and (d) the ENS concept. All standardized reference *S–N* curves (characteristic, $P_s = 97.7\%$) have a slope parameter of $m = 3$ [7]. FAT is the fatigue strength (in MPa) at two million cycles.

Fig. 17 shows the predicted computational fatigue lives with respect to the experimental results.

4. Discussion

In the present study, the effect of plate misalignment on the fatigue performance of fillet-welded NLCX joints was evaluated by conducting experimental fatigue tests for NLCX fillet weld joints made of t = 8 mm S1100 UHSS grade. In addition, numerical analyses were carried out to investigate the stress concentrations induced by the misaligned, and the effect of geometry parameters (plate and throat thickness, and weld penetration) on the magnitude of SCFs, and to investigate the degree of misalignment (e/L ratio) inducing the maximum SCF. The SCFs were investigated using the structural HS stress-based methods, determined using the LSE method and Xiao–Yamada method [31], and the ENS method with the reference radius of $r_{ref} = 1.0$ mm. In addition, the fatigue life predictions were conducted with a multiparametric notch stress-based approach, the 4R method, and LEFM.

In prior investigations related to the topic [25,26], a low degree of misalignment was investigated by the fracture mechanics-based evaluation, and, in those studies, only minor effects on the fatigue life were found. As shown in this study, the maximum SCF (K_{tot}) is induced when the misalignment to the joint width ratio is e/L = 0.2–0.4, see

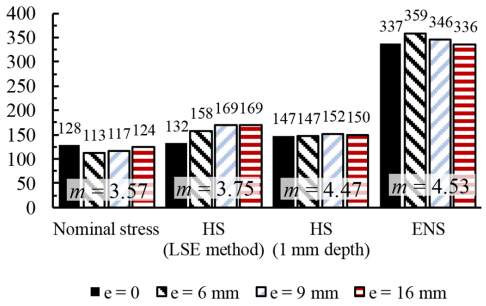

Fig. 12. Experimental mean fatigue strength ($P_s = 50\%$) value for different stress criteria using a free slope parameter of the *S–N* curve.

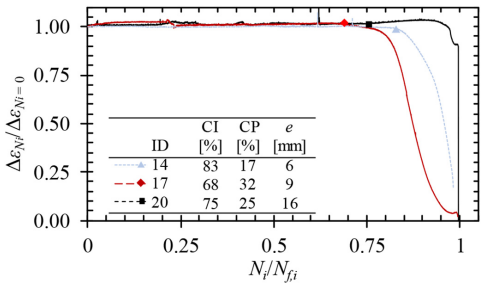

Fig. 13. Strain gage measurements during the fatigue tests: CI and CP periods of the total fatigue life, based on the strain drop at weld toe having a fatigue crack.

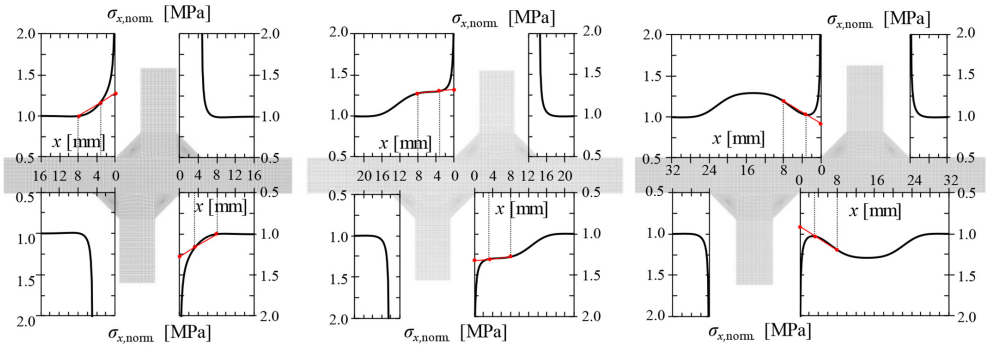

Fig. 14. Normalized normal stress ($\sigma_{x,norm.}$) distributions of the misaligned NLCX joints obtained using FEA: (a) $e/L = 0.25$, (b) $e/L = 0.75$ and (c) $e/L = 1.25$.

Figs. 15–16. Consequently, the fatigue strength is influenced by the misalignment. Experimental fatigue tests showed a decrease of 12% in fatigue strength for the misaligned joint compared to the joint without misalignment (corresponding to 36% in fatigue life) when using the nominal stress approach. Depending on the joint geometry, the maximum stress concentration induced by the misalignment is derived when the degree of misalignment is $e/L = 0.2$–0.4. As shown in a prior investigation [28], fillet-welded single-sided non-load carrying transverse (NLCT) joint has a lower notch SCF than a double-sided NLCX joint, which was also clearly indicated by this study as, when

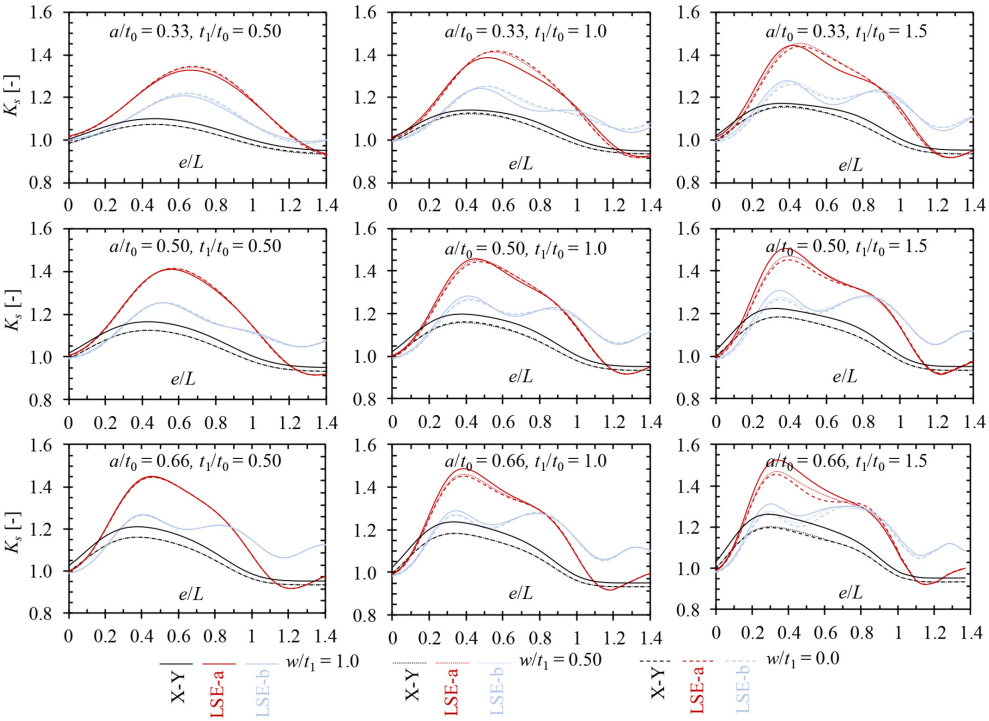

Fig. 15. Results of parametric analyses: structural SCFs obtained using the Xiao–Yamada (X-Y) method (1 mm below depth), 'a' type of LSE (LSE-a), and 'b' type of LSE (LSE-b).

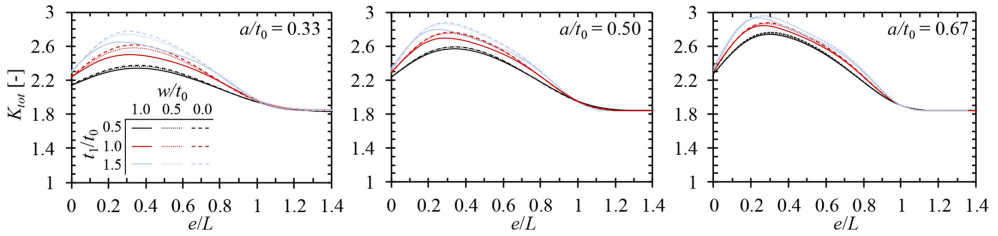

Fig. 16. Results of parametric analyses: SCFs in terms of the ENS system.

Table 7
Characteristic model parameters for different fatigue strength assessment approaches (units are in mm, MPa and N). C_{4R} is the fatigue capacity for the 4R method, σres is the residual stress, r is the weld toe radius applied in the FE model, H and n are the strain hardening coefficient and exponent, respectively, and C is the crack propagation coefficient.

Approach	Parameters	Ref.
Nominal stress	FAT80, $m = 3$	[7,38]
Structural HS stress	FAT100, $m = 3$	[7]
ENS	FAT225, $m = 3$	[7]
4R	$C_{4R} = 10^{17.94}$, $m = 4.65$ $\sigma_{res} = 0$, $R = 0.1$, $r = 1.3$ mm $H = 1391$ MPa, $n = 0.03$	[33]
LEFM	$C = 3.0{\cdot}10^{-13a}$, $m = 3$, $a_i = 0.1$ mm	[7]

[a] Based on the prior value. The current more conservative estimation is $C = 5.21{\cdot}10^{-13}$.

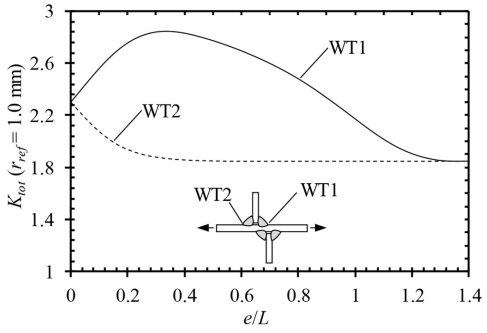

Fig. 18. Comparison of notch SCFs at outer and inner weld toes (WTs) for the tested specimens.

$e/L > 1.0$, the notch SCF for T joint is 80%–85% of the corresponding notch SCF of X joint, see Fig. 16. It is also worth noting that, in the case of T joint ($e/L > 1.0$), the joint geometry parameters do not have influence on the notch SCF; $K_{tot} = 1.84$ was derived for all geometries, while for the X joints ($e/L = 0$), the notch SCF depends on the joint geometry (throat thickness, the thickness of adjoined plate component, and weld penetration). The results of this study can also reflect on, for instance, welding-repaired fatigue cracks in welded components [39]; as the weld toes are not aligned after repairing, in axial loading the outer weld toe has lower stress concentration, as also demonstrated in Fig. 18.

When observing the applicability of local stress-based approaches for evaluating the effect of plate misalignment on the fatigue performance of the fillet welded NLCX joints, it was clearly indicated that the LSE method with extrapolation points (type 'a' or type 'b') is not able to evaluate the structural SCF correctly, because the extrapolation points are influenced by the through-thickness stress distribution of the adjacent (outer) weld toe. Consequently, more local approaches are needed for the fatigue analysis of misaligned joints. In this study, a structural stress method using stress value at the 1 mm depth after Xiao and Yamada [31], and the ENS concept were utilized in the fatigue assessments. Both methods showed good agreement with the experimental results, i.e. similar fatigue strengths were obtained for different misalignment degrees, see Fig. 12. However, it is worth noting that the magnitude of structural stress at the 1 mm depth is significantly influenced by the stress distribution in through-thickness direction, and for thicker or thinner plates the stress distribution is different.

Fig. 19 summarizes the fatigue test results in comparison with applied fatigue strength assessment approaches. The effect of plate misalignment is evaluated by comparing the fatigue strength of a misaligned ($e/L > 0$) NLCX joint to an NLCX joint without misalignment ($e/L = 0$) in terms of nominal stress applied in the base plate. In this regard, an LEFM-based evaluation on the plate misalignment effects gives

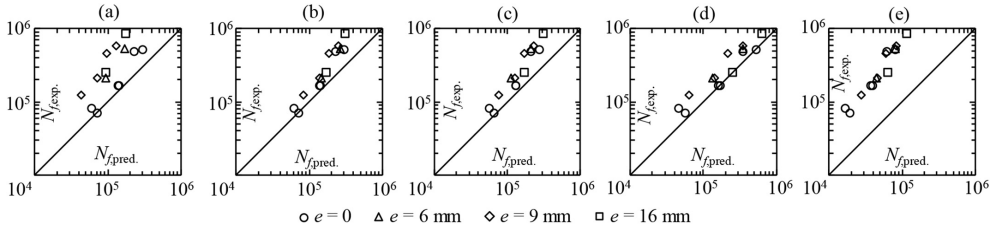

Fig. 17. Fatigue test results in comparison with predicted fatigue lives: (a) HS with LSE method, (b) Structural stress method using stress at 1 mm depth, (c) ENS method, (d) 4R method, and (e) LEFM.

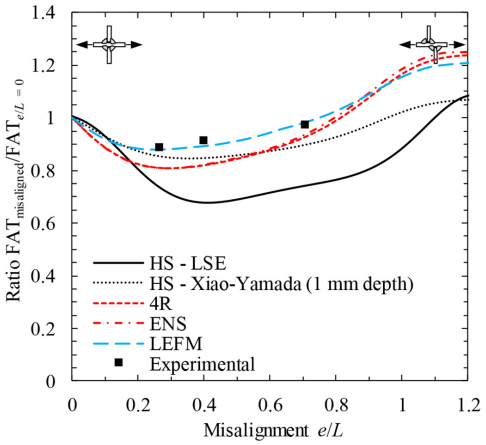

Fig. 19. Comparison of the effect of plate misalignment on the fatigue strength capacity converted to the nominal stress system.

the closest estimation with respect to the experimental result but, on the other hand, offers very conservative estimations for fatigue life, as clearly demonstrated in Fig. 17e, while Fig. 19 provides the proportional comparison of fatigue strengths only. When comparing the fatigue life predictions using different approaches, the notch-stress based system, the ENS method and particularly the 4R method all showed a good correspondence between the experimental lives, Fig. 17.

In the experiments of the present study, a robotized GMAW was employed to produce constant welding quality through all test welds and fatigue test specimens to diminish the effect of changes in weld geometry easily produced by manual welding. The changes in weld size alter the degree of misalignment along the weld, and the changes in local weld toe geometry have a significant influence on the notch stress concentration that may disable concluding the effects of misalignment. Nevertheless, the weldments of this study were prepared at the PB position (horizontal plate in the loading direction, see Fig. 4) and, consequently, quite a sharp transition was produced, i.e. $r_{true,avg} = 0.3$ mm. This signifies a rather sharp notch but, however, no initial fatigue crack was present at the weld toe, and the major share of total fatigue life, up to 80%, was comprised of the fatigue crack initiation period, as demonstrated in Fig. 13. Reflecting on the prior investigations of crack initiation share, the result is quite typical for welded UHSS joints [28,29]. By changing the welding procedure, or implementing post-weld treatments, the fatigue performance of weld toes in UHSS joints can be significantly improved [40,41], and the fatigue life is even more controlled by the local notch stress. Consequently, further experiments should be conducted for various weld toe qualities and applied stress ratios, and considerations made on the effect of plate misalignment on the fatigue strength of misaligned joints in the case of bending load.

5. Conclusions

In the present study, the fatigue strength of axially loaded misaligned thin-walled ($t = 8$ mm) NLCX joints was evaluated experimentally by conducting fatigue tests on NLCX joints made of S1100 UHSS material, and numerically conducting FEAs to determine the SCFs induced by the misalignments. Based on the results of the numerical and experimental studies, the following conclusions can be drawn:

- In the misaligned fillet-welded NLCX joints, the inner weld toe is the fatigue critical weld toe under axial cyclic loading, not the outer one due to stress concentration induced at the inner weld toe (see experimental fatigue failures in Fig. 10 and stress distributions in Fig. 14);
- The fatigue strength of NLCX joints decreases by up to 12% when a plate misalignment of adjoined plate components occurs. The maximum SCF occurs when the misalignment to joint width ratio is $e/L = 0.2$–0.4, while the misaligned joint has a lower SCF when the misalignment is more than $e/L = 0.6$–0.8, as the NLCT joints have lower notch SCF than the corresponding NLCX joints in axial loading;
- An increase in the plate thickness of the adjoined plate component or throat thickness results in higher magnitude of misalignment effect on the SCF. The degree of weld penetration has a negligibly small effect on the SCF, particularly in the case of the small plate thickness of adjoined plate component or large throat thickness;
- Notch stress-based methods seem to be applicable for evaluating the effect of plate misalignment on the fatigue performance of misaligned fillet-welded NLCX joint – a scatter range value of $T_\sigma = 1{:}1.13$ was found. A structural HS approach using the LSE method is not applicable for evaluating the SCF as the stress values at the extrapolation points are affected by the notch stress distribution of adjacent notch detail (see Fig. 11b and Fig. 14).

Declaration of Competing Interest

The authors declare that they have no known competing financial interests or personal relationships that could have appeared to influence the work reported in this paper.

Acknowledgements

This work was supported by Business Finland in the Intelligent Steel Applications (ISA) project (Grant ID: 7386/31/2018). Furthermore, the authors wish to thank SSAB Europe for their funding of experimental fatigue testing.

References

[1] H. Ban, G. Shi, A review of research on high-strength steel structures, Struct. Build. 171 (2018).
[2] C. Miki, K. Homma, T. Tominaga, High strength and high performance steels and their use in bridge structures, J. Constr. Steel Res. 58 (2002) 3–20, https://doi.org/10.1016/S0143-974X(01)00028-1.
[3] C.M. Sonsino, Light-weight design chances using high-strength steels, Mater. Sci. Eng. Technol. 38 (2007) 9–22, https://doi.org/10.1002/mawe.200600090.
[4] A.M.P. De Jesus, R. Matos, B.F.C. Fontoura, C. Rebelo, L. Simões Da Silva, M. Veljkovic, A comparison of the fatigue behavior between S355 and S690 steel grades, J. Constr. Steel Res. 79 (2012) 140–150, https://doi.org/10.1016/j.jcsr.2012.07.021.
[5] P.J. Haagensen, S.J. Maddox, IIW Recommendations on Methods for Improving the Fatigue Strength of Welded Joints, Woodhead Publishing, 2013.
[6] G.B. Marquis, Z. Barsoum, IIW Recommendations for the HFMI Treatment - for Improving the Fatigue Strength of Welded Joints, Springer Singapore, Singapore, 2016 https://doi.org/10.1007/978-981-10-2504-4.
[7] A. Hobbacher, Recommendations for Fatigue Design of Welded Joints and Components, 2nd ed. Springer International Publishing, Cham, 2016.
[8] DNVGL-RP-C203, Fatigue Design of Offshore Steel Structures, 2016.
[9] BS7608:2014 +A1:2015, Guide to Fatigue Design and Assessment of Steel Products, 2015.
[10] L. Eggert, W. Fricke, H. Paetzold, Fatigue strength of thin-plated block joints with typical shipbuilding imperfections, Weld. World. 56 (2012) https://doi.org/10.1007/BF03321402.
[11] I. Lotsberg, Stress concentrations due to misalignment at butt welds in plated structures and at girth welds in tubulars, Int. J. Fatigue 31 (2009) 1137–1345, https://doi.org/10.1016/j.engfailanal.2016.11.006.
[12] H. Remes, W. Fricke, Influencing factors on fatigue strength of welded thin plates based on structural stress assessment, Weld. World. 58 (2014) 915–923, https://doi.org/10.1007/s40194-014-0170-7.
[13] A.J. Pachoud, P.A. Manso, A.J. Schleiss, New parametric equations to estimate notch stress concentration factors at butt welded joints modeling the weld profile with splines, Eng. Fail. Anal. 72 (2017) 11–24, https://doi.org/10.1016/j.engfailanal.2016.11.006.
[14] M. Dabiri, M. Ghafouri, H. Rohani Raftar, T. Björk, Utilizing artificial neural networks for stress concentration factor calculation in butt welds, J. Constr. Steel Res. 138 (2017) 488–498, https://doi.org/10.1016/j.jcsr.2017.08.009.

[15] M.J. Ottersböck, M. Leitner, M. Stoschka, W. Maurer, Analysis of fatigue notch effect due to axial misalignment for ultra high-strength steel butt joints, Weld. World. 63 (2019) 851–865, https://doi.org/10.1007/s40194-019-00713-4.
[16] H. Jakubczak, G. Glinka, Fatigue analysis of manufacturing defects in weldments, Int. J. Fatigue 8 (1986) 51–57, https://doi.org/10.1016/0142-1123(86)90053-8.
[17] M. Skorupa, Fatigue life prediction of cruciform joints failing at the weld toe, Weld. Res. (1992) 269–276.
[18] R.M. Andrews, The effect of misalignment on the fatigue strength of welded cruciform joints, Fatigue Fract. Eng. Mater. Struct. 19 (1996) 755–768, https://doi.org/10.1111/j.1460-2695.1996.tb01320.x.
[19] R. Goyal, G. Glinka, Fracture mechanics-based estimation of fatigue lives of welded joints, Weld. World. 57 (2013) 625–634, https://doi.org/10.1007/s40194-013-0060-4.
[20] S. Xing, P. Dong, P. Wang, A quantitative weld sizing criterion for fatigue design of load-carrying fillet-welded connections, Int. J. Fatigue 101 (2017) 448–458, https://doi.org/10.1016/j.ijfatigue.2017.01.003.
[21] C. Cui, Q. Zhang, Y. Bao, J. Kang, Y. Bu, Fatigue performance and evaluation of welded joints in steel truss bridges, J. Constr. Steel Res. 148 (2018) 450–456, https://doi.org/10.1016/j.jcsr.2018.06.014.
[22] Y. Dong, C.G. Soares, On the fatigue crack initiation point of load-carrying fillet welded joints, in: C. Guodes Soares, R. Dejhalla, D. Pavletic (Eds.),Towar. Green Mar. Technol. Transp 2015, pp. 407–416, https://doi.org/10.1201/b18855.
[23] A. Ahola, T. Björk, Z. Barsoum, Fatigue strength capacity of load-carrying fi llet welds on ultra-high-strength steel plates subjected to out-of-plane bending, Eng. Struct. 196 (2019) 109282, https://doi.org/10.1016/j.engstruct.2019.109282.
[24] R. Ghafoori-Ahangar, Y. Verreman, Fatigue behavior of load-carrying cruciform joints with partial penetration fillet welds under three-point bending, Eng. Fract. Mech. 215 (2019) 211–223, https://doi.org/10.1016/j.engfracmech.2019.05.015.
[25] L. Zong, G. Shi, Y.Q. Wang, Z.X. Li, Y. Ding, Experimental and numerical investigation on fatigue performance of non-load-carrying fillet welded joints, J. Constr. Steel Res. 130 (2017) 193–201, https://doi.org/10.1016/j.jcsr.2016.12.010.
[26] H. Su, J. Wang, J. Du, Fatigue behavior of uncorroded non-load-carrying bridge weathering steel Q345qDNH fi llet welded joints, J. Constr. Steel Res. 164 (2020) 105789, https://doi.org/10.1016/j.jcsr.2019.105789.
[27] M.M.P. Mbeng, Effective Notch Method Assessment of Misalignment for Fatigue Loaded Welds, Master's thesis Lappeenranta University of Technology, 2007.
[28] A. Ahola, T. Nykänen, T. Björk, Effect of loading type on the fatigue strength of asymmetric and symmetric transverse non-load carrying attachments, Fatigue Fract. Eng. Mater. Struct. 40 (2017) 670–682, https://doi.org/10.1111/ffe.12531.
[29] M.J. Ottersböck, M. Leitner, M. Stoschka, W. Maurer, Crack initiation and propagation fatigue life of ultra high-strength steel butt joints, Appl. Sci. 9 (2019) https://doi.org/10.3390/app9214590.
[30] E. Niemi, W. Fricke, S.J. Maddox, Structural Hot-Spot Stress Approach to Fatigue Analysis of Welded Components, 2nd Editio, Springer Singapore, Singapore, 2017 https://doi.org/10.1007/978-981-10-5568-3.
[31] Z.G. Xiao, K. Yamada, A method of determining geometric stress for fatigue strength evaluation of steel welded joints, Int. J. Fatigue 26 (2004) 1277–1293, https://doi.org/10.1016/j.ijfatigue.2004.05.001.
[32] C.M. Sonsino, W. Fricke, F. De Bruyne, A. Hoppe, A. Ahmadi, G. Zhang, Notch stress concepts for the fatigue assessment of welded joints - background and applications, Int. J. Fatigue 34 (2012) 2–16, https://doi.org/10.1016/j.ijfatigue.2010.04.011.
[33] A. Ahola, T. Skriko, T. Björk, Fatigue strength assessment of ultra-high-strength fillet weld joints using 4R method (in press), J. Constr. Steel Res. (2019) https://doi.org/10.1016/j.jcsr.2019.105861.
[34] T. Skriko, M. Ghafouri, T. Björk, Fatigue strength of TIG-dressed ultra-high-strength steel fillet weld joints at high stress ratio, Int. J. Fatigue 94 (2017) 110–120, https://doi.org/10.1016/j.ijfatigue.2016.09.018.
[35] E. Niemi, W. Fricke, S.J. Maddox, Fatigue Analysis of Welded Components: Designer's Guide to the Structural Hot-Spot Stress Approach, 2nd Editio, Springer Nature, Singapore, 2018 https://doi.org/10.1533/9781845696665.
[36] J. Baumgartner, T. Bruder, An efficient meshing approach for the calculation of notch stresses, Weld. World. 57 (2013) 137–145, https://doi.org/10.1007/s40194-012-0005-3.
[37] Cornell Fracture Group, Software, http://cfg.cornell.edu/software/ 2020 (accessed January 9, 2020).
[38] EN 1993-1-9, Eurocode 3 - Design of steel structures - Part 1–9: Fatigue, 2005.
[39] J. Schubnell, A. Sarmast, E. Carl, M. Farajian, P. Ladendorf, P. Knödel, T. Ummenhofer, Fatigue performance of repaired welded joints made of S355 and S960 steel, 72nd IIW Annu. Assem. Int. Conf. - Comm. XIII - WG2, 2019.
[40] J. Berg, N. Stranghöner, Fatigue behaviour of high frequency hammer peened ultra high strength steels, Int. J. Fatigue 82 (2016) 35–48, https://doi.org/10.1016/j.ijfatigue.2015.08.012.
[41] A. Ahola, T. Skriko, T. Björk, Experimental investigation on the fatigue strength assessment of welded joints made of S1100 ultra-high-strength steel in as-welded and post- weld treated condition, 7 Th Int. Conf. Struct. Eng. Mech. Comput., Cape Town, South Africa 2019, pp. 1–6.

Publication III

Ahola, A., Björk, T., and Barsoum, Z.

Fatigue strength capacity of load-carrying fillet welds on ultra-high-strength steel plates subjected to out-of-plane bending

Reprinted with permission from
Engineering Structures
Vol. 196, 109282, 2019

Engineering Structures 196 (2019) 109282

Contents lists available at ScienceDirect

Engineering Structures

journal homepage: www.elsevier.com/locate/engstruct

Fatigue strength capacity of load-carrying fillet welds on ultra-high-strength steel plates subjected to out-of-plane bending

A. Ahola[a,*], T. Björk[a], Z. Barsoum[b]

[a] School of Energy Systems, Lappeenranta-Lahti University of Technology LUT, P.O. Box 20, FI-53851 Lappeenranta, Finland
[b] Department of Aeronautical and Vehicle Engineering, KTH Royal Institute of Technology, Teknikringen 8, SE-10044 Stockholm, Sweden

ARTICLE INFO

Keywords:
Fatigue assessment
Welded joints
Weld root fatigue strength
Bending
Ultra-high-strength steel
Load-carrying joint

ABSTRACT

Weld root fatigue strength capacity is an important design criterion in load-carrying (LC) fillet welded joints subjected to cyclic loads. This paper elaborates on the weld root fatigue strength capacity of fillet welded LC joints made of ultra-high-strength steel (UHSS) and subjected to out-of-plane bending. Experimental fatigue tests are carried out using constant amplitude loading with an applied stress ratio of $R = 0.1$ with both pure axial, i.e. DOB = 0 (degree of bending, bending stress divided by total stress) and bending, i.e. DOB = 1.0, load conditions. The applicability of different approaches – nominal weld stress, effective notch stress concepts, and 2D linear elastic fracture mechanics (LEFM) – for the fatigue strength assessment of weld root capacity is evaluated. Furthermore, a parametric LEFM analysis is used to evaluate the effect of weld penetration on the root fatigue strength capacity in axial and bending loading. The results indicate that in the case of bending, nominal weld stress can be calculated using the linear stress distribution over the joint section and FAT36 as a reference curve. In the bending loading, for the joints failing from the weld toe, a mean fatigue strength of up to 185 MPa in the nominal stress system was achieved, indicating that the reference curve FAT63 is overly conservative. The ENS concept with FAT225 seemed to be slightly unconservative for assessing the root fatigue strength capacity. LEFM analyses revealed that in the case of increasing weld penetration and bending loading, weld root fatigue strength capacity seemed to correlate with the nominal weld stress calculated using effective weld throat thickness, while in axial loading, weld stress should be calculated using external throat thickness summed with penetration length.

1. Introduction

Lightweight structures have a reduced environmental impact as they allow a decrease in material usage, weight, and production resources used. The introduction of lightweight structures is connected to the possibility of using high-strength steel (HSS). Higher structural performance and energy efficiency of metal structures is increasingly required in many fields, such as in the automotive, construction and offshore industry. The objective to optimize structures with the minimized weight and cost, and increase thus the structural performance and energy efficiency, pose challenges for the designers and analysts. Structures made of HSS or ultra-high-strength steel (UHSS) plates incorporate typically welding, and an awareness regarding the potential failure mechanisms is also needed. One of the main challenges when using HSS to achieve lightweight design of welded structures and components is to obtain high weld quality and simultaneously, minimize the scatter of quality in manufacturing. Other important aspects are the accurate assessment of the fatigue life of welded structures and adequate concepts for these assessments. One of the critical steps in the fatigue life assessment of welded structures is the adequate determination of effective stress, which is one of the uncertainty parameters that results in a variation in the life estimation. A common engineering practice is to consider the most conservative approach, which often leads to unnecessarily over dimensioned welded joints and structures.

Weld root fatigue strength capacity, due to unpenetrated weld or insufficient throat thickness, is an essential design criterion in load-carrying (LC) joints. Depending on the weld size and its location, the share of secondary bending stresses at the adjoined plate member, and potentially conducted post-weld treatments, a fatigue crack may initiate from the weld toe or the weld root [1–3]. Fatigue strength capacity of the weld root can be assessed using stress-based approaches, i.e. nominal stress, hot spot (HS) stress or effective notch stress (ENS) or using fracture mechanics and crack propagation analysis. Of these, the nominal stress method is the most elementary of the fatigue assessment

* Corresponding author.
E-mail address: antti.ahola@lut.fi (A. Ahola).

https://doi.org/10.1016/j.engstruct.2019.109282
Received 20 December 2018; Received in revised form 6 June 2019; Accepted 6 June 2019

approaches. In a pure axial loading, the nominal weld stress (NWS) range $\Delta\sigma_w$ is calculated at the shortest ligament of the weld, usually corresponding to throat thickness, and fatigue life is obtained using characteristic reference curve FAT36 [4–6].

For LC joints with throat bending, structural weld stress methods have been established. Fricke et al. [7] proposed a method that is based on the structural stress at the weld leg length following the failure path of the root failure. Alternatively, structural stress can be calculated at the throat section following the procedure proposed by Sørensen et al. [8]. However, these methods have not been officially included in the design codes and guidelines, and are thus not the focus of this study. In more complex structural components, the ENS concept can be applied for the fatigue assessment of the weld root using the reference radius r_{ref} = 1.00 mm and the reference curve FAT225 or FAT200 for the maximum principal or von Mises stress criterion, respectively [9]. Recently, Sundermeyer et al. [10] analyzed and tested partially and fully penetrated single-sided welded thick-walled T-joints (t = 24.5 mm), indicating that the increasing penetration depth improved the fatigue strength of the weld root in terms of the ENS system. In the partially penetrated joints with an initial crack due to an infusible weld root face, FAT225 appeared to be unconservative. This issue was also previously reported by Fricke and Kahl [11] for fillet welded hollow sections with an end or intermediate plate. In their studies, the fatigue test results barely exceeded the FAT225 reference curve.

Due to the insidious characteristics of root side failures, i.e. the fact that the failure cannot be visually monitored until the crack has propagated through the weld or parent material, the fatigue strength properties of LC joints have been comprehensively investigated in recent decades. Also, different load conditions, such as shear loading and multiaxial loads, have come under investigation. Kim et al. [12] studied the effect of the direction of uniaxial loading, i.e. the share of shear load component, on the fatigue capacity of LC joints. Khurshid et al. [13] and Frendo and Bertini [14] investigated tubular joints subjected to multiaxial loads. However, the vast majority of previous experimental studies [15] have focused on single- or double-sided fillet welds where the adjoined plate member is subjected to axial membrane loading having only secondary bending due to the angular distortion or the axial offset of adjoined plate members, as in [16] . Supposedly, there are two main reasons for this: Firstly, the root fatigue capacity of double-sided fillet welded joints subjected to bending is much higher than joint subjected under axial tension and consequently, careful consideration of potential root fatigue is particularly required in the case of axial loading [17–19]. Secondly, due to complexity of bending test procedure, axial tension tests have been preferred [20].

The existence of bending stresses induced by external bending loading, axial misalignment or angular distortion in an adjoined plate member, see Fig. 1, cannot totally be neglected and should be taken into account in fatigue strength assessment. Moreover, current design codes do not give instructions for the consideration of bending stresses in the weld root fatigue strength assessment of double-sided fillet welded joints. Fatigue strength properties of non-load carrying joints made of HSS or UHSS have been widely studied in recent years but less attention has been paid to the root fatigue strength properties of strength-matching weld metals.

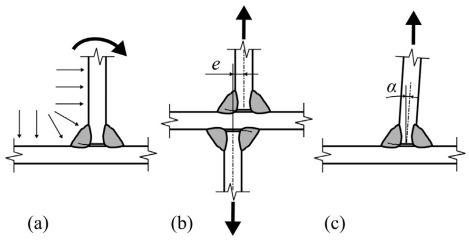

Fig. 1. Fillet welded LC joints where bending stresses are induced by: (a) external bending loading or structural discontinuity, (b) plate axial offset, and (c) angular misalignment.

This paper evaluates the root side fatigue strength capacity of double-sided fillet welded LC joints made of UHSS. Experimental fatigue tests were carried out using constant amplitude loading with an applied stress ratio of R = 0.1. The focus of this paper is on DOB = 1.0 (degree of bending, bending stress divided by total stress) out-of-plane loading but DOB = 0 axial loading was also considered to have a reasonable comparison between different load conditions. Hereby, an analytical fatigue assessment procedure for the calculation of the weld root stresses under bending loading is proposed. Furthermore, the paper discusses the applicability of the ENS approach and two-dimensional linear elastic fracture mechanics (LEFM) for the fatigue assessment of root side failures and the effect of weld penetration on the root side fatigue strength capacity of double-side fillet welded joints.

2. Experimental program

2.1. Materials

Experimental fatigue tests were carried out for LC joints made of direct-quenched S960 MC sheet metals. With the direct-quenching, high mechanical properties can be obtained with the minimized need for the alloying. Böhler Union X96 (Ø1.0 mm), which is a strength-matching filler material for S960 steels, was used in the preparation of the test specimens. The chemical compositions and mechanical properties of the base and filler materials are presented in Table 1 and Table 2, respectively. In Tables 1 and 2, the measured items represent the values obtained from the material certificate provided by the material supplier.

2.2. Test specimens

Load carrying fillet welded joints were fabricated of t = 9 mm S960 MC plates using a gas metal arc welding (GMAW) process (1 3 5) [21] and a welding robot to achieve a uniform metallurgical quality and weld reinforcement geometry. Two types of test specimens were fabricated: For the axial (DOB = 0) tests, specimens with widenings for clamping, Fig. 2a, and for the bending (DOB = 1.0) tests, specimens with a uniform width, Fig. 2b, were fabricated. Due to the high weld root fatigue capacity of bending loaded joints, small throat thicknesses were preferred and a = 4 mm throat thickness was solely pursued within these joints. In the axially loaded joints, the weld root is more critical than weld toe and consequently, both a = 4 mm and a = 5 mm target throat thicknesses were manufactured and tested; see Table 4. In two specimens (FWB_DYN7 and FWB_DYN8), double beveling was used to test the effect of weld penetration and reinforcement location on the fatigue strength capacity. In the other specimens, no groove preparation was conducted. The main welding parameters are presented in Table 3 for the two different throat thicknesses. The realized values are presented in Table 4.

Preliminary tests, conducted for joints in AW condition and subjected to a DOB = 1 loading, indicated that the weld root fatigue capacity was substantially higher than the weld toe, resulting in fatigue failures from the weld toe, see Table 5 in Section 2.4. Consequently, high frequency mechanical impact (HFMI) treatment was employed at the weld toe in the remaining specimens to achieve a fatigue failure from the weld root. The HFMI treatment resulted in improved weld toe geometry in terms of a higher toe radius and beneficial compressive residual stresses; see Fig. 3. Plate surface normal residual stresses parallel to the loading direction were measured using an X-ray diffractometer (Stresstech Xstress G3000) in the selected specimens representing the test series. Table 4 presents the test matrix and conducted procedures for each specimen. In Table 4, n/a refers to not

Table 1
Chemical compositions of the studied materials [weight-%].

Material	Type	C	Si	Mn	P	S	Cr	Ni	Mo	Cu	Nb	N
S960 MC	maximum	0.12	0.25	1.30	0.02	0.01						
	measured	0.097	0.20	1.09	0.008	0.001	1.13	0.38	0.191	0.033	0.001	0.005
Union X96	nominal*	0.12	0.8	1.9			0.45	2.35	0.55			

* Undiluted weld metal

relevant for the specimens failing from the weld toe.

2.3. Test set-up

For joints subjected to out-of-plane bending, a four-point bending device producing a constant bending moment with no shear stress between the inner press rolls was assembled; see Fig. 4b. For joints subjected to axial loading, a conventional test rig, whereby the specimen is clamped to jaws, was used; see Fig. 4a. In both test set-ups, the force was produced using a servo-hydraulic cylinder. During tests, the minimum and maximum of applied load and displacements were recorded. Despite almost nonexistent secondary bending stresses due to the straightness of specimens and the loading type in the case of bending, each specimen was instrumented with a strain gage at a $0.4\,t = 3.6$ mm distance from the weld toe. The failure criterion for the end of a test was a fracture of the specimen.

2.4. Results

Table 5 presents the fatigue test results for all tested joints. In the axially loaded specimens that failed from the weld root, the weld stress range is calculated for the gross weld area according to the design codes [4–6,23] as follows:

$$\Delta\sigma_w = \frac{t}{2a_{eff}}\Delta\sigma \tag{1}$$

where t is the plate thickness, a_{eff} is the effective throat thickness (considering the weld penetration; see Table 4) and $\Delta\sigma$ is the maximum nominal stress at the adjoined plate component; see Fig. 5. Respectively, for the bending loaded specimens, an elastic stress distribution in the gross cross section of the weld areas, as this paper proposes, was assumed. A similar concept regarding elastic stress distribution for single-sided welds has been applied previously by Sundermeyer et al. [10]. By adopting this concept concerning the reference weld root stress in bending loading, for double-sided fillet welded joints, the corresponding elastic stress range at the weld root is:

$$\Delta\sigma_w = \frac{\Delta M c}{I} = \frac{\frac{\Delta\sigma t^2}{6}\frac{w}{2}}{\frac{(w+2a_{eff})^3 - w^3}{12}} = \frac{\Delta\sigma t^2 w}{6a_{eff}w^2 + 12wa_{eff}^2 + 8a_{eff}^3} \tag{2}$$

where ΔM is the moment range acting on the adjoined plate component, I is the second moment of area, w is the width of the non-fused weld root and c is the distance from the neutral axis to the weld root ($c = w/2$ in the case of symmetric welds); see Fig. 5.

In both loading types, the penetration obtained by macro graphic investigations, see Fig. 8 and Table 4, was included in the calculation of the root stress to obtain more conservative results. Only the specimens with an observable failure from weld root (WR) were considered in the calculation of the root fatigue strength; see Table 5. The joints failing from the weld toe, i.e. the AW joints FWB_DYN1-3 and FWB_DYN7-8, were included in the analysis of the weld toe fatigue strength, respectively. The test results of the FWB_DYN4 and FWB_DYN13 specimens were excluded from further analysis since they failed from the base material. For the ENS system, 2D FEA was employed to obtain SCF $k_t(r_{ref} = 1\text{ mm})$ values, and to convert nominal plate stress to ENS at weld root or weld toe depending on the failure location. A more detailed description of the FE modeling can be found in Section 3.

The mean fatigue strength for each approach, was calculated using the standard procedure according to the IIW Recommendations [4], i.e. stress as an independent variable and fatigue life as the dependent variable. In the joints failing from the weld root, only the fixed slope of the S-N curve ($m = 3$) was used in the fatigue strength assessment; see Fig. 6. For the weld root failures, the FAT36 characteristic design curve following the IIW Recommendations [4] and EC3 [5] was chosen for a comparison.

The test results of the joints with a toe failure indicated that a shallower slope would fit the test data more comprehensively, and consequently, both m = free and $m = 3$ regression analyses were conducted; see Fig. 7. No distinct improvement, however, was found in the joints with partial K-groove preparation with regard to purely fillet welded joints; see Fig. 7. For that reason, all weld toe failure test results were included in the same regression analysis. In the case of bending loading, it must be considered that no secondary bending stress is induced by the angular distortion, and the nominal stress is thus equal to the structural hot spot stress.

3. Numerical analysis

3.1. Computational fatigue capacity

Two-dimensional (2D) plane strain modeling was employed when computational fatigue strength capacities were obtained for the tested joints. The ENS concept and LEFM were applied in the analysis. Preprocessing and analysis of the ENS models were carried out using FEMAP/NxNastran v11.4.0 (Siemens PLM Software), and the crack propagation analysis and subsequent stress intensity factor (SIF), $\Delta K(a)$ evaluation was conducted using Casca/Franc2D v4 distributed by Cornell University [24]. The crack paths were calculated using maximum tangential stress criterion at the crack tip and SIFs were obtained utilizing the J-integral approach implemented in the Franc2D software. The geometry for each model was modeled following the measured geometry. The throat thicknesses and width of unpenetrated root gap were measured from the polished section at the center of the crack, as presented in Section 2.4, Fig. 8. As shown in Fig. 8, neither excessive convexity nor concavity were found in the weldments, which could have affected the fatigue strength capacity. Consequently, the weld

Table 2
Mechanical properties of the studied materials.

Material	Type	Proof strength $R_{p0.2}$ [MPa]	Ultimate strength R_m [MPa]	Ultimate elongation A [%]	Min. impact toughness KVC [J]
S960 MC	nominal	960	980–1250	7	27 (-40 °C)
	measured	1041	1210	11	65 (-40 °C)
Union X96	nominal	930	980	14	80 (+20 °C) 47 (-50 °C)

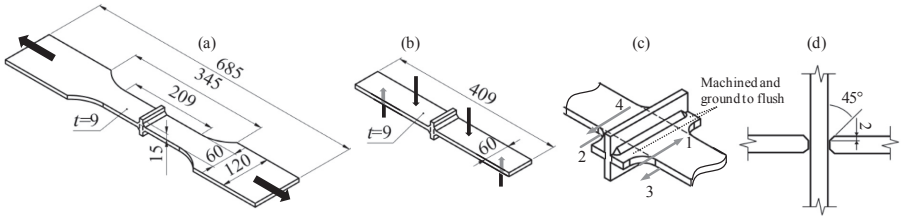

Fig. 2. Shape (after removing weld run-on and run-off parts) and dimensions of the test specimens: (a) axially and (b) bending loaded LC joints; (c) sequence of welds and preparation of the specimens; and (d) partial K-groove preparation used in the FWB_DYN7 and FWB_DYN8 specimens (all dimensions in mm).

profile was simplified in terms of modeling only triangle-shaped geometry, as shown in Figs. 9 and 10.

Fig. 11 illustrates the notch stress distribution along the circumference of the fictitious radius in terms of normalized stress and the maximum principal stress criterion (SCF = $\sigma_{max}/\sigma_{nom}$). The maximum values were used as representative SCFs in the fatigue strength assessment in the ENS concept, see Table 5 and Figs. 6 and 7. In bending loading, the maximum SCF = 0.73–0.81 was induced at approximately 100°, i.e. 10°from leg length section in the direction of the attached plate. In axial loading, the maximum SCF = 3.85–3.93 was at 80°, i.e. 10°from the leg length section in the direction of the weld reinforcement. The locations of the maximum SCFs correspond well to the directions of early crack propagation; see Fig. 8.

Computational fatigue lives were obtained using mean S-N curves and the crack propagation coefficient (C_{mean}) for stress-based approaches and LEFM analyses, respectively. In the case of nominal stress and ENS approaches, mean S-N curves were obtained from characteristic design curves using safety factor of j_σ = 1.37 [25] representing the usual scatter bandwidth and failure probability of 2.3% (mean – 2Stdv). Thus, the computational mean fatigue strengths are 49 MPa (FAT36) for the nominal stress approach, and 308 MPa (FAT225) for the ENS concept. Paris' law and a numerical integrator were used when predicted fatigue life $N_{f,pred}$ was obtained using an LEFM-based analysis:

$$N_{f,pred} = \int_{a=a_i}^{a=a_f} \frac{da}{C \cdot \Delta K(a)^m} \tag{3}$$

where a_i is the initial crack depth, a_f is the final crack depth, C is the crack propagation coefficient, $\Delta K(a)$ is the SIF range as a function of crack depth, and m is the slope of Paris' law. For the LEFM and subsequent fatigue life analysis, the mean values of crack propagation coefficients m and C were applied. Currently, the IIW Recommendations [4] propose $C_{char} = 5.21 \cdot 10^{-13}$ (da/dN in mm/cycle and ΔK in MPa·mm$^{1/2}$) , which was chosen as the reference crack propagation coefficient in this study. C_{mean} was obtained using the same ratio between C_{char} and C_{mean} as in [26,27], i.e. 3.0/1.7 = 1.76, resulting in $C_{mean} = 5.21 \cdot 10^{-13}/1.76 = 2.95 \cdot 10^{-13}$. In addition, the computational design fatigue lives were also obtained using the characteristic crack propagation coefficient. Fig. 12 presents the results for the computational fatigue lives with respect to the test results. Excluding one axially loaded test specimen (FWB_DYN15), the experimental fatigue life was higher than the predicted design fatigue life in all approaches. In general, the ENS system seems to be slightly unconservative, or there is no redundant safety with respect to the experimental test results. When using the LEFM or NWS system, there is no major difference between these approaches. Using LEFM and NWS, the predicted mean fatigue lives correspond quite well to the experimental test results, and on the other hand, design fatigue lives are distinctly lower compared with the experimentally obtained fatigue lives.

3.2. Efficiency of weld penetration on improving fatigue strength capacity

Weld penetration plays an important role when assessing the weld root fatigue strength of LC joints. On the basis of the LEFM-based analysis, Maddox [28] showed that decreasing the infusible root face improves the weld root fatigue strength proportionally more than the weld toe capacity. However, previous studies have focused only on LC joints subjected to axial loading. Consequently, a parametric analysis on the effect of an increasing degree of weld penetration on the improvement level of the weld root fatigue strength capacity was carried out. The objective of this analysis was to investigate whether weld stress, see Eqs. (1) and (2), should be calculated on the basis of effective throat thickness or leg length (external throat thickness summed with penetration length).

The analyses were conducted for a geometry corresponding to the tested specimens, i.e. a t = 9 mm LC joint with symmetric double-sided fillet welds. A total number of four different throat thicknesses were analyzed; a/t = 1/3, a/t = 1/2 and a/t = 2/3 with a flank angle of θ = 45°. Four different degrees of weld penetration were analyzed, focusing on the small degree of penetration, i.e. p/t = 0 (no penetration), p/t = 0.05, p/t = 0.1, p/t = 0.15 and p/t = 0.2 resulting in the total number of 30 LEFM analyses when both pure tensile and bending load conditions were considered. Otherwise, the model configuration, and boundary and load conditions were similar to the ones presented in Fig. 10. The improvement level was assessed relatively by comparing the fatigue strength capacity of the weld with penetration with welds without penetration as follows (LEFM data points in Figs. 13 and 14):

$$k = \frac{FAT_{\text{penetrated}}}{FAT_{\text{fillet weld}}} = \frac{\left(\frac{N_{f,i}}{2{\cdot}10^6}\right)^{\frac{1}{m}}\Delta\sigma}{\left(\frac{N_{f,p=0}}{2{\cdot}10^6}\right)^{\frac{1}{m}}\Delta\sigma} = \frac{N_{f,i}^{\frac{1}{m}}}{N_{f,p=0}^{\frac{1}{m}}} \tag{4}$$

where index i corresponds to the penetrated case $p = i$. In addition, the

Table 3
Welding parameters for the different target throat thicknesses (a_{target}): average value measured for each pass and the corresponding standard deviations (stdv). Heat input Q calculated according to EN 1011-1 [22] using a thermal efficiency of k = 0.8 for the GMAW process.

a_{target} [mm]	Pass ID	Type	Current I [A]	Voltage U [V]	Travel speed v [mm/s]	Wire feed rate w [m/min]	Heat input Q [kJ/mm]
4	1–4	average	233	27.6	9.5	13.2	0.54
4		stdv	1.4	0.15	*	*	$3.2{\cdot}10^{-3}$
5	1–4	average	232	28.3	5.9	13.2	0.90
5		stdv	0.76	0.11	*	*	$3.1{\cdot}10^{-3}$

* Pre-set constant value for the welding robot, no variation

Table 4
Test matrix and weld reinforcement geometry. a_1 and a_2 are the throat thicknesses of the failed weld pair (the welds 1 and 3, or the welds 2 and 4; see Fig. 2c), $a_{i,eff}$ is the corresponding effective throat thickness calculated considering the weld penetration, w is the width of the non-fused weld root, and ΔM_{exp} and ΔF_{exp} are the experimental test moment and force, respectively. AW signifies the as-welded condition.

Specimen ID	Load type A = axial B = bending	Test condition	Groove preparation	a_1 [mm]	a_2	$a_{1,eff}$	$a_{2,eff}$	w	ΔM_{exp} [Nm]	ΔF_{exp} [kN]
FWB_DYN1	B	AW	–	3.7	3.7	n/a	n/a	n/a	278	–
FWB_DYN2	B	AW	–	3.4	3.4	n/a	n/a	n/a	263	–
FWB_DYN3	B	AW	–	3.8	3.8	n/a	n/a	n/a	223	–
FWB_DYN4	B	HFMI	–	n/a	n/a	n/a	n/a	n/a	306	–
FWB_DYN5	B	HFMI	–	4.0	4.1	4.9	4.9	6.7	371	–
FWB_DYN6	B	HFMI	–	4.1	4	4.8	4.7	7.0	412	–
FWB_DYN7	B	AW	Partial K	3.2	3.2	n/a	n/a	n/a	344	–
FWB_DYN8	B	AW	Partial K	3.6	3.6	n/a	n/a	n/a	257	–
FWB_DYN9	B	HFMI	–	4.0	4.2	4.8	4.9	6.8	512	–
FWB_DYN10	B	HFMI	–	4.1	3.9	4.9	4.8	6.6	430	–
FWB_DYN11	B	HFMI	–	4.2	4	5	4.8	6.7	485	–
FWB_DYN12	B	HFMI	–	3.8	3.7	4.6	4.5	6.7	548	–
FWB_DYN13	B	HFMI	–	n/a	n/a	n/a	n/a	n/a	439	–
FWB_DYN14	A	HFMI	–	4.2	4	4.8	4.6	7.2	–	81.6
FWB_DYN15	A	HFMI	–	3.9	4.3	4.6	5.1	6.9	–	55.3
FWB_DYN16	A	HFMI	–	4.5	5.1	5	5.5	7.7	–	73.2
FWB_DYN17	A	HFMI	–	4.7	5.3	5.2	5.7	7.7	–	64.2

Table 5
Fatigue test results.

Specimen ID	Loading type A = axial B = bending	$\Delta\sigma$ [MPa]	$\Delta\sigma_w$ [MPa] Eqs. (1) and (2)	$\Delta\sigma_{ens}$ [MPa]	N_f [10^3 cycles]	Failure location WR = weld root WT = weld toe BM = base material
FWB_DYN1	B	344	n/a	660	192	WT
FWB_DYN2	B	325	n/a	632	343	WT
FWB_DYN3	B	275	n/a	528	1 163	WT
FWB_DYN4	B	378	n/a	n/a	946	BM
FWB_DYN5	B	458	60	334	774	WR
FWB_DYN6	B	509	69	392	556	WR
FWB_DYN7	B	424	n/a	809	128	WT
FWB_DYN8	B	317	n/a	599	486	WT
FWB_DYN9	B	632	84	461	324	WR
FWB_DYN10	B	531	70	393	557	WR
FWB_DYN11	B	599	78	454	506	WR → WT + BM
FWB_DYN12	B	676	102	547	229	WR → BM
FWB_DYN13	B	542	n/a	n/a	418	BM
FWB_DYN14	A	153	145	593	120	WR
FWB_DYN15	A	103	95	395	320	WR
FWB_DYN16	A	136	117	536	206	WR
FWB_DYN17	A	119	99	461	290	WR

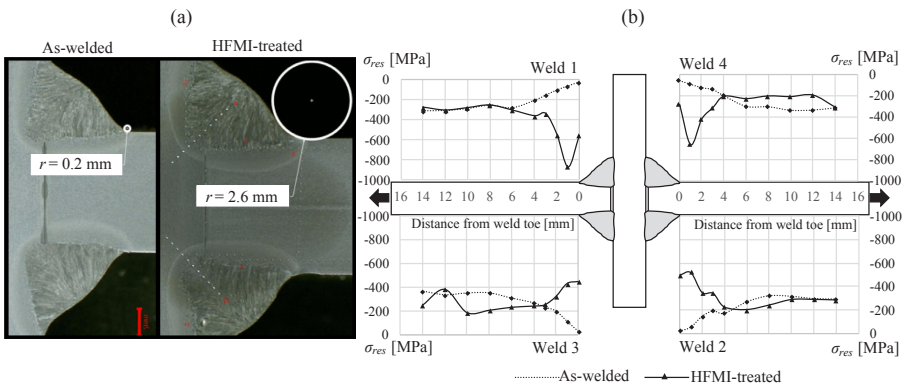

Fig. 3. (a) Weld toe geometry; (b) surface residual stress distribution along specimen surface in as-welded and HFMI-treated conditions.

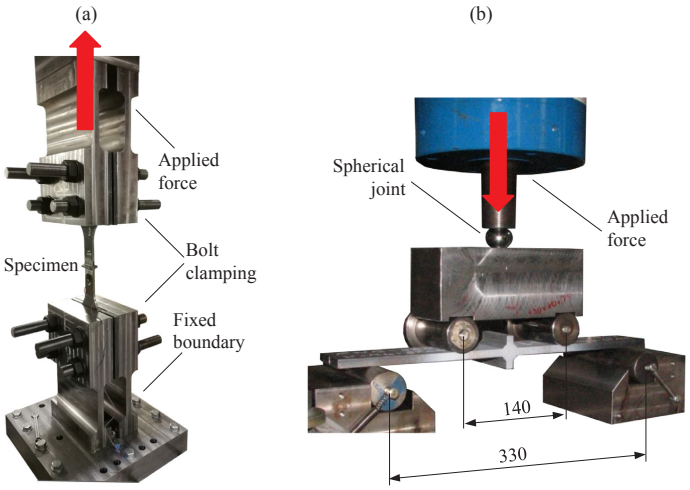

Fig. 4. Test set-ups: (a) axial and (b) bending tests.

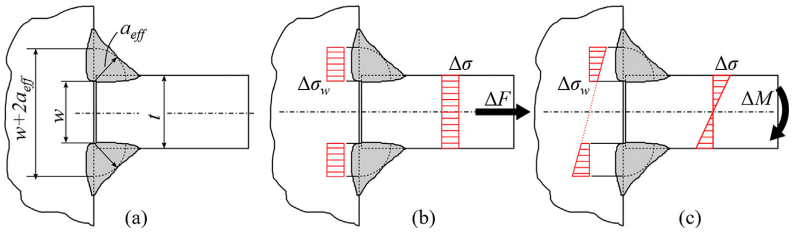

Fig. 5. (a) Dimensions of LC joints, and weld stresses for (b) axially and (c) bending loaded specimens in terms of the nominal stress system.

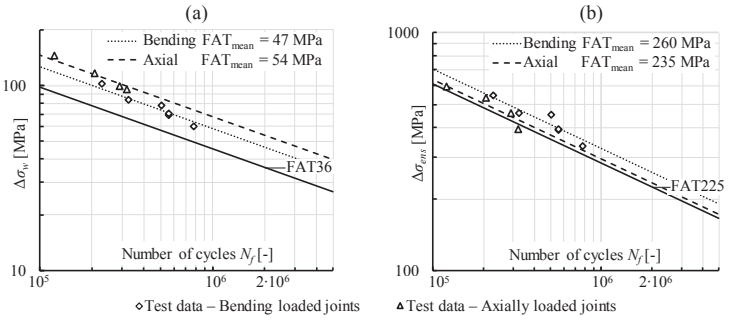

Fig. 6. Fatigue test results for joints with root failure and the derived S-N curves in terms of (a) the NWS and (b) ENS system. The slope of the S-N curve $m = 3$ is used in all cases.

improvement level was assessed using Eqs. (1) and (2) for axial and bending loading, respectively. Effective throat thickness a_{eff} (solid black line, Figs. 13 and 14) and external throat thickness summed with penetration length, i.e. $a + p$ (dashed black line, Figs. 13 and 14) were used as reference lengths for the fatigue strength assessment. In the axial loading, the fatigue strength capacity is linearly dependent on the length of the ligament (a_{eff} or $a + p$) but in the case of bending loading, the length of the ligament has a quadratic effect on the fatigue strength capacity; see Eqs. (1) and (2).

4. Discussion

In this study, the weld root fatigue strength capacity of double-sided fillet welds on steel plates subjected to out-of-plane bending was

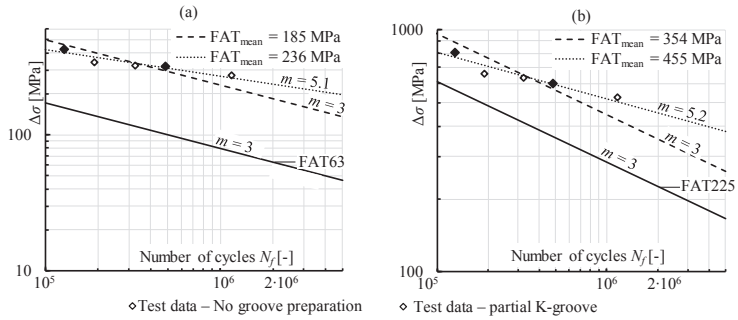

Fig. 7. Fatigue test results for bending loaded joints with toe failure and the derived S-N curves in terms of (a) NWS = HS stress, (b) ENS system.

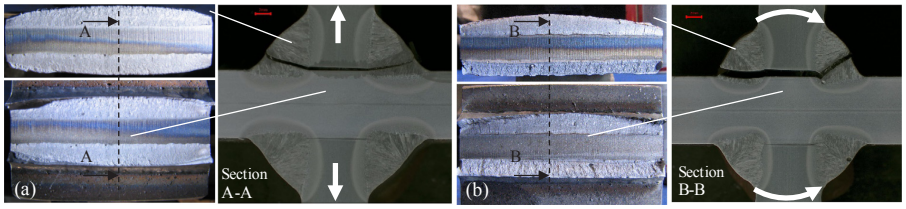

Fig. 8. Typical fracture surface and failure paths in (a) axially loaded joints (FWB_DYN17) and (b) bending loaded joints (FWB_DYN5).

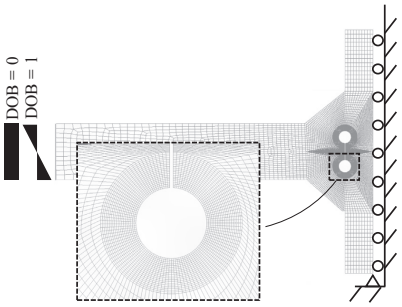

Fig. 9. ENS model with the reference radius of r_{ref} = 1.0 mm and showing the load and boundary conditions.

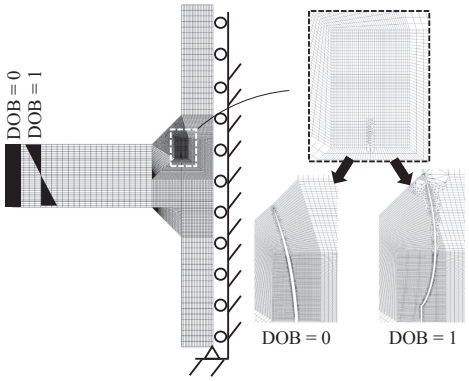

Fig. 10. Casca/Franc2D LEFM model with the initial and final cracks.

experimentally and numerically investigated. In the joints subjected to out-of-plane bending, nominal weld stresses were derived using linear-elastic stress distribution over the joint section, and the stress value at the non-propagated notch root (see Fig. 5 and Eq. (2)) was used as the basis for the calculation procedure.

In both the axial and bending load cases, effective throat thickness was used to consider the weld penetration in the tested joints. Using this approach, mean fatigue strengths of 47 MPa for bending loaded joints and 54 MPa for axially loaded joints, with the S-N curve slope of $m = 3$, were acquired; see Fig. 6. Since a reasonable accordance in the fatigue strengths between the axially and bending loaded joints was achieved using a linear elastic stress distribution over the joint section, it can be proposed for design purposes. However, it must be recognized that this proposal is based on a limited number of test results, and further experimental verification should be conducted for various plate and throat thickness ratios and for other steel materials. It is also worth noting that the crack paths for the axial and bending loading vary, see Figs. 8 and 10, and consequently, further experimental and numerical studies should be conducted considering different DOB ratios to see the combined effect of different load components on the root side fatigue strength capacity.

In terms of the ENS system, mean fatigue strengths computed separately for the axially and bending loaded joints (see Fig. 6b) exceeded the characteristic design curve FAT225. For bending loaded joints mean fatigue strength of 260 MPa was obtained, while for axially loaded joints, mean fatigue strength was 235 MPa. However, when considering the usual scatter in the design curves, the test results did not achieve the computed mean fatigue strength of 308 MPa (j_σ = 1.37) that has been also obtained for butt-welded joints with toe failure by Nykänen and Björk [29]. The unconservative nature of the use of the ENS concept for the fatigue strength assessment of root side failures has been

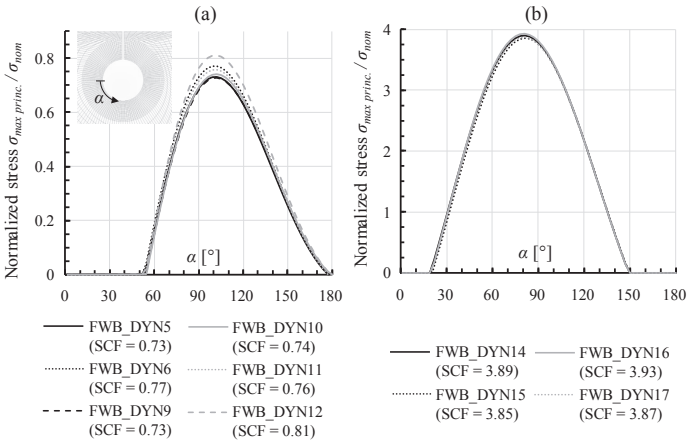

Fig. 11. Normalized stress along the circumference of fictitious notch radius, and the obtained SCFs for test specimens: (a) bending and (b) axially loaded joints.

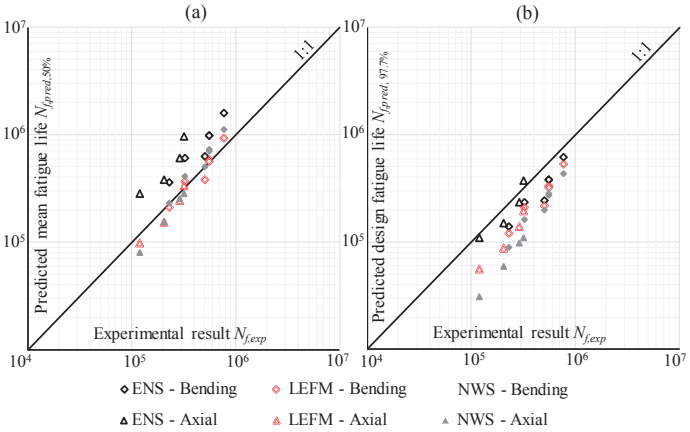

Fig. 12. Correlation between predicted fatigue life and experimental test result using (a) computational mean fatigue strength coefficients and (b) characteristic design coefficients in different fatigue strength assessment approaches.

exemplified in the previous works undertaken by Sundermeyer et al. [10] and Fricke and Kahl [11]. On the other hand, the weld root fatigue strength capacity is mainly associated with the gross ligament, i.e. throat thickness in fillet welds, and residual stress field at the weld root. Thus, the scatter in the test results is lower in the case of weld root failure than weld toe failure. However, since reasonably margin with respect to the FAT225 design curve was not found, a detailed scrutiny on the designed and realized weld throat thickness and penetration should be supervised.

In structural design and analysis, the weld penetration should be generally neglected unless a consistent weld penetration can be trustworthily achieved [30] and confirmed by non-destructive testing, such as radiographical or ultrasonic inspection. However, the consideration of weld penetration is of paramount importance when deriving the S-N curves since it significantly affects the obtained weld stress values. Further insight into the previous studies conducted in the field of weld root fatigue does not fully reveal whether the weld penetration was considered or weld stresses were calculated on the basis of external throat thickness. In this study, macrographic investigations, see Fig. 8 and Table 4, were conducted for each failed specimen to measure the length of the infusible weld root. These measures were used in the subsequent analyses to obtain analytical weld stresses and to create finite element models for the ENS system and LEFM. In addition, a parametric analysis was conducted to investigate the effect of weld penetration on the root side fatigue strength capacity. This analysis revealed that in the case of bending loading, the improvement level corresponded to the analytical weld stress calculated on the basis of the effective throat thickness (a_{eff}), as shown in Fig. 13. Respectively, in the case of axial loading, the improvement level corresponded to the analytical weld stress calculated based on the external throat thickness summed with weld penetration; see Fig. 14. An explanatory factor for this issue has been presented in Fig. 15, in which the normalized stress distribution through the leg length section is plotted. The stress distributions were obtained from FE models of which detailed element

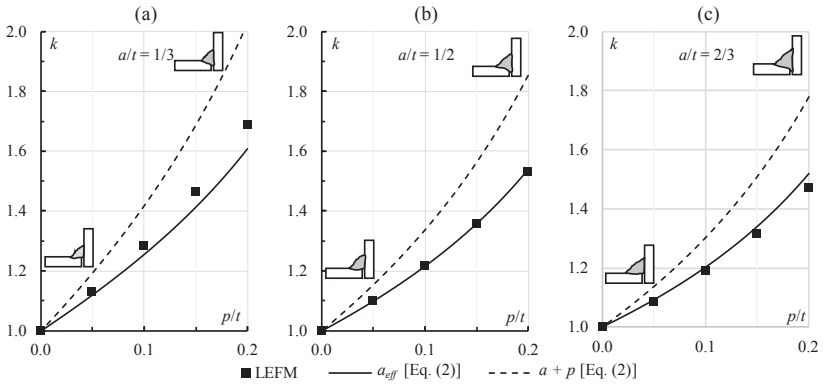

Fig. 13. Improvement level of weld root fatigue strength capacity in the bending loading using LEFM-based analysis for the different a/t ratios; (a) $a/t = 1/3$, (b) $a/t = 1/2$ and (c) $a/t = 2/3$.

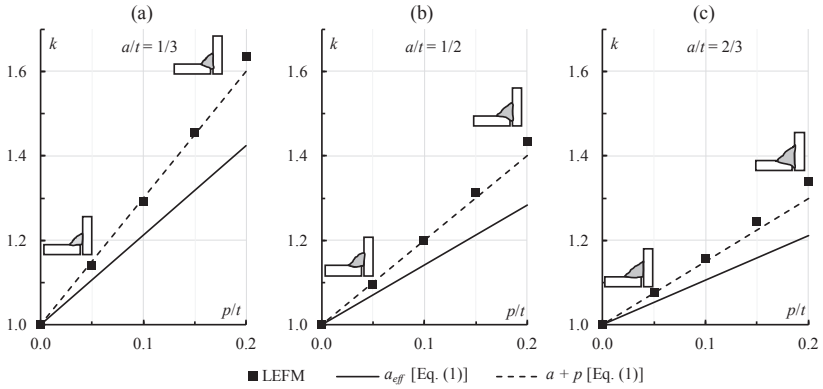

Fig. 14. Improvement level of weld root fatigue strength capacity in the axial loading using LEFM-based analysis for the different a/t ratios; (a) $a/t = 1/3$, (b) $a/t = 1/2$ and (c) $a/t = 2/3$.

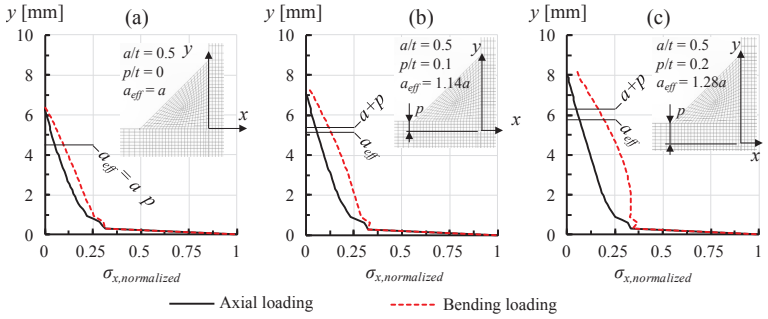

Fig. 15. Normalized normal stress ($\sigma_x/\sigma_{x,peak}$) distribution along the leg length section with different weld penetration lengths obtained by the FEA; (a) $p/t = 0$, (b) $p/t = 0.1$ and (c) $p/t = 0.2$.

meshes are shown in Fig. 15. Otherwise, the joint dimensions, and load and boundary conditions followed the models described in Figs. 9 and 10. In the case of axial loading, the stress distribution is constantly decreasing through the leg length section while in the bending loading, a curved stress distribution can be seen and the top of the weld reinforcement near the weld toe does not sustain any significant load. Consequently, in the bending loading, the leg length is not fully effective near the weld toe, particularly when considering the analytical stress distribution shown in Fig. 5, and the weld root fatigue strength in the bending loading seems to correlate with the effective throat thickness.

Root side fatigue strength capacities were computed employing numerical methods. 2D plane strain models were used to obtain the SCFs for the ENS concept and the SIFs for the LEFM analysis. For a comparison, fatigue strength capacities were also obtained using an analytically determined NWS. Fig. 12 shows the results of these analyses, indicating that both the analytical and LEFM analyses resulted in a good correspondence with the experimental results. When using characteristic design coefficients, a reasonable safety margin between the characteristic design life (survival probability of 97.7%) and the experimental result was obtained. The ENS concept gave, again, unconservative results.

Within this study, the tests were carried out using the external stress ratio of $R = 0.1$, and the results are thus applicable for the joints subjected to the pulsating load conditions. Depending on the contact mechanism within the base plate and adjoined plate component, single-pass fillet weld may induce high compressive residual stress at the weld root [31,32], which makes the fatigue strength capacity susceptible to the external stress ratio. Nevertheless, for similar LC joints and filler materials used in this study, Ahola et al. [33] reported only 15% decrease in the weld root fatigue strength capacity when increasing the external stress ratio from $R = 0.1$ to $R = 0.5$. Due to these discrepancies, the further studies should pay attention to the formation of residual stress at the weld root in the UHSS materials, and to the effect of external stress ratio on the weld root fatigue strength capacity.

5. Conclusions

In the present paper, numerical and experimental analyses of the fatigue behavior of LC joints made of UHSS were carried out. According to the results of this study, the following conclusions can be drawn:

- Linear elastic stress distribution over the joint section can be used as a basis for the nominal weld stress (NWS) calculation for the bending loading. The characteristic FAT36 design curve for weld root failure, according to the design codes and guidelines [4–6], is applicable in this case.
- No significant improvement was found in the case of ultra-high-strength filler materials when weld root fatigue crack propagation was the critical design criterion. However, the FAT63 design curve for the toe failure in the bending loading was overly conservative. Furthermore, fatigue strength in terms of the ENS concept was very high in bending loading, whereby mean fatigue strength of 354 MPa ($m = 3$) was obtained for the joints failing from the weld toe. Plate bending stress induces a lower SCF than membrane stress; secondly, a stress gradient in the through thickness direction contributes to the achievement of a high fatigue strength.
- In bending, the fatigue strength improvement level at the weld root by increasing the weld penetration seems to correlate with the effective throat thickness, i.e. the shortest ligament, while in axial loading, the fatigue strength improvement seems to correlate with the external throat thickness summed with the weld penetration length.
- LEFM ($C_{mean} = 2.95{\cdot}10^{-13}$ √mm/MPa·cycle) and the NWS system (computational mean fatigue strength of 49 MPa) estimate the mean fatigue lives with a reasonable margin of error for both axial and bending loading. Respectively, considering the fatigue test results of this study and previous work on fillet welded joints, the ENS system gives unconservative fatigue life estimations for weld root failures.

Acknowledgements

This work was supported by Business Finland in the Digi-TuoTe project. In addition, the authors wish to thank M.Sc. (Tech.) Markus Haajanen for the significant contribution in the management of experimental testing.

References

[1] Xing S, Dong P, Wang P. A quantitative weld sizing criterion for fatigue design of load-carrying fillet-welded connections. Int J Fatigue 2017;101:448–58. https://doi.org/10.1016/j.ijfatigue.2017.01.003.
[2] Cui C, Zhang Q, Bao Y, Kang J, Bu Y. Fatigue performance and evaluation of welded joints in steel truss bridges. J Constr Steel Res 2018;148:450–6. https://doi.org/10.1016/j.jcsr.2018.06.014.
[3] Singh PJ, Achar DRG, Guha B, Nordberg H. Fatigue life prediction of gas tungsten arc welded AISI 304L cruciform joints with different LOP sizes. Int J Fatigue 2002;25:1–7. https://doi.org/10.1016/S0142-1123(02)00067-1.
[4] Hobbacher A. Recommendations for Fatigue Design of Welded Joints and Components. 2nd ed. Cham: Springer International Publishing; 2016.
[5] EN 1993-1-9. Eurocode 3 - Design of steel structures - Part 1-9: Fatigue, 2005.
[6] DNVGL-RP-C203. Fatigue Design of Offshore Steel Structures, 2016.
[7] Fricke W, Kahl A, Paetzold H. Fatigue assessment of root cracking of fillet welds subject to throat bending using the structural stress approach fatigue assessment of root cracking of fillet welds subject to throat bending using the structural stress approach for structural stress. Weld World 2006;50:64–74. https://doi.org/10.1007/BF03266538.
[8] Sørensen JD, Tychsen J, Andersen JU, Brandstrup RD. Fatigue analysis of load-carrying fillet welds. J Offshore Mech Arct Eng 2006;128:65. https://doi.org/10.1115/1.2163876.
[9] Sonsino CM, Fricke W, De Bruyne F, Hoppe A, Ahmadi A, Zhang G. Notch stress concepts for the fatigue assessment of welded joints - Background and applications. Int J Fatigue 2012;34:2–16. https://doi.org/10.1016/j.ijfatigue.2010.04.011.
[10] Sundermeyer W, Fricke W, Paetzold H. Investigation of weld root fatigue of single-sided welded T-joints. In: Soares Guedes C, Shenoi RA, editors. Anal. Des. Mar. Struct. V, London: Taylor & Francis Group; 2015, p. 309–15.
[11] Fricke W, Kahl A. Fatigue assessment of weld root failure of hollow section joints by structural and notch stress approaches. In: Packer JA, Willibald S, editors. Proc. 11th Int. Conf. Tubul. Struct., 2006, p. 593–600.
[12] Kim IT, Kainuma S. Fatigue life assessment of load-carrying fillet-welded cruciform joints inclined to uniaxial cyclic loading. Int J Press Vessel Pip 2005;82:807–13. https://doi.org/10.1016/j.ijpvp.2005.07.004.
[13] Khurshid M, Barsoum Z, Däuwel T, Barsoum I. Root fatigue strength assessment of fillet welded tube-to-plate joints subjected to multi-axial stress state using stress based local methods. Int J Fatigue 2017;101:209–23. https://doi.org/10.1016/j.ijfatigue.2017.02.007.
[14] Frendo F, Bertini L. Fatigue resistance of pipe-to-plate welded joint under in-phase and out-of-phase combined bending and torsion. Int J Fatigue 2015;79:46–53. https://doi.org/10.1016/j.ijfatigue.2015.04.020.
[15] Gurney TR, MacDonald K. Literature survey on fatigue strengths of load-carrying fillet welded joints failing in the weld. Report OTH 1995;91:356.
[16] Jakubczak H, Glinka G. Fatigue analysis of manufacturing defects in weldments. Int J Fatigue 1986;8:51–7.
[17] Song W, Liu X, Razavi SMJ. Fatigue assessment of steel load-carrying cruciform welded joints by means of local approaches. Fatigue Fract Eng Mater Struct 2018:1–16. https://doi.org/10.1111/ffe.12870.
[18] Radaj D, Helmers K. Bewertung von Scheißverwindungen hinsichtlich Schwingfestingkeit nach dem Kerbspannungskonzept (in German). Konstruktion 1997;49:21–7.
[19] Lie ST, Lan S. A boundary element analysis of misaligned load-carrying cruciform welded joints. Int J Fatigue 1998;20:433–9. https://doi.org/10.1016/S0142-1123(97)00133-3.
[20] Kang W, Kim WS, Paik YM. Fatigue strength of fillet welded steel structure under out-of-plane bending. Int J Korean Weld Soc 2002;2:33–9.
[21] EN ISO 4063. Welding and allied processes. Nomenclature of processes and reference numbers (Corrected version 2010-03-01)., 2018.
[22] EN 1011-1. Welding - Recommendations for welding of metallic materials - Part 1: General quidance for arc welding, 2009.
[23] BS7608:2014 +A1:2015. Guide to Fatigue Design and Assessment of Steel Products, 2015.
[24] Cornell University. Software 2018. (accessed October 23, 2018). < http://cfg.cornell.edu/software/ > .
[25] Radaj D, Sonsino CM, Fricke W. Fatigue Assessment of Welded Joints by Local Approaches. 2nd ed. Cambridge: Woodhead Publishing; 2006.
[26] Lohne P. A fracture mechanics approach to fatigue analysis of welded joints in offshore structures. J Nor Marit Res 1979;7:12–20.
[27] King RN, Stacey A, Sharp J V. A review of fatigue crack growth rates for offshore steels in air and seawater environments. In: Mercati D, editor. Proc. 15th Int. Conf.

Offshore Mech. Arct. Eng. OMAE, 1996, p. 341–8.
[28] Maddox S. Assessing the significance of flaws in welds subject to fatigue. Weld J 1974;53:401–10.
[29] Nykänen T, Björk T. Assessment of fatigue strength of steel butt-welded joints in as-welded condition - Alternative approaches for curve fitting and mean stress effect analysis. Mar Struct 2015;44:288–310. https://doi.org/10.1016/j.marstruc.2015.09.005.
[30] EN 1993-1-8. Eurocode 3 - Design of steel structures - Part 1-8: Design of joints, 2005.
[31] Mori T, Ichimiya M. Fatigue crack initiation point in load carrying fillet-welded cruciform joints. Weld Int 1999;10:786–94.
[32] Barsoum Z, Lundbäck A. Simplified FE welding simulation of fillet welds - 3D effects on the formation residual stresses. Eng Fail Anal 2009;16:2281–9. https://doi.org/10.1016/j.engfailanal.2009.03.018.
[33] Ahola A, Skriko T, Björk T. Experimental investigation on the fatigue strength assessment of welded joints made of S1100 ultra-high-strength steel in as-welded and post-weld treated condition (in press). In: Zingoni A, editor. Proc. 7th Int. Conf. Struct. Eng. Mech. Comput. Cape Town, South Africa, 2-4 Sept. 2019, 2019, p. 1–6.

Publication IV

Ahola, A., Skriko, T., and Björk, T.

Fatigue strength assessment of ultra-high-strength steel fillet weld joints using 4R method

Reprinted with permission from
Journal of Constructional Steel Research
Vol. 167, 105861, 2020

Journal of Constructional Steel Research 167 (2020) 105861

Contents lists available at ScienceDirect

Journal of Constructional Steel Research

journal homepage: www.elsevier.com/locate/ijcard

Fatigue strength assessment of ultra-high-strength steel fillet weld joints using 4R method

A. Ahola*, T. Skriko, T. Björk

Laboratory of Steel Structures, Lappeenranta-Lahti University of Technology LUT, P.O. Box 20, FI-53851, Lappeenranta, Finland

ARTICLE INFO

Article history:
Received 14 August 2019
Received in revised form
4 November 2019
Accepted 6 November 2019
Available online 30 November 2019

Keywords:
Fatigue
Welded joint
Ultra-high-strength steel
Post-weld treatment
4R method

ABSTRACT

A fatigue analysis on experimentally tested transverse fillet-welded non-load-carrying T- and X-joints made of S960 and S1100 ultra-high-strength steel was carried out in the present study. The test data consisted of welded joints in the as-welded, high frequency mechanical impact-treated, and tungsten inert gas-dressed conditions, that were fatigue tested using uniaxial constant amplitude loading with an applied stress ratio of $R = 0.1-0.5$. The weld geometry and residual stress measurements were carried out, and for each joint, the fatigue strength was assessed using a multiparametric notch stress approach, entitled the 4R method, which incorporates the consideration of four parameters, i.e. notch stress range $\Delta\sigma_k(r)$, applied stress ratio R, material ultimate strength R_m, and residual stress σ_{res} in the fatigue assessment. In the 4R method, the local cyclic elastic-plastic behavior at the notch root is obtained, and the Smith-Watson-Topper parameter is applied to conduct a mean stress correction to commeasure all results into a single S-N curve. The results showed that the applied stress ratio had a distinct influence on the fatigue strength capacity for both joints in the as-welded and post-weld treated conditions when using the conventional stress-based approaches, i.e. nominal stress, structural hot-spot stress and effective notch stress concepts. Nevertheless, the 4R method resulted in a good agreement between the experimental test results and the fatigue strength assessments, regardless of the load and joint conditions.

1. Introduction

The use of ultra-high-strength steels (UHSSs) has gained increasing interest for many applications, such as in cranes, aerial work vehicles and transport equipment since UHSSs enable weight reduction with improved structural performance in comparison to conventional mild steels. However, to exploit the full potential of cyclically loaded structures made of welded UHSS components, the implementation of post-weld treatments (PWTs) is essential, together with a convenient structural design and high fabrication quality. Numerous studies have been conducted in the field of high frequency mechanical impact (HFMI) treatment [1–5] and tungsten inert gas (TIG) dressing [6–8] on welded joints made of UHSS showing a significant improvement in fatigue strength capacity with respect to the S-N curves for the corresponding joints in as-welded (AW) condition [9–12].

Conventionally, in the fatigue strength assessment of a welded joint in the AW condition, the presence of high tensile residual stresses is assumed. As a consequence, the increasing mean stress level of externally applied loading does not significantly decrease the fatigue strength capacity [13]. However, it is well-known that the applied stress ratio has a significant effect on the improvement level of the PWT methods if the fatigue strength improvement is based on the modified residual stress state at the notch root, such as in the HFMI treatment. The improvement level, obtained by the HFMI treatment, is also associated with the material strength [14]. Consequently, according to the IIW Recommendations [15], a higher improvement level can be claimed for a welded detail made of higher material strength, although a reduction in the improvement level depending on the R ratio is proposed.

TIG dressing, by means of re-melting the transition region from the base material to the weld reinforcement, lowers the stress concentration at the weld toe, contributing to the achievement of high fatigue strength. The residual stress after the TIG dressing seems to be related to the microstructure properties of the base metal. Hensel et al. [16] reported near zero residual stresses for S355 steel and tensile residual stresses for S960QL steel, similar to Ahola et al. [17] for S1100QT steel. In contrast, Skriko et al. [6] reported compressive residual stresses for TIG-dressed S960QC

* Corresponding author.
E-mail address: antti.ahola@lut.fi (A. Ahola).

https://doi.org/10.1016/j.jcsr.2019.105861
0143-974X/

weldments. In general, the potential existence of tensile residual stresses posits that the improvement due to the TIG dressing is less sensitive to the increase in the mean stress level.

The prevailing concept in engineering is that the different PWTs and load conditions (R) are considered in the fatigue strength assessment by either introducing material strength-, PWT- and R-specific reduction or improvement factors, or using PWT-specific S-N curves that are based on experimental verifications. Such factors can be applicable in many cases but might also result in redundant conservatism and, in particular, offer no physical explanation for the increase or reduction in the fatigue strength capacity. Hensel et al. [18,19] introduced a fatigue bonus factor related to the effective stress ratio that can be used to evaluate the effect of stabilized residual stress, in association with material strength and the external stress ratio, on fatigue strength capacity, but the factor lacks the consideration of notch stress concentrations potentially influenced by the welding technique or PWT.

Recently, various local approaches [20–22] have been introduced to evaluate fatigue strength of weld toe and weld root failures. However, high quality UHSS weldments without initial flaws, either in the AW or post-weld treated condition, require advanced methods to consider parameters affecting the fatigue performance. To overcome the issues related to the combined effect of the different load and residual stress conditions, in conjunction with material strength and notch stress concentration, on the fatigue strength capacity, Nykänen et al. [23–25] introduced a notch stress-based fatigue strength assessment approach, entitled the 4R method after the four parameters included in the analysis, i.e. notch stress range $\Delta\sigma_k(\boldsymbol{r})$, applied stress ratio $\boldsymbol{R}$, residual stress $\sigma_{\boldsymbol{r}es}$ and material ultimate strength $\boldsymbol{R}_m$, see bolded R and r letters as an introduction to the name. In the 4R method, the local stress ratio R_{local} acting at the notch root is determined considering the aforementioned parameters. Material ultimate strength R_m and residual stress state σ_{res} determine the material behavior at the notch root under external cyclic load configuration, i.e. the applied notch stress range $\Delta\sigma_k$ based on the weld toe radius r and applied stress ratio R. The well-known Smith Watson and Topper (SWT) equation [26], i.e. $\sigma_{max}\varepsilon_a =$ constant, is adopted in the fatigue strength assessment to consider the mean stress effect on the fatigue strength capacity. The applicability of the SWT parameter to the mean stress correction in welded joints has also been corroborated in Refs. [27,28].

The applicability of the 4R method for various steel materials and grades, and applied stress ratios has been shown in the previous studies [24,29], while less has been paid attention to the UHSS joints in the post-weld treated condition. This study aims to verify the applicability of the 4R method for UHSS fillet weld joints in the AW and post-weld treated condition, including HFMI treatment and TIG dressing as PWT methods. Although UHSS fillet weld joints have been widely studied experimentally in recent years, geometry (weld profiles and weld toe radii) or residual stress measurements have not been conducted or reported precisely enough to apply the fatigue test data in the fatigue analyses using the 4R method. Consequently, experimental fatigue test data of UHSS fillet weld joints, reported in Refs. [17,30], are used as a basis of the fatigue analysis and in addition, fatigue tests in the AW and HFMI-treated condition are carried out for non-load-carrying X-joints (NLCX) made of S1100 UHSS grade to supplement the fatigue test data. The NLCX-joints in the AW condition are fatigue tested using $R = 0.1$ and $R = 0.5$ applied stress ratios of external loading. Based on the findings in a previous study [17], the HFMI-treated joints were tested with various R values in the $R = 0.1$–0.4 regime to investigate the effect of increased mean stress on the improvement level of the HFMI treatment. Comprehensive geometry and residual stress measurements are carried out for the test data, and the collected data are analyzed using the 4R method.

2. Experimental data

2.1. Applied fatigue test data

In this study, the recently published fatigue test results were applied for the notch stress analysis. The fatigue test results with the relevant information related to the test specimens, such as the weld toe radius, residual stress condition and secondary bending stress, were collected from recent studies. Numerous experimental studies have been conducted on welded UHSS joints in the AW and PWT conditions, but either the secondary bending stress, residual stress or weld geometry (including weld toe radius, throat thickness and weld flank angle) measurements were not conducted precisely enough in terms of the 4R method or the results were not available. Consequently, fatigue test data of such studies were not included in this study. The applied data consisted of fillet-welded NLCT- and NLCX-joints. Table 1 summarizes the key information regarding the experimental test data. Further details regarding the preparation of the test specimens and measurements can be found in the original references [17,30].

2.2. Additional fatigue tests

The fatigue tests were carried out for NLCX-joints made of S1100MC UHSS. Fig. 1 shows the shape and dimensions, and welding preparation of the test specimens, and Tables 2 and 3 present the nominal mechanical properties and chemical compositions of the base material and filler metal, respectively. All specimens were prepared using a robotic gas metal arc welding (GMAW) with a Ø 1.0 mm Union X96 solid wire targeting a nominal throat thickness of $a = 5$ mm. Total number of 12 specimens were prepared and fatigue tested, of which eight specimens were tested in the AW condition, and four specimens were tested in the HFMI-treated condition. Residual stress and geometry measurements (weld profiles and toe radii) were measured before fatigue testing, and the further details and results of those measurements can be found in Table 7 in Section 3.2.

The fatigue tests were carried out using uniaxial constant amplitude cyclic loading with applied stress ratios of $R = 0.1$–0.5. The specimen-specific test condition (applies stress range and ratio) can be found in Appendix A. Each specimen was equipped with a strain gage installed at the $0.4t$ distance from the weld toe, see Fig. 1d, to obtain macrogeometric bending stress induced by the

Table 1
Fatigue test data of axially loaded transverse T- and X-joints included in this study.

Ref.	Base material	Joint type	Joint condition	R of external loading	No. of tests
Ahola et al. [17]	S1100	T-joint	AW	0.1 and 0.5	6
	S1100	T-joint	HFMI	0.1 and 0.5	4
	S1100	T-joint	TIG	0.1 and 0.5	4
Ahola et al. [30]	S960	T-joint	AW	0.1	2
	S960	X-joint	AW	0.1	2

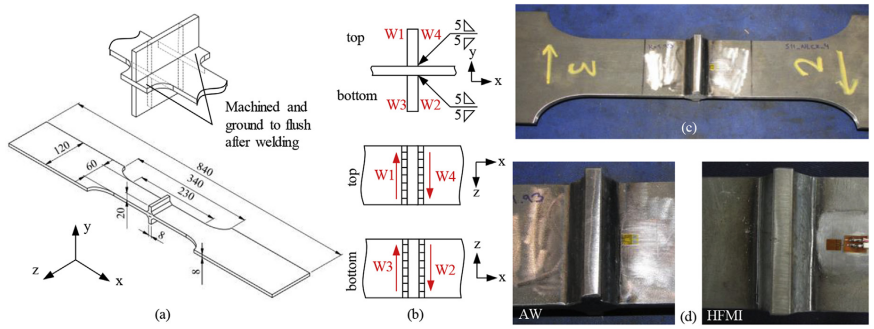

Fig. 1. NLCX fatigue test specimens tested within this study: (a) shape and dimensions of the test specimens (all dimensions in mm), (b) sequence and direction of weld passes (W1−W4), (c) example of welded specimen, and (d) detailed views on joint areas and strain gages in specimens in the AW and HFMI-treated condition.

Table 2
Nominal mechanical properties of the studied materials.

Material	Proof strength $R_{p0.2,min}$ [MPa]	Ultimate strength R_m [MPa]	Elongation $A_{5,min}$ [%]	Impact Energy KV [J] (at temp.)
S1100	1100	1130−1350	10	27 (−40 °C)
Union X96[a]	930	≥980	14	47 (−50 °C)

[a] Mechanical properties of undiluted weld metal.

Table 3
Nominal chemical composition [weight-%] of the studied materials (the most important alloying components).

Material	C_{max}	Si_{max}	Mn_{max}	P_{max}	S_{max}	Al_{min}
S1100	0.20	0.50	1.80	0.02	0.005	0.015
	C_{max}	Si_{max}	Mn_{max}	Cr_{max}	Ni_{max}	Mo_{max}
Union X96[a]	0.12	0.8	1.9	0.45	2.35	0.55

[a] Chemical composition of undiluted weld metal.

angular misalignment of specimen. A servo-hydraulic testing machine, see Fig. 2a, was used in the fatigue tests and the applied failure criterion was the total rupture of the specimen. Fig. 2b presents a rupture and polished cross-section of a failed specimen.

2.3. Results

The fatigue test data points are presented in Appendices A and B. The details regarding the geometry and residual stress measurements can be found in Section 3.2. A standard statistical analysis [9], with the free and fixed slopes of the *S-N* curve, was conducted on the test results. Due to the distinguishing notch stress factors and amount of the secondary bending stress induced by the angular distortion [30], the NLCT and NLCX joints showed different fatigue strength capacities in the nominal and structural stress systems. In the ENS system, all test results were embedded in the same statistical analysis. For the joints in the AW condition, a fixed $m = 3$ slope was used while for the TIG-dressed and HFMI-treated joints, $m = 4$ [31] and $m = 5$ [15] were applied, respectively. Fig. 3 shows the data point plots with the corresponding standard or recommended curves, and Tables 4–6 present the results of the statistical analyses regarding the fatigue strengths. FE modeling and analysis were employed to obtain stress concentration factors (SCFs) for the ENS analysis. According to the ENS approach, fictitious weld toe radius of $r_{ref} = 1.0$ mm has been suggested for AW and HFMI-treated specimens [15,32], and this approach was also used in this study. For the TIG-dressed joints, the $r_{true} + 1$ mm concept was used due to the large weld toe radius. A typical element mesh used in the analyses is presented in Fig. 8 (Section 3.2). The SCFs were obtained separately for membrane and bending stress (see Table 7), and the ENS was calculated as follows:

$$\Delta\sigma_{ens} = K_{t,m}(r = 1\ \text{mm})\Delta\sigma_m + K_{t,b}(r = 1\ \text{mm})\Delta\sigma_b \quad (1)$$

where $\Delta\sigma_{ens}$ is the ENS range, $K_{t,m}$ and $K_{t,b}$ are the SCFs for membrane and bending stress, respectively, $\Delta\sigma_m$ is the membrane stress due to the axial loading, and $\Delta\sigma_b$ is the bending stress induced by the macrogeometric angular distortion, and measured by a strain gage during the test.

3. 4R fatigue analysis

3.1. Theoretical background

The 4R method is a notch stress-based approach for the fatigue strength assessment of welded joints. In the 4R method, the material cyclic behavior is simulated considering the material strength, residual stress, weld toe quality, and thus the effective notch stress acting at the notch root, and the applied stress ratio of external loading. Effective notch stress with the stress averaging concept, i.e. $r = r_{true} + 1$ mm, is used as a basis for the fatigue analysis. In a prior investigation [24], $r = 1$ mm was also used for the HFMI-treated joints but within this study, the $r = r_{true} + 1$ mm concept is applied and proposed for these joints. The Ramberg-Osgood elastic-plastic material model with the kinematic hardening rule is applied to describe the material cyclic behavior at the notch root, which can be formulated as follows:

$$\varepsilon = \varepsilon_e + \varepsilon_p = \frac{\sigma}{E} + \left(\frac{\sigma}{H}\right)^{\frac{1}{n}} \quad (2)$$

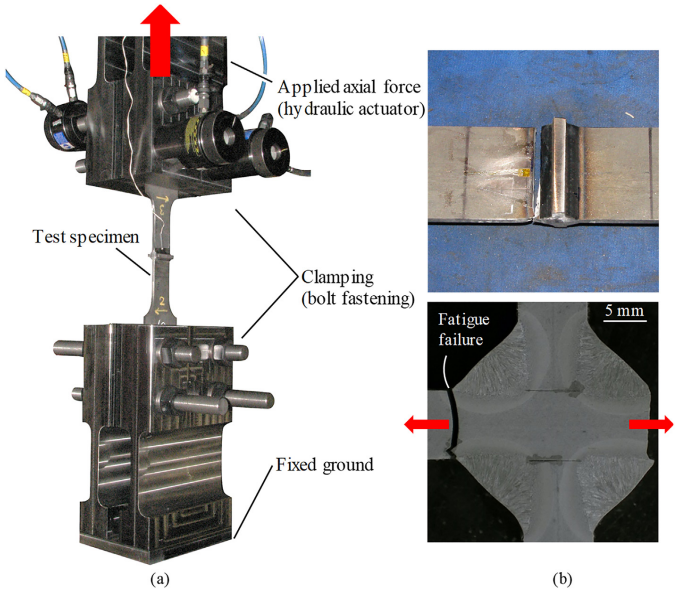

Fig. 2. (a) Fatigue test set-up, and (b) rupture and polished cross-section of a failed specimen.

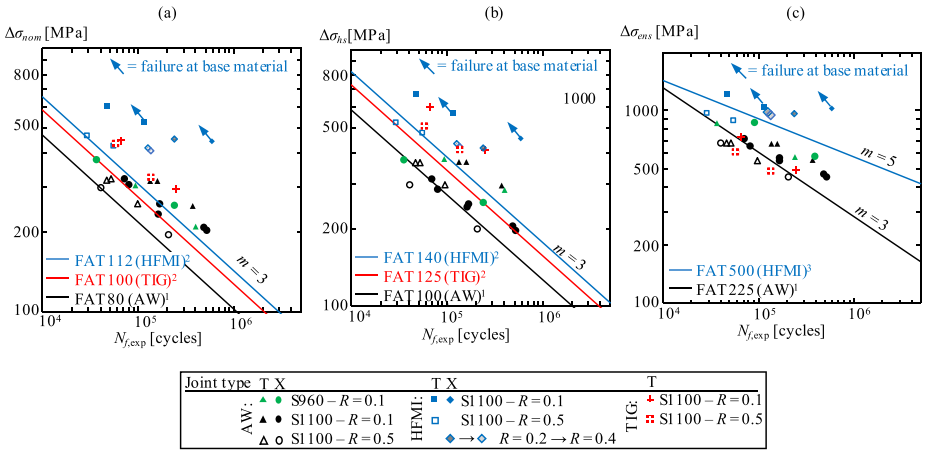

Fig. 3. Data points with the reference *S-N* curves for the AW and PWT joints after [1]Haagensen and Maddox [33], [2]Hobbacher [9] and [3]Marquis and Barsoum [15] in the (a) nominal stress $\Delta\sigma_{nom}$, (b) structural stress $\Delta\sigma_{hs}$, and (c) ENS system $\Delta\sigma_{ens}$ (r_{ref} = 1.0 mm). $N_{f,exp}$ is the experimental fatigue life.

$$\Delta\varepsilon = \Delta\varepsilon_e + \Delta\varepsilon_p = \frac{\Delta\sigma}{E} + 2\left(\frac{\Delta\sigma}{2H}\right)^{\frac{1}{n}} \quad (3)$$

where ε, ε_e, ε_p are the total, elastic, and plastic strain, respectively, σ is the stress, E is the modulus of elasticity, H is the strain hardening coefficient and n is the strain hardening exponent. In Eq. (3), the symbols denoted with Δ represent the same variables but correspond to the range values. Neuber's rule with hyperbolae and counter hyperbolae are employed to obtain maximum and minimum stress, respectively, as follows:

Table 4
Obtained mean fatigue strengths for the joints in the AW and PWT condition in the nominal stress system (survival probability of $P_s = 50\%$).

Joint type Stress ratio	m = fixed				m = free			
	0.1		0.5		0.1		0.5	
	m	FAT [MPa]	m	FAT [MPa]	m	FAT [MPa]	m	FAT [MPa]
NLCT - AW	3	126	3	92	3.26	134	3.11	96
NLCT - HFMI	5	285	5	204	n/a	n/a	6.93	253
NLCT - TIG	4	181	4	172	3.00	144	2.87	127
NLCX - AW	3	111	3	86	4.29	144	3.98	110

Table 5
Obtained mean fatigue strengths for the joints in the AW and PWT conditions in the HS stress system ($P_s = 50\%$).

Joint type Stress ratio	m = fixed				m = free			
	0.1		0.5		0.1		0.5	
	m	FAT [MPa]	m	FAT [MPa]	m	FAT [MPa]	m	FAT [MPa]
NLCT - AW	3	155	3	107	4.72	205	3.32	119
NLCT - HFMI	5	315	5	228	n/a	n/a	7.57	297
NLCT - TIG	4	250	4	209	3.45	219	3.90	205
NLCX - AW	3	111	3	87	4.33	144	4.09	114

Table 6
Obtained mean fatigue strengths for the joints in the AW and PWT conditions in the ENS system using the reference radius of $r_{ref} = 1.0$ mm ($P_s = 50\%$).

Joint type Stress ratio	m = fixed				m = free			
	0.1		0.5		0.1		0.5	
	m	FAT [MPa]	m	FAT [MPa]	m	FAT [MPa]	m	FAT [MPa]
All joints - AW	3	269	3	200	4.15	338	3.71	246
All joints – HFMI	5[a]	586[a]	5	425	4.97[a]	584[a]	7.89	564
All joints – TIG[b]	4	303	4	252	3.33	264	3.92	248

[a] All test results of $R = 0.1–0.4$ but excluding base material failures (see Appendices A and B).
[b] $r_{ref} = r_{true} + 1$ mm = 7.4 mm (see Table 7, Section 3.2).

Table 7
Average values and corresponding standard deviations for geometric variables derived from the 2D geometry measurements along with the corresponding SCFs. n is the number of measurements conducted within each test group.

Group	Joint type	Weld geometry measurements							SCF (r = 1 mm)		SCF (r = rtrue + 1 mm)	
		$r_{true,avg}$	Stdv$_r$	θ_{avg}	Stdv$_\theta$	a_{avg}	$Stdv_a$	n	Kt,m	Kt,b	Kt,m	Kt,b
S960 - AW [30]	NLCT	0.30	0.07	43	1.1	5.1	0.12	24	1.85	2.06	1.73	1.90
S960 - AW [30]	NLCX	0.29	0.07	43	1.5	5.2	0.17	12	2.32	1.79	2.14	1.66
S1100 - AW [17]	NLCT	0.35	0.22	36	1.2	4.5	0.16	12	1.85	2.03	1.71	1.87
S1100 - HFMI [17]	NLCT	2.3	0.49	37	1.7	4.5	0.09	8	1.85	2.03	1.38	1.48
S1100 - TIG [17]	NLCT	6.4	1.8	37	1.5	4.5	0.11	8	1.85	2.03	1.20	1.24
S1100 - AW this study	NLCX	0.3	0.11	44	1.9	5.2	0.18	32	2.30	1.78	2.12	1.66
S1100 - HFMI this study	NLCX	2.3	0.21	43	2.3	5.2	0.23	16	2.30	1.78	1.62	1.32

$$\varepsilon = \frac{\left(\frac{\Delta\sigma_k}{1-R} + \sigma_{k,res}\right)^2}{\sigma E} \tag{4}$$

$$\Delta\varepsilon = \frac{\Delta{\sigma_k}^2}{\Delta\sigma E} \tag{5}$$

where $\Delta\sigma_k$ is the notch stress range obtained using the $r = r_{true} + 1$ mm concept, R is the external stress ratio, and $\sigma_{k,res}$ is the local residual stress. Within the fatigue tests conducted in this and prior studies, relaxed and subsequently stabilized residual stresses were not measured during the fatigue test. For that reason, the initial residual stress state was assumed with conservative assumptions, see Section 3.2. Fig. 4 summarizes the key aspects related to the determination of local stress ratio R_{local} at the notch root on the basis of the aforementioned concepts for the different residual stress states with and without residual stress relaxation, including the following steps:

a. At the notch root, linear elastic effective notch stress (σ_k) fluctuates cyclically under external constant amplitude loading and as a result, a time-stress history is received;

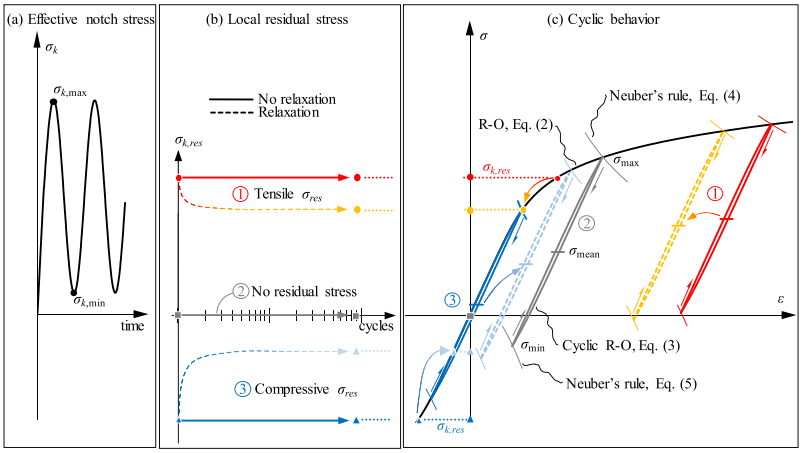

Fig. 4. Schematic representation of cyclic behavior following Eqs (2)–(5): (a) constant amplitude effective notch stress due to external loading, (b) local residual stresses at the notch root with and without the residual stress relaxation, and (c) cyclic behavior and hysteresis loops influenced by the effective notch stress range and residual stresses.

b. Local residual stress ($\sigma_{k,res}$) can be tensile or compressive depending on the joint condition. Local residual stress posits the initial stress occurring at the notch root, i.e. the starting point at the R–O curve in Fig. 4c is derived. The relaxation of residual stresses can be taken into account by changing the starting point at the R–O curve;
c. The local cyclic behavior and, subsequently, the hysteresis loops are determined based on the effective notch stress range and the initial residual stress. As a result, the local minimum and maximum stress (σ_{min} and σ_{max}) acting at the notch are derived.

Both tensile and compressive welding residual stresses can significantly relax under cyclic loading [34,35]. As shown in Fig. 4, the stabilization of residual stress in the case of compressive residual stresses, e.g. as a result of the HFMI treatment, increase distinctly mean stress level of local stress ratio. A decrease in the high residual stress, however, does not have a significant influence on the mean stress level, as local yielding occurs with the maximum loading even at the low level of loading. Nevertheless, is must be noted that the given example is presented for a cyclic loading at the low stress ratio, i.e. $R = 0.1$, and at high stress ratios, the effect of residual stress state on the cyclic behavior and subsequently on the fatigue strength is lower. The ratio of the local minimum and maximum stresses (σ_{min} and σ_{max}) determine the local stress ratio R_{local}, whereby the reference notch stress range $\Delta\sigma_{k,ref}$ can be defined by reformulating the SWT parameter [24] as follows:

$$R_{local} = \frac{\sigma_{min}}{\sigma_{max}} \tag{6}$$

$$\Delta\sigma_{k,ref} = \frac{\Delta\sigma_k(r_{true} + 1\ \text{mm})}{\sqrt{1 - R_{local}\left[\Delta\sigma_k(r_{true} + 1\ \text{mm}), n, H, \sigma_{k,res}, R_{eff}\right]}} \tag{7}$$

where R_{eff} is the effective stress ratio (see further details in Section 3.2). Further details concerning the theoretical background of the 4R method can be found in Refs. [23,24,29].

3.2. 4R parameters

The tests were conducted mainly at the intermediate life, i.e. around 100 000 cycles with a maximum ENS of 1000 MPa; no reversed plasticity was present in the tests with the studied high-strength materials, and fully elastic stress ranges can be assumed. If no cyclic softening or hardening is assumed, the monotonic stress-strain-behavior describes the material behavior in the tests. In a recent study, Amraei et al. [36] determined the material behavior of the studied S960 and S1100 grades in non-welded and butt-welded components. From these tests, the Ramberg-Osgood (R–O) material models for the base materials can be obtained. The engineering force-displacement behavior was converted to true stress-true strain curves and subsequently, the plastic strain characteristics were derived for the R–O material models by conducting a linear regression analysis on the plastic strain and true stress, as shown in Ref. [37]:

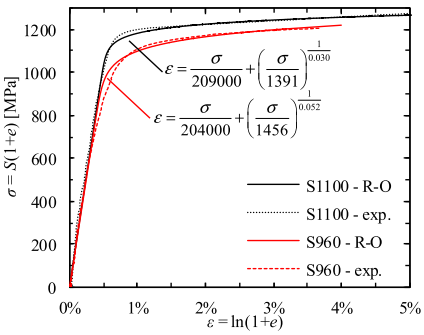

Fig. 5. Material models of the S960 and S1100 steels used in this study. ε and σ are the true strain and stress, respectively, obtained from the corresponding engineering values (e, S) determined on the basis of the test force and displacement.

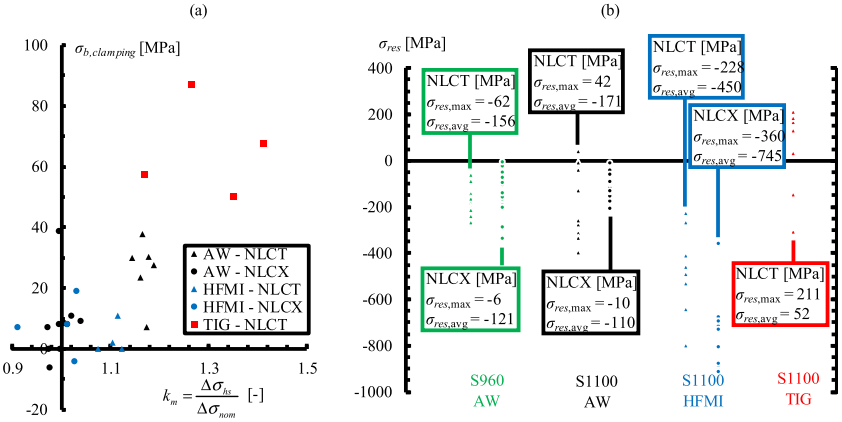

Fig. 6. (a) Clamping-induced stresses as a function of k_m factor in the test, and (b) results of residual stress measurements for the NLCT and NLCX specimens in the AW and PWT condition.

$$\log\varepsilon_p = \frac{1}{n}(\log\sigma - \log H) \tag{8}$$

Young's moduli for the S960 and S1100 materials were determined on the basis of the digital image correlation (DIC) system, and $E_{S960} = 204$ GPa and $E_{S1100} = 209$ GPa were derived [36]. Fig. 5 presents the obtained material models for the studied S960 and S1100 base materials.

The fatigue tests were carried out using the applied stress ratios from $R = 0.1$ to $R = 0.5$. However, due to the angular distortion of the specimens, the clamping led to an additional increase in the mean stress level, as also shown by Leitner [38]. Thus, each specimen was equipped with a strain gage and the clamping-induced stress was recorded when the specimens were inserted into the test rig. Appendices A and B provide the effective stress ratio (R_{eff}) values, in which the clamping-induced bending stress, the straightening of the specimen due to axial loading, and the distinguishing notch factors [30] were considered as follows:

$$R_{eff} = \frac{K_{t,m}\sigma_{m,\min} + K_{t,b}\left(\sigma_{b,clamping} + \sigma_{b,\min}\right)}{K_{t,m}\sigma_{m,\max} + K_{t,b}\left(\sigma_{b,clamping} + \sigma_{b,\max}\right)} \tag{9}$$

where $\sigma_{m,\min}$ and $\sigma_{m,\max}$, and $\sigma_{b,\min}$ and $\sigma_{b,\max}$ are the minimum and maximum of membrane and bending stresses, respectively, induced by the axial loading and the angular distortion in the test. In the NLCX joints, no significant clamping-induced bending stress was found, i.e. $\sigma_{b,clamping} < 10$ MPa, while the highest stresses due to the clamping were recorded in the TIG-dressed T-joints due to high angular distortion caused by the asymmetric joint geometry and thus, unequal welding and PWT heat inputs. In the TIG-dressed specimens, clamping stresses up to $\sigma_{b,clamping} = 90$ MPa were found, see Fig. 6a. The surface residual stresses, parallel to the loading direction, were measured using an X-ray diffractometer (Stresstech X3000 G3 device) at the centerline of the specimens. In the 4R analysis, the characteristic maximum value of residual stress representative of joint type and condition was used since there was variation in the measurements, as shown in Fig. 6b, and the failure did not always occur at the center of the specimen where the measurements were conducted. For the HFMI-treated joints, relaxation of the residual stresses during the early stage of cyclic loading has been demonstrated by Leitner et al. [34]. Although the chosen maximum values for the HFMI-treated joints distinguish from the measured values up to 900 MPa compressive residual stresses, see Fig. 6b, it can be noted that due to the relaxation, the stabilized residual stresses are lower in compression. However, in the studied joints, the stabilized residual stresses were not measured during the fatigue tests.

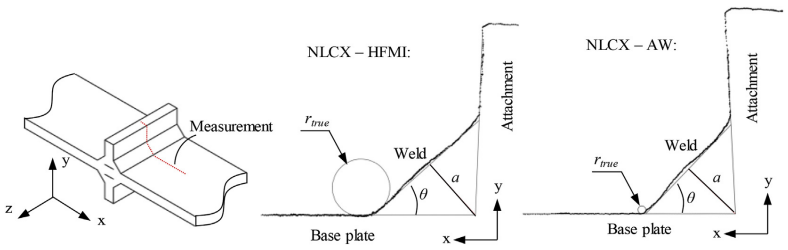

Fig. 7. (a) Measurement line of 2D geometry measurement and (b) results of the measurements of NLCX joints made of S1100 steel in the AW and HFMI-treated condition (see measured values in Table 7).

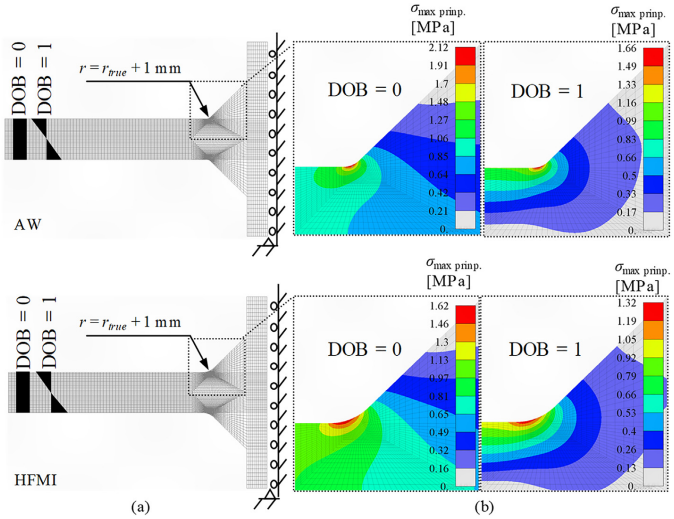

Fig. 8. (a) Half-symmetric FE models of the NLCX joints in the AW and HFMI-treated conditions with load and boundary conditions, and (b) the corresponding results of the SCFs for membrane and bending loading (a seed load of 1 MPa was used in the analysis). DOB is the degree of bending (bending stress divided by the total stress).

Geometry measurements were conducted for all specimens and welds at the centerline of the specimens using a 2D coordinate measuring device with an inductive displacement transducer and a laser displacement sensor, see Fig. 7a. Based on the measurements, the weld toe radius r_{true}, flank angle θ and throat thickness a were determined, see Fig. 7b. A summary of these analyses can be found in Table 7. From the obtained geometry, a 2D quadratic 8-node plane strain element model with both $r = 1$ mm and $r = r_{true} + 1$ mm weld toe radius was modeled and analyzed to obtain SCFs for notch stress analyses (the ENS concept and 4R method). At the notch root, the element size of $r/20$, e.g. element size of 0.05 mm × 0.05 mm for a weld toe radius of 1 mm, was chosen based on the mesh convergence study on notch stresses undertaken by Baumgartner and Bruder [39]. All analyses were carried out using Femap (Siemens PLM Software) with Nx Nastran. Since all specimens were prepared using a robotic GMAW, almost constant weld profile was obtained, as indicated by the standard deviations (Stdv) of the measured values. As shown in Table 7, in the HFMI-treated and TIG-dressed specimens higher scatter was found regarding the weld toe radius as the treatments were conducted manually. Consequently, no specimen-specific finite element analysis (FEA) was carried out, instead the average (avg) values were used in each model representing the test series. Fig. 8a shows the load and boundary conditions applied in the models and Fig. 8b presents FEA results. For the 4R method, the acting notch stresses $\Delta\sigma_k$ were obtained using Eq. (1) except now the SCFs based on $r = r_{true} + 1$ mm were used in the analysis.

3.3. Fatigue strength predictions

Utilizing the concept introduced in Section 3.1 and the parameters presented in Section 3.2, the elastic plastic cyclic behavior was obtained for each test. For the test results ($\Delta\sigma_{k,ref,i}$, $N_{f,i}$), Deming's regression [40], i.e. minimization of the sum of the squared perpendicular distances (MSSPD), was conducted. Conventionally, in regression analysis, only the scatter in the fatigue life is determined and considered. However, since the *S-N* curve is meant to describe the fatigue strength characteristics, and there is always uncertainty related to the stress acting at the local point causing the fatigue failure, the scatter should be regarded also in the stress value. Consequently, the stress range becomes partly unknown variable and the use of the MSSPD approach is justifiable. Fig. 9 shows all the fatigue test results presented in terms of the reference stress range $\Delta\sigma_{k,ref}$ with the corresponding *S-N* curves. The *S-N* curve of the 4R method can presented as follows:

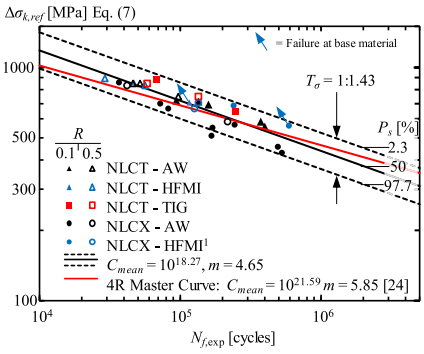

Fig. 9. Fatigue test results using the 4R method with the mean and characteristic *S-N* curves obtained by means of the MSSPD approach. [1]For HFMI-treated NLCX-joints, the $R = 0.1$ and $R = 0.5$ data points represent the tests carried out using $R = 0.1$–0.2 and $R = 0.3$–0.4 loads, respectively (see details in Appendix 1).

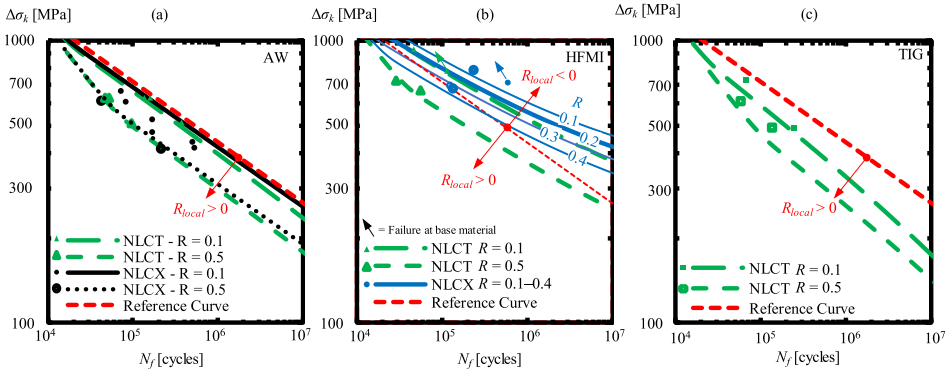

Fig. 10. *S-N* curves of the 4R method with a R_{local} correction, and the original data points ($N_{f,i}$, $\Delta\sigma_{k,i}$) for the S1100 joints in (a) AW, (b) HFMI-treated and (c) TIG-dressed condition. For the reference curve, $C_{mean} = 10^{18.27}$ and $m = 4.65$ (see Fig. 9).

$$N_{f,4R} = \left(\frac{\sqrt{1 - R_{local}}}{\Delta\sigma_k}\right)^{m_{4R}} C_{4R} \tag{10}$$

where the C_{4R} is the fatigue capacity and m_{4R} is the slope of the *S-N* curve according to the 4R method. Fig. 10 presents the fatigue test results corresponding to the notch stress range, and the S-N curves are obtained from the reference curve, which is modified according to the R_{local} values following Eq. (10).

4. Discussion

4.1. Fatigue strength capacity

The fatigue strength capacity of transverse NLC-joints made of UHSS was experimentally tested in the AW and PWT condition. The experimental data were collected from recently published studies [17,30], and supplemented with additional tests on NLCX-joints made of S1100 grade steel. Due to the configuration of the test specimens, i.e. small-scale specimens and no deformations were prevented in the welding, almost zero residual stresses were obtained, also for the AW specimens, see Fig. 6, as also noted in prior studies [30,41]. In fact, the highest tensile residual stresses were obtained in the TIG-dressed S1100 specimens, whereby a maximum of 200 MPa parallel to the loading direction was measured. Nevertheless, to demonstrate the effect of high tensile residual stresses on the fatigue strength capacity, the tests were carried out using applied stress ratios of $R = 0.1$–0.5.

The tests with the $R = 0.1$ loading showed a good correspondence with the design guidelines [9–12]; a reasonable margin with respect to the design *S-N* curves with a survival probability of $P_s = 97.7\%$ was found. For the HFMI-treated joints at low stress ratios, i.e. $R = 0.1$, FAT500 seemed to be applicable, see Fig. 3 and Table 6. However, the increasing mean stress level had a decreasing influence on the improvement level of the HFMI treatment. Due to the lack of design guidelines for the notch stress concept for the TIG-dressed joints [42], $r = r_{true} + 1$ mm was employed in this study, following the stress averaging concept with the fictitious notch rounding [43]. Using this concept, the *S-N* curve for the TIG-dressed joints ($R = 0.1$) did not reach the corresponding curve for the AW joints ($r = 1.0$ mm). However, the TIG-dressed joints tested with $R = 0.5$ loading, converged with the corresponding AW curve; see Fig. 3 and Table 6. In the TIG-dressed joints, the presence of tensile residual stresses make them less sensitive to the increase in the mean stress level. This finding is in agreement with the results acquired by Skriko et al. [6,44].

Of the geometry measurements conducted in this study, the average weld toe radius was determined to represent the test series, i.e. joints with similar joint configuration and welding parameters; see Fig. 7 and Table 7. A welding robot was used in the preparation of the test specimens and no significant variation was thus observed within the measurements and subsequent geometry analysis results. Although the HFMI and TIG treatments were performed manually, the geometrical variations were also minor in these specimens. In general, the test results (Fig. 3) showed that the specific *S-N* curves for the different *R* ratios and joint conditions (AW or PWT) are required to reach a reasonable accuracy in fatigue strength predictions. To avoid the need for this, the 4R method was adopted using the concept $r = r_{true} + 1$ mm for all joints, regardless of the joint condition (AW, HFMI, TIG).

The aim of this study was to further verify the applicability of the 4R method for the fatigue strength assessment of fillet-welded joints made of UHSS. The results showed that the 4R method can be applied for UHSS joints in the AW and PWT condition, regardless of the applied stress ratio. In the previous work undertaken by Nykänen et al. [23,24], the applicability of the 4R method for joints in the AW and HFMI-treated conditions was introduced, following the $r_{ref} = 1.0$ mm concept recommended by the IIW Recommendations [15]. Nevertheless, the fatigue test conducted at higher stress ratio, i.e. $R = 0.5$, indicated that fatigue strength improvement with the HFMI treatment can be claimed also at high stress ratios; see Fig. 3. The main influencing factor for that was obviously the increase in weld toe radius, as shown in Table 7. Consequently, the stress averaging concept, i.e. $r_{true} + 1$ mm, was adopted different to a previous study [24] showing good accordance with fatigue test results in terms of the 4R method.

The results of the 4R analysis showed a drastic decrease in the

scatter of the test results, i.e. all data points converged in a single *S-N* curve with a scatter range ($P_s = 97.7\%$: $P_s = 2.3\%$) of $T_\sigma = 1{:}1.43$; see Fig. 9. This results in a mean fatigue strength of $C_{4R,mean} = 10^{18.27}$ (FAT = 375 MPa at two million cycles) and a characteristic fatigue strength capacity of $C_{4R,char} = 10^{17.91}$ ($P_s = 97.7\%$, FAT = 314 MPa) with the slope of the *S-N* curve $m = 4.65$. The present study estimated a steeper slope with respect to the previous studies related to the 4R method, in which $m = 5.85$ was obtained [24,29]. Nevertheless, the Master Curve obtained by Nykänen and Björk [24] for C-Mn steels including various material strengths ($R_{p0.2} = 224–1100$ MPa) fits the experimental results of this study, as shown in Fig. 9. When conducting a statistical analysis with a similar slope of $m = 5.85$, $C_{4R,mean} = 10^{21.68}$ was received, which corresponds well with the Master Curve of $C_{4R,mean} = 10^{21.59}$.

4.2. Efficient fatigue design practices

From the engineering design point of view, the 4R method poses challenges to designers in the selection of trustworthy 4R parameters, i.e. without drawing unconservative assumptions and yet without redundant conservatism. In this study, an X-ray diffractometer, and 2D geometry measurement devices were employed to measure the residual stresses and weld profiles, respectively, for the 4R analysis. In fatigue design engineering, such facilities are not always available and, thus, the worst-case assumptions, such as tensile residual stresses equal to yield strength and a sharp $r_{true} = 0$ weld toe radius, are typically used to avoid making unconservative fatigue life predictions. This concept can also be adopted when using the 4R method [45]. For the HFMI treatment, a conservative assumption of $\sigma_{res} = -0.255R_m$ was given in Ref. [24] based on the measurements of existing studies, and the assumption seems to correspond to the residual stress measurements of this study. Regarding the residual stresses after the TIG dressing, the authors did not find studies, in which the TIG dressing of UHSSs and subsequent residual stress measurements were conducted for joints in the high tensile residual stress field.

Nevertheless, the increasing demands for structural and weight optimization are leading to more comprehensive utilization of structural performance, and methods to examine the realized values are needed. In this regard, quality assurance in fabrication [46] plays an important role; the desired quality level must be reached and verified. Although there exist many non-destructive measurement techniques for measuring the residual stresses in the structures, they are not commonly used in the practical engineering work. To overcome the need for the measurements, simulation of welding processes [47,48] and PWTs [49–51] for UHSSs can be adopted to estimate the residual stress state for the fatigue strength assessment, together with the analytical [52] and numerical [34] methods to estimate the stabilized residual stresses.

4.3. Future work

Within this study, HFMI treatment and, with a limited scope, TIG dressing were considered as PWTs for fillet-welded joints, showing the efficiency of the 4R method for the fatigue strength assessment of welded joints made of UHSS. To further validate the 4R method for TIG-dressed joints, additional fatigue tests and detailed research on the residual stress state after treatment for different steel grades should be carried out. In addition, the incorporation of other post-weld improvement techniques, such as burr grinding [33] and laser dressing [44], under the 4R methodology needs further verification. In the 4R method, the residual stress relaxation can be considered; see Fig. 4. Nevertheless, in the studied joints, stabilized residual stresses were not measured, and the effects of it on the use of the 4R method should be paid attention in future works.

This study showed a decrease in the improvement level of the HFMI treatment when the *R* ratio increases. Experimental tests were conducted at the intermediate regime, i.e. near 100 000 cycles. It should be noted that the HFMI treatment shows a particularly beneficial effect at the high cycle regime, hence additional experimental tests should be carried out to verify the 4R method at this regime. The fatigue testing of HFMI-treated welded joints at the high cycle regime, however, may result in failures outside the joint area, particularly at low stress ratios, as also observed in this study. To diminish the affecting parameters causing scatter in the fatigue test results, small-scale specimens are typically preferred to study a certain phenomenon. As with many other fatigue design concepts, the 4R method also requires further validation by testing with large-scale specimens and structures.

5. Conclusions

Within this study, the experimental fatigue test data for fillet-welded joints with transverse attachments made of UHSS was extracted from literature. The tests were complemented with the fatigue tests conducted for the NLCX-joints made of the S1100 UHSS. All tests were carried out using CAL with the applied stress ratio of $R = 0.1–0.5$. The fatigue strengths were obtained using conventional stress-based approaches; the nominal stress, structural HS stress and ENS method. The 4R method was employed to investigate the mean stress correction by means of the local stress ratio acting at the notch root. On the basis of the experimental work and subsequent fatigue analysis, the following conclusions can be drawn:

- The fatigue test results with low stress ratios, i.e. $R = 0.1$, exceeded the characteristic curves ($P_s = 97.7\%$) of the design codes and guidelines [9–12].
- The design curves [9–12] were unconservative for the joints in the AW condition and tested at high stress ratio, i.e. $R = 0.5$. For the HFMI-treated joints tested at high stress ratio, higher fatigue strength was found than suggested by the IIW Recommendations [15].
- The conventional fatigue strength assessment methods, such as the nominal stress, HS and ENS concepts, recall specific *S-N* curves for different PWTs, and careful consideration of applied stress ratio is needed to reach a reasonable accuracy in the fatigue strength assessment.
- The 4R method enables fatigue strength assessment of transverse fillet-welded UHSS joints with good accuracy regardless of joint condition or applied stress ratio using a single *S-N* curve with the SWT mean stress correction.

Acknowledgements

The authors wish to thank Business Finland and SSAB Europe for the funding through the Digi-TuoTe project (grant ID 3558/31/2016) that enabled the experimental program and this study to be completed.

Appendices

Appendix A
Fatigue test data of S1100 NLCX specimens tested in this study.

Specimen ID	Joint type	Joint condition	Material	$\Delta\sigma_{nom}$ [MPa]	$\Delta\sigma_{hs}$[a] [MPa]	$\Delta\sigma_{ens}$ [MPa]	$\Delta\sigma_{k,4R}$ [MPa]	R [−]	R_{eff} [−]	$N_{f,exp}$ [cycles]	Remarks
S11_NLCX_1	NLCX	AW	S1100	314	312	719	663	0.1	0.12	71 872	
S11_NLCX_2	NLCX	AW	S1100	301	317	721	610	0.1	0.12	82 578	
S11_NLCX_3	NLCX	AW	S1100	254	247	572	527	0.1	0.10	169 415	
S11_NLCX_4	NLCX	AW	S1100	231	241	549	476	0.1	0.13	167 322	
S11_NLCX_5	NLCX	AW	S1100	206	205	472	438	0.1	0.10	496 828	
S11_NLCX_6	NLCX	AW	S1100	201	196	453	417	0.1	0.08	528 328	
S11_NLCX_7	NLCX	AW	S1100	291	294	675	613	0.5	0.50	42 103	
S11_NLCX_8	NLCX	AW	S1100	193	197	450	415	0.5	0.50	216 073	
S11_NLCX_9H	NLCX	HFMI	S1100	444	448	1029	712	0.1	0.11	592 164	Failure at base material
S11_NLCX_10H	NLCX	HFMI	S1100	409	419	958	676	0.4	0.38	135 617	
S11_NLCX_11H	NLCX	HFMI	S1100	420	432	987	696	0.3	0.30	125 826	
S11_NLCX_12H	NLCX	HFMI	S1100	452	412	968	787	0.2	0.18	238 488	

[a] Corresponding to the failure locations. In some specimens, the failure occurred at the opposite side of specimen to the side of maximum HS stress. The HS stresses corrected to correspond the stress value at the failure location, as shown in Ref. [53]. Consequently, $\Delta\sigma_{hs} < \Delta\sigma_{nom}$.

Appendix B
Fatigue test data of S960 and S1100 specimens tested in Refs. [17,30].

Specimen ID	Joint type	Joint condition	Material	$\Delta\sigma_{nom}$ [MPa]	$\Delta\sigma_{hs}$ [MPa]	$\Delta\sigma_{ens}$ [MPa]	$\Delta\sigma_{k,4R}$ [MPa]	R [−]	R_{eff} [−]	$N_{f,exp}$ [cycles]	Remarks
S11_NLCT_1	NLCT	AW	S1100	311	365	683	631	0.1	0.11	159 573	
S11_NLCT_3	NLCT	AW	S1100	310	365	683	631	0.1	0.16	135 643	
S11_NLCT_5	NLCT	AW	S1100	250	297	558	515	0.1	0.17	376 238	
S11_NLCT_2	NLCT	AW	S1100	313	363	680	628	0.5	0.51	46 422	
S11_NLCT_4	NLCT	AW	S1100	318	364	681	629	0.5	0.51	52 181	
S11_NLCT_6	NLCT	AW	S1100	254	296	554	511	0.5	0.53	97 383	
S11_NLCT_7H	NLCT	HFMI	S1100	604	667	1242	929	0.1	0.10	47 174	
S11_NLCT_8H	NLCT	HFMI	S1100	526	565	1048	784	0.1	0.10	116 617	Failure at base material
S11_NLCT_9H	NLCT	HFMI	S1100	465	518	965	721	0.5	0.48	29 305	
S11_NLCT_10H	NLCT	HFMI	S1100	423	475	888	664	0.5	0.48	56 474	
S11_NLCT_11T	NLCT	TIG	S1100	446	602	730	730	0.1	0.16	67 404	
S11_NLCT_13T	NLCT	TIG	S1100	289	408	494	494	0.1	0.22	247 632	
S11_NLCT_12T	NLCT	TIG	S1100	434	507	612	612	0.5	0.52	58 140	
S11_NLCT_14T	NLCT	TIG	S1100	323	408	493	493	0.5	0.54	135 812	
AAT5	NLCT	AW	S960	299	377	715	664	0.1	0.21	93 948	
AAT6	NLCT	AW	S960	210	284	541	503	0.1	0.25	399 921	
AAX5	NLCX	AW	S960	373	371	864	796	0.1	0.16	36 761	
AAX6	NLCX	AW	S960	250	251	583	537	0.1	0.12	244 214	

References

[1] E. Harati, L. Svensson, L. Karlsson, M. Widmark, Effect of high frequency mechanical impact treatment on fatigue strength of welded 1300 MPa yield strength steel, Int. J. Fatigue 92 (2016) 96–106, https://doi.org/10.1016/j.ijfatigue.2016.06.019.

[2] T. Nykänen, T. Björk, R. Laitinen, Fatigue strength prediction of ultra high strength steel butt-welded joints, Fatigue Fract. Eng. Mater. Struct. 36 (2012) 469–482, https://doi.org/10.1111/ffe.12015.

[3] M. Leitner, S. Gerstbrein, M.J. Ottersböck, M. Stoschka, Fatigue strength of HFMI-treated high-strength steel joints under constant and variable amplitude block loading, Procedia Eng. 101 (2015) 251–258, https://doi.org/10.1016/j.proeng.2015.02.036.

[4] M. Leitner, M. Stoschka, W. Eichlseder, Fatigue enhancement of thin-walled, high-strength steel joints by high-frequency mechanical impact treatment, Weld. World 58 (2014) 29–39, https://doi.org/10.1007/s40194-013-0097-4.

[5] J. Berg, N. Stranghöner, Fatigue behaviour of high frequency hammer peened ultra high strength steels, Int. J. Fatigue 82 (2016) 35–48, https://doi.org/10.1016/j.ijfatigue.2015.08.012.

[6] T. Skriko, M. Ghafouri, T. Björk, Fatigue strength of TIG-dressed ultra-high-strength steel fillet weld joints at high stress ratio, Int. J. Fatigue 94 (2017) 110–120, https://doi.org/10.1016/j.ijfatigue.2016.09.018.

[7] S.H.J. Van Es, M.H. Kolstein, R.J.M. Pijpers, F.S.K. Bijlaard, TIG-dressing of high strength butt welded connections - Part 2: physical testing and modelling, Procedia Eng. 66 (2013) 126–137, https://doi.org/10.1016/j.proeng.2013.12.068.

[8] T. Dahle, Design fatigue strength of TIG-dressed welded joints in high-strength steels subjected to spectrum loading, Int. J. Fatigue 20 (1998) 677–681, https://doi.org/10.1016/S0142-1123(98)00031-0.

[9] A. Hobbacher, Recommendations for Fatigue Design of Welded Joints and Components, second ed., Springer International Publishing, Cham, 2016.

[10] DNVGL-RP-C203, Fatigue Design of Offshore Steel Structures, 2016.

[11] BS7608:2014 +A1:2015, Guide to Fatigue Design and Assessment of Steel Products, 2015.

[12] EN 1993-1-9, Eurocode 3 - design of steel structures - Part 1-9, Fatigue (2005).

[13] C.M. Sonsino, Effect of residual stresses on the fatigue behaviour of welded joints depending on loading conditions and weld geometry, Int. J. Fatigue 31 (2009) 88–101, https://doi.org/10.1016/j.ijfatigue.2008.02.015.

[14] H.C. Yıldırım, G.B. Marquis, Fatigue strength improvement factors for high strength steel welded joints treated by high frequency mechanical impact, Int. J. Fatigue 44 (2012) 168–176, https://doi.org/10.1016/j.ijfatigue.2012.05.002.

[15] G.B. Marquis, Z. Barsoum, IIW Recommendations for the HFMI Treatment - for Improving the Fatigue Strength of Welded Joints, Springer Singapore, Singapore, 2016, https://doi.org/10.1007/978-981-10-2504-4.

[16] J. Hensel, T. Nitschke-pagel, K. Dilger, Fatigue performance of welded steel longitudinal stiffeners, in: Proc. 22nd Int. Offshore Polar Eng. Conf. Held Rhodes, Greece, 17-22 June, 2012, 2012, pp. 187–192.

[17] A. Ahola, T. Skriko, T. Björk, Experimental investigation on the fatigue strength assessment of welded joints made of S1100 ultra-high-strength steel in as-welded and post-weld treated condition, in: A. Zingoni (Ed.), Proc. 7th Int. Conf. Struct. Eng. Mech. Comput. (SEMC 2019). Cape Town, South Africa, 2-4 Sept. 2019, 2019, pp. 1254–1259.

[18] J. Hensel, T. Nitschke-Pagel, K. Dilger, Residual stress–based fatigue design of welded structures, Mater. Perform. Charact. 7 (2018) 630–642, https://doi.org/10.1520/mpc20170113.

[19] J. Hensel, Mean Stress Correction in Fatigue Design Under Consideration of Welding Residual Stress. Henry Granjon Prize Catecory C: Design and Structural Integrity. IIW-document XIII-2795-19, 2019.

[20] C. Cui, Q. Zhang, Y. Bao, J. Kang, Y. Bu, Fatigue performance and evaluation of welded joints in steel truss bridges, J. Constr. Steel Res. 148 (2018) 450–456, https://doi.org/10.1016/j.jcsr.2018.06.014.
[21] P. Luo, Q. Zhang, Y. Bao, Predicting weld root notch stress intensity factors for rib-to-deck welded joint under deck loading modes, Int. J. Fatigue 128 (2019) 105212, https://doi.org/10.1016/j.ijfatigue.2019.105212.
[22] J. Li, Q. Zhang, Y. Bao, J. Zhu, L. Chen, Y. Bu, An equivalent structural stress-based fatigue evaluation framework for rib- to-deck welded joints in orthotropic steel deck, Eng. Struct. 196 (2019) 109304, https://doi.org/10.1016/j.engstruct.2019.109304.
[23] T. Nykänen, T. Björk, Assessment of fatigue strength of steel butt-welded joints in as-welded condition - alternative approaches for curve fitting and mean stress effect analysis, Mar. Struct. 44 (2015) 288–310, https://doi.org/10.1016/j.marstruc.2015.09.005.
[24] T. Nykänen, T. Björk, A new proposal for assessment of the fatigue strength of steel butt-welded joints improved by peening (HFMI) under constant amplitude tensile loading, Fatigue Fract. Eng. Mater. Struct. 39 (2016) 566–582, https://doi.org/10.1111/ffe.12377.
[25] T. Nykänen, H. Mettänen, T. Björk, A. Ahola, Fatigue assessment of welded joints under variable amplitude loading using a novel notch stress approach, Int. J. Fatigue 101 (2017) 177–191, https://doi.org/10.1016/j.ijfatigue.2016.12.031.
[26] K.N. Smith, T.H. Topper, P. Watson, A stress–strain function for the fatigue of metals, J. Mater. 5 (1970) 767–778, https://doi.org/10.1179/1752270612Y.0000000008.
[27] Ö. Karakas, Consideration of mean-stress effects on fatigue life of welded magnesium joints by the application of the Smith-Watson-Topper and reference radius concepts, Int. J. Fatigue 49 (2013) 1–17, https://doi.org/10.1016/j.ijfatigue.2012.11.007.
[28] J. Baumgartner, T. Bruder, Influence of weld geometry and residual stresses on the fatigue strength of longitudinal stiffeners, Weld. World 57 (2013) 841–855, https://doi.org/10.1007/s40194-013-0078-7.
[29] T. Björk, H. Mettänen, A. Ahola, M. Lindgren, J. Terva, Fatigue strength assessment of duplex and super-duplex stainless steels by 4R method, Weld. World 62 (2018) 1285–1300, https://doi.org/10.1007/s40194-018-0657-8.
[30] A. Ahola, T. Nykänen, T. Björk, Effect of loading type on the fatigue strength of asymmetric and symmetric transverse non-load carrying attachments, Fatigue Fract. Eng. Mater. Struct. 40 (2017) 670–682, https://doi.org/10.1111/ffe.12531.
[31] H.C. Yıldırım, Recent results on fatigue strength improvement of high-strength steel welded joints, Int. J. Fatigue 101 (2017) 408–420, https://doi.org/10.1016/j.ijfatigue.2016.10.026.
[32] C.M. Sonsino, W. Fricke, F. De Bruyne, A. Hoppe, A. Ahmadi, G. Zhang, Notch stress concepts for the fatigue assessment of welded joints - background and applications, Int. J. Fatigue 34 (2012) 2–16, https://doi.org/10.1016/j.ijfatigue.2010.04.011.
[33] P.J. Haagensen, S.J. Maddox, IIW Recommendations on Post Weld Improvement of Steel and Aluminium Structures. IIW-Document XIII-2200r7-07 (Revision 6 July 2010, 2010.
[34] M. Leitner, M. Khurshid, Z. Barsoum, Stability of high frequency mechanical impact (HFMI) post-treatment induced residual stress states under cyclic loading of welded steel joints, Eng. Struct. 143 (2017) 589–602, https://doi.org/10.1016/j.engstruct.2017.04.046.
[35] C. Cui, Q. Zhang, Y. Bao, S. Han, Y. Bu, Residual stress relaxation at innovative both-side welded rib-to-deck joints under cyclic loading, J. Constr. Steel Res. 156 (2019) 9–17, https://doi.org/10.1016/j.jcsr.2019.01.017.
[36] M. Amraei, A. Ahola, S. Afkhami, A. Heidarpour, T. Björk, X.-L. Zhao, Effects of heat input on the mechanical properties of butt-welded high and ultra-high strength steels, Eng. Struct. 198 (2019) 109460, doi:j.engstruct.2019.109460.
[37] N.E. Dowling, Mechanical Behavior of Materials. Engineering Methods for Deformation, Fracture, and Fatigue, Prentice Hall, 2006.
[38] M. Leitner, Influence of effective stress ratio on the fatigue strength of welded and HFMI-treated high-strength steel joints, Int. J. Fatigue 102 (2017) 158–170, https://doi.org/10.1016/j.ijfatigue.2017.03.008.
[39] J. Baumgartner, T. Bruder, An efficient meshing approach for the calculation of notch stresses, Weld. World 57 (2013) 137–145, https://doi.org/10.1007/s40194-012-0005-3.
[40] W.E. Deming, Statistical Adjustment of Data, Dover Publication Inc., 1943.
[41] M. Leitner, W. Mössler, A. Putz, M. Stoschka, Effect of post-weld heat treatment on the fatigue strength of HFMI-treated mild steel joints, Weld. World 59 (2015) 861–873, https://doi.org/10.1007/s40194-015-0265-9.
[42] J. Baumgartner, P.G. Ruiz, H.C. Yıldırım, Fatigue assessment of TIG-dressed joint with local approaches, IIW Intermed. Meet. Held Braunschweig, 23 March 2018, 2018. IIW-Document XIII-WG3-56-18.
[43] D. Radaj, C.M. Sonsino, W. Fricke, Fatigue Assessment of Welded Joints by Local Approaches, second ed., Woodhead Publishing, Cambridge, 2006.
[44] T. Skriko, Dependence of Manufacturing Parameters on the Performance Quality of Welded Joints Made of Direct Quenched Ultra-high-strength Steel, Lappeenranta University of Technology, 2018. Doctoral Dissertation.
[45] T. Björk, A. Ahola, T. Skriko, 4R method for consideration of the fatigue performance of welded joints - background and applications, in: S.-L. Chan, T.-M. Chan, S. Zhu (Eds.), Ninth Int. Conf. Adv. Steel Struct. (ICASS 2018), 2018, pp. 1159–1168, https://doi.org/10.18057/ICASS2018.P.141. Hong Kong.
[46] T. Stenberg, Z. Barsoum, E. Åstrand, A. Ericson Öberg, C. Schneider, J. Hedegård, Quality control and assurance in fabrication of welded structures subjected to fatigue loading, Weld. World 61 (2017) 1003–1015, https://doi.org/10.1007/s40194-017-0490-5.
[47] J. Hensel, T. Nitschke-pagel, K. Dilger, On the effects of austenite phase transformation on welding residual stresses in non-load carrying longitudinal welds, Weld. World (2015) 179–190, https://doi.org/10.1007/s40194-014-0190-3.
[48] J. Zhu, M. Khurshid, Z. Barsoum, Accuracy of computational welding mechanics methods for estimation of angular distortion and residual stresses, Weld. World (2019), https://doi.org/10.1007/s40194-019-00746-9.
[49] P. Ferro, F. Berto, M.N. James, A simplified model for TIG-dressing numerical simulation, Model. Simul. Mater. Sci. Eng. 25 (2017).
[50] C. Deng, Y. Niu, B. Gong, Y. Liu, D. Wang, Numerical assessment of fatigue design curve of welded T-joint improved by high-frequency mechanical impact (HFMI) treatment, Adv. Eng. Software 114 (2017) 154–162, https://doi.org/10.1016/j.advengsoft.2017.06.017.
[51] Y. Liu, B. Gong, C. Deng, C. Zhao, X. Liu, D. Wang, Numerical analysis of optimum treatment parameters by high frequency mechanical impact, J. Constr. Steel Res. 150 (2018) 23–30, https://doi.org/10.1016/j.jcsr.2018.08.004.
[52] S. Han, T. Lee, B. Shin, Residual stress relaxation of welded steel components under cyclic load, Steel Res. Int. 73 (2002) 414–420, doi:srin.200200008|.
[53] T. Skriko, T. Björk, T. Nykänen, Effects of weaving technique on the fatigue strength of transverse loaded fillet welds made of ultra-high-strength steel, Weld. World 58 (2014) 377–387, https://doi.org/10.1007/s40194-014-0123-1.

Publication V

Ahola, A., Muikku, A., Braun, M., and Björk, T.
Fatigue strength assessment of ground fillet-welded joints using 4R method

Reprinted with permission from
International Journal of Fatigue
Vol. 142, 105916, 2021

International Journal of Fatigue 142 (2021) 105916

Contents lists available at ScienceDirect

International Journal of Fatigue

journal homepage: www.elsevier.com/locate/ijfatigue

Fatigue strength assessment of ground fillet-welded joints using 4R method

Antti Ahola[a,*], Arttu Muikku[a], Moritz Braun[b], Timo Björk[a]

[a] Laboratory of Steel Structures, Lappeenranta-Lahti University of Technology LUT, P.O. Box 20, FI-53851 Lappeenranta, Finland
[b] Institute for Ship Structural Design and Analysis, Hamburg University of Technology, Am Schwarzenberg Campus 4C, D-21073 Hamburg, Germany

ARTICLE INFO

Keywords:
Fatigue
Welded joint
Grinding
Peening
4R method

ABSTRACT

In the present paper, a fatigue analysis for welded joints made of mild, and high- and ultra-high-strength steel grades and post-weld-treated with grinding and combined grinding and peening methods is carried out using literature data. The 4R method was used to re-analyze the data points considering material strength, residual stress, applied stress ratio, and weld toe radius. The use of the 4R method, instead of local fatigue strength assessment approaches, enabled residual stresses to be taken into consideration and accurately predicted the fatigue strength of joints in the as-welded and post-weld-treated conditions, including grinding and combined grinding and peening methods.

1. Introduction

A wide range of steel constructions and components undergo fluctuating and cyclic load conditions during service. Hence, fatigue strength is among the most important design criteria. In welded components, the consideration of fatigue behavior is even more important as welding is associated with thermal cycles, causing tensile residual stresses, as well as welding deformations. High tensile residual stresses, equal to up to the yield strength of the material, increase local mean stress level at the fatigue-critical details, and welding deformations and misalignments can cause an increase in macro-geometric stresses, thus exposing welded joints to fatigue failures. In addition, a sharp transition from the plate component to the weld reinforcement, even if no initial flaws are present, introduces a local notch stress concentration, which makes the weld toes susceptible to fatigue crack initiation (CI) and subsequently crack propagation (CP). To overcome the issues causing low fatigue strength of welded joints in the as-welded (AW) condition, the implementation of post-weld treatments (PWTs) has attracted both academic and industrial interest, and a wide range of PWT methods has been developed in recent decades. In general, PWTs can be divided into two categories: methods for improving the weld toe geometry and thus lowering the notch stress concentration, and methods for modifying residual stress state at the weld toe [1]. Notch stress concentration at weld toes can be reduced by introducing machining methods, such as burr and disc grinding, or re-melting methods, such as tungsten inert gas (TIG), laser or plasma dressing. Residual stresses can be modified either globally, for example by thermal treatments, or locally by introducing overloads or peening methods, such as high-frequency mechanical impact (HFMI) treatments. Full descriptions of these methods are given in the IIW guidelines for PWTs [1] and partial ones covered in design codes [2,3].

To select an appropriate PWT method for a given engineering application, careful consideration of material characteristics and load conditions is needed. Re-melting methods might change the metallurgy of the dressed region and, consequently, affect the corrosion behavior of stainless steel grades [4], as well as the ultimate strength and ductility of direct-quenched ultra-high-strength steels [5,6]. Peening methods are notably more effective for high- and ultra-high-strength steel joints than for mild steels [7,8], while the beneficial effect of the HFMI treatment is lost at high mean stress levels [1] and overload peaks [9]. Consequently, grinding is a recommended PWT method to enhance the fatigue strength of welded joints although it is not the most cost-effective one [10–12]. The grinding procedure, nevertheless, usually provides at least a moderate improvement in fatigue strength compared to joints in the AW condition, regardless of the environmental [13] or load conditions [14], and material strength [15]. Furthermore, grinding tools are normally readily accessible and can thus be easily adopted in workshops, and treatment quality can be simply inspected by determining the radius and depth resulting from the grinding treatment.

One concern related to the implementation of PWTs is the consideration of the fatigue strength improvement of fatigue assessment of welded joints. The most rudimentary and conventional approach has been to assess the fatigue strength using the nominal stress approach, and fatigue strength improvements can be incorporated in fatigue analysis by implementing an increase in the fatigue class (FAT). Nevertheless, due to the increased computational capacity achieved in

* Corresponding author.
E-mail address: antti.ahola@lut.fi (A. Ahola).

https://doi.org/10.1016/j.ijfatigue.2020.105916
Received 24 July 2020; Received in revised form 19 August 2020; Accepted 24 August 2020
Available online 29 August 2020

recent decades, a more common engineering approach is to evaluate the fatigue strength of welded joints using local approaches, particularly notch stress-based concepts employing finite element (FE) modeling, even large-scale components. Pedersen *et al.* [16] conducted an extensive fatigue data analysis for various welded details in the AW and post-weld-treated (burr-ground, TIG-dressed, HFMI-treated) conditions using a notch stress approach with a fixed reference radius of r_{ref} = 1.0 mm after the effective notch stress (ENS) concept [17], regardless of the joint condition. Using this approach, a characteristic design fatigue strength of FAT320 with the slope parameter of *S-N* curve of m = 3 was suggested for both burr-ground and TIG-dressed joints, and of FAT360 with m = 5 for HFMI-treated joints. In a recent study, Mecséri and Kövesdi [18] re-analyzed experimental fatigue test data of welded specimens post-weld-treated with grinding considering the radius of ground weld toe, finding a good correspondence with numerically and experimentally determined mean fatigue strengths using the ENS concept. Another means of considering notch stresses in the fatigue analysis is to apply the theory of critical distance (TCD) or stress averaging concepts. Baumgartner *et al.* [19,20] statistically evaluated the critical distances of a = 0.6 mm and a = 0.1 mm, based on the maximum principal stress hypothesis, for welded steel joints in the AW and TIG-dressed condition, respectively. It is also worth mentioning that reasonable accuracies were found with different critical distances between a = 0.1–1 mm [19,20]. Karakaş *et al.* [21] found a critical distance of a = 0.06 mm for welded magnesium alloys. In addition, Braun *et al.* [22] have demonstrated the applicability of the stress averaging concept for ground specimens.

Notch stress-based approaches, with multiple different definitions and concepts, take local stress into account in fatigue assessment. However, they do not take into consideration of material strength (if not considered in micro-support length or notch sensitivity), applied stress ratio, or residual stresses. Moreover, current design codes and guidelines do not address the effect of combined PWTs, for example weld toe grinding (TG) followed by peening, for which higher fatigue strengths have been obtained in prior studies [23–25], than those joints obtained from individually-applied grinding or peening treatments. To consider the combined effect of residual stresses and external load conditions, in association with notch effects and material strength, Nykänen and Björk [26,27] introduced an ENS-based approach combined with the Smith-Watson-Topper (SWT) mean stress correction for the fatigue strength assessment of C-Mn steel welded joints in the AW and HFMI-treated condition. While this approach was in development, the authors named the 4R method after four '*R*'-letter parameters considered in the analysis (applied stress ratio R, material ultimate strength R_m, residual stress σ_{res} and weld toe radius r). The applicability of the approach was also verified for variable amplitude loads [28], duplex and super-duplex stainless steel grades [29], and TIG-dressed joints [30,31].

Prior studies of the 4R method have not addressed welded joints post-weld-treated with either grinding methods or combined grinding and peening (G&P) methods. The aim of the current study is to use the 4R method to assess the fatigue strength of fillet weld joints post-weld-treated with grinding methods and, thus, show the general applicability of the approach for assessing the fatigue strength of joints treated with various PWT methods. An extensive literature research was carried out to collect fatigue test data for fillet-welded joints in the AW condition and post-weld-treated using burr grinding, disc grinding, weld profiling (WP), and combined G&P methods, and tested under uniaxial constant amplitude loading. From these studies, the weld profile and toe geometries were evaluated based on the available macro graphs, geometry measurements, and details related to preparation of grinding. For each test series, a three-dimensional (3D) solid element FE model was created to obtain the notch stress concentration factors (SCFs). Furthermore, the available residual stress measurements for joints in the AW, ground, and G&P condition is collected to approximate the residual stresses. Local stress–strain behavior was analytically approximated at the location of the maximum stress at the notch root for each test result to obtain the local stress ratio, and the mean stress correction was conducted based on the local stress ratio acting at the notch root. The results obtained under 4R method are compared with those obtained under the ENS approach.

2. Fatigue strength improvement with grinding

2.1. Treatment procedures and current design guidelines

Fatigue strength improvement by grinding PWT methods is based on the removal of material from the weld toe using tools with a rounded profile, such as rotary burrs and discs. In butt-welded details, the whole weld reinforcement can be ground flat; in the case of fillet welds, however, typically the fillet weld is profiled with grinding tools or, alternatively, the grinding is applied only locally at the weld toe. WP requires more material to be removed than under toe treatments but typically provides a smoother transition from the base material to the filler metal. To implement a successful grinding treatment, the resulting radius at the weld toe should be higher than 0.2 t (where t is the plate thickness) and have a minimum grinding depth of d = 0.5 mm but no more than 7% of plate thickness, as per the IIW Recommendations for grinding PWTs [1].

As in many other PWT methods, the improvement in fatigue strength gained by grinding can be limited by the change in fatigue failure location, particularly in load-carrying (LC) joints but also in non-load-carrying (NLC) joints. Prior investigations [23,32] have clearly demonstrated the weld root failures in post-weld-treated longitudinal gusset joints. Fig. 1 demonstrates fatigue failures at inter-bead toes in multi-pass fillet-welded joints. Weld root failures can be avoided by increasing weld penetration through the use of groove preparation or welding techniques while, as demonstrated in Fig. 1b, inter-bead fatigue cracking can be efficiently avoided by extending the ground region to also cover the weld face, thus realizing full potential of fatigue strength improvement.

The current codes and design guidelines for the fatigue design of ground welds cover nominal stress and structural hot-spot (HS) stress approaches. A 30% increase in fatigue strength is provided for ground joints by the IIW Recommendations for PWTs [1]. In the nominal stress approach, this refers to a two-fatigue class improvement, and in the structural HS stress approach, design curves of FAT125 and FAT112 with *S-N* curve slope parameter of m = 3 are recommended for ground NLC and LC welded joints, respectively. In the fatigue design guidelines for offshore steel structures [2], a higher slope parameter of m = 3.5 is

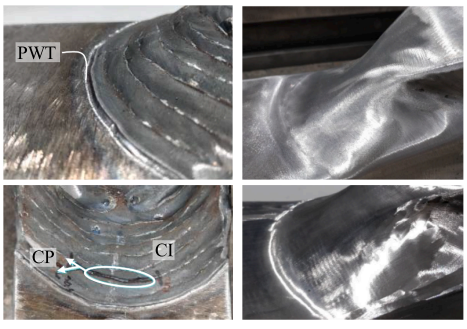

Fig. 1. (a) Fatigue CI and CP at a HFMI-treated joint at the inter-bead toe of a multi-pass weldment, and (b) corresponding ground joint with longitudinal finishing.

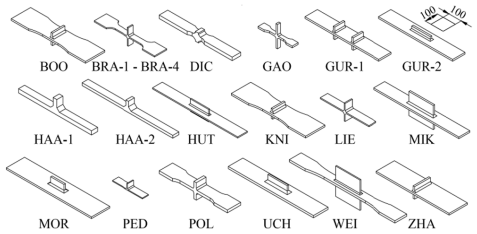

Fig. 2. Joint types in the extracted data (dimensions in scale and in mm), see acronyms in Table 1.

given for ground joints. In a recent study [33], a *S-N* curve slope parameter of $m = 4$ was proposed based on a literature review of experimental findings. Nevertheless, although treatment procedures are given in design guidelines [1–3], the nominal stress and structural HS stress approaches do not address the geometrical effects, that is, the resulting grinding radius and depth, on the fatigue strength capacity of a ground joint.

2.2. Fatigue test data of specimens in the as-welded and ground condition

A literature review of the existing experimental studies related to the fatigue strength of welded post-weld-treated with grinding methods was carried out to collect fatigue test data to evaluate fatigue strength using the 4R method, described in Section 3. The main objective of the literature review was to collect the data on ground welded specimens but also data of joints in the AW condition was collected for purposes of comparison. The collected data consisted of various grinding methods: TG, covering both burr and disc grinding methods; WP, in which the weld reinforcement is profiled; combined G&P methods, in which the grinding is followed by mechanical peening to introduce beneficial compressive residual stresses.

From these studies, together with the extracted test data points, details regarding the specimen and weld geometry were evaluated to prepare FE models. Weld profiles and weld toe geometries were primarily determined based on the measurements and analyses conducted within the studies or defined based on the available etched or polished sections. In most cases, weld toe radii for AW specimens were not available, as described in Table 1, and for those test series, $r_{true} = 0$ was assumed according to the worst-case assumption [34]. In a few test series, neither geometry measurements nor macro graphs were available but the details regarding the applied burr tool and treatment were comprehensively described. In such ground joints, the weld toe radius was assumed to be equal to the radius of the grinding tool. Expectedly, for practical reasons, the resulting true weld toe radius is slightly higher than the radius of burr tool but as described in Section 4, when the weld toe radius produced by the BG increases, its effect on the notch SCF significantly decreases. Consequently, reasonably small error in the estimation of weld toe radius leads to a small but conservative overassessment of notch SCF.

The literature research revealed several comprehensive studies were found. However, in some of these, the *S-N* curves or tables providing experimental results were unreadable or untraceable in terms of data points. Furthermore, some studies did not provide any essential information on the grinding treatment or weld geometry. Ambiguous fatigue test series such as these were excluded from the fatigue analysis of this study. Fatigue-tested specimens were still available for further analyses from a recent study by Braun *et al.* [15], and the un-failed side of the NLC cruciform specimens were 3D-scanned with a Hexagon Romer device to obtain weld geometries – the resulting geometries are shown in Fig. 3. Table 1 summarizes the extracted fatigue test data series and gives the details of load and joint conditions. A total number of 607 fatigue test results was extracted from the literature, and the joint conditions were categorized into AW, TG, WP and G&P joints.

3. Fatigue assessment of as-welded and ground joints using the 4R method

3.1. Theoretical foundation

The 4R method is based on the determination of cyclic behavior at the notch root accounting for material strength properties (stress–strain curve), local residual stress σ_{res} induced by the welding and subsequently potentially modified by the PWTs, applied stress ratio R, and weld toe quality r_{true}. Prior investigations (see, for example, [27,28,30,48]) have given fill descriptions of the theoretical foundation of the 4R method and the related equations. The 4R method aims to determine the local stress ratio, shown in Fig. 4, which is applied with the SWT mean stress correction:

$$\Delta\sigma_{k,ref} = \frac{\Delta\sigma_k}{\sqrt{1 - R_{local}}} \quad (1)$$

In Eq. (1), $\Delta\sigma_{k,ref}$ is the mean stress-corrected reference notch stress range, $\Delta\sigma_k$ is the (linear elastic) ENS range, and R_{local} is the local stress ratio ($\sigma_{\min}/\sigma_{\max}$), as demonstrated in Fig. 4. The use of the reference ENS range, in terms of the local cyclic behavior and notch stress concentration, commeasures the fatigue test data points into a single *S-N* curve. When adopting the 4R method for ground joints, no modifications in the basic theory are conducted. The grinding and combined G&P methods are in the main focus of this study, which follows the basic concepts accordingly. The 4R analysis, illustrated in in Fig. 4, can be summarized as follows:

(a) A welded joint can be in the AW or post-weld-treated condition. If grinding is adopted, a reduction of notch SCF is achieved. The joint can be treated with peening methods which do not significantly affect the weld toe geometry but introduce beneficial compressive residual stresses.
(b) Nominal (external) cyclic stress (σ_{nom}) is identical for the AW and ground joints. The ENS range is obtained based on external loading and notch SCFs (see Section 3.2.2 for further details). Due to the increased weld toe radius, the notch stress range is lower for ground joints.
(c) In welded joints in the AW condition, tensile residual stresses, equal to up to the yield strength of the material, are typically present. Notch SCF is reduced by grinding, and a decrease in tensile residual stresses can occur locally at the weld toe as the global residual stresses are not superposed with high notch SCFs. If peening methods are employed, compressive residual stresses are introduced (see Section 3.2.1 for further details). During the cyclic loading, the residual stresses may relax due to over- or underloads or the stabilization of compressive residual stresses.
(d) Residual stress sets the starting point at the stress–strain (R-O) curve. The linear elastic stress range (b) is converted to elastic plastic behavior at the notch root, and the local stress ratio is determined based on the local minimum and maximum stress ($\sigma_{\min}$ and $\sigma_{\max}$).

3.2. 4R parameters

3.2.1. Residual stress

For joints in the AW condition, tensile residual stresses up to the yield strength of the material at the weld toes can be assumed in fatigue design [49]. This is a conservative, but justifiable, assumption in engineering design since welded structural components cannot deform freely due to the stiffness of the whole structure. In small-scale fatigue test specimens, however, the deformation are not usually prevented; consequently, the residual stresses are also significantly lower [50,51].

Table 1
Extracted fatigue test data for the ground specimens. $f_y/R_{p0.2}$ is the yield or proof strength of material, n is the number of test specimens in the series (failure at the investigated area), and d_{true} is the grinding depth.

Ref.	t [mm]	Steel grade	$f_y/R_{p0.2}$ [MPa]	Joint type[a]	Load type[b]	Joint cond.	Tool[c]	n [-]	R [-]	r_{true} [mm]	d_{true} [mm]	Acr.
[14]	12.5	BS 43A	260[e]	NLCX	A	AW	–	12	−1 & 0.5	0	0	BOO
[14]	12.5	BS 43A	260[e]	NLCX	A	TG	DG	16	−1 & 0.5	2.65	0.8	BOO
[15]	8	S900	972[d]	NLCX	A	AW	–	9	0	0.4	0	BRA-1
[15]	8	S900	972[d]	NLCX	A	WP	LG	11	0	9.6	0.2	BRA-1
[35]	8	S690	735[d]	NLCX	A	AW	–	12	0	0.6	0	BRA-2
[35]	8	S690	735[d]	NLCX	A	WP	LG	21	0	8.2	0.5	BRA-2
[35]	8.4	1.4462	608[d]	NLCX	A	AW	–	12	0	0.8	0	BRA-3
[35]	8.4	1.4462	608[d]	NLCX	A	WP	LG	17	0	8.3	0.4	BRA-3
[35]	8	S355	450[d]	NLCX	A	AW	–	9	0	0.7	0	BRA-4
[35]	8	S355	450[d]	NLCX	A	WP	LG	15	0	8.4	0.45	BRA-4
[23]	12.7	BS 15	280[d]	NLCX	A	AW	–	7	−1	0	0	GUR-1
[23]	12.7	BS 15	280[d]	NLCX	A	TG	BG	7	0	3.4	0.1	GUR-1
[23]	12.7	BS 968	350[d]	NLCX	A	TG	BG	6	0	3.4	0.1	GUR-1
[23]	12.7	BS 15	280[d]	NLCX	A	WP	BG	11	−1 & 0	6.8	0.25	GUR-1
[23]	12.7	BS 968	350[d]	NLCX	A	WP	BG	9	−1 & 0	6.8	0.25	GUR-1
[23]	12.7	BS 15	280[d]	NLCX	A	G&P	BG	5	0	6.8	0.25	GUR-1
[23]	12.7	BS 968	350[d]	LG	A	AW	–	4	0	0	0	GUR-2
[23]	12.7	BS 15	280[d]	LG	A	TG	BG	6	0	1.2	0.1	GUR-2
[23]	12.7	BS 15	280[d]	LG	A	WP	BG	17	−1 & 0	6.8	0.25	GUR-2
[23]	12.7	BS 968	350[d]	LG	A	WP	BG	6	0	6.8	0.25	GUR-2
[24]	30	C-Mn steel	380[d]	NLCT	4B	AW	–	7	0.1	0	0	HAA-1
[24]	30	C-Mn steel	380[d]	NLCT	4B	TG	BG	6	0.1	6	0.5	HAA-1
[24]	30	C-Mn steel	380[d]	NLCT	4B	G&P	BG	6	0.1	6	0.5	HAA-1
[36]	20	S420	463[d]	NLCT	4B	AW	–	56	0.1	0	0	HAA-2
[36]	20	S420	463[d]	NLCT	4B	TG	BG	47	0.1	6	0.8	HAA-2
[25]	12.7	DH36	375[d]	NLCX	A	AW	–	13	0	0.8	0	GAO
[25]	12.7	DH36	375[d]	NLCX	A	TG	BG	11	0	3.2	0.9	GAO
[25]	12.7	DH36	375[d]	NLCX	A	G&P	BG	10	0	3.2	0.9	GAO
[37]	12.7	BS 43A	245[e]	NLCX	A	AW	–	9	0	0	0	KNI
[37]	12.7	BS 43A	245[e]	NLCX	A	TG	DG	13	0	3.5	0.6	KNI
[37]	12.7	Superelso 70	685[e]	NLCX	A	AW	–	5	0	0	0	KNI
[37]	12.7	Superelso 70	685[e]	NLCX	A	TG	DG	4	0	3.5	0.6	KNI
[38]	12.5	S355	406[d]	NLCX	A	TG	BG	2	0.1	4.2	0.8	ZHA
[38]	12.5	S355	406[d]	NLCX	A	G&P	BG	4	0.1	4.2	0.8	ZHA
[39]	20	DH36	355[e]	NLCX	A	AW	–	11	0.1	0	0	POL
[39]	20	DH36	355[e]	NLCX	A	BG	BG	5	0.1	6.5	0.55	POL
[40]	16	SM490YA	425[d]	LG	A	AW	–	8	0–0.1	1.1	0	UCH
[40]	16	SM490YA	425[d]	LG	A	TG	BG	18	0–0.1	3	0.1;0.5;1.5	UCH
[40]	16	SM490YA	425[d]	LG	A	TG	BG	16	0–0.1	5	0.1;0.5;1.5	UCH
[41]	6	S700	700[e]	NLCT	4B	AW	–	17	0.1	0	0	PED
[41]	6	S700	700[e]	NLCT	4B	TG	BG	11	0.1	3	0.3	PED
[42]	8	S700	794[d]	NLCX	A	AW	–	30	0.2–0.73	2.3	0	LIE
[42]	8	S700	794[d]	NLCX	A	TG	BG	9	0.2	4.3	0.5–0.8	LIE
[43]	8	S700	700[e]	LG	A	AW	–	7	0.1 & 0.5	0.7	0	HUT
[43]	8	S700	700[e]	LG	A	TG	BG	8	0.1 & 0.5	5.2	0.5	HUT
[44]	16	S690	719[d]	LG	A	AW	–	9	0.1	1.5	0	WEI
[44]	16	S690	719[d]	LG	A	TG	BG	8	0.1	2.66	0.5	WEI
[45]	24	A515 Grade 70	411[d]	LCX	A	AW	–	4	0	0	0	DIC
[45]	24	A515 Grade 70	411[d]	LCX	A	TG	BG	4	0	3.8;8.5	0.8	DIC
[46]	12	SBHS500	633[d]	LG	A	AW	–	6	0.1	0.2	0	MIK
[46]	12	SBHS500	633[d]	LG	A	TG	BG	4	0.1	2.7	0.5	MIK
[46]	12	SBHS500	633[d]	LG	A	G&P	BG	14	0.1	3.2;2.9	0.8;0.6	MIK
[47]	12	SM490YA	417[d]	LG	A	AW	–	6	0–0.1	1.4	0	MOR
[47]	12	SM490YA	417[d]	LG	A	AW[f]	DG	5	0–0.1	1.4	0	MOR
[47]	12	SM490YA	417[d]	LG	A	TG	BG	1	0–0.1	6.2	0.4	MOR
[47]	12	SM490YA	417[d]	LG	A	WP	DG	1	0–0.1	11.4	0.1	MOR

[a] X = cruciform joint, T = T-joint, LG = longitudinal gusset joints (see also Fig. 2).
[b] Load type: A = axial loading, 4B = four-point bending.
[c] Grinding tool: disc grinder (DG), lamellar grinder (LG), burr grinder (BG).
[d] Measured value.
[e] Nominal value.
[f] Weld face ground but no treatment at the weld toe (BI specimens).

Furthermore, the magnitude of residual stresses can be influenced by the welding sequence and interpass temperature [52,53]. The magnitude of residual stresses in small-scale specimens is also related to joint type. For instance, in transverse weldments, such as butt-welded joints and transverse attachment joints without preventing deformations, angular distortion can occur freely, which reduces the formation of residual stresses. In contrast, in fillet-welded LG joints, the free contradiction of weld metal at the cooling phase is prevented due to the axial stiffness of the adjoined plate components, which results in higher residual stresses.

The above-described concepts regarding welding residual stresses in small-scale specimens are widely supported by experimental findings: for transverse attachments in the AW condition, nearly zero residual stresses were reported, and the grinding does not have a significant

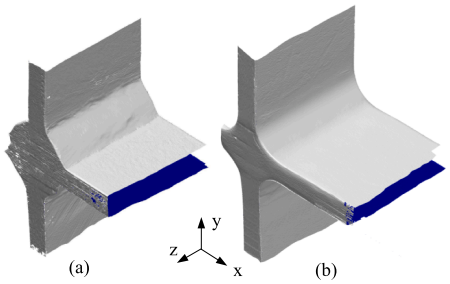

Fig. 3. 3D-scanned geometries for the S900 NLCX joints tested in [15]: (a) a NLCX joint in the AW condition, and (b) a weld-profiled NLCX joint.

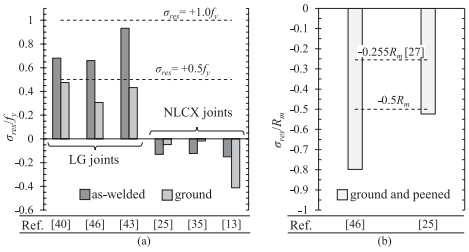

Fig. 5. Results of published residual stress measurements: (a) LG and NLCX joints in the AW and ground condition, and (b) ground and subsequently pneumatically peened joints.

influence on the negligible low residual stresses (see, for example, [13,25,35]). In LG joints, high tensile residual stresses parallel to the loading direction have been measured up to $\sigma_{res} = +0.9f_y$ in the vicinity of the weld toe, while grinding can reduce the tensile residual stresses to some extent [40,43,46]. Beneficial compressive residual stresses can be introduced using peening methods. Nykänen and Björk [27] reported a conservative approximation for residual stresses after peening of $\sigma_{res} = -0.255R_m$, covering various peening methods. For ground and pneumatically peened joints, even higher compressive residual stresses have been reported in prior studies [25,46]. Fig. 5 summarizes the results of residual stress measurements indicated in the studies from which the data points were extracted for the present paper.

Most of the experimental studies extracted for the present study, see Table 1, lack residual stress measurements, or these were not reported. Consequently, the residual stresses were approximated on the basis of the published results, as shown in Fig. 5, using conservative assumptions. Furthermore, the relaxation of residual stresses was neglected in this study. The following approximations of residual stresses were conducted (see also Fig. 5 for a comparison):

- AW condition: in LG joints, $\sigma_{res} = +f_y$ and in transverse fillet weld joints, $\sigma_{res} = 0$
- Ground condition: in LG joints, $\sigma_{res} = +0.5f_y$ and in transverse fillet weld joints, $\sigma_{res} = 0$
- Ground and peened: $\sigma_{res} = -0.5R_m$

3.2.2. *Effective notch stress range*

FE analyses were employed to obtain the notch SCFs and, subsequently, the ENS for the fatigue analysis. To consider the fatigue effective notch factors, the notch SCFs were obtained using fictitious radii of $r = r_{true} + 1$ mm according to the ENS concept [17] and 4R method [27,30]. When enlarging the radius by 1 mm to obtain the fatigue-effective SCF, the undercut (dent) depth was held as original. For joints in the AW condition, $r_{true} = 0$ was assumed if no further information was available, as shown Table 1, and the notch SCFs for the 4R method correspond to the ENS concept with the reference radius of $r_{ref} = 1.0$ mm. The SCFs were obtained numerically using linear hexahedral solid element mesh models and the maximum principal stress criterion. At weld toes, a mesh size less than $r/20$ corresponding to 125 elements over a 360° arc was used to obtain SCFs accurately, following the mesh convergence study by Baumgartner and Bruder [54]. Fig. 6 depicts the element mesh used in the FEAs.

As clearly indicated in a prior study [55], notch SCFs are different for membrane and bending stress loads. Consequently, notch SCFs were obtained separately for such loads, that is, DOB = 0 and DOB = 1. Braun *et al.* [15,35] reported welding-induced angular distortions and subsequent bending stresses for each fatigue-tested NLCX specimen, with misalignment factors varying between $k_m = 1.5$–2.4, $k_m = 1.0$–1.2, $k_m = 1.0$–1.8, and $k_m = 1.0$–1.2 for BRA-1 (S900), BRA-2 (S690), BRA-3 (1.4462), and BRA-4 (S355) data sets, respectively. In other experimental studies conducted for axially loaded joints, and included in this study, neither angular distortions nor secondary

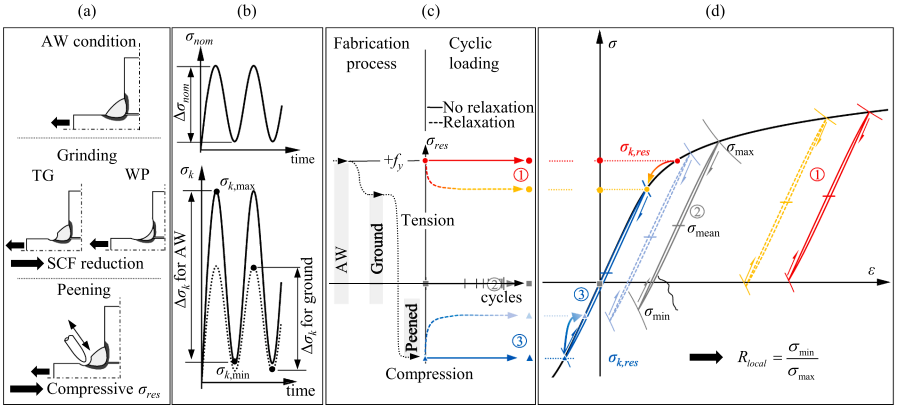

Fig. 4. Steps to determine the cyclic behavior of welded joints in the AW and ground conditions under CA loading: (a) joint characteristics, (b) notch stress range based on the external loading and SCF, (c) local residual stresses after welding, PWT and under cyclic loading, and (d) local cyclic stress loops for the joints.

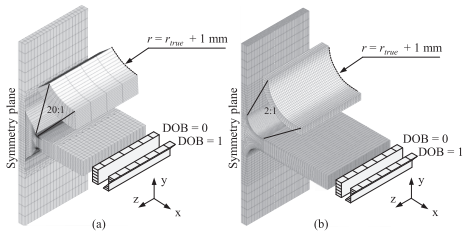

Fig. 6. FE models to obtain notch SCFs: (a) a NLCX joint in the AW condition and (b) a weld-profiled NLCX joint, corresponding to the specimen geometries presented in Fig. 3. DOB is the degree of bending (bending stress divided by the total stress).

bending stresses were available or reported, as the nominal stress method covers only a certain degree of misalignment in *S-N* curves. Consequently, a fixed distortion and misalignment factor of $k_m = 1.25$ was approximated according to the IIW Recommendations [56]. In the case of four-point bending, the angular distortion does not cause any secondary stresses, and notch stress ranges can be calculated directly using bending stresses and the corresponding notch SCF. The ENS was calculated with the superposition principle as follows for axially loaded joints:

$$\begin{aligned}\Delta\sigma_k &= K_{t,m}(r)\Delta\sigma_{m,nom} + K_{t,b}(r)\Delta\sigma_{b,nom} \\ &= [K_{t,m}(r) + K_{t,b}(r)(k_m - 1)]\Delta\sigma_{m,nom}\end{aligned} \quad (2)$$

and for four-point bending-loaded joints simply:

$$\Delta\sigma_k = K_{t,b}(r)\Delta\sigma_{b,nom} \quad (3)$$

In Eqs. (2) and (3), $K_{t,m}(r)$ and $K_{t,b}(r)$ are the notch SCFs for membrane and bending stresses, respectively, using a toe radius of r, and $\Delta\sigma_{m,nom}$ and $\Delta\sigma_{b,nom}$ are the membrane and bending stress ranges, respectively. In the case of LG joints, the $K_{t,m}$ and $K_{t,b}$ SCFs also includes the structural SCF induced by the gusset. Fig. 7 presents the notch SCFs for the extracted specimens in the AW and ground conditions. For the G&P specimens, the notch SCFs are similar to the ground specimens since peening does not majorly modify the geometrical shape of notch root.

3.2.3. Material behavior and applied stress ratio

All extracted fatigue test data series included information about the materials used in the experimental program. From the perspective of 4R analysis, it is essential to include material behavior in the fatigue analysis, as it describes the local maximum and minimum stress from which the local stress ratio is obtained. Nevertheless, the strain amplitude is not employed in the fatigue assessment, and the result is therefore not affected by uncertainties related to the obtained strain amplitudes. Instead, it is important to consider stress behavior, that is, the maximum and minimum stresses should be estimated as accurately as possible. For low-alloyed mild steels, a strain hardening coefficient of $H' = 1.65R_m$ and exponent of $n' = 0.15$ can be estimated [57] for the Ramberg-Osgood (R-O) material curve. This assumption does not, however, necessarily provide correct yield/proof and ultimate strengths for the estimated R-O curve as the parameters are fixed based on the ultimate strength. In addition, for high- and ultra-high-strength steel grades, the yield strength to ultimate strength ratio is usually higher than it is for mild steels [58,59].

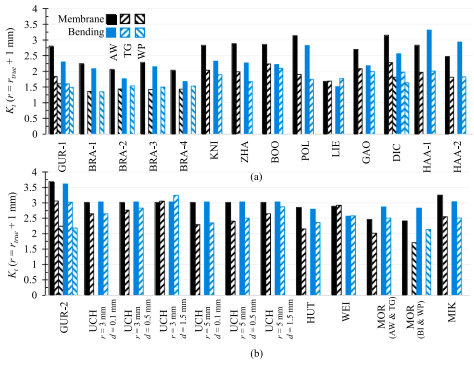

Fig. 7. Numerically obtained notch SCFs for joints in the AW and ground condition: (a) transversely welded joints (NLCT, NLCX, LCX), and (b) LG joints.

In the present study, a simplified method for estimating the R-O parameters was employed due to the lack of comprehensive material data. The strain hardening coefficient and exponent were derived based on the yield and ultimate strength and corresponding elongation values. The engineering stress and strains (σ and ε) were converted to true stress-true strain ($\bar{\sigma}$ and $\bar{\varepsilon}$) values, namely $\bar{\varepsilon} = \ln(1+\varepsilon)$and $\bar{\sigma} = (1+\varepsilon)\sigma$ [60], and R-O parameters were fitted according to the plastic strain at the known yield and ultimate strength points using a log-conversion of the plastic term of the R-O equation in comparison with a linear formula, as follows:

$$\bar{\varepsilon}_p = \left(\frac{\bar{\sigma}}{H}\right)^{\frac{1}{n}} \Leftrightarrow \log\bar{\varepsilon}_p = \frac{1}{n}(\log\bar{\sigma} - \log H) \Rightarrow y = \frac{1}{k}(x - b) \quad (4)$$

Applied stress ratios or, alternatively, the minimum or maximum of applied nominal stress were provided in all the extracted fatigue test data series. Recent studies [30,61,62] have indicated the need to consider specimen clamping-induced increase in mean stress and reduction in angular distortion to accurately obtain the effective applied stress ratio, and secondary bending stresses. Due to the lack of strain gage measurements and/or available data, these effects were excluded from the 4R analysis undertaken for this study.

3.3. Fatigue strength predictions

For each data point, cyclic behavior was analytically determined based on the concepts presented in Section 3.1, and the mean stress correction was conducted according to Eq. (1). The reference stress range was analyzed using linear elastic stress range and the 4R parameters: material strength, weld toe radius, residual stress and applied stress ratio. The approximations conducted in the 4R parameters and secondary bending stresses result in a certain level of uncertainty in the obtained stress range (see Eq. (1)). Consequently, the statistical analyses of *S-N* curves should account for the uncertainty in the obtained stress range, and not only in the fatigue life, as conventionally regarded [56]. Therefore, when determining the *S-N* curve in the 4R method, the minimization of the sum of squared perpendicular distances (MSSPD) statistical approach (Deming's regression [63]) is also applied for *S-N* curve fitting, in addition to the standard method with linear regression ($\Delta\sigma$ as known variable and N_f as unknown variable). The data plots are divided into four categories as follows: AW, TG, WP, and G&P. When applying the 4R method with the mean stress-corrected reference stress range, no significant difference between the different categories was observed, as shown in Fig. 8.

As regards the ENS concept, the AW data points were obtained with the reference radius of $r_{ref} = 1.0$ mm, and TG, WP, and G&P data points considering the true radius, that is, $r = r_{true} + 1$ mm. To enable a more comprehensive comparison between different data sets (AW, TG, WP, and G&P joints), the slope parameter of the *S-N* curve, mean fatigue strength (for a survival probability of $P_s = 50\%$), and scatter range T_σ (between $P_s = 10\%$ and $P_s = 90\%$) were determined from a data series

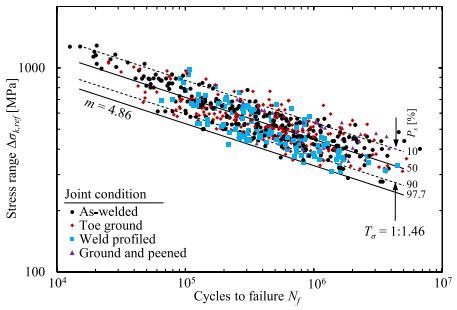

Fig. 8. *S-N* data plots for the 4R method and the S-N curves obtained using the MSSPD approach.

including all specimens. Subsequently, the mean fatigue strengths ($FAT_{mean,i}$, Tables 2, and 3) were obtained separately for different data sets using the obtained slope parameter. In the ENS concept, a similar approach was applied, except that the G&P joints were excluded from the statistical analysis of mean fatigue strength for all specimens as they showed significantly higher fatigue strength than AW, TG, and WP joints. A fixed slope parameter of $m = 3$ was also applied in the statistical analysis.

4. Discussion

Grinding methods are widely used in industrial applications to enhance the fatigue strength of welded joints due to their ready accessibility and suitability for a range of steel joints and components. Current fatigue design recommendations for weld toe grinding only cover the nominal stress and structural HS stress approaches for ground specimens [1]. The aim of this study was to re-analyze existing fatigue test data of joints in the AW and ground conditions using the notch stress-based approach, known as the 4R method, which employs the fatigue-effective fictitious radius concept with the SWT mean stress correction. Fatigue test results from a total number of 607 data points, as well as related details regarding the weld and specimen geometries, were extracted from published research papers and reports. Notch SCFs were obtained based on the geometry details using FE analysis. For each data point, the local cyclic behavior at the fatigue critical weld toe was analytically approximated to obtain the local stress ratio, which was used to mean stress-correct the notch stress range using SWT correction, as shown in Fig. 2 and Eq. (1).

4.1. Comparisons between the 4R method and ENS concept

The S-N data points, including all joint conditions (AW, TG, WP, and G&P), were plotted using the reference ENS range and the data points lay in one scatter band with a reasonably low scatter when the 4R method was applied. The reference ENS obtained using the SWT mean stress-correction commeasures the effect of the local stress ratio influenced by the applied stress ratio, material strength, residual stresses, and weld toe radius. The mean fatigue strength of $FAT_{mean} = 388$ MPa (the slope parameter of $m = 4.86$) was derived for all data points with the scatter value of $T_\sigma = 1{:}1.46$ between $P_s = 10\%$ and $P_s = 90\%$ curves, as presented in Table 2. Scatter values below $T_\sigma = 1{:}1.50$ are generally regarded as acceptable for individual series [21,57], and can be achieved using the 4R method for various joint types and conditions, steel grades, and applied stress ratios. The slope parameter of the *S-N* curve obtained for the extracted data was slightly lower than that obtained for the master data of the 4R method [27], in which high tensile residual stresses, $\sigma_{res} = +f_y$, were assumed for small-scale butt weld specimens. Assumption of high tensile residual stresses affects the cyclic behavior and local stress ratio particularly at a high-cycle regime, and increases the reference stress range (see R_{local} effects in Eq. (1)) resulting in a larger slope parameter. In this study, based on the available residual stress measurements, negligible small residual stress were assumed for the transversely welded small-scale specimens in the AW and ground condition, see Fig. 5. The resulting slope parameter was $m = 4.86$, which is in line with the 4R results obtained in recent studies [30,31]. As the reference stress range represents a mean stress-corrected value, the results of the 4R method cannot directly be compared to the ENS method.

The ENS concept, with $r_{ref} = 1.0$ mm for joints in the AW condition and $r = r_{true} + 1$ mm for ground joints, had good correspondence with the FAT225 curve, as shown Table 3. This finding supports previous research on the applicability of the ENS approach for ground joints [18]. However, insight on data plots (see Fig. 9) reveals that the G&P specimens were furthest away from the design curve, as the ENS method only takes geometrical improvements into account. Consequently, these results were excluded from the statistical analysis when evaluating the design curves presented in Table 3. For the HFMI-treated specimens, IIW [64] provides the design curves for the ENS method using $r_{ref} = 1.0$ mm in accordance with the material strength and applied stress ratio. Fig. 10 shows the data plots of G&P specimens in comparison with the design curves of HFMI-treated welded joints, indicating that the design curves are overly conservative for these PWT methods. Grinding preceding the peening treatment provides a significant reduction of notch SCF; thus, the combined effect of reduced notch SCF and compressive residual stresses should be taken into account more comprehensively. G&P specimens showed a distinctly higher fatigue strength than the AW, TG, and WP specimens, and an increase of 30–40% in fatigue strength – depending on the statistical approach applied – was found for the ENS concept (see Table 3).

In the statistical analyses for obtaining *S-N* curves, two different statistical approach were applied, namely the standard method (fatigue life is unknown variable), and the MSSPD approach (both fatigue life and stress range are unknown variables). The use of MSSPD approach resulted in larger slope parameters and lower scatter range values compared to the standard method (see Tables 2 and 3). In the context of this study, there is a certain level of uncertainty related to the stress range and, consequently, the use of the MSSPD approach is justifiable. The consideration of uncertainties in stress ranges should also be paid attention in further studies, and the MSSPD approach should, thus, potentially be employed.

4.2. Effects of compressive residual stresses

The 4R method provides a fatigue strength assessment approach

Table 2
Results of statistical analyses for the 4R method with different data sets.

Statistical approach	All specimens				$FAT_{mean,i}$ [MPa] (ratio $FAT_{mean,i}/FAT_{mean}$)			
	m [-]	FAT_{mean} [MPa]	FAT_{char} [MPa]	T_σ [-]	AW	TG	WP	G&P
Standard	3.55	345	243	1:1.57	345 (1.00)	344 (1.00)	325 (0.94)	395 (1.15)
MSSPD	4.86	388	288	1:1.46	393 (1.01)	387 (1.00)	366 (0.94)	418 (1.08)

Table 3
Results of statistical analyses for the ENS method with different data sets.

Statistical approach	All specimens[a]				$FAT_{mean,i}$ [MPa] (ratio $FAT_{mean,i}/FAT_{mean}$)			
	m [-]	FAT_{mean} [MPa]	FAT_{char} [MPa]	T_σ [-]	AW	TG	WP	G&P
Standard	3.20	368	258	1:1.57	381 (1.04)	367 (1.00)	337 (0.92)	509 (1.39)
Standard	3[b]	355	243	1:1.62	371 (1.04)	355 (1.00)	326 (0.92)	502 (1.41)
MSSPD	4.10	410	301	1:1.49	428 (1.04)	408 (0.99)	374 (0.91)	535 (1.30)

[a] Excluding data points of G&P joints.
[b] Fixed slope parameter of $m = 3$ in accordance with the design codes and guidelines [2,56].

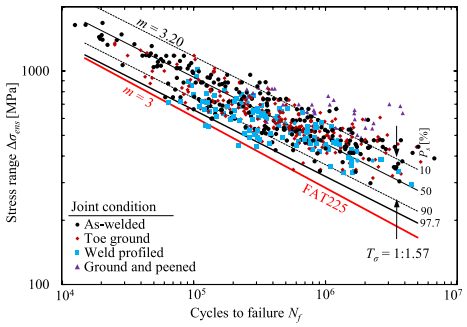

Fig. 9. *S-N* data plots for the ENS method and the S-N curves obtained using the standard statistical approach.

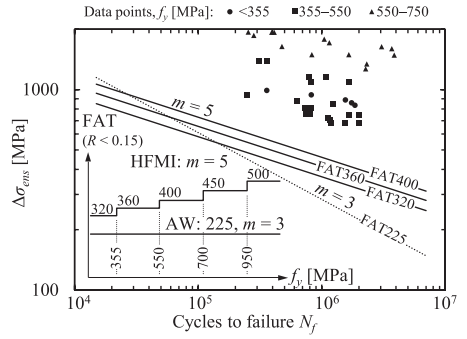

Fig. 10. Fatigue test results of G&P specimens using r_{ref} = 1.0 mm compared to the *S-N* curves for the HFMI-treated joints, after the IIW recommendations for the HFMI treatment [64].

which numerically accounts for the magnitude of residual stresses in association with the geometrical improvement. By examining more closely the 4R results of individual data sets covering joints in the AW, ground, and ground and peened condition, it can be seen that the data points lie in a single *S-N* curve, as shown in Fig. 11. The study by Miki *et al.* [46] also covered two type of peening methods after grinding (cleaning) treatment, resulting in different magnitude of compressive residual stresses, these being electric peening (CEP specimens) with $\sigma_{res} \approx -240$ MPa and pneumatic peening (CPP specimens) with $\sigma_{res} \approx -450$ MPa at the notch root. In their study [46], the highest fatigue strength was experimentally obtained for the CPP specimens, while the 4R method commeasures their effect on the fatigue performance, as demonstrated in Fig. 11d. For all G&P specimens (see Table 2), a 8% increase in mean fatigue strength ($FAT_{mean,G\&P}$ = 418 MPa) was found with respect to the mean fatigue strength of all specimens (FAT_{mean} = 388 MPa). However, in should be noted that the residual stresses were conservatively estimated, see Fig. 5, and the number of G&P specimens was limited; thus, more comprehensive data on the experimental fatigue test results and residual stresses is expected to improve the accuracy of the fatigue strength predictions.

4.3. Efficient grinding treatments

In grinding methods, a smoother transition from the base material to the weld reinforcement is acquired, and thus reducing the SCF and improving the fatigue strength. This was demonstrated in data sets applying both TG and WP methods in comparison with the AW joints (see Fig. 7). However, as the grinding methods are based on the removal of material, it requires they are laborious and redundant grinding should be avoided. Fig. 12 presents the notch SCFs for a ground NLCX joint under axial and bending loading as a function of toe radius. In this consideration, the grinding depth is kept constant at d = 0.5 mm, although for larger radii, the grinding depth typically slightly increases for practical reasons. It can be noted that notch SCF is reduced; however, with higher radii, the reduction of SCF fades out and approaches a specific value. Furthermore, it is noticeable that the reduction of net cross section due to the grinding depth is more detrimental for bending loads than axial loads due to the reduction of section modulus. In a notch SCF analysis, grinding depth can be considered directly in an FE model, while its effects on the fatigue assessments are excluded when the nominal or structural stress approaches are applied.

4.4. Reliability, sensitivity, and need for further studies

In axially loaded joints, angular distortion needs to be taken into account when evaluating *S-N* curves due to the secondary bending effects. In the extracted data, only the results of Braun *et al.* [15,35] provided the angular distortion-corrected stress values; consequently, a stress magnification factor of k_m = 1.25 was assumed for all other test specimens, as per the IIW Recommendations [56]. Such assumption is needed to compare the results with prior studies on the 4R method in which the macro geometric bending stresses were taken into account. Supposedly, the magnitude of angular distortion varies between the test series and individual specimens, and increases the scatter in the test results, although reasonably high accuracy was obtained with the assumption (see Tables 2 and 3). A higher accuracy with the 4R method could be expected if the welding residual stress and specimen-specific geometry details had been available for all data sets. The majority of prior studies unfortunately lacked information on welding residual stresses. Fatigue strength assessments of joints made of high- and ultra-high-strength steel grades, and peened specimens have a higher sensitivity in particular to the effects caused by welding residual stresses. A higher accuracy could also be expected for the ENS method in the fatigue strength assessment of G&P joints if a mean stress-correction is applied. However, it would require a joint condition-specific description and verification.

The 4R method applies residual stress, material strength, applied stress ratio, and weld toe radius numerically in the fatigue strength

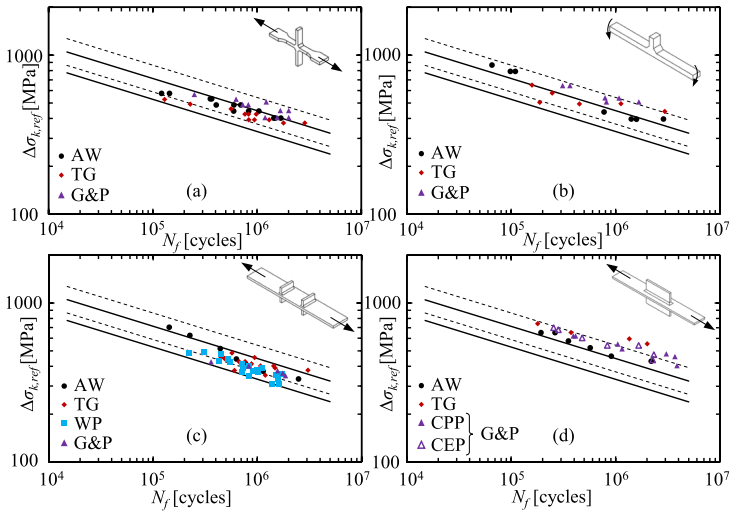

Fig. 11. Comparison of 4R fatigue strength predictions ground and peened data series: (a) Gao *et al.* [25], (b) Haagensen [24], (c) Gurney [23], and (d) Miki *et al.* [46]. The *S-N* curves correspond to those presented in Fig. 8 and Table 2.

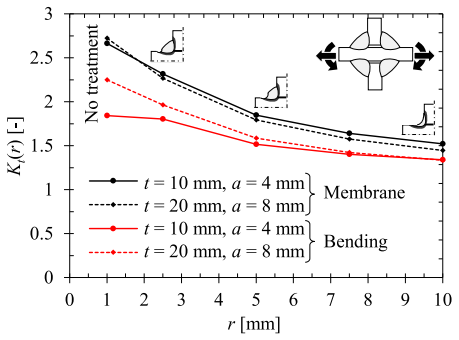

Fig. 12. Notch SCFs as a function of toe radius for a NLCX joint with plate thicknesses of t = 10 mm and t = 20 mm and a grinding depth of d = 0.5 mm.

assessment of welded joints, and the uncertainties related to the 4R parameters and their effects on the accuracy of predictions are important subjects from both academic and engineering viewpoints. To address these aspects, a sensitivity analysis of the 4R parameters was performed. In this analysis, a fillet-welded NLCX joint with different residual stress states (high tensile, low and compressive), applied stress ratio (pulsating and fully reversed) and steel grades (mild steel S355 and UHSS S960 grades) were investigated. Each 4R parameter was varied according to the 'one variable at the time' principle. Table 4 presents the baseline scenarios and chosen range of variations for each parameter. Ushikorawa's analytical formula [65] for notch SCF was applied when determining notch SCFs for the NLCX joint with different weld toe radii.

The results of the sensitivity analysis are presented in Fig. 13. Evidently, in joints with high tensile residual stresses, fatigue strength prediction is insensitive to the changes in residual stresses and applied stress ratios. Nevertheless, in joints with low or compressive residual stresses, significantly higher sensitivity to the changes in residual stresses and applied stress ratio was found. These aspects are in line with current knowledge concerning stress ratio effects on the fatigue strength of welded joints [1,56], and highlight that the effect of an individual parameter on fatigue strength cannot be unambiguously determined unless applied stress ratio and residual stress are not specified. When comparing mild steel and UHSS grades, no major difference was found, except that mild steels appear more sensitive to the changes in yield strength. Of the 4R parameters, weld toe radius is not severely affected by other parameters. On the other hand, the sensitivity of the parameters relating to applied load range should be noted. In general, under a high-cycle regime and low stress levels, higher sensitivity is present.

The fatigue assessments showed good correspondence between the joints in the AW and ground conditions when using a fictitious radius of $r = r_{true} + 1$ mm. Nevertheless, further studies could critically evaluate the value of fictitious radius and conduct comparisons with other fatigue-effective notch stress concepts, such as the stress averaging and critical distance concepts. Grinding quality in terms of surface

Table 4
Baseline scenarios and range of variations of the 4R parameters in the sensitivity analysis.

	S355 ($\Delta\sigma_m$ = 150 MPa)				S960 ($\Delta\sigma_m$ = 300 MPa)			
4R parameter	r_{true} [mm]	$R_{p0.2}$ [MPa]	σ_{res} [MPa]	R [-]	r_{true} [mm]	$R_{p0.2}$ [MPa]	σ_{res} [MPa]	R [-]
Baseline scenarios	0.5	355	250; 0; −100	0.5; 0; −1	0.5	960	850; 0; −300	0.5; 0; −1
Range of variation	± 0.5	± 100	± 100	± 0.2	± 0.5	± 100	± 100	± 0.2

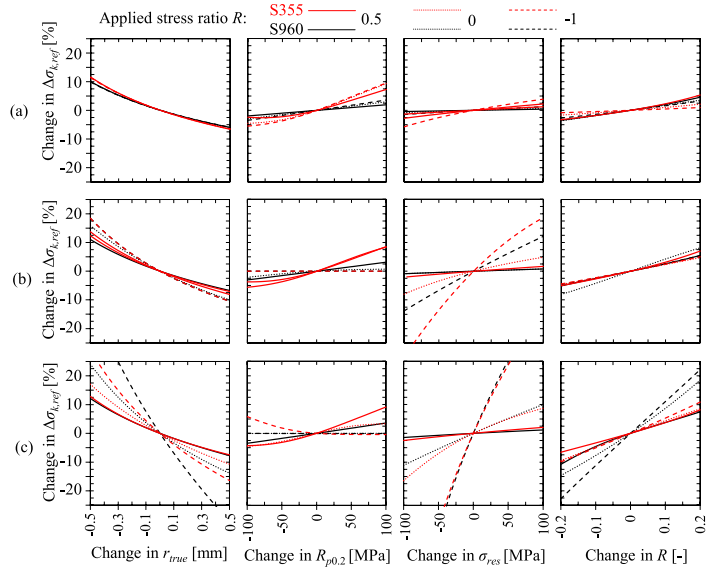

Fig. 13. Results of sensitivity analyses: (a) high tensile residual stress, (b) negligible low residual stress and (c) compressive residual stress.

roughness has a significant influence on the fatigue limit, particularly in high-strength materials [66], and its effects on the fatigue performance of ground joints should be addressed in further studies. In fatigue testing, small-scale specimens are widely employed, while fatigue test data analysis of large-scale components would further-verify the findings of this study in engineering applications. To account for the relaxation of residual stresses in fatigue assessments, further studies should be undertaken to investigate, in particular, the residual stress relaxion under the manufacturing procedures and mechanical loading conditions of ground and peened joints. Grinding methods have shown their potential to increase the fatigue strength in large-scale components [67–70]. However, these studies were excluded from the 4R analysis carried out for the present study due to the lack of comprehensive geometry data.

5. Conclusions

In the present study, the fatigue strength of ground specimens was evaluated using the 4R method. The 4R method is a versatile approach for the fatigue strength assessment of welded joints but, naturally, requires higher amount of modeling and analysis work, together with the proper estimations of the 4R parameters in comparison with the ENS approach. Fatigue test data and relevant information regarding the weld geometries were extracted from the literature. For each data series, linear FE analyses were carried out to obtain SCFs for notch stress analysis. All data points were converted to a reference notch stress system with the SWT mean stress correction, and the results were compared with the conventional ENS approach. The following conclusions can be drawn from the present study:

- The ENS-based evaluation with fictitious radius concept leads to similar results to those obtained using the 4R method and complies with the FAT225 curve, when excluding peened specimens. Grinding followed by additional peening treatment introduces compressive residual stresses and thus improves fatigue strength by 30–40% in addition to the fatigue strength enhancement related to the geometrical improvement.
- The 4R method was successfully applied, and led to a scatter range of T_σ = 1:1.46, for joints in AW, ground, and ground and peened condition. Consequently, the study shows that the 4R method can be regarded as a generic method for predicting the fatigue strength of welded joints in AW and post-weld-treated conditions, including PWTs based on both geometrical and residual stress improvement.
- The 4R method showed a good accuracy of fatigue strength predictions for joints improved by G&P (an 8% higher mean fatigue strength for the G&P joints compared to all joints), as well as demonstrated a high accuracy for joints in the AW and ground conditions in particular. Implementation of the 4R method enables the methodological consideration of compressive residual stresses introduced by peening methods at the ground weld toe.

Declaration of Competing Interest

The authors declare that they have no known competing financial interests or personal relationships that could have appeared to influence the work reported in this paper.

Acknowledgements

The work was supported by Business Finland in the Intelligent Steel Applications (ISA) project (Grant ID: 7386/31/2018). In addition, the authors wish to thank all assisting research colleagues for providing support and access to their fatigue test data.

Appendix A. Supplementary material

Supplementary data to this article can be found online at https://doi.org/10.1016/j.ijfatigue.2020.105916.

References

[1] Haagensen PJ, Maddox SJ. IIW recommendations on methods for improving the fatigue strength of welded joints. Woodhead Publishing; 2013.
[2] DNVGL-RP-C203. Fatigue design of offshore steel structures; 2016.
[3] BS7608:2014 +A1:2015. Guide to fatigue design and assessment of steel products; 2015.
[4] Gooch TG. Corrosion behavior of welded stainless steel. Weld J 1996:135–54.
[5] Amraei M, Dabiri M, Björk T, Skriko T. Effects of workshop fabrication processes on the deformation capacity of S960 ultra-high strength steel. 121007 J Manuf Sci Eng 2016;138. https://doi.org/10.1115/1.4033930.
[6] Björk T, Ahola A, Tuominen N. On the design of fillet welds made of ultra-high strength steel. Weld World 2018;62:985–95. https://doi.org/10.1007/s40194-018-0624-4.
[7] Yıldırım HC, Marquis GB. Fatigue strength improvement factors for high strength steel welded joints treated by high frequency mechanical impact. Int J Fatigue 2012;44:168–76. https://doi.org/10.1016/j.ijfatigue.2012.05.002.
[8] Leitner M, Gerstbrein S, Ottersböck MJ, Stoschka M. Fatigue strength of HFMI-treated high-strength steel joints under constant and variable amplitude block loading. Procedia Eng 2015;101:251–8. https://doi.org/10.1016/j.proeng.2015.02.036.
[9] Schubnell J, Carl E, Farajian M, Gkatzogiannis S, Knödel P, Ummenhofer T, et al. Residual stress relaxation in HFMI-treated fillet welds after single overload peaks. Weld World 2020. https://doi.org/10.1007/s40194-020-00902-6.
[10] Smith IFC, Hirt M. A review of fatigue strength improvement methods. Can J Civ Eng 1984;12:166–83. https://doi.org/10.1139/l85-016.
[11] Jármai K, Pahlke H, Farkas J. Cost savings using different post-welding treatments on an I-beam subject to fatigue load. Weld World 2014;58:691–8. https://doi.org/10.1007/s40194-014-0150-y.
[12] Kirkhope KJ, Bell R, Caron L, Basu RI, Ma K-T. Weld detail fatigue life improvement techniques. Part 1: review. Mar Struct 1999;12:447–74. https://doi.org/10.1016/S0951-8339(99)00013-1.
[13] Baptista R, Infante V, Branco CM. Study of the fatigue behavior in welded joints of stainless steels treated by weld toe grinding and subjected to salt water corrosion. Int J Fatigue 2008;30:453–62. https://doi.org/10.1016/j.ijfatigue.2007.04.011.
[14] Booth GS. The fatigue life of ground or peened fillet welded steel joints - the effect of mean stress. Met Constr 1981;13:112–5.
[15] Braun M, Grimm JH, Hoffmeister H, Ehlers S, Fricke W. Comparison of fatigue strength of post-weld improved high strength steel joints and notched base material specimens. Ships Offshore Struct 2018;13:47–55. https://doi.org/10.1080/17445302.2018.1425522.
[16] Pedersen MM, Mouritsen OØ, Hansen MR, Andersen JG. Experience with the Notch Stress Approach for Fatigue Assessment of Welded Joints Experience with the Notch Stress Approach for Fatigue Assessment of Welded Joints. In: Barsoum Z, Samuelsson J, editors. Proc. Swedish Conf. Light Weight Optim. Welded Struct., 2010.
[17] Sonsino CM, Fricke W, De Bruyne F, Hoppe A, Ahmadi A, Zhang G. Notch stress concepts for the fatigue assessment of welded joints - Background and applications. Int J Fatigue 2012;34:2–16. https://doi.org/10.1016/j.ijfatigue.2010.04.011.
[18] Mecséri BJ, Kövesdi B. Assessment of grinding weld treatment methods using effective notch stresses. Weld World 2020. https://doi.org/10.1007/s40194-020-00894-3.
[19] Baumgartner J, Schmidt H, Ince E, Melz T, Dilger K. Fatigue assessment of welded joints using stress averaging and critical distance approaches. Weld World 2015;59:731–42. https://doi.org/10.1007/s40194-015-0248-x.
[20] Baumgartner J, Yıldırım HC, Barsoum Z. Fatigue strength assessment of TIG-dressed welded steel joints by local approaches. Int J Fatigue 2019;126:72–8. https://doi.org/10.1016/j.ijfatigue.2019.04.038.
[21] Karakaş Ö, Zhang G, Sonsino CM. Critical distance approach for the fatigue strength assessment of magnesium welded joints in contrast to Neuber's effective stress method. Int J Fatigue 2018;112:21–35. https://doi.org/10.1016/j.ijfatigue.2018.03.004.
[22] Braun M, Grimm J-H, Milaković A-S, Hoffmeister H, Canaletti A, Ehlers S, et al. Bewertung der Schwingfestigkeit ausgeschliffener Schweißnähte aus hochfesten Stählen und Vergleich mit gekerbten Grundmaterialproben (in German). 19. Tagung Schweißen der Marit. Tech. und im Ingenieurbau 2019:76–91.
[23] Gurney TR. Effect of peening and grinding on the fatigue strength of fillet welded joints. Br Weld J 1968;15:601–9.
[24] Haagensen PJ. The effect of grinding and peening on the fatigue strength of welded T-joints. Trans Eng Sci 1993:2.
[25] Gao W, Wang D, Cheng F, Deng C, Liu Y, Xu W. Enhancement of the fatigue strength of underwater wet welds by grinding and ultrasonic impact treatment. J Mater Process Technol 2015;223:305–12. https://doi.org/10.1016/j.jmatprotec.2015.04.013.
[26] Nykänen T, Björk T. Assessment of fatigue strength of steel butt-welded joints in as-welded condition - Alternative approaches for curve fitting and mean stress effect analysis. Mar Struct 2015;44:288–310. https://doi.org/10.1016/j.marstruc.2015.09.005.
[27] Nykänen T, Björk T. A new proposal for assessment of the fatigue strength of steel butt-welded joints improved by peening (HFMI) under constant amplitude tensile loading. Fatigue Fract Eng Mater Struct 2016;39:566–82. https://doi.org/10.1111/ffe.12377.
[28] Nykänen T, Mettänen H, Björk T, Ahola A. Fatigue assessment of welded joints under variable amplitude loading using a novel notch stress approach. Int J Fatigue 2017;101:177–91. https://doi.org/10.1016/j.ijfatigue.2016.12.031.
[29] Björk T, Mettänen H, Ahola A, Lindgren M, Terva J. Fatigue strength assessment of duplex and super-duplex stainless steels by 4R method. Weld World 2018;62:1285–300. https://doi.org/10.1007/s40194-018-0657-8.
[30] Ahola A, Skriko T, Björk T. Fatigue strength assessment of ultra-high-strength steel fillet weld joints using 4R method. J Constr Steel Res 2019. https://doi.org/10.1016/j.jcsr.2019.105861.
[31] Mettänen H, Nykänen T, Skriko T, Ahola A, Björk T. Fatigue strength assessment of TIG-dressed ultra-high-strength steel fillet weld joints using the 4R method. 105745 Int J Fatigue 2020;139. https://doi.org/10.1016/j.ijfatigue.2020.105745.
[32] Marquis G, Nykänen T, Björk T. Fatigue crack patterns in ultrasonic peened welded structures during constant and variable amplitude loading. Proc. Int. Conf. Crack Paths (CP 2009), 2009, p. 273–84.
[33] Braun M, Wang X. Fatigue strength improvement by weld toe grinding: a data review. IIW-document XIII-2861-2020; 2020.
[34] Fricke W. IIW recommendations for the fatigue assessment of welded structures by notch stress analysis. Woodhead Publishing; 2012.
[35] Braun M, Hensel J, Song S, Ehlers S. Fatigue strength of normal and high strength steels joints improved by weld profiling (under preparation); 2020.
[36] Haagensen PJ. IIW's round robin and design recommendations for improvement methods. In: Maddox SJ, Prager M, editors. Proc. IIW 50th Annu. Assem. Conf., New York: Welding Research Council; 1997, p. 305–16.
[37] Knight JW. Improving the fatigue strength of fillet welded joints by grinding and peening. IIW-document XIII-851-77; 1977.
[38] Zhang YH, Maddox SJ. Fatigue life prediction for toe ground welded joints. Int J Fatigue 2009;31:1124–36. https://doi.org/10.1016/j.ijfatigue.2009.01.003.
[39] Polezhayeva H, Kang J-K, Heo J-H, Kim K-S. Effect of weld toe burr grinding on the fatigue strength of transverse welded specimens made from DH36 steel. Proc. ASME 28th Int. Conf. Ocean. Offshore Arct. Eng. OMAE2009 2009:1–5. https://doi.org/10.1115/OMAE2009-79331.
[40] Uchida D, Mori T, Sasaki Y. Influence of grinding depth on fatigue strength of out-of-plane gusset joints with finished weld toes (in Japanese). Japanese Soc Steel Constr 2016;23:51–8. https://doi.org/10.11273/jssc.23.89_51.
[41] Pedersen MM, Mouritsen OØ, Hansen MR, Andersen JG, Wenderby J. Comparison of post-weld treatment of high-strength steel welded joints in medium cycle fatigue. Weld World 2010;54:208–17. https://doi.org/10.1007/BF03263506.
[42] Lieurade HP, Huther I, Lefebvre F. Effect of weld quality and postweld improvement techniques on the fatigue resistance of extra high strength steels. Weld World 2008;52:106–15. https://doi.org/10.1007/BF03266658.
[43] Huther I, Suchier Y, Lieurade HP. Fatigue behaviour of longitudinal non-load-carrying joints improved by burr gringing, TIG dressing. IIW-document XIII-2108-06; 2006.
[44] Weich I. Ermüdungsverhalten mechanisch nachbehandelter Schweißverbindungen in Abhängigkeit des Randschichtzustands (in German) Doctoral thesis Technical University of Braunschweig; 2009.
[45] Dickerson T, Moura Branco C. Weld improvement methods for low cycle fatigue applications. Final report EUR 17823; 1997.
[46] Miki C, Tai M. Fatigue strength improvement of out-of-plane welded joints of steel girder under variable amplitude loading. Weld World 2013;57:823–40. https://doi.org/10.1007/s40194-013-0076-9.
[47] Mori T, Inomata T, Hirayama S. Influence of grinding method on fatigue strength of out-of-plane gusset welded joints (in Japanese). Japanese Soc Steel Constr 2004;11:55–62. https://doi.org/10.11273/jssc1994.11.42_55.
[48] Björk T, Mettänen H, Ahola A, Lindgren M, Terva J. Fatigue strength assessment of duplex and super-duplex stainless steels by 4R method. Weld World 2018;62. https://doi.org/10.1007/s40194-018-0657-8.
[49] Sonsino CM. Effect of residual stresses on the fatigue behaviour of welded joints depending on loading conditions and weld geometry. Int J Fatigue 2009;31:88–101. https://doi.org/10.1016/j.ijfatigue.2008.02.015.
[50] Gkatzogiannis S, Knoedel P, Ummenhofer T. FE welding residual stress simulation: Influence of boundary conditions and material models. In: Jönsson J, editor. Proc. Eurosteel 2017, vol. 1, Wiley; 2017, p. 443–52. doi:10.1002/cepa.80.
[51] Farajian M. Welding residual stress behavior under mechanical loading. Weld World 2013;57:157–69. https://doi.org/10.1007/s40194-013-0024-8.
[52] Leggatt RH. Residual stresses in welded structures. Int J Press Vessel Pip 2008;85:144–51. https://doi.org/10.1016/j.ijpvp.2007.10.004.
[53] Chen B-Q, Guedes SC. Effect of welding sequence on temperature distribution, distortions, and residual stress on stiffened plates. Int J Adv Manuf Technol 2016;86:3145–56. https://doi.org/10.1007/s00170-016-8448-0.
[54] Baumgartner J, Bruder T. An efficient meshing approach for the calculation of notch stresses. Weld World 2013;57:137–45. https://doi.org/10.1007/s40194-012-0005-3.
[55] Ahola A, Nykänen T, Björk T. Effect of loading type on the fatigue strength of asymmetric and symmetric transverse non-load carrying attachments. Fatigue Fract Eng Mater Struct 2017;40:670–82. https://doi.org/10.1111/ffe.12531.
[56] Hobbacher A. Recommendations for fatigue design of welded joints and components. 2nd ed. Cham: Springer International Publishing; 2016.
[57] Radaj D, Sonsino CM, Fricke W. Fatigue assessment of welded joints by local approaches. 2nd ed. Cambridge: Woodhead Publishing; 2006.
[58] Pavlina EJ, Van Tyne CJ. Correlation of yield strength and tensile strength with hardness for steels. J Mater Eng Perform 2008;17:888–93. https://doi.org/10.1007/s11665-008-9225-5.
[59] Webster S, Bannister A. Structural integrity assessment procedure for Europe - of the SINTAP programme overview. Eng Fract Mech 2000;67:481–514. https://doi.org/10.1016/S0013-7944(00)00070-9.
[60] Dowling NE. Mechanical behavior of materials. Engineering methods for deformation, fracture, and fatigue. Prentice Hall; 2006.

[61] Leitner M. Influence of effective stress ratio on the fatigue strength of welded and HFMI-treated high-strength steel joints. Int J Fatigue 2017;102:158–70. https://doi.org/10.1016/j.ijfatigue.2017.03.008.
[62] Baumgartner J, Bruder T. Influence of weld geometry and residual stresses on the fatigue strength of longitudinal stiffeners. Weld World 2013;57:841–55. https://doi.org/10.1007/s40194-013-0078-7.
[63] Deming WE. Statistical adjustment of data. Dover Publication Inc.; 1943.
[64] Marquis GB, Barsoum Z. IIW Recommendations for the HFMI Treatment - For Improving the Fatigue Strength of Welded Joints. Singapore: Springer Singapore; 2016. doi:10.1007/978-981-10-2504-4.
[65] Iida K, Uemura T. Stress concentration factor formulae widely used in Japan. Fatigue Fract Eng Mater Struct 1996;19:779–86. https://doi.org/10.1111/j.1460-2695.1996.tb01322.x.
[66] Parmentier G, Huther M. S-N curves for welded, non-welded or improved welded details of marine structures. 5th Fatigue Des. Conf. Fatigue Des. 2013. Procedia Eng., vol. 66, 2013, p. 49–61. doi:10.1016/j.proeng.2013.12.061.
[67] Qian X, Petchdemaneengam Y, Swaddiwudhipong S, Marshall P, Ou Z, Thang C. Fatigue performance of tubular X-joints with PJP + welds: I - Experimental study. J Constr Steel Res 2013;90:49–59. https://doi.org/10.1016/j.jcsr.2013.07.016.
[68] Choi S-M, Tateishi K, Hanji T. Fatigue strength improvement of weld joints with cope Hole. Int J Steel Struct 2013;13:683–90. https://doi.org/10.1007/s13296-013-4009-7.
[69] Lotsberg I, Fjeldstad A, Helsem MR. Fatigue life improvement of welded doubling plates by grinding and ultrasonic peening. Weld World 2014;58:819–30. https://doi.org/10.1007/s40194-014-0161-8.
[70] Puthli R, Herion S, Bergers J. Influence of longitudinal attachments on the fatigue behaviour of high strength steels. Proc. 16th Int. Offshore Polar Eng. Conf., vol. 4, 2006, p. 120–6.

ACTA UNIVERSITATIS LAPPEENRANTAENSIS

899. MAMELKINA, MARIA. Treatment of mining waters by electrocoagulation. 2020. Diss.

900. AMBAT, INDU. Application of diverse feedstocks for biodiesel production using catalytic technology. 2020. Diss.

901. LAAPIO-RAPI, EMILIA. Sairaanhoitajien rajatun lääkkeenmääräämistoiminnan tuottavuuden, tehokkuuden ja kustannusvaikuttavuuden arviointi perusterveydenhuollon avohoidon palveluprosessissa. 2020. Diss.

902. DI, CHONG. Modeling and analysis of a high-speed solid-rotor induction machine. 2020. Diss.

903. AROLA, KIMMO. Enhanced micropollutant removal and nutrient recovery in municipal wastewater treatment. 2020. Diss.

904. RAHIMPOUR GOLROUDBARY, SAEED. Sustainable recycling of critical materials. 2020. Diss.

905. BURGOS CASTILLO, RUTELY CONCEPCION. Fenton chemistry beyond remediating wastewater and producing cleaner water. 2020. Diss.

906. JOHN, MIIA. Separation efficiencies of freeze crystallization in wastewater purification. 2020. Diss.

907. VUOJOLAINEN, JOUNI. Identification of magnetically levitated machines. 2020. Diss.

908. KC, RAGHU. The role of efficient forest biomass logistics on optimisation of environmental sustainability of bioenergy. 2020. Diss.

909. NEISI, NEDA. Dynamic and thermal modeling of touch-down bearings considering bearing non-idealities. 2020. Diss.

910. YAN, FANGPING. The deposition and light absorption property of carbonaceous matter in the Himalayas and Tibetan Plateau. 2020. Diss.

911. NJOCK BAYOCK, FRANCOIS MITERAND. Thermal analysis of dissimilar weld joints of high-strength and ultra-high-strength steels. 2020. Diss.

912. KINNUNEN, SINI-KAISU. Modelling the value of fleet data in the ecosystems of asset management. 2020. Diss.

913. MUSIKKA, TATU. Usability and limitations of behavioural component models in IGBT short-circuit modelling. 2020. Diss.

914. SHNAI, IULIIA. The technology of flipped classroom: assessments, resources and systematic design. 2020. Diss.

915. SAFAEI, ZAHRA. Application of differential ion mobility spectrometry for detection of water pollutants. 2020. Diss.

916. FILIMONOV, ROMAN. Computational fluid dynamics as a tool for process engineering. 2020. Diss.

917. VIRTANEN, TIINA. Real-time monitoring of membrane fouling caused by phenolic compounds. 2020. Diss.

918. AZZUNI, ABDELRAHMAN. Energy security evaluation for the present and the future on a global level. 2020. Diss.

919. NOKELAINEN, JOHANNES. Interplay of local moments and itinerant electrons. 2020. Diss.

920. HONKANEN, JARI. Control design issues in grid-connected single-phase converters, with the focus on power factor correction. 2020. Diss.

921. KEMPPINEN, JUHA. The development and implementation of the clinical decision support system for integrated mental and addiction care. 2020. Diss.

922. KORHONEN, SATU. The journeys of becoming ang being an international entrepreneur: A narrative inquiry of the "I" in international entrepreneurship. 2020. Diss.

923. SIRKIÄ, JUKKA. Leveraging digitalization opportunities to improve the business model. 2020. Diss.

924. SHEMYAKIN, VLADIMIR. Parameter estimation of large-scale chaotic systems. 2020. Diss.

925. AALTONEN, PÄIVI. Exploring novelty in the internationalization process - understanding disruptive events. 2020. Diss.

926. VADANA, IUSTIN. Internationalization of born-digital companies. 2020. Diss.

927. FARFAN OROZCO, FRANCISCO JAVIER. In-depth analysis of the global power infrastructure - Opportunities for sustainable evolution of the power sector. 2020. Diss.

928. KRAINOV, IGOR. Properties of exchange interactions in magnetic semiconductors. 2020. Diss.

929. KARPPANEN, JANNE. Assessing the applicability of low voltage direct current in electricity distribution - Key factors and design aspects. 2020. Diss.

930. NIEMINEN, HARRI. Power-to-methanol via membrane contactor-based CO2 capture and low-temperature chemical synthesis. 2020. Diss.

931. CALDERA, UPEKSHA. The role of renewable energy based seawater reverse osmosis (SWRO) in meeting the global water challenges in the decades to come. 2020. Diss.

932. KIVISTÖ, TIMO. Processes and tools to promote community benefits in public procurement. 2020. Diss.

933. NAQVI, BILAL. Towards aligning security and usability during the system development lifecycle. 2020. Diss.

934. XIN, YAN. Knowledge sharing and reuse in product-service systems with a product lifecycle perspective. 2020. Diss.

935. PALACIN SILVA, VICTORIA. Participation in digital citizen science. 2020. Diss.

936. PUOLAKKA, TIINA. Managing operations in professional organisations – interplay between professionals and managers in court workflow control. 2020. Diss.

ISBN 978-952-335-594-1
ISBN 978-952-335-595-8 (PDF)
ISSN-L 1456-4491
ISSN 1456-4491
Lappeenranta 2020